Molecular regulation of synaptic α_5-$GABA_A$ receptors

Carmen Kivisild

A thesis submitted to University College London for the degree of

Doctor of Philosophy

Department of Neuroscience, Physiology and Pharmacology

University College London

December 14, 2021

I, Carmen Kivisild, confirm that the work presented in this thesis is my own. Where information has been derived from other sources, I confirm that this has been indicated in the work.

Abstract

In the adult brain, the main role for γ-aminobutyric acid receptors ($GABA_ARs$) is to control neural excitability via transient synaptic and persistent tonic inhibition. These forms of inhibition are distinct and mediated by receptors located at inhibitory synapses (phasic), and by extrasynaptic receptors (tonic). Although receptors containing the α_5 subunit (α_5-$GABA_ARs$) are predominantly located extrasynaptically, there are also synaptic α_5-$GABA_ARs$, which, due to their significant expression in the hippocampus, are thought to play an important role in learning and memory. Consequently, selective allosteric modulators of α_5-$GABA_ARs$ have been proposed as therapeutic options for cognitive dysfunction associated with conditions such as Down syndrome, Alzheimer's disease, schizophrenia, and autistic spectrum disorder. However, how hippocampal synaptic inhibition via α_5-$GABA_ARs$ is regulated, remains largely unknown. Here, online prediction software for post-translational modification and mass-spectrometry analyses were used to discover phosphorylation sites in the intracellular domain of the α_5 subunit that may regulate the subcellular location of the α_5-$GABA_ARs$. To assess this, one of the key phosphorylated residues ${\alpha_5}^{S374}$ was mutated to phosphomimetic and phospho-dead residues. Whole-cell patch clamp recordings in wild-type and mutant transfected HEK293 cells were used to reveal that ${\alpha_5}^{S374}$ has a significant role in receptor function and is likely to be phosphorylated by the kinase GSK3β. By using a combination of electrophysiology and structured illumination microscopy (SIM) in transfected cultured hippocampal neurons, phosphorylation of ${\alpha_5}^{S374}$ was found to regulate the synaptic location of α_5-$GABA_ARs$ and thus control phasic inhibition. The underlying molecular mechanism behind modified α_5-receptor trafficking is likely

to be altered binding between phosphorylated α_5-$GABA_A$Rs and inhibitory synaptic scaffold proteins. Although several drugs can target α_5-$GABA_A$Rs, a greater understanding of the molecular mechanisms by which neurons control their accumulation at synaptic sites, and thus regulate phasic inhibition, is greatly needed to elucidate the role of α_5-$GABA_A$Rs in cognition.

Impact statement

The α_5-GABA$_A$R isoform is quite unique for the GABA$_A$ receptor family. These receptors show a discrete brain distribution being particularly and substantially expressed in the hippocampus. It is also unusual by exhibiting both synaptic and extrasynaptic subcellular localization and thus is ideally-placed to contribute towards both phasic and tonic inhibition mediated by GABA. It also has a so far unique interaction with a receptor associated molecule radixin that may influence its synaptic, perisynaptic and extrasynaptic accumulation. The α_5-GABA$_A$R innately displays slow kinetics and numerous studies support a key role in higher order function including synaptic plasticity and in terms of behaviour, cognitive function.

The key physiological role played by α_5-GABA$_A$Rs is exemplified by the consequences when there are deficits in α_5-GABA$_A$Rs function. Such deficits are associated with multiple neuropathological diseases and again consequentially, several drugs have been developed to target these receptors. Despite this background, very little is known about the molecular and cellular regulation of this unique receptor subtype which will be of paramount importance for normal healthy brain function, and which will also influence our view of its role as a developing therapeutic target.

In the present study, by using a combination of methods designed for precise experimental interrogation, we provide a new contribution towards what is known about the molecular regulation of α_5-GABA$_A$Rs. Significantly, strong evidence is obtained demonstrating that the accumulation of α_5-GABA$_A$Rs at inhibitory synapses is negatively regulated by the phosphorylation of a key serine residue at position 374 located in the intracellular domain of the α_5 subunit. The consensus sequence that includes $\alpha_5{}^{S374}$ implicates glycogen synthase kinase-3 iso-

form β(GSK3β) as the partner phosphorylating kinase and links the regulation of α_5-$GABA_A$Rs to a variety of signalling pathways. This represents a new pathway for controlling and modulating α_5-$GABA_A$R function and will impact on the sub-cellular localisation of these receptors with implications for their contribution to both phasic and tonic GABA-mediated inhibition.

Given the pivotal role of the α_5-$GABA_A$Rs in controlling synaptic plasticity and excitatory transmission within the hippocampus, this phosphorylation-dependent regulation of α_5-$GABA_A$Rs is likely to be important for underpinning their involvement in memory and cognition. Therefore, in conclusion, this study describes the importance and impact of post-translational modification in $GABA_A$R signalling, and in particular this work broadens our fundamental knowledge about the specific regulation of α_5-$GABA_A$Rs. Consequently, it further highlights the therapeutic potential of these receptors.

Acknowledgements

I would like to start with Prof Trevor Smart. Trevor, thank you so much for opening the door of opportunity to me by taking in a person from a distant country called Estonia and who had no previous experience with electrophysiology. I didn't even know what GABA was before I joined your lab. You have always seen the best in me and encouraged my curiosity. Your friendly face, greeting me every morning, gave me positive energy even when I felt low. Thank you!

Dr Damian Bright, you are next. Damian, words don't do justice to how amazingly well we work together. Every day, I waited impatiently for you to come to work so I could bounce some ideas off you. Your logical and critical thinking greatly balances my, sometimes overwhelming, eagerness and wild imagination. I don't know why I am still surprised by how Bright you are. You are also a great friend. Whenever you have asked me "How are you?", I know that you have always meant that. So, thank you for these most interesting scientifical conversations and thank you so much for being my best friend in the lab.

Dr Philip Thomas and Dr Martin Mortensen, a great duo located in the same office. I really enjoyed visiting you, frequently. You two are the most useful people in the lab: whenever I wanted something I came straight to you. "Did you get my email?", "Where can I find...?" or "Help needed!" were the main phrases I yelled when storming into your office. Thank you both for all the help throughout my PhD. And special thanks to Mamo for organizing the best parties ever!

Dr Saad Hannan, my culture mentor. Saad, you are the most skilled in the lab, and I feel happy that I had a chance to learn from the best. Thank you for teaching me how to become an expert in preparing hippocampal cultures.

Valentina and Dr Marco, thank you both for keeping my spirits up and boosting my mental health with picnics in the park, trip to Cotswold and most importantly – by bringing me cinnamon buns.

I would also like to thank past and current members of the lab whom I haven't specifically mentioned here. Each of you have helped me to get where I am today. Also, thank you LMCB for providing me the opportunity to do my PhD at UCL. Thank you!

And last, but not least! From the bottom of my heart, Risto, thank you for always supporting my dreams. I could have not done it without your unconditional love and patience. Thank you for holding everything together while I had to work hard on my thesis. I promise to be there for you next year when you finish your PhD. I love you.

Contents

List of Figures

List of Tables

List of Abbreviations

5-HT3	Type-3 serotonin receptors
ANOVA	Analysis of variance
BLA	Basolateral complex of the amygdala
BSA	Bovine serum albumin
BZ	Benzodiazepine binding site
CAMKII	Calcium/calmodulin-dependent kinase
CB	Collybistin
CeA	Central nucleus of the amygdala
CeL	Lateral subdivision of CeA
CeM	Medial subdivision of CeA
CDK5	Cyclin-dependent kinase 5
CHS	Cholesteryl hemisuccinate
CK1	Casein kinase 1
CNS	Central nervous system
CR	Calretinin
CRC	Concentration-response curve
cryo-EM	Cryo-electron microscopy
DDM	n-Dodecyl β-D-maltoside
DIV	Days in vitro
DMEM	Dulbecco‘s modified Eagle‘s medium
DMSO	Dimethyl sulfoxide
DTT	Dithiothreitol
ECD	Extracellular domain
EC50	Half maximal effective concentration
ELM	Eukaryotic linear motif
EPM	Elevated plus maze
ER	Endoplasmic reticulum
ERK1/2	Extracellular signal–regulated kinase 1/2
FBS	Fetal bovine serum
GABA	γ-Aminobutyric acid
$GABA_A$Rs	γ-Aminobutyric acid type A receptors
GBD	Gephyrin binding domain

GFP	Green fluorescent protein
Grin1	Mouse model for schizophrenia
GSK3	Glycogen synthase kinase-3
HBS	HEPES-buffered saline
HBSS	Hanks' balanced salt solution
HEK293	Human embryonic kidney cells
HEPES	4-(2-hydroxyethyl)-1-piperazineethanesulfonic acid
IAA	Iodoacetamide
ICD	Intracellular domain
iLTD	Inhibitory long-term depression
iLTP	Inhibitory long-term potentiation
IN	Interneuron
IP	Immunoprecipitation
IPSC	Inhibitory postsynaptic current
LB	Luria Broth
LC-MS	Liquid chromatography–mass spectrometry
LHFPL4/GARLH4	Lipoma HMGIC Fusion Partner-Like 4
LIR	LC3-interacting region
LTD	Long-term depression
LTP	Long-term potentiation
MAM	Mouse model for schizophrenia
MAPK	Mitogen-activated protein kinase
MDD	Major depressive disorder
MEM	Minimum Essential Medium
MS	Mass spectrometry
NAM	Negative allosteric modulator
NEK2	NIMA-related kinase 2
NGS	Normal goat serum
NL2	Neuroligin 2
NMDA	N-methyl-d-aspartate
NMDARs	N-methyl-d-aspartate receptors
O-LM	Oriens/lacunosum-moleculare
PALM	Photoactivated localization microscopy
PAM	Positive allosteric modulator
PBS	Phosphate-buffered saline
PCR	Polymerase chair reaction
PFA	Paraformaldehyde
PKA	Protein kinase A
PKC	Protein kinase C
pLGIC	Pentameric ligand-gated ion channels
PLGS	Protein Lynx Global Server
PMA	phorbol 12-myristate 13-acetate, PKC activator
PSD	Postsynaptic density

PTX	Picrotoxin
QToF	Quadrupole time-of-flight
RM	Repeated measurements
ROI	Region of interest
SDS	Sodium dodecyl sulphate
SEM	Standard error of the mean
SH2 and SH3	Src homology 2 and 3 domains
SIM	Structured illumination microscopy
SR	Super resolution
SSD	Subsynaptic domain
SST	Somatostatin
SST-IN	Somatostatin-positive interneuron
STAT5	Signal transducer and activator of transcription 5 protein
STED	Stimulated emission depletion
STORM	Stochastic optical reconstruction microscopy
TBS	Tris-buffered saline
TBS	Theta burst stimulation
TE	Tris/EDTA buffer
TM1-TM4	Transmembrane regions 1-4
TRAF2	TNF receptor-associated factor 2
Ts65Dn	Mouse model for Down Syndrome
VIAAT	Vesicular inhibitory amino acid transporter
VIP	Vasoactive intestinal polypeptide
ZAC	Zn^{2+}-activated ion channel

Chapter 1

Introduction

1.1 $GABA_A$ receptor structure, subunit composition and assembly

γ-Aminobutyric acid receptors ($GABA_A$Rs) are the major mediators of inhibitory neurotransmission within the mammalian central nervous system (CNS), which is caused by opening of anion-permeable pentameric ligand-gated ion channels (pLGIC) leading to an increased membrane conductance and often the hyperpolarization of the postsynaptic cell. In this case, GABA is released by the presynaptic axon terminal boutons and binds to these receptors which, in turn, leads to an increased influx of chloride ions and a reduction in neuronal excitability (Sallard et al., 2021). Although chloride ion flux accounts for most of the $GABA_A$R membrane conductance *in vivo*, these currents will also have a smaller contribution from bicarbonate ion flux. Furthermore, in ion substitution experiments, formate, propionate, acetate, cyanide, and halides can also permeate through the GABA ion channel. The relative conductance and permeability for these anions is controlled by ion selectivity filters, transmembrane electrochemical ion gradients and the pore diameter (Fatima-Shad and Barry, 1993).

$GABA_A$Rs are members of the pLGIC (formerly Cys-loop receptor) family together with anion-selective glycine receptors, cation-selective nicotinic acetylcholine receptors and type-3 serotonin (5-HT3) receptors, and the Zn^{2+}-activated ion channel (ZAC) in vertebrate species (Corringer et al., 2012). Like other recep-

tors in this family, $GABA_A$Rs assemble as pentamers with all five subunits arranged pseudo-symmetrically around the central pore (Figure 1.1A). Each subunit comprises three main domains: an extracellular domain (ECD), a transmembrane domain (TMD), and an intracellular domain (ICD). The ECD has a highly conserved domain organization which comprises an N-terminal α-helix, followed by two inner and outer sheets comprising ten β strands arranged orthogonally. The structural signature of the Cys-loop family is a loop formed by a disulfide bridge between two cysteine residues on strands β6 and β7 (Kim and Hibbs, 2021). The ECD is important as it contains two orthosteric (GABA) binding sites and several other binding sites for allosteric modulators (Kim et al., 2020; Masiulis et al., 2019; Zhu et al., 2018). By comparisons to the ECD, the TMD is composed of four transmembrane α-helices (M1–M4), with the M2 helices of each subunit contributing to form the pore. The amino acid sequence of the large ICD that lies between the M3 and M4 TMD helices, is variable between subunits (Kim and Hibbs, 2021). Despite recent advances in our understanding from structural studies of $GABA_A$Rs (Laverty et al., 2019; Miller and Aricescu, 2014; Miller et al., 2018, 2017; Phulera et al., 2018) the structure of the ICD is still poorly understood and described as intrinsically disordered (Figure 1.1B). However, the ICD is believed to adapt a defined conformation when bound to intracellular binding partners or receptor-associated molecules (Kim and Hibbs, 2021). The ICD is the focus of this project as it is important for receptor trafficking (Charych et al., 2004; Kittler et al., 2008) and the fine tuning of GABA channel kinetics (Kittler et al., 2005) as well as mediating interactions with synaptic anchoring proteins (Brady and Jacob, 2015; Mukherjee et al., 2011; Tretter et al., 2008, 2011; Ye et al., 2021).

The subunits constituting $GABA_A$ heteropentameric receptors are derived from a diverse number of families. Based on the exact combination of the subunits, receptors are divided into subtypes, each possessing a specific pharmacology and distinct distribution in the brain. Mammals have 19 genes coding for $GABA_A$Rs subunits (Simon et al., 2004), classified into homologous classes (α, β, γ, ρ, ϑ, ε, π and δ) with some of these exhibiting multiple isoforms ($\alpha_{1\text{-}6}$, $\beta_{1\text{-}3}$, $\gamma_{1\text{-}3}$ and $\rho_{1\text{-}3}$) (Olsen

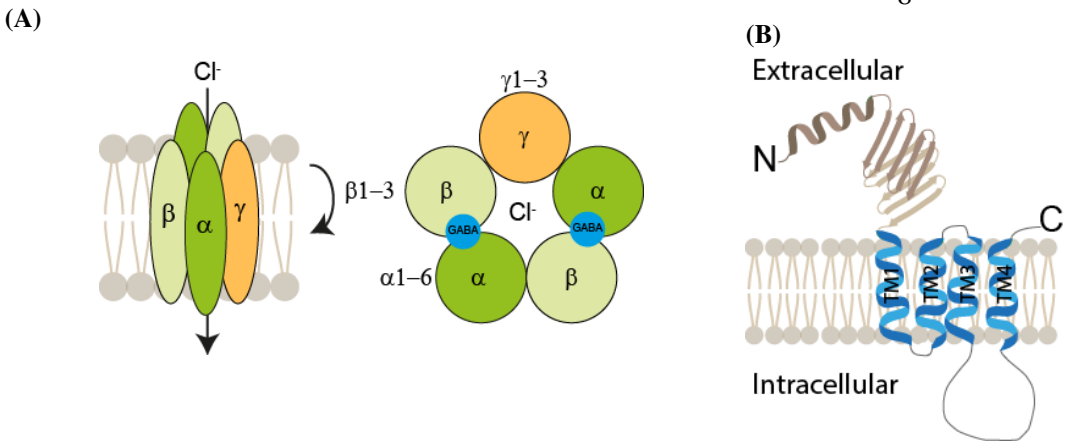

Figure 1.1: Schematic of heteropentameric $GABA_A$ receptor and their subunits. **(A)** Left, the stoichiometric arrangement of the subunits as viewed from the plane of the membrane and right, looking down on the extracellular surface. Each chloride permeable $GABA_AR$ is composed of five subunits typically arranged as γ-β-α-β-α (orange - light green - green - light green - green), when read counter-clockwise, although other subunit combinations also exist. There are two GABA binding sites (blue), both located at the β+/α− interfaces. **(B)** Schematic of one $GABA_A$ subunit that comprises an extracellular domain (β-sheets, in light brown), four membrane-spanning α-helices (TM1–TM4, in blue) and a large cytoplasmic domain (grey) between TM3 and TM4.

and Sieghart, 2008). The diversity of subunits is further increased by alternative splicing where γ_2 subunits are found in long (γ_{2L}) and short versions (γ_{2S}) serving as the best example. The only difference between these two isoforms is a cytoplasmic insertion of 8 residues in γ_{2L} which also contains a protein kinase C (PKC) phosphorylation site (Cheng et al., 1997; Kofuji et al., 1991; Krishek et al., 1994; Whiting et al., 1990).

The largest population of receptors in the brain are thought to be composed of two α, two β and one γ subunit, where both alpha and beta subunits are most often, but not always, of the same isoform (Olsen and Sieghart, 2008, 2009). However, other stoichiometries can be observed: a ϑ subunit can replace a β subunit (Bonnert et al., 1999) and ε, π and δ subunits can replace a γ subunit (Araujo et al., 1998; Hedblom and Kirkness, 1997; Neelands et al., 1999). The subunits in the same class share approximately 70% sequence identity, whereas only approximately 20-40% sequence identity is observed between members of different classes (Olsen and Tobin, 1990). From structural studies, the stoichiometric arrangement of subunits is

γ-β-α-β-α, when read counter-clockwise looking down onto the extracellular face. The receptor carries two GABA binding sites, both located at the β+/α− interfaces in the ECD of the receptor, where + stands for "principal" and – for "complementary" faces of the subunit (Figure 1.1A). Upon the binding of the agonist to the orthosteric-binding sites, a cascade of conformational changes is initiated leading to the opening of the chloride-permeable central pore and a resultant flux of ions (Baumann et al., 2001, 2002, 2003).

Given the heteromeric nature of $GABA_A$Rs *in vivo*, the long list of subunits together with the splice variants gives rise to a huge number of theoretically possible subunit combinations. However, experimental evidence only exists for a few dozen combinations *in vivo*, suggesting that the assembly process of $GABA_A$Rs is selective and not based simply on permutations (Olsen and Sieghart, 2008). It is likely that assembly rules are different depending on the expression and availability of partner subunits (Pirker et al., 2000) and also multiple residues in different domains may be involved in oligomerization with the same neighbouring subunit (Sarto-Jackson and Sieghart, 2008). Yet, few universal rules have been established. For an example, most studies data suggests that both α and β subunits are obligatory for the surface expression of fully functional pentameric receptors (Connolly et al., 1996). In addition, most $GABA_A$Rs subtypes contain only one non-α/β subunit, making non-α/β subunits most likely mutually exclusive within a pentamer (Araujo et al., 1998).

1.2 $GABA_A$ receptor trafficking

Under physiological conditions, $GABA_A$Rs are believed to cycle continuously between the neuronal cell surface and intracellular compartments. $GABA_A$Rs can be inserted into the plasma membrane either as newly assembled receptor complexes via a *de novo* secretory pathway or reinserted following internalization. First, the monomers are oligomerized into dimers and trimers and eventually pentamers in the endoplasmic reticulum (ER) and are then transported to the Golgi apparatus for further maturation and onward transportation (Luscher et al., 2011). Proteins cannot

exit the ER until they have achieved their correctly-folded conformation. Unassembled monomers are subject to poly-ubiquitination that targets them for proteasomal degradation (Gallagher et al., 2007). Following correct assembly and quality control, $GABA_A$Rs are trafficked to the Golgi apparatus and segregated into vesicles for transport to and insertion into the plasma membrane facilitated by several receptor-associated proteins (Luscher et al., 2011). On the plasma membrane $GABA_A$Rs diffuse laterally between synaptic and extrasynaptic locations and between adjacent synapses (Bogdanov et al., 2006; Thomas et al., 2005; Triller and Choquet, 2005), before they are internalized by clathrin-mediated endocytosis (Kittler et al., 2000). Most internalized $GABA_A$Rs are rapidly recycled back to the plasma membrane and non-recycled $GABA_A$Rs are targeted for lysosomal degradation (Figure 1.2) (Kittler et al., 2004, 2005, 2008).

1.3 Synaptic and extrasynaptic subcellular location of $GABA_A$ receptors

Immunocytochemistry and *in situ* hybridization experiments in rodent brain have demonstrated that synaptic $GABA_A$Rs primarily consist of α, β, and γ_2 subunits whereas those lacking γ_2 are predominantly or exclusively extrasynaptic (Heldt and Ressler, 2007; Hörtnagl et al., 2013). For these latter receptors, most often, the γ_2 subunit in the pentamer is replaced by δ (Nusser et al., 1998a) or with an ε subunit in some specific brain areas (Jones and Henderson, 2007; Neelands et al., 1999). It should be emphasised that extrasynaptic $GABA_A$Rs are not restricted to those lacking the γ_2 subunit. Although γ_2 subunits in complex with α_1 or α_2 subunits are densely clustered at inhibitory synapses, the total amount of both of these subtypes expressed at inhibitory synapses of CA1 pyramidal cells is similar to that found in the extrasynaptic membrane (Kasugai et al., 2010). The γ_2 subunit is probably a "licence" or anchor to permit synaptic localisation, but it is most likely not solely responsible for guiding $GABA_A$Rs to synapses (Alldred et al., 2005; Essrich et al., 1998; Kerti-Szigeti et al., 2014; Schweizer, 2003). The α-subunit expression within synaptic receptors varies, but predominantly these are α_1, α_2, or

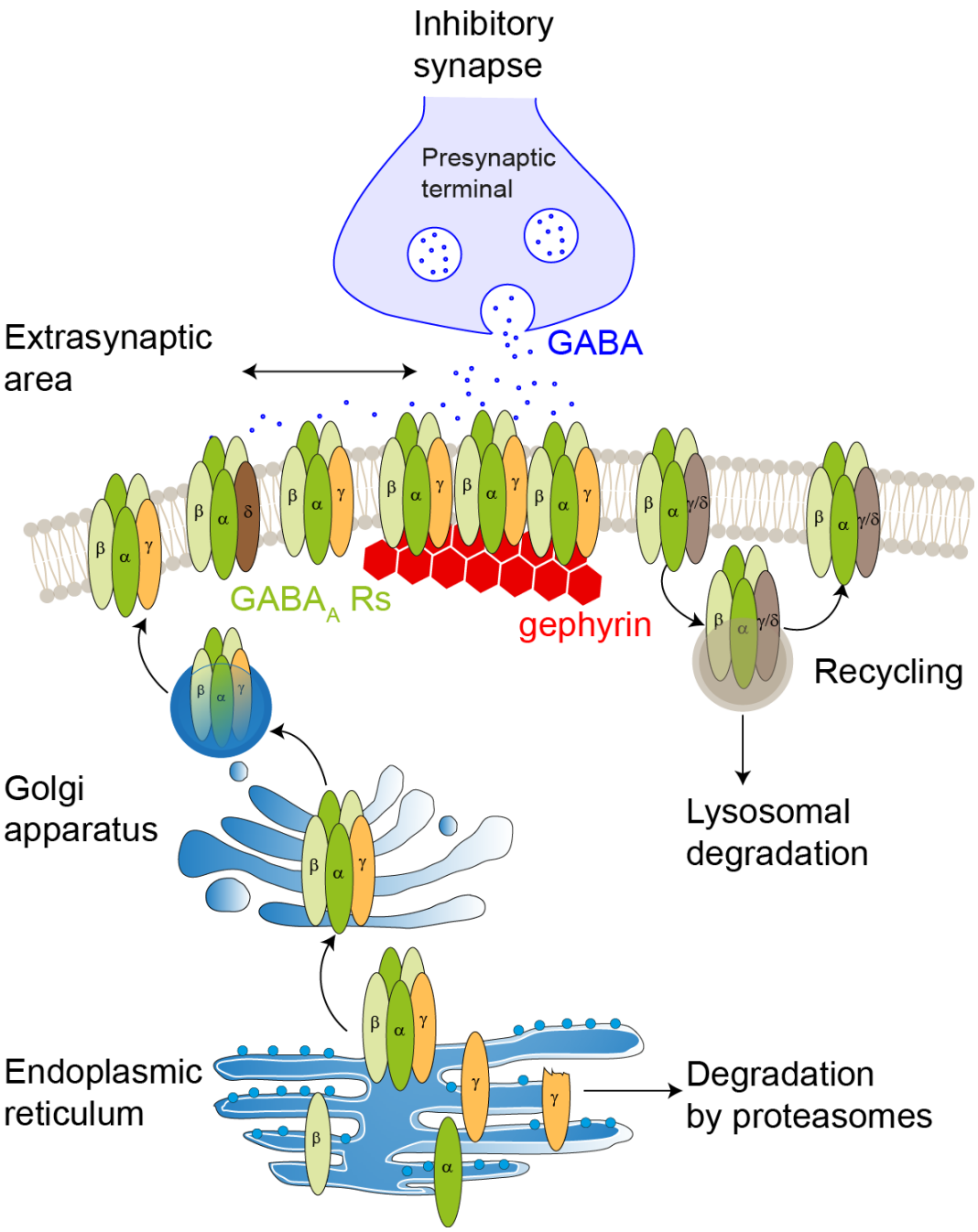

Figure 1.2: Schematic of GABA$_A$Rs trafficking.
Newly synthesised GABA$_A$R monomers are assembled into higher-order oligomers and eventually pentamers in the endoplasmic reticulum and sent to the Golgi apparatus for further maturation. Ubiquitination targets wrongly or unassembled monomers for proteasomal degradation. Fully functional pentamers enter the plasma membrane via fusion of secretory vesicles in extrasynaptic areas. These GABA$_A$Rs can then laterally move to synaptic sites where receptors are captured by synaptic anchoring proteins such as gephyrin. Receptors can be removed from the plasma membrane by endocytosis and then recycled back to the cell surface as required. Dispensable receptors are degraded in the lysosomes.

α_3 subunits (Fujiyama et al., 2000; Gross et al., 2011; Nusser et al., 1996; Sassoè-Pognetto et al., 2000). On the other hand, subunits α_4 and α_6 in complex with δ subunit are perisynaptic or extrasynaptic (Herd et al., 2013; Nusser et al., 1998a; Sun et al., 2018; Wei et al., 2003), and α_5 subunit-containing $GABA_A$Rs are found at both, synaptic and extrasynaptic sites (Brady and Jacob, 2015; Christie and de Blas, 2002a; Hausrat et al., 2015; Loebrich et al., 2006; Serwanski et al., 2006; Zarnowska et al., 2009).

To enable synaptic transmission, $GABA_A$Rs are captured at synapses by post-synaptic scaffold proteins such as gephyrin (Kneussel et al., 1999), collybistin (Papadopoulos et al., 2007) and Lipoma HMGIC Fusion Partner-Like 4 (LHFPL4/ GARLH4) (Davenport et al., 2017; Yamasaki et al., 2017), along with other trans-synaptic proteins in the postsynaptic density like neuroligins (Chiu et al., 2019; Poulopoulos et al., 2009). Scaffold proteins are key components in the organization of functional synapses by binding to cytoskeletal anchoring elements and to receptors thus providing a physical link between them (Ko et al., 2015).

Gephyrin has a major role in anchoring, clustering, and stabilizing $GABA_A$Rs at synaptic sites although these processes can also occur independently from gephyrin (Kneussel et al., 2001; Lévi et al., 2004). Different research groups have shown that gephyrin can directly bind to a specific gephyrin binding domain (GBD) in the intracellular loop of $\alpha_{1\text{-}3}$ and α_5 subunits, and β_2, and β_3 subunits (Brady and Jacob, 2015; Kowalczyk et al., 2013; Mukherjee et al., 2011; Tretter et al., 2008, 2011), but it is an essential synaptic organizer only for α_2 subunit-containing $GABA_A$Rs as demonstrated by knock-out experiments (Kneussel et al., 1999, 2001; Lévi et al., 2004). Interestingly, prior studies have indicated that the GBD is located in the same region of the intracellular loop for all the aforementioned α subunits, but the amino acid sequence in that region is not conserved (Figure 1.3), which points to a higher order structure or an unidentified common feature that is conserved among these subunits (Tretter et al., 2012). Although the α subunits seem to be the main subunit in the pentamer that interacts with gephyrin, the process is most likely more

complicated and involving other subunits such as γ_2 (Alldred et al., 2005; Essrich et al., 1998).

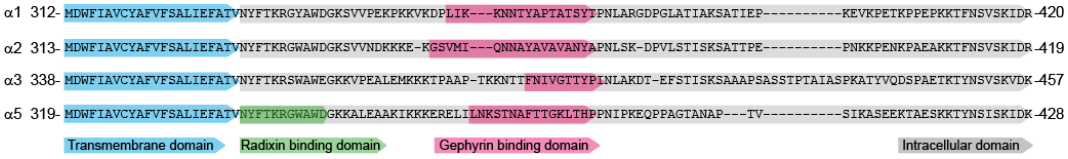

Figure 1.3: Alignment of the mouse α-subunits from the beginning of the TM3 to the end of the intracellular domain.
Gephyrin binding domain (highlighted in pink) has been identified in $\alpha_{1\text{-}3}$ and α_5 subunits, radixin on the other hand has only been shown to bind to α_5 subunits (binding domain highlighted in green). Conserved transmembrane region TM3 is highlighted in blue, and the intracellular part of the subunits is in grey. Data obtained from UniProt entry numbers: α_1 P62812, α_2 P26048, α_3 P26049, α_5 Q8BHJ7. Exact amino acid numbers are marked at the beginning and at the end of the sequence based on the whole protein sequence including signalling peptide.

Collybistin (CB) is another important synaptic scaffold protein that binds to gephyrin (Grosskreutz et al., 2001; Kins et al., 2000) and $GABA_A$Rs in a region-specific manner (Papadopoulos et al., 2007). Evidence has highlighted the role of CB in strengthening the interactions between α_2 and gephyrin by forming a ternary complex (Saiepour et al., 2010), but the role in clustering other gephyrin-dependent $GABA_A$Rs remains controversial (Patrizi et al., 2012; Wagner et al., 2021). Neuroligin2 (NL2) is an inhibitory synaptic cell adhesion molecule that is located in the postsynaptic membrane (Varoqueaux et al., 2004) and binds to gephyrin and collybistin to contribute to the formation and stabilization of GABAergic synapses (Poulopoulos et al., 2009). Recently it was shown that LHFPL4 is also enriched at inhibitory synapses and forms a complex with γ_2 subunits in $GABA_A$Rs and NL2 and is thus considered to be a major regulator of synaptic localization of $GABA_A$Rs in hippocampal pyramidal neurons. Furthermore, synaptic accumulation and clustering of gephyrin itself also requires GARLH expression (Davenport et al., 2017; Wu et al., 2018; Yamasaki et al., 2017). The γ_2 subunit was shown to be absolutely necessary for the formation of the tripartite complex NL2/LHFPL4/$GABA_A$Rs (Yamasaki et al., 2017), which is consistent with previous studies showing that the γ_2 subunit is required for synaptic localization of $GABA_A$Rs (Essrich et al., 1998; Schweizer, 2003).

In contrast to δ subunit-containing $GABA_A$Rs, which exhibit a diffuse distribution on the extrasynaptic membrane (Nusser et al., 1998a; Sassoè-Pognetto et al., 2000), extrasynaptic α_5 subunit-containing receptors are clustered by radixin (Loebrich et al., 2006). Interestingly, α_5 is the only subunit so far to be reported to interact directly with radixin even though the corresponding regions in $\alpha_{1\text{-}3}$ subunits have very similar (or in the case of α_2, identical) amino acid sequences to the radixin binding motif found in α_5 (Figure 1.3) (Hausrat et al., 2015; Loebrich et al., 2006).

However, none of these proteins completely explain the mechanisms that control which receptor subtypes are targeted to specific inhibitory synapses. Fritschy and colleagues proposed that the α-subunit is a prime candidate for providing receptor domains that direct subcellular receptor targeting (Fritschy et al., 1998). Moreover, it was directly demonstrated that α subunits, together with γ_2, can guide the synaptic localization of $GABA_A$Rs (Wu et al., 2012).

1.4 Phasic and tonic inhibition mediated by $GABA_A$ receptors

Following vesicular release of GABA by the presynaptic neuron, the peak concentrations of GABA briefly reach 1-3 millimolar in the synaptic cleft as each vesicle is thought to release several thousand GABA molecules (Mozrzymas et al., 2003; Scimemi and Beato, 2009). Tens to hundreds of $GABA_A$Rs concentrated at postsynaptic sites are then transiently activated which gives rise to phasic inhibition characterized by a fast rising and slower decaying synaptic conductance waveform (Nusser et al., 1997, 1998b). $GABA_A$Rs at the synapses have a lower apparent affinity for GABA than their extrasynaptic counterparts (Mortensen et al., 2011) to ensure that the GABA molecules only occupy the receptors for a very short duration, with a time constant for the clearance of synaptic GABA of a few hundred microseconds (Mozrzymas, 2004; Mozrzymas et al., 2003). The functions of phasic inhibition in the adult CNS are to provide a temporally and spatially precise means of counterbalancing excitatory inputs to rapidly prevent over-excitation of neurons and to generate coordinated rhythmic activities in neuronal networks. This

fine control of neuronal excitation is vital for all aspects of signal processing and normal brain function (Farrant and Nusser, 2005) (Figure 1.4).

In contrast to the high levels of GABA present in the synapse, extrasynaptic $GABA_A$Rs distributed over the neuronal surface are persistently activated by low nanomolar to micromolar GABA concentrations (Christensen et al., 2014; Mortensen and Smart, 2006; Nyitrai et al., 2006). These receptors display a higher affinity for GABA as they are usually, only exposed to low ambient levels of GABA in the extracellular space (Mortensen et al., 2011), resulting from overspill from the synaptic cleft on the same or nearby neurons. Other non-vesicular sources of ambient GABA include reversed transport by GABA transporters and GABA permeation through specific anion channels (Brickley and Mody, 2012). Extrasynaptic $GABA_A$Rs provide a basal low level but persistent inhibitory membrane conductance, termed tonic inhibition, which makes the generation of action potentials by the postsynaptic cell, less likely (Figure 1.4) (Bright and Smart, 2013a). Interestingly, it has been postulated, that postsynaptic scaffold proteins like gephyrin contribute to tonic, as well as to phasic, inhibition, adding an extra level of regulation for both forms of inhibition (Marchionni et al., 2009).

1.5 Post-translational modifications regulate GABAergic postsynaptic plasticity

The regulation of GABAergic inhibition involves multiple processes including diverse post-translational modifications such as protein phosphorylation, SUMOylation, acetylation, palmitoylation, ubiquitination and nitrosylation, of both $GABA_A$Rs and scaffold proteins (Lorenz-Guertin and Jacob, 2018; Nakamura et al., 2015). Phosphorylation serves as a key post-translational modification, as GABA channel function as well the postsynaptic plasticity of $GABA_A$Rs are all regulated by phosphorylation (Abramian et al., 2010; Brandon et al., 2000, 2001, 2002a). For example, the phosphorylation of residue S^{383} within the β_3 subunit by calcium/calmodulin-dependent kinase (CAMKII) promotes $GABA_A$Rs insertion and clustering on the plasma membrane (Houston et al., 2008, 2009; Mcdonald

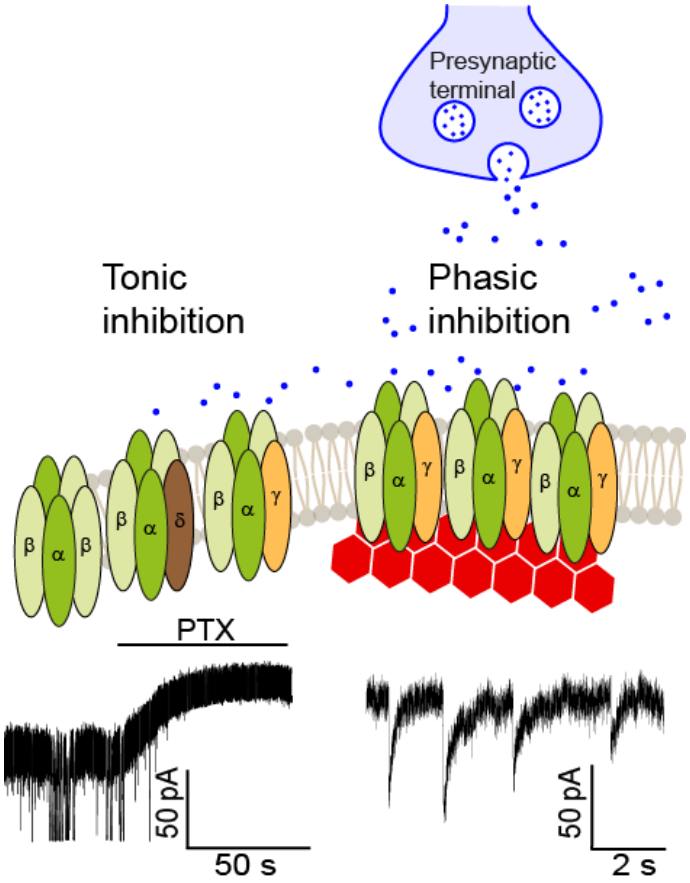

Figure 1.4: Schematic of phasic and tonic inhibition mediated by $GABA_A$ receptors. Depending on the subunit composition $GABA_A$Rs can locate synaptically or extrasynaptically, where they mediate phasic and tonic inhibition respectively. Neurotransmitter GABA, released from the presynaptic terminals, quickly acts on $GABA_A$ receptors located directly at inhibitory synapses. Receptors residing at extrasynaptic sites are activated by GABA that has 'escaped' from the synaptic cleft. Tonic inhibition is mostly generated by α_5 or δ subunit-containing and some α/β heteromers $GABA_A$Rs, whereas phasic inhibition mostly depends on α_1-α_3, β and γ_{2L} subunit-containing $GABA_A$Rs. Tonic inhibition (trace in the left bottom corner) is revealed by the change in holding current after application of the $GABA_A$R antagonist picrotoxin (PTX). On the other hand, the inhibitory postsynaptic currents (IPSCs, trace on right bottom corner) that mediate phasic inhibition are apparent as spontaneous deflections in the holding current and are shaped by the properties and number of $GABA_A$Rs at the synapse. Both example traces originate from this project.

and Moss, 1997; Petrini et al., 2014; Saliba et al., 2012). Other well characterized phosphorylation sites in β_3 subunit are S^{408}/S^{409} phosphorylated by PKC and protein kinase A (PKA) that regulate $GABA_AR$ cell surface levels and function (Kittler et al., 2005; Mcdonald and Moss, 1997; McDonald et al., 1998). Also, the phosphorylation of residue S^{443} in α_4 subunit by PKC has been shown to increase the stability of receptors on the cell surface (Abramian et al., 2010), but the exact effects remain controversial (Bright and Smart, 2013b). The number of phosphorylation sites identified in $GABA_ARs$ so far is surprisingly low, considering that the major intracellular domain between TM3 and TM4 of the each $GABA_AR$ subunit contains numerous consensus sites for phosphorylation by both serine/threonine and tyrosine protein kinases (Luscher et al., 2011; Moss and Smart, 1996; Moss et al., 1995).

GABAergic postsynaptic plasticity relies on the type and dynamic number of $GABA_ARs$ at the synapses which is largely controlled by the interaction between $GABA_ARs$ and synaptic scaffold proteins (Barberis, 2020). These receptor-scaffold interactions are not only regulated by the phosphorylation of $GABA_ARs$ but also by the phosphorylation of scaffold proteins. The phosphorylation of gephyrin is well described, and depending on the specific residue, can lead to either an increased or decreased clustering of $GABA_ARs$ at synapses (Flores et al., 2015; Lorenz-Guertin and Jacob, 2018; Tyagarajan et al., 2011, 2013).

1.6 Heterogeneous expression of $GABA_A$ receptors in the brain

$GABA_AR$ receptors are present on nearly all neurons in the brain (Mody and Pearce, 2004). The regional distribution of $GABA_ARs$ is broad and very heterogeneous throughout the brain (Heldt and Ressler, 2007; Hörtnagl et al., 2013; Pirker et al., 2000; Sperk et al., 2020). The most abundant and ubiquitously distributed subtype in the mammalian nervous system is $\alpha_1\beta_2\gamma_2$ accounting for approximately 60% of all $GABA_ARs$ in rodents. Two other major subtypes, receptors containing the α_2 or α_3 subunits frequently co-expressed with the β_3 and γ_2 subunits, account for approx-

imately 15-20% and 10-15% respectively, of all $GABA_A$Rs in the brain (Whiting et al., 1995). Receptors containing the α_5 subunit account for less than 5% of all $GABA_A$Rs in the rodent brain but are highly concentrated in CA1 to CA3 areas in the hippocampus (Möhler et al., 2002). Receptors containing the α_4-subunit are generally expressed at very low abundance but more prominently in thalamus and dentate gyrus. Those containing the α_6-subunit are restricted to the granule cell layer of the cerebellum and to the cochlear nucleus (Heldt and Ressler, 2007; Hörtnagl et al., 2013; Pirker et al., 2000). These expression profiles highlight the regional diversity for $GABA_A$Rs, but it is also important to note that the subunit composition of $GABA_A$Rs is very plastic and is often specific to certain types of neurons in one brain region and may even vary in single neurons in a cell compartment dependent manner, for example α_2 subunit-containing receptors are specifically clustered around the axon initial segment (Nathanson et al., 2019) and $\beta_{2/3}$ subunits show differential expression patterns on single Purkinje neurons in the cerebellum (He et al., 2015).

1.7 $GABA_A$Rs containing the α_5 subunit

Receptors containing the α_5 subunit (α_5-$GABA_A$Rs), have recently received a lot of interest due to their special role in cognition and unique anatomical expression pattern in the brain (Jacob, 2019; Mohamad and Has, 2019). There are three main features that make α_5-$GABA_A$Rs an attractive target for research. First, α_5-$GABA_A$Rs, usually $\alpha_5\beta_3\gamma_{2L}$ (Sur et al., 1998), are found at both synaptic and extrasynaptic areas, where they mediate phasic and tonic inhibition respectively (Glykys and Mody, 2006; Serwanski et al., 2006; Vargas-Caballero et al., 2010; Zarnowska et al., 2009). Secondly, α_5-$GABA_A$Rs are expressed in several parts of the brain including the cortex, amygdala, olfactory bulb and hypothalamus, but they are most abundant in dendritic regions of the CA1–CA3 subfields of the hippocampus (Heldt and Ressler, 2007; Hörtnagl et al., 2013; Pirker et al., 2000; Sperk et al., 1997). This particularly restricted localization of α_5 subunits in the brain suggests the great importance of α_5-$GABA_A$Rs subtype in the physiological processes underlying learning and memory (Collinson et al., 2002, 2006; Dawson et al., 2006; Martin et al., 2010; Prut et al., 2010). Therefore, several selective negative and positive allosteric modulators (NAM/PAMs) of α_5-$GABA_A$Rs have been proposed as therapeutic targets for cognitive dysfunction associated with disorders such as Down syndrome (Block et al., 2017; Braudeau et al., 2011; Martínez-Cué et al., 2014), Alzheimer's disease (Vinnakota et al., 2020; Xu et al., 2018), schizophrenia (Gill and Grace, 2014; Gill et al., 2011; Hauser et al., 2005), autism spectrum disorder (Mesbah-Oskui et al., 2017; Zurek et al., 2016) and major depressive disorder (MDD) (Fee et al., 2021). Third, synaptic currents mediated by α_5-GABARs show a characteristic kinetic profile, with slow decays (Cao et al., 2020; Capogna and Pearce, 2011; Magnin et al., 2019; Prenosil et al., 2006; Salesse et al., 2011; Schulz et al., 2018; Vargas-Caballero et al., 2010; Zarnowska et al., 2009).

1.8 Synaptic location of α_5-$GABA_A$Rs

Controversies regarding the subcellular location of α_5-$GABA_A$Rs have been mainly fuelled by the conflicting reports about these receptors colocalising with the synap-

tic scaffold protein gephyrin (Brady and Jacob, 2015; Brünig et al., 2002; Christie and de Blas, 2002a; Crestani et al., 2002; Serwanski et al., 2006). There are several reasons behind this. First, it is widely accepted that postsynaptic gephyrin anchors $GABA_A$Rs at inhibitory synapses, yet gephyrin-independent mechanisms have also been described (Kneussel et al., 2001; Lévi et al., 2004). Secondly, contrary to popular belief that synaptic $GABA_A$Rs accumulation requires the presence of gephyrin molecules at synaptic sites, the insertion of $GABA_A$Rs at synapses may occur prior to the formation of the synaptic gephyrin clusters (Petrini et al., 2014). Even more, gephyrin may form complexes with extrasynaptic $GABA_A$Rs (Danglot et al., 2003) and radixin-α_5-$GABA_A$Rs complexes can be found at synapses (Magnin et al., 2019). Therefore, the sole use of gephyrin as a postsynaptic marker will not accurately describe the full complexity of the organization of inhibitory synapses.

For many years, it was thought that α_5-$GABA_A$Rs are predominantly or exclusively extrasynaptic as early immunofluorescence staining experiments in dissociated cultures of rat hippocampal neurons and confocal laser scanning microscopy of CA1 pyramidal cells in mice and rat hippocampal sections failed to detect colocalization between α_5-$GABA_A$Rs and gephyrin (Brünig et al., 2002; Crestani et al., 2002). Interestingly, although Brünig and colleges laid the foundation of the extrasynaptic nature of α_5-$GABA_A$Rs, they also demonstrated that approximately 24% of α_5-$GABA_A$Rs were located directly opposed to synapsin I-positive boutons, a presynaptic marker used for GABAergic and glutamatergic synapses. To explain this observation, they postulated that these synapsin clusters were presynaptic to neighbouring synapses not containing α_5-$GABA_A$Rs or α_5-$GABA_A$Rs were clustered at postsynaptic sites independently of gephyrin, but this result was not hugely influential for the research community. In addition, gephyrin knockout studies indicated that clustering of α_5-$GABA_A$Rs *per se* does not require gephyrin (Kneussel et al., 2001).

Using a novel in house developed affinity-purified antibody against the α_5 subunit and fluorescence immunocytochemistry, Christie and De Blas challenged the

idea that α_5-GABA$_A$Rs are exclusively extrasynaptic in pyramidal neurons and for the first time, officially reported the synaptic location and the colocalization between α_5-GABA$_A$Rs and gephyrin. They also showed clustering and not diffuse staining of extrasynaptic α_5-GABA$_A$Rs (Christie and de Blas, 2002a). Later, the same laboratory described three different types of α_5-GABA$_A$Rs clusters in the rat brain based on the triple-label colocalization with gephyrin and a presynaptic marker glutamic acid decarboxylase (GAD) (Serwanski et al., 2006). In addition to imaging studies, direct interaction between α_5-GABA$_A$Rs and gephyrin was shown by immunoprecipitating the complex from both cultured neurons and adult rat brains (Brady and Jacob, 2015). This interaction has been supported by the observation that gephyrin/collybistin clusters can trap surface α_5-GABA$_A$Rs in recombinant cells (George et al., 2021).

Based on the most recent research, it is clear that the subcellular location of α_5-GABA$_A$Rs is highly dynamic and these receptors are indeed expressed at both synaptic and extrasynaptic locations (Davenport et al., 2021; Hausrat et al., 2015). Yet, despite the strong evidence of synaptic α_5-GABA$_A$Rs, the focus in research remains still on the extrasynaptic pool of α_5-GABA$_A$Rs mediating tonic inhibition thus forming the main basis for investigation in this PhD project.

1.9 Distinct functional roles of extrasynaptic and synaptic α_5-GABA$_A$Rs

The participation of extrasynaptic α_5-GABA$_A$Rs in tonic inhibition was first described by Caraiscos and colleges in cultured mouse hippocampal neurons and hippocampal CA1 pyramidal cells on brain slices (Caraiscos et al., 2004) and later in other brain areas (Bonin et al., 2007; Glykys and Mody, 2006; Glykys et al., 2008). Functional roles attributed to these high-affinity extrasynaptic α_5-GABA$_A$Rs include the control of neuronal network activity (Bonin et al., 2007; Lee and Maguire, 2014), to avoid pathological hyperactivity (Donegan et al., 2019) and to regulate gamma frequency oscillations (Glykys et al., 2008; Towers et al., 2004). Gamma oscillations occur in different cognitive tasks including memory processing

and impaired gamma oscillations lead to deficits in synchronised network activity (Lisman and Buzsáki, 2008). In addition, extrasynaptic α_5-$GABA_A$Rs are also a conduit for modulating inhibitory postsynaptic plasticity (Davenport et al., 2021). α_5-$GABA_A$Rs are clustered at extrasynaptic sites by activated radixin and the disruption of this complex leave these receptors free to accumulate at synaptic sites (Davenport et al., 2021; Hausrat et al., 2015).

Inhibitory postsynaptic currents (IPSCs) can be categorised on the basis of their kinetics into $GABA_{A,fast}$ and $GABA_{A,slow}$ IPSCs (Capogna and Pearce, 2011). α_5-$GABA_A$Rs mediate slowly rising and slowly decaying $GABA_{A,slow}$ currents and this unique feature has been used as a signature to show the presence of this receptor subtype at synapses (Cao et al., 2020; Capogna and Pearce, 2011; Magnin et al., 2019; Prenosil et al., 2006; Salesse et al., 2011; Schulz et al., 2018; Vargas-Caballero et al., 2010; Zarnowska et al., 2009). Moreover, α_5-$GABA_A$Rs have been shown to specifically contribute to a large-amplitude subset of $GABA_{A,slow}$ IPSCs and the pharmacological data suggests that this type of synaptic current may be responsible for the modulation of cognitive function by α_5-$GABA_A$R targeting drugs (Zarnowska et al., 2009).

1.10 Cell- and synapse-type specific expression of α_5-$GABA_A$Rs

Although α_5-$GABA_A$Rs constitute about 5% of the total $GABA_A$Rs population in the brain, this subtype is highly concentrated on pyramidal neurons in the CA1 and CA3 regions of the hippocampus, where α_5-$GABA_A$Rs make up almost 25% of the total $GABA_A$Rs population (Brünig et al., 2002; Caraiscos et al., 2004; Crestani et al., 2002; Sur et al., 1998, 1999). Recent work has suggested that α_5-$GABA_A$Rs are also expressed in CA1 somatostatin positive interneurons (Magnin et al., 2019; Salesse et al., 2011).

Interestingly, under basal conditions in CA1 pyramidal neurons, α_5-$GABA_A$Rs mostly contribute to tonic inhibition and although these receptors can be synaptic as well, involvement in synaptic inhibition is rather limited (Davenport et al., 2021)

or specific to certain synapses only (Schulz et al., 2018). Even more, the synaptic location of α_5-GABA$_A$Rs on pyramidal neurons in the neocortex declines rapidly during development in the first two postnatal weeks, which results in weakening of synaptic inhibition onto these cells (Cao et al., 2020). Nevertheless, synaptic contribution of α_5-GABA$_A$Rs on neocortical pyramidal neurons can be detected throughout the development (Ali and Thomson, 2008).

Synaptic inhibition of pyramidal neurons in the hippocampus is mediated by numerous classes of GABAergic interneurons (IN), which all express different molecular markers and have different connectivity, but two of the major classes are relevant to this project: somatostatin (SST)-positive oriens/lacunosum-moleculare (O-LM) cells that target the distal dendrites of the pyramidal cells and interneuron-selective, vasoactive intestinal polypeptite (VIP)- and/or calretinin (CR)-positive interneurons, that specifically target other inhibitory neurons and drive the network disinhibition (Harris et al., 2018).

In hippocampus, between interneurons, α_5-GABA$_A$Rs are preferentially targeted to the inhibitory synapses made by the VIP- and CR-positive terminals onto dendrites of SST-INs (Magnin et al., 2019; Salesse et al., 2011). Between interneurons and principal cells, α_5-GABA$_A$Rs are targeted to synapses formed by SST-INs onto the dendrites of pyramidal cells (Cao et al., 2020; Schulz et al., 2018)(Figure 1.5). It should be noted that the expression of synaptic α_5-GABA$_A$Rs is not restricted to these types of cells and can be found at other classes of interneurons as well (Petrache et al., 2020).

It is very likely that pyramidal and interneuronal expression of α_5-GABA$_A$Rs serves distinct functions in cognitive processing. Elegant work by Magnin and colleges separated the specific impacts of hippocampal α_5-GABA$_A$Rs mediated inhibition at synapses formed by interneuron-interneuron or interneuron-pyramidal cells and demonstrated that phasic inhibition via VIP/CR input to SST-INs was responsible for the control of anxiety-like behaviour whereas tonic inhibition via SST-INs onto pyramidal neurons controlled spatial learning (Magnin et al., 2019).

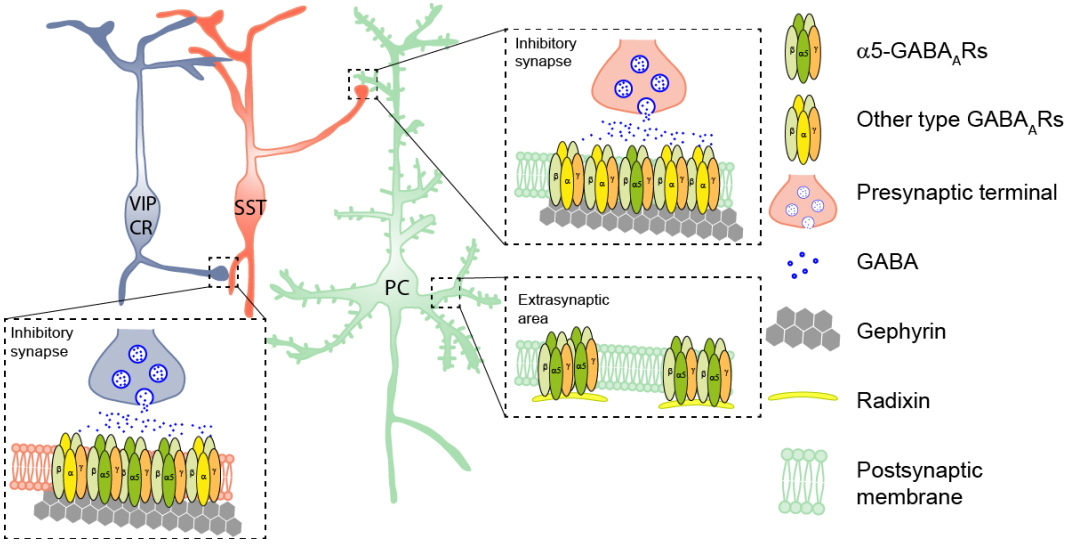

Figure 1.5: Schematic of cell- and synapse-type specific expression of α_5-GABA$_A$Rs. In the hippocampus, α_5-GABA$_A$Rs receptors are expressed on somatostatin-positive (SST) interneurons and pyramidal cells (PC). On SST interneurons, α_5-GABA$_A$Rs are mostly synaptic whereas on pyramidal neurons, most α_5-GABA$_A$Rs are extrasynaptic and only few of these receptors can be found at synapses under basal conditions.

1.11 Phosphorylation as a key post-translational modification for regulating inhibitory synapse plasticity

Little is known about the molecular mechanisms that control the accumulation of α_5-GABA$_A$Rs at inhibitory synapses, but compelling evidence suggests that phosphorylation and dephosphorylation of GABA$_A$Rs and/or postsynaptic scaffold protein gephyrin are the key events for induction of inhibitory synaptic plasticity (Nakamura et al., 2015, 2020; Tyagarajan and Fritschy, 2010; Tyagarajan et al., 2011). There are no phosphorylation sites identified to date on the α_5 subunit, but the phosphorylation sites identified in α_1 (T^{375}) and α_2 (S^{359}) subunits support this idea linking phosphorylation and plasticity. On both subunits, phosphorylation of residues negatively impacts on the binding of the α subunit to gephyrin or gephyrin/collybistin complexes respectively, and therefore decreases receptor accumulation at synapses (Mukherjee et al., 2011; Nakamura et al., 2020). It is very likely that similar mechanisms also exist for α_5-GABA$_A$Rs.

On the other hand, phosphorylation and other post-translational modifications of gephyrin have been extensively investigated. For example, the activity-dependent phosphorylation of S^{305} in gephyrin by calcium/calmodulin-dependent kinase (CAMKII) promotes $GABA_A$Rs clustering (Flores et al., 2015). By contrast, gephyrin phosphorylation by extracellular signal–regulated kinase 1/2 (ERK1/2) and glycogen synthase kinase 3 isoform β (GSK3β) at residues S^{268} and S^{270} respectively, reduces $GABA_A$Rs aggregation and enhances gephyrin proteolysis by calpain (Tyagarajan et al., 2011, 2013). In addition, while gephyrin palmitoylation stabilizes the receptors at synapses, gephyrin nitrosylation and SUMOylation decrease its synaptic clustering (Dejanovic and Schwarz, 2014; Dejanovic et al., 2014; Ghosh et al., 2016).

1.12 Negative and positive allosteric modulators of α_5-$GABA_A$Rs

The notable subtype diversity of $GABA_A$Rs provides these receptors with a rich pharmacology and considerable therapeutic potential, which is best implemented by targeting a specific α subunit (Olsen, 2018; Sieghart and Savić, 2018). $GABA_A$Rs subtypes containing the α_1, α_2, α_3 or α_5 together with γ_2 subunit, but not those containing the α_4 or α_6 subunit, are sensitive to benzodiazepines, positive allosteric modulators (PAM-s) of $GABA_A$Rs that have been in clinical use for decades (Sieghart, 2006). The sensitivity to benzodiazepines is determined by a critical histidine in α subunits, ${\alpha_1}^{H101}$, which is conserved in benzodiazepine-sensitive but not in benzodiazepine-insensitive subunits (Duncalfe et al., 1996; Wieland et al., 1992). Benzodiazepines bind to the benzodiazepine binding site (BZ site), located at the α+/γ_2– interfaces and potentiate GABA-induced activation of the receptor (Miller et al., 2018; Sigel, 2002; Zhu et al., 2018). However, their use is limited by side effects and their addictive properties. Therefore, in addition to benzodiazepines, other compounds have been developed that either bind to the same site as benzodiazepines or bind to an overlapping site (Maramai et al., 2020; Rudolph and Knoflach, 2011; Solomon et al., 2019).

Increased hippocampal activity in the ageing human brain (Koh et al., 2013), in schizophrenia patients (Gill and Grace, 2014) or in neuropsychiatric disorders with cognitive deficits (Engin et al., 2015) has highlighted the potential use of α_5-GABA$_A$Rs specific PAMs. Reduction of excess neuronal activity by enhancing α_5-GABA$_A$Rs mediated inhibition could significantly improve the treatment of these disorders (Jacob, 2019; Maramai et al., 2020). Unfortunately, only a few α_5-PAM compounds with limited selectivity for α_5-GABA$_A$Rs are available: SH-053-2'F-R-CH3 (Savić et al., 2008), compound 44 (Chambers et al., 2003), compound 6 (van Niel et al., 2005), and MP-III-022 (Stamenić et al., 2016), thus their impact on cognitive tasks needs further investigation.

Negative allosteric modulators (NAMs) that selectively reduce GABAergic transmission through α_5-GABA$_A$Rs have been heavily investigated for their potential cognitive enhancing effects (Atack, 2011; Jacob, 2019; Maramai et al., 2020). Reducing the expression levels or inhibiting α_5-GABA$_A$Rs activity has been shown to be beneficial in various hippocampal-dependent cognitive tasks (Collinson et al., 2002; Crestani et al., 2002; Engin et al., 2020; Martin et al., 2009; Milić et al., 2013; Yee et al., 2004). From the many NAMs developed, L-655,708 (Quirk et al., 1996), has been widely investigated in preclinical studies (Atack et al., 2006; Clarkson et al., 2010; Inoue et al., 2021; Khodaei et al., 2020; Lake et al., 2015; Zurek et al., 2012, 2014).

The α_5 NAM L-655,708 is an α_5 subunit-selective partial inverse agonist that binds to the benzodiazepine site of α_5-GABA$_A$Rs, but at higher concentrations also to α_1, α_2, and α_3 subunit-containing GABA$_A$Rs. Effects of blocking α_5-GABA$_A$Rs in the hippocampus by L-655,708 include reduction of tonic inhibition, enhanced LTP, improved cognitive performance and generation of spontaneous gamma oscillations (Atack et al., 2006; Caraiscos et al., 2004; Glykys et al., 2008; Khodaei et al., 2020). Unfortunately, L-655,708 also exhibits anxiogenic effects (Navarro et al., 2002), which has prevented its further development and use in humans (Atack, 2011).

1.13 Thesis aims

Maintaining inhibitory synaptic transmission is essential for normal function of neuronal networks and disruption to $GABA_ARs$ mediated inhibition will cause profound alterations to brain function, which has been linked with several pathological conditions (Rudolph and Möhler, 2014). Inhibitory synaptic plasticity is primarily mediated by the modulation of $GABA_ARs$ number at postsynaptic sites and their interaction with synaptic scaffold protein gephyrin also plays a significant role. Yet, the molecular mechanisms underlying the plasticity of GABAergic synapses are poorly understood (Barbaris 2020). As emphasised previously, α_5-$GABA_ARs$ are the focus of this project due to their dual subcellular location, great importance in hippocampal-dependent cognitive tasks and therapeutic potential. This project investigates the molecular mechanisms controlling the synaptic accumulation of α_5-$GABA_ARs$ by exploring the role of phosphorylation of residue S^{374} in the α_5 subunit. The aims of this PhD project are to:

1. **Identify phosphorylation sites and explore which potential kinases phosphorylate the gephyrin binding domain in the α_5 subunit**.

   At present, there are no phosphorylation sites identified in the α_5 subunit despite it containing numerous kinase consensus sequences. Using different online prediction tools and mass-spectrometry analysis, I aim to specifically find phosphorylation sites within the gephyrin binding domain of the α_5 subunit. In addition, I explore potential kinases that can phosphorylate selected residues in α_5 subunits.

2. **Characterise the functional effects of phosphorylating the gephyrin binding domain in the α_5 subunit.**

   Using site-directed mutagenesis I generate phospho-null and phosphomimetic α_5 cDNAs for transfecting recombinant and primary neuronal cells. Next, I perform whole-cell patch clamp recordings from transfected cells to assess the potential effects of phosphorylation on the function of α_5-$GABA_ARs$.

3. **Investigate the hypothesis that phosphorylation of gephyrin binding domain in α_5 subunit controls the synaptic accumulation of α_5-GABA$_A$Rs.**

   This aim is the main emphasis of this project. Using whole-cell patch clamp recordings from transfected cells and super-resolution imaging I search for evidence of increased synaptic location of phospho-null mutant α_5-GABA$_A$Rs. In addition, I assess the role of gephyrin in this process and discuss the potential importance of our findings.

Chapter 2

Material and Methods

2.1 Mass-spectrometry

Mass spectrometry was performed in the laboratory of Prof Konstantinos Thalassinos (Structural & Molecular Biology, Division of Biosciences, UCL). Carmen Kivisild prepared samples, Abubakar Hatimy and Shaan Subramaniam carried out data acquisition and analysis.

2.1.1 Sample preparation and immunoprecipitation of $GABA_A$Rs

Two set of cell samples were used in these experiments: recombinant receptors expressed in HEK293 cells and native neuronal receptors from rat brain lysates.

HEK293 cells plated on 10 cm culture dishes and transiently transfected with cDNAs expressing mouse myc-tagged α_5, flag-tagged β_3 and untagged γ_{2L} subunits were cultured for 24 h before harvesting the cells. All three constructs were previously made and already available in the lab (details in Appendix Table A.2). HEK293 cells were maintained and transfected as described in Section 2.4.1. At 15 min prior to the sample collection, half of the cell samples were treated with the protein kinase C activator phorbol 12-myristate 13-acetate (200 nM, PMA) and the other half were exposed to the PMA vehicle, dimethyl sulfoxide (DMSO) as a control. All of the following procedures were carried out on ice. The media was removed, and cells were briefly washed in 5 ml ice cold tris-buffered saline (TBS, pH 7.6). The TBS was then removed, 0.9 ml of pre-chilled lysis buffer A (20 mM HEPES, 300 mM NaCl) supplemented with a protease inhibitor cocktail (cOmplete,

Mini Protease Inhibitor Tablets, Roche) was added to the cells. The dishes were immediately placed into a -80°C freezer for 3 min to disrupt cell structure and break up the membranes. The dishes were then removed from the freezer and the cells were scraped off from the dish, transferred into a pre-chilled microcentrifuge tube and homogenized by pipetting samples through Microlance 21-gauge and 23-gauge needles, 10 times each.

The second set of samples were prepared from rat brain lysates. Female adult rat brains were rapidly removed, hippocampi were extracted using a dissecting microscope and the meninges removed. Dissected hippocampi were immediately frozen in liquid nitrogen and stored at -80°C for further experiments. Samples were then taken out from the freezer and two hippocampi were transferred to a hand-held Dounce glass homogenizer. 1 ml of lysis buffer A supplemented with the protease inhibitor cocktail (cOmplete) was added and samples were homogenized with 10 manual up-and-down strokes. The homogenate was transferred into a new pre-chilled microcentrifuge tube and further homogenised by pipetting samples through Microlance 21-gauge and 23-gauge needles, 10 times each. Finally, the samples were put into a -80°C freezer for 3 min to disrupt cell structure and break up cell membranes.

Both sets of samples were then incubated on ice for 10 min and centrifuged at 1000g for 10 min at +4°C. The pellet was removed, and the supernatant transferred into a pre-chilled microcentrifuge tube. To solubilize cell membranes, 100 μl of a 10x n-Dodecyl β-D-maltoside/cholesteryl hemisuccinate (DDM/CHS) stock solution (final concentrations: 20 mM (1%, w/v) DDM, 4 mM (0.25% Trizma salt, w/v, equivalent to 0.2% free acid form) CHS) was added dropwise. The samples were incubated for 1 h at +4°C with a gentle rotating motion. Solubilized proteins were collected by centrifugation at 16 000 g for 30 min at +4°C and the supernatant was transferred into a fresh pre-chilled microcentrifuge tube.

Magnetized Protein A or Protein G Dynabeads (50 μl per sample, Invitrogen) were washed once with lysis buffer A and then the buffer was removed. Primary antibodies were diluted in 500 μl of lysis buffer A and added to the beads. The fol-

lowing primary antibodies were used: 15 μg of anti-myc tag antibody (clone 9E10, Abcam) and anti-flag tag antibody (clone M2, Sigma-Aldrich) to pull down recombinant receptor complexes from HEK293 cells and 2.5 μl of α_5 subunit specific antisera (gift from Jean-Marc Fritschy) (Fritschy et al., 1997) was used to immunoprecipitate α_5-$GABA_A$Rs from hippocampal lysates (details about antibodies used in Appendix Table A.4). Anti-myc tag and anti-flag tag primary antibodies were conjugated to Dynabeads Protein G and the anti-α_5 subunit primary antibody was conjugated to Dynabeads Protein A by incubation for 30 min at room temperature (22°C) with agitation, and then washed twice with 500 μl of lysis buffer A. The buffer was removed, and samples containing solubilized receptors were added to the beads conjugated to an appropriate primary antibody and then incubated on a rotating platform overnight at +4°C to allow receptor complexes to bind to the Dynabeads. Next day, the receptor-antibody-beads complexes were washed three times with washing buffer (0.05% w/v DDM, 0.0125% w/v CHS in lysis buffer A) to remove non-specific binding. After the final wash, the washing buffer was removed and the receptor-antibody-bead complex was resuspended in 35 μl of SDS sample buffer (10% v/v glycerol, 2.5% w/v sodium dodecyl sulfate (SDS), 62.5 mM tris-HCl (pH 6.8), 2.5 mg/ml bromophenol blue, 2 M urea, 100 mM dithiothreitol (DTT)) to elute the proteins. Beads were separated from the immunoprecipitate by exposure to a magnet for 1 min, the samples were collected, and then incubated for 30 min at room temperature prior to loading onto gels.

2.1.2 Protein separation and digestion

Eluted proteins were run on NuPAGE 4-12% Bis-Tris 1.5 mm gel (Invitrogen) along with a pre-stained protein marker (New England Biolabs) in MOPS buffer (0.1 mM MOPS, 0.1 mM Tris, 0.1% SDS, 5 mM sodium bisulfite). Proteins resolved by electrophoresis were visualized using Coomassie staining, and target protein bands were excised. Gel bands were cut into smaller pieces and washed twice with 500 μl of AmBic buffer (40% acetonitrile, 60% of a 50 mM ammonium bicarbonate solution (AmBic, pH 8.6)) for 30 min on a shaker and then shrunk with 500 μl of acetonitrile. Acetonitrile was then discarded, and the gel pieces were dried at 50 °C.

For reduction and alkylation, 200 µl of 10 mM dithiothreitol (DTT) buffer (15.4 mg DTT in 10 ml of 50 mM AmBic) was added and samples were incubated for 60 min at 56 °C. Then 200 µl of 55 mM iodoacetamide (IAA) buffer (102 mg IAA in 10 ml 50 mM AmBic) was added and incubated for 45 min at room temperature in the dark. Next, the reducing and alkylating solution was removed, and gel pieces were washed with 1000 µl of 50 mM AmBic, shrunk with 500 µl of acetonitrile before swelling again with 500 µl 50 mM AmBic. The shrinkage and swelling steps were repeated twice. After the last shrinkage, the gel pieces were dried completely using the SpeedVac concentrator at 50°C.

Sequencing-grade, lyophilized trypsin (Promega) was reconstituted according to the manufacturer's instructions and diluted to a final concentration of 10 ng µl in 25 mM ammonium bicarbonate (pH 8.6). Gel pieces were placed in 200 µl of the trypsin solution and incubated overnight at 37°C. On the following day, the enzyme solution was removed and retained. Peptides were extracted by adding 100 µl of extraction buffer (0.5% formic acid, 20% acetonitrile in water) to the gel pieces, followed by vigorous shaking for 15 min. The extraction buffer was removed and added to the retained enzyme solution. This extraction process was repeated twice. All three solutions were pooled (200 µl enzyme solution + 2x 100 µl extraction buffer) and the SpeedVac concentrator was used at 50°C to reduce the volume to $\sim$10 µl.

2.1.3 Sample desalting with StageTips method

The stop-and-go-extraction tips (StageTips) were assembled using P200 pipette tips with Empore C18 disk cores as described previously (Rappsilber et al., 2007). Assembled StageTips were washed with 50 µl of methanol, then equilibrated with 50 µl of solution 2 (0.5% Acetic acid in water), 50 µl of solution 3 (0.5% Acetic acid in 80% acetonitrile) and then again with 50 µl of solution 2. Next, the concentrated peptides extracted from the gel pieces were resuspended in 50 µl of solution 2 before being applied to the StageTips, washed with 50 µl of solution 2, and finally eluted with 50 µl of solution 3.

2.1.4 Data independent liquid chromatography–mass spectrometry (LC/MS^E)

Two mass-spectrometry compatible solvents were injected at appropriate proportions to generate a gradient for the separation of peptides by reversed phase nano-Ultra Performance Liquid Chromatography (15 kpsi NanoAcquity UPLC, Waters Corp.). These are: Solvent A (0.1% Formic acid in Water; Thermo Scientific) and Solvent B (0.1% formic acid in Acetonitrile). For each sample 1 µl – 5 µl was loaded onto a reverse-phase UPLC Symmetry C18 trap column (180 µm internal diameter, 20 mm length, 5 µm particle size, Waters Corp.). Samples were desalted (99.9% Solvent A) at a flow rate of 8 µl/min for 2 min. Peptides were subsequently separated by a linear gradient (0.3 µl/min, 35°C; 3% - 40% Solvent B) using a BEH130 C18 nano-column (75 µm internal diameter, 250 mm length, 1.7 µm particle size, Waters Corp.) over the course of 60 min.

The nanoLC was coupled through a nanoflow sprayer to a quadrupole time-of-flight (QToF) mass spectrometer (HDMS Synapt G2-Si; Waters Corp.) operating in Resolution mode. The ToF analyser was externally calibrated from 175.11 to 1285.54 m/z using the fragment ions from a 320 fmol µl solution of [Glu1]-fibrinopeptide B (FPB, Sigma-Aldrich Aldrich). Data were lockmass-corrected following acquisition using the monoisotopic mass of the doubly-charged precursor of FPB (785.8426 m/z), delivered to the mass spectrometer via a LockSpray interface. This reference spray was sampled every 30 s. Mass measurements were made using a data independent mode (LC-MS^E) of acquisition. Briefly, energy in the collision cell was alternated from low energy (4 eV) to high energy (energy ramp from 16-38 eV) whilst continuously acquiring MS data. Measurements were made over an m/z range of 50-2000 Da with a scan time of 0.6 s One cycle of MS and MS^E data were acquired every 1.2 s.

2.1.5 Data analysis

LC-MS data were processed as described earlier (Geromanos et al., 2009) using the Protein Lynx Global Server (PLGS) v3.0.2 (Waters Corporation). Data were queried against a Homo sapiens protein database (UniProt proteome:UP000005640) concatenated with a list of common contaminants obtained from the Global Pro-

teome Machine (ftp://ftp.thegpm.org/fasta/cRAP). Carbamidomethylation of cysteine was specified as a fixed modification. Phosphorylation (of serine, threonine and tyrosine residues) and oxidation (of methionine) were specified as variable modifications. A maximum of two missed cleavages were tolerated in the analysis to account for incomplete digestion. For peptide identification, three corresponding fragment ions were set as a minimum criterion whereas for protein identification a minimum of seven fragment ions were required. Protein false positive discovery rate was set at 1% as estimated by the number of proteins identified from a randomised database.

2.2 Online bioinformatic tools

The NetPhos 3.1 server (https://www.cbs.dtu.dk/services/NetPhos/) (Blom et al., 2004) was used to predict the phosphorylation consensus sites for serine, threonine and tyrosine residues, and the eukaryotic linear motif (ELM) resource (https://elm.eu.org) (Kumar et al., 2020) was used to find consensus phosphorylation motifs within the major intracellular loop of the α_5 subunit. For both tools, the primary sequence for the intracellular loop of the mouse α_5 subunit (UniProt - Q8BHJ7, amino acids 342-428 in the α_5 protein) was uploaded into the software. For ELM, the cell compartment was set to 'plasma membrane' and 'cytosol', and the species name was set to *Mus musculus*. Details of different software used are in Appendix Table A.5.

2.3 Molecular biology

2.3.1 Site-directed mutagenesis

The coding regions of murine γ-aminobutyric acid type A ($GABA_A$) receptor α_5, β_3 and γ_{2L} subunits were previously cloned into the pRK5 expression vector (Gielen et al., 2015) and this plasmid was used as a template for following PCR reactions. Single-amino acid mutations (S^{374A} and S^{374D}) were introduced into the wild-type or into myc-tagged $GABA_A$ α_5 nucleotide sequence by site-directed mutagenesis using standard PCR methods.

PCR amplification was carried out with Phusion High-Fidelity DNA Polymerase (New England Biolabs) according to the manufacturer's protocol. Briefly, all reactions were performed in a total volume of 50 μl and under the following conditions: pre-incubation at 98°C for 30 s, denaturation at 98°C for 10 s, primer annealing for 30 s (temperature according to primers used), extension at 72°C for 60 s, 35 cycles. All the forward and backward primers (Sigma-Aldrich) used are listed in Appendix Table A.1. The resultant PCR products were purified using QIAquick Gel Extraction Kit (Qiagen).

The purified PCR product (16 μl) was transferred into a new microcentrifuge tube and incubated for 5 min at 70°C. Next, 2 μl of T4 ligase buffer and 1 μl of T4 polynucleotide kinase were added to the samples and incubated for 30 min at 37°C. Then 2 μl of T4 ligase was added and the samples were incubated overnight at 16°C. All the reagents used for DNA ligation were obtained from New England Biolabs.

pRK5 plasmids containing the appropriate inserts were then transformed into 5-alpha Competent E. coli cells (New England Biolabs) according to the manufacturer's instructions, before plating of the transformed bacterial cells onto Luria Broth (LB) agar plates supplemented with ampicillin at 100 μg/ml for overnight incubation at 37°C. Colonies were picked and incubated in 100 ml of LB supplemented with ampicillin with shaking overnight at 37°C. Plasmid DNA was purified using a Qiagen Plasmid Maxi kit (Qiagen) following the manufacturer's protocol. The concentration of plasmid DNA was determined using a Nanodrop (Thermo Fischer). The correct sequence of the plasmid was verified by DNA sequencing across the insert (Source Bioscience).

All constructs generated and used in this project are listed in Appendix Table A.2. HA-GSK3β S9A pcDNA3 was a gift from Jim Woodgett (Addgene plasmid # 14754).

2.4 HEK293 cell culture and electrophysiology

2.4.1 Culture preparation and transfections

All cell culture reagents were acquired from Thermo Fisher Scientific unless otherwise stated. Human embryonic kidney (HEK293) cells were cultured and transiently transfected as described previously (Hannan et al., 2013; Thomas and Smart, 2005). Briefly, HEK293 cells were maintained in Dulbecco‘s modified Eagle‘s medium (DMEM) supplemented with 10% v/v fetal bovine serum (FBS), 100 U/ml penicillin and 100 μg/ml streptomycin at 37°C in humidified air with 5% CO2. For electrophysiology experiments, cells were plated onto 22 mm glass coverslips (VWR international) coated with poly-L-lysine (100 μg/ml, Sigma-Aldrich) and on 100 mm culture dishes (Greiner-Bio-One GmbH) for routine secondary culture and for proteomics. Using the calcium phosphate precipitation method, HEK293 cells were transiently transfected 4-6 h post-plating with various combinations of cDNA constructs encoding for α_5 (wt and mutated), β_3 and γ_{2L} subunits, GSK3β S9A and enhanced green fluorescent protein (eGFP). The expression of eGFP was used for identifying transfected cells, as well as estimating transfection efficiency. For transfections, appropriate cDNAs were mixed in 1:1 ratio to a total amount of 4 μg for electrophysiology and 24 μg for proteomics, usually in a total volume of 4 μl or 24 μl respectively. Then, 20 μl of 340 mM $CaCl_2$ was added to the 4 μg DNA mixture following by 24 μl HEPES-buffered saline (HBS; 280 mM NaCl, 2.8 mM Na2HPO4, 50 mM HEPES (pH 7.2)) and vortexed vigorously. Solution volumes were adjusted accordingly for proteomics experiments. The mixture was added dropwise to the cultured cells and before their return to the incubator. Further experiments commenced around 24 h after plating the cells. The transfection efficacy was estimated around 70%.

2.4.2 Whole-cell patch clamp recordings from HEK293 cells

Whole-cell patch-clamp recordings were performed at room temperature with an Axopatch 200B amplifier (Molecular Devices). GABA-evoked membrane currents were recorded from single eGFP-fluorescent HEK293 cells expressing $GABA_A$Rs containing wild-type or mutated α_5 subunits along with β_3 and γ_{2L} subunits. Cells

were voltage-clamped at -20 mV and continuously perfused with Krebs solution containing: 140 mM NaCl, 4.7 mM KCl, 1.2 mM $MgCl_2$, 2.52 mM $CaCl_2$, 11 mM Glucose and 5 mM HEPES, adjusted to pH 7.4 with 1 M NaOH. All recordings were performed using thin-walled borosilicate glass pipettes with resistance of 2.5 - 3 MΩ (World Precision Instruments). These were filled with an internal solution containing 120 mM KCl, 1 mM $MgCl_2$, 11 mM EGTA, 10 mM HEPES, 1 mM $CaCl_2$ and 2 mM K_2ATP, adjusted to pH 7.2 with 1 M NaOH. The osmolarity of this intracellular solution was 300 ± 10 mOsm/L. Currents were filtered at 5 kHz (4-pole Bessel filter) and digitized at 50 kHz with a Digidata 1440A (Molecular Devices). The series resistance was measured at regular intervals and recordings in which the series resistance changed by more than 25% were discarded. All chemicals used to prepare solutions were purchased from Sigma-Aldrich.

2.4.3 Drug treatments

All the drugs used in this study were bath-applied in Krebs solution, including GABA (Sigma-Aldrich), protein kinase C activator phorbol 12-myristate 13-acetate (PMA, 200 nM, Calbiochem) and GSK3β kinase inhibitor CHIR99021 (CHIR, 1 μM, Calbiochem) (details in Appendix Table A.3). Different GABA concentrations (0.01 μM to 300 μM) were rapidly applied using a modified U-tube system with a solution exchange time of $<$100 ms (Mortensen and Smart, 2007). PMA or CHIR99021 were applied continuously during the recordings in appropriate experiments. Control responses using the maximum concentration of GABA (300 μM) were obtained at regular intervals. The number of cells recorded for each condition is noted in each figure legend.

2.4.4 Data analysis

2.4.4.1 Concentration-response curve (CRC) fitting

Clampex 10.3 and Clampfit 10.3 software (Molecular Devices) were used for data acquisition and analysis respectively. Concentration–response relationships (CRC) were generated for each recorded cell and accrued using Origin 2020 software (OriginLab). The peak amplitudes of GABA-activated currents were measured relative to the baseline holding current prior to GABA application. GABA responses

at all concentrations were normalised to the peak current in response to the maximal GABA concentration (300 μM). After normalization, concentration response data were curve fitted using the Hill equation:

$$I = \frac{I_{\max}}{1 + (\frac{EC_{50}}{[GABA]})^n} \tag{2.1}$$

where I is the measured current, I_{max}x is the maximum current, [GABA] is the concentration of applied GABA, EC_{50} represents the concentration of GABA that evokes 50% of maximum response and n represents the Hill coefficient.

2.4.4.2 Calculation of whole-cell parameters, current densities and macroscopic kinetic parameters

Membrane currents in response to 10 mV hyperpolarising steps were used to calculate series resistance (Rs, MΩ), input resistance (R_{in}, MΩ), membrane tau (τ, ms), and membrane capacitance (Cm, pF) using the following equations:

Equation 2.2, series resistance:

$$R_s = \frac{-10}{I_{peak}} \times 1000 \tag{2.2}$$

Equation 2.3, input resistance:

$$R_{in} = (\frac{-10}{I_{ss}} \times 1000) - R_s \tag{2.3}$$

Equation 2.4, membrane tau value:

$$\tau = \frac{area}{I_{peak} - I_{ss}} \tag{2.4}$$

Equation 2.5, membrane capacitance:

$$C_m = \frac{\tau \times (R_s + R_{in})}{R_s \times R_{in}} \times 1000 \tag{2.5}$$

Where I_{peak} is the peak current, I_{ss} is the steady current, and the area is determined from under the current response.

Current densities (pA/pF) were calculated from the peak current, I_{peak} in response to maximal concentrations of GABA using the following equation:

Equation 2.6, current density:

$$current\ density = \frac{I_{peak}}{C_m} \tag{2.6}$$

In addition, the kinetics of maximal GABA-activated currents - receptor activation, desensitisation, and deactivation phases, were characterised. Activation time was quantified as the 20 – 80% rise time of the peak current whilst exponential time constants for desensitisation and deactivation were obtained by fitting exponential functions to the relevant phase of current decay. The desensitising current was fitted with a single exponential, whilst the deactivation phase was fitted with either one or two exponential components, with the accuracy of the fit judged by visual inspection. For those responses in which the decay was better fit by a biexponential function, the weighted time constant (τ_w) was calculated using equation:

Equation 2.7, weighted time constant:

$$\tau_w = \frac{(A_1 \times \tau_1) + (A_2 \times \tau_2)}{A_1 + A_2} \tag{2.7}$$

Where A represent the amplitude and τ represents the exponential time constant of each component.

2.5 Primary neuronal cultures and electrophysiology

2.5.1 Culture preparation and transfections

Primary neuronal cultures were prepared from E18 Sprague-Dawley rat embryos of either sex. This procedure was performed under UK Home Office guidelines by authorised Home Office licence holders. Pregnant dams of various ages were sacrificed by a team member of UCL Biological Services in accordance with the UK Animals (Scientific Procedures) Act 1986. Pups were taken out and hippocampi were extracted in ice cold Hanks' balanced salt solution (HBSS) and placed into HBSS supplemented with 0.1% w/v trypsin (Sigma-Aldrich) for 10 min at 37°C.

Enzymatic dissociation was followed by mechanical trituration into single cells using fire-polished glass Pasteur pipettes. Cells were plated onto 22 mm glass coverslips (VWR international) for electrophysiology or onto 1.5H 18 mm glass coverslips (Marienfeld) for imaging experiments, both coated with 100 μg/mg poly-L-ornithine (Sigma-Aldrich). The plating medium contained Minimum Essential Medium (MEM) supplemented with 5% v/v FBS, 5% v/v horse serum, penicillin-G/streptomycin (100 U/ml and 100 μg/ml), 20 mM glucose (Millipore), and 2 mM L-glutamine. After 2 h, the plating media was replaced with a maintenance medium (Neurobasal-A with 1% v/v B-27 supplement, penicillin-G/streptomycin (50 U/ml / 50 μg/ml), 0.5% v/v Glutamax, 35 mM glucose). Neurons were grown in a humidified incubator (37°C, 5% CO2).

Primary hippocampal neurons in culture were transfected after 7 days *in vitro* (DIV) using a calcium phosphate precipitation method (Hannan et al., 2013), with neurons subsequently being used for electrophysiological recordings between 12 – 16 DIV or fixed for imaging on 14 DIV. For transfections, 54 μl of TE buffer (10 mM Tris-HCl (pH 8.0), 0.1 mM EDTA) was mixed with 1.5 μl of eGFP cDNA and 2.5 μl of the appropriate α_5 (wild-type/mutated/tagged/untagged) cDNA. Next, 2.5 μl of 2.5 M $CaCl_2$ was added, and the mixture was then transferred dropwise into a new microcentrifuge tube containing 60 μl of 2x HEPES buffered saline (HBS; 42 mM HEPES, 274 mM NaCl, 10 mM KCl, 1.4 mM Na2HPO4, 15 mM D-glucose; pH 7.11) while continuously vortexing. The mixture was then incubated at room temperature for 30 min with vortexing every 5 min. Meanwhile, the media from the neuronal dishes was replaced with pre-warmed (37°C) and filter-sterilized 2 mM kynurenic acid in Neurobasal-A supplemented with penicillin-G/streptomycin (100 U/ml and 100 μg/ml). The DNA mixture (60 μl) was added dropwise to each coverslip and cells were returned to the incubator for 30 min. Cells were then washed twice with 1 ml of pre-warmed Neurobasal-A supplemented with penicillin-G/streptomycin (100 U/ml and 100 μg/ml) before replenishment with neuronal maintenance media. The transfection efficacy was estimated around 1%.

2.5.2 Whole-cell patch clamp recordings from neuronal cultures

Neurons were removed from the incubator (between 12 - 16 DIV) and placed into a bath continuously perfused with Krebs solution supplemented with 2 mM kynurenic acid (Sigma-Aldrich) to block ionotropic glutamate receptors. Cells were voltage-clamped at -60 mV and recorded at room temperature. The patch pipette was filled with an internal solution consisting of 140 mM CsCl, 2 mM NaCl, 10 mM HEPES, 5 mM EGTA, 2 mM $MgCl_2$, 0.5 mM $CaCl_2$, 2 mM Na_2ATP, 0.5 mM Na_2GTP, 2 mM QX-314 (Tocris), pH 7.4, with an osmolarity of 300 $\pm$ 10 mOsm/L. CsCl and QX-314 were included in the internal solution to block voltage-gated K^+ and Na^+ currents respectively. The pH of the intracellular solution was adjusted using 1 M CsOH.

2.5.3 Drug treatments

L-655,708 (Santa Cruz Biochemicals, sc-204040) is an α_5-$GABA_A$Rs selective inverse agonist or negative allosteric modulator/inhibitor and was used to block α_5-$GABA_A$Rs mediated currents. Picrotoxin (PTX, Sigma-Aldrich, P1675) is an antagonist of all $GABA_A$Rs subtypes and was used to reveal the total tonic current in cultured hippocampal neurons. Stock solutions in DMSO (5 mM for L-655,708, 100 mM for PTX) were diluted into Krebs solution to make appropriate working solutions (50 nM for L-655,708, 100 μM for PTX) (details in Appendix Table A.3. Both drugs were applied continuously onto cells through a modified U-tube (Mortensen and Smart, 2007) after a period of stable control recording and allowed to equilibrate for at least 3 min before starting with subsequent recordings. In experiments where both drugs were used, recordings were made for approximately 10-15 min in L-655,708 before subsequent application of PTX.

2.5.4 Peptide treatment

All experiments with peptides were performed by a PhD student Seth Liebowitz and analysed by Carmen Kivisild. Two peptides were used in this study: (1) a blocking peptide mimicking the gephyrin binding domain (residues 370-385) on the α_5 subunit (Brady and Jacob, 2015) and (2) a scrambled peptide with the same amino acids in random sequence. Both peptides, synthesised by Biomatik, were

dissolved as 3 mM stock solutions in water and stored at -18°C. Peptides were added to the internal solution on the day of the experiment to a final concentration of 30 μM. Currents were recorded approximately 5 min after patching the cell to allow enough time for the peptide to act. The sequences of peptides were as follows:
Blocking peptide: acetyl-KSNAFTTGKLTHPPN-amide
Scrambled peptide: acetyl-TSTLFPTHKKPNNAG-amide
N- and C- terminal modifications (acetylation and amidation) were made to the peptides to remove the charge from both termini of the peptide. In addition, these modifications make the peptides more stable and increase their biological activity.

2.5.5 Electrophysiology data analysis

Spontaneous inhibitory postsynaptic currents (sIPSCs) were recorded from transfected neurons expressing wild-type or mutated α_5 subunits along with eGFP. The recordings were imported into WinEDR (V3.9.5, Strathclyde Electrophysiology Software, Dr J Dempster) for event detection using an amplitude threshold method (threshold was set to -4 pA). All detected synaptic events were verified by visual inspection of individual traces and the frequency and the amplitude of sIPSCs were calculated. Average baseline current levels were calculated during a 2 ms epoch immediately before each detected event and the peak amplitude was calculated relative to this value.

Selected synaptic events were imported into WinWCP software (V5.5.5, Strathclyde Electrophysiology Software, Dr J Dempster) for further analysis. Events that exhibited monotonic rises and an uncontaminated decay phase were aligned on their rising phases and mean synaptic IPSC waveforms were constructed by averaging $>$50 sIPSCs for each cell. The sIPSC 10 – 90% rise times and decay times were calculated from the mean IPSC waveforms. Decay times were characterised by fitting the decay phase of the mean IPSC waveform with a standard mono- or bi-exponential decay function, and weighted time constants were calculated using Equation 2.7.

Next, all synaptic currents were pooled within one transfection group and amplitude distributions fitted with the sum of three or four Gaussian functions of the form:

Equation 2.8, Gaussian function:

$$y = y_0 + \frac{A}{w\sqrt{\frac{\pi}{2}}} \times e^{\frac{-2(x-x_c)^2}{w^2}} \tag{2.8}$$

Where A is the area, y_0 defines the pedestal of the distribution, x_c is the mean amplitude current and w is the half-height width of the Gaussian curve. The distributions were fitted using Gaussian functions programmed in Origin (Ver 6). Synaptic currents were then subdivided into small- and large-amplitude groups using a threshold based upon the Gaussian fits. Cumulative probability plots and histograms were generated for both frequency and amplitude distributions in small- and large-amplitude groups using GraphPad Prism 9 software (GraphPad).

2.6 Structured illumination microscopy (SIM)

2.6.1 Immunostaining

Myc-tagged (protein sequence: EQKLISEEDL) constructs were created to distinguish transfected α_5 from endogenous α_5 subunits. A previously engineered cDNA construct expressing a myc-tagged mouse α_5 subunit was used as a template to generate myc-tagged α_5 mutants as described in Section 2.3.1. The myc-tag at the beginning of the mature protein, between amino acids 28 and 29 in the α_5 subunit including the signalling peptide (UniProt Q8BHJ7).

Cultured hippocampal neurons were transfected at 7 DIV with cDNA expressing one of the following variants: wild-type α_5, mutated $\alpha_5{}^{S374A}$ or $\alpha_5{}^{S374D}$ subunits as described in Section 2.5.1. Seven days after transfection (14 DIV), coverslips were removed from the incubator, gently washed with ice-cold phosphate-buffered saline (PBS) and fixed with paraformaldehyde (4% v/v PFA/ 4% w/v sucrose/ PBS, pH 7.0) for 5 mins before washing twice in PBS. Surface proteins were blocked with 10% v/v normal goat serum (NGS) in PBS for 20 min at room temperature and

then the coverslips were washed once with 1% w/v bovine serum albumin (BSA) in PBS. All following washes used 1% BSA in PBS. $GABA_A$Rs at the cell membrane were labelled by incubating coverslips in a primary antibody solution diluted in 3% NGS for 1 h at room temperature. Anti-myc primary antibody (Abcam, ab9106 and ab32) and α_5 subunit specific antisera (Fritschy et al., 1997), diluted 1:2000 and 1:500 respectively, were used to label α_5 subunits expressed at the cell surface. Cell surface expressed endogenous α_1 subunits were labelled using anti-α_1 primary antibody (Abcam, ab33299) diluted 1:200 (details about antibodies used are in Appendix Table A.4). After washing the cells once, they were permeabilised to stain for intracellular proteins using 0.1% Triton X-100 in PBS for 5 mins and then washed twice more. Next, the cells were incubated in a blocking solution (10% NGS in PBS) for 30 mins, washed and intracellular endogenous vesicular inhibitory amino acid transporter (VIAAT) and gephyrin proteins were labelled by incubating coverslips in primary antibody solution diluted in 3% NGS for 1 h at room temperature. Anti-VIAAT (Alomone labs, AGP-129) and anti-gephyrin (Synaptic Systems, SYSY3B11) primary antibodies were used, diluted by 1:500 and 1:200 respectively. Cells were then washed three times and incubated in a secondary antibody mixture consisting of anti-rabbit Alexa Flour 488 (Invitrogen, A-11034), anti-mouse Alexa Flour 555 (Invitrogen, A-21424) and anti-guinea pig Alexa Flour 647 (Invitrogen, A-21450), all diluted by 1:500 in 3% NGS. Cells were subsequently washed four times and coverslips were mounted on microscope slides using Prolong Glass mounting medium (Invitrogen) for SIM imaging.

2.6.2 Imaging

Multichannel 3D-SIM images were acquired using an Axio Observer.Z1 SR Zeiss ELYRA PS.1 microscope with Plan-Apochromat DIC M27 63x 1.4 NA oil objective lens immersed in halogen-free (HF) immersion oil (SPI Supplies) at room temperature. Fluorophores were excited by illumination from 488 nm, 561 nm, and 642 nm lasers (HR Diode and HR DPSS) and emitted light was detected by a pco.edge sCMOS camera controlled via ZEN Black software (v. 11.0.2.190, Zeiss). Structured illumination was provided by diffracting incident laser light using a 100 nm

grating pattern at three angles with five rotations per angle. Camera exposure time was maintained at 100 ms and laser power at 10% of maximum. 10-15 z-stacks were acquired for each 12-bit image. For channel alignment, 200 nm TetraSpeck fluorescent microspheres (Invitrogen) were imaged using the same settings. Raw images were corrected for chromatic aberration using the channel alignment algorithm and reconstructed into super-resolution images using the SIM reconstruction mode with default settings in ZEN Black software.

2.6.3 Data analysis

Reconstructed images were analysed using an ImageJ-based plugin called DiAna (Gilles et al., 2017). Briefly, images were opened in ImageJ and a region of interest (ROI) was drawn using the freehand selection tool. Only proximal dendrites were chosen, and the soma was excluded from the analysis. Next, 5-10 z-stack slices were selected where the clusters from all three channels were in focus and out of focus slices were excluded. The background area outside of the ROI was deleted and the three channels were split. The DiAna plugin was then used to perform 3D segmentation for object extraction using a global intensity thresholding procedure. Appropriate thresholds for each channel were assigned by visual inspection and fixed during the analysis. Other parameters of the segmentation were kept on default settings. Following the segmentation procedure, 3D measurements (volume and mean grey value), colocalization and distance analysis were performed. Clusters were defined as colocalised if they overlapped with each other, with the distance between two clusters measured from centre-to-centre. All data were saved as Excel files, which were then imported into MATLAB 2020 (Mathworks) for further analysis. A custom-made MATLAB code (by Risto Jamul, Kings College London, UK) was used to find mean values and quantify the percentage of colocalization in each cell.

2.7 Statistical analysis and software used

All data visualisation and statistical analyses were performed using GraphPad Prism 9 software. In all figures, bars represent the overall mean values and individual cir-

cles correspond to mean values from each cell. One-way ANOVA and two-way repeated measurements (RM) ANOVA analysis followed by appropriate post-hoc tests were performed depending on the number of variables. For cumulative probability plots Kruskal-Wallis with Dunn's post hoc tests were used. The threshold for statistical significance was set at $p < 0.05$. In all figures: non-significant (ns) $p > 0.05$, $* \, p \leq 0.05$, $** \, p > 0.01$, $*** \, p > 0.001$. All values are presented as mean $\pm$ standard error of the mean (SEM). All graphs were plotted in GraphPad Prism and figures including multiple panels were composed in Adobe Illustrator CS6 (Adobe).

Chapter 3

Phosphorylation of S^{374} in the gephyrin binding domain of the α_5 subunit by glycogen synthase kinase 3 alters the α_5-$GABA_A$Rs function

3.1 Introduction

As discussed in previous sections, phosphorylation of $GABA_A$Rs is a key post-translational modification in regulating inhibitory postsynaptic plasticity (Nakamura et al., 2015; Tyagarajan and Fritschy, 2010). Mass-spectrometry (MS) is a powerful tool for investigating the phosphorylation of different proteins (Dephoure et al., 2013). Considerable effort has been made to expand our knowledge about regulatory domains contained within the primary sequences of $GABA_A$R subunits (Kang and Lubec, 2009) as well as the technical aspects for investigating $GABA_A$Rs using MS (Chen et al., 2012). Yet, there are only a few comprehensive studies using this technique to describe the phosphorylation status of $GABA_A$Rs (Jurd et al., 2010; Kang et al., 2011; Nakamura et al., 2016, 2020) as it has been challenging, because $GABA_A$Rs are strongly hydrophobic transmembrane proteins (Kang and Lubec, 2009; Kang et al., 2008). Nevertheless, MS has been utilised to find novel binding partners for $GABA_A$Rs (Nakamura et al., 2016), to identify co-associations

between different $GABA_AR$ subunits (Ghafari et al., 2017; Ju et al., 2009), and also to sequence, with near complete coverage, individual $GABA_AR$ subunits (Chen et al., 2012; Kang and Lubec, 2009; Kang et al., 2008, 2009).

The main challenges for identifying novel phosphorylation sites in $GABA_ARs$ are the low abundance of phosphorylated proteins compared to unphosphorylated counterparts and the need for a large sample of pure protein (Dephoure et al., 2013). Another approach that can be taken to support the use of MS is to use computational-based prediction tools to tentatively identify protein kinase consensus sites. There are several computational methods that can be used to predict phosphorylation sites, which can be broadly categorized into two groups: (1) methods based on machine learning and (2) methods that seek consensus phosphorylation motifs by screening primary sequences. The NetPhos 3.1 (https://services.healthtech.dtu.dk/service.php?NetPhos-3.1) server uses previously trained artificial neural networks to predict serine (S), threonine (T) or tyrosine (Y) phosphorylation consensus sites in eukaryotic proteins (Blom et al 1999). The Eukaryotic Linear Motif (ELM, https://ELM.eu.org/) is a prediction tool that scans a library of user-submitted protein sequences for matches to experimentally validated or putative motifs. The current version of the ELM database contains 289 motif classes and 3523 individual protein motifs including phosphorylation and protein binding motifs (Kumar et al 2020). A combination of MS and online prediction tools is therefore a powerful approach for identifying phosphorylation sites in α_5 subunits.

The function of $GABA_ARs$ is finely regulated by phosphorylation (Kittler et al., 2005; Nakamura et al., 2015). Intrinsic electrophysiological parameters have been used to describe the changes in $GABA_AR$ function. Most described macroscopic kinetic parameters of GABA-evoked currents are known as: activation, desensitisation, and deactivation (Figure 3.1). Activation phase is described as a rapid increase in current upon exposure to agonist, desensitisation phase is a progressive decrease in current in the continued presence of agonist and deactivation phase is a decay of any remaining current upon removal of agonist. These three phases can be characterised by parameters reflecting the duration or rate of current change or, in

the case of desensitisation, the extent of current decrease. Activation time is the delay associated with a step change in GABA concentration and receptor/channel response, which depends on the receptor affinity for GABA and thus speed of GABA binding leading to a series of conformational changes to the receptor and opening of the central pore. Desensitization is a process in which $GABA_AR$s lose their ability to remain open upon sustained agonist binding (Sallard et al., 2021). Intuitively, this mechanism would protect neural networks from abnormally strong inhibitory signals, but it can also act as an initiator of synaptic plasticity (Baker et al., 2002; Bianchi and Macdonald, 2002; Field et al., 2021). During the deactivation phase, GABA unbinds from its orthosteric site on the $GABA_AR$ and consequently the central pore closes, thus ending usually the hyperpolarisation of the cell (Sallard et al., 2021). At given agonist concentrations, and when exposed to agonist for the same duration, these kinetic parameters can be used to identify the receptor subtype involved by its signature current profiles (Bianchi et al., 2002; Chen et al., 2017; Gingrich et al., 1995; Picton and Fisher, 2007) and also to investigate the alterations to receptor function following mutations when comparing the same receptor subtype (Laha and Tran, 2013; Terejko et al., 2020, 2021). In this chapter, macroscopic kinetic parameters are used to describe the functional changes of α_5-$GABA_AR$s caused by mutating the phosphorylated residue in the α_5 subunit. In addition, advantage is taken of the distinct α_5-$GABA_AR$s kinetic profile to describe the synaptic accumulation of these receptors under specific circumstances.

The changes to $GABA_AR$ function are classically described using the functional parameters derived by fitting concentration response curves to a series of GABA responses: the EC_{50} and Hill coefficient. The EC_{50} is the GABA concentration at which the current peak reaches half of the maximal current amplitude and reflects directly the potency of GABA, it will also be affected by the receptor's affinity for GABA and GABA efficacy (Colquhoun, 1998). The Hill coefficient of a $GABA_AR$ reflects the slope of the concentration response curve, and it has been used to describe the changes in the number of and cooperativity between GABA binding sites (Sallard et al., 2021) although the information on the latter aspects is

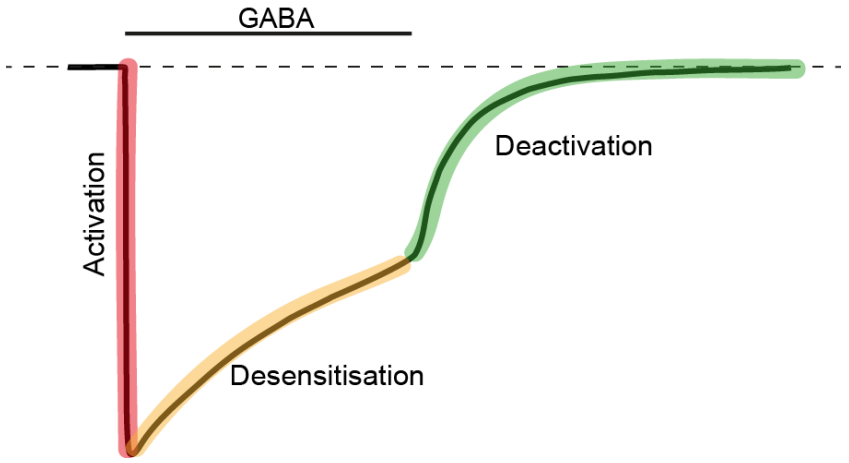

Figure 3.1: Schematic showing macroscopic kinetic phases of a GABA-activated current.
Whole-cell membrane current evoked by 300 μM GABA (bar) depicting the three macroscopic kinetic phases analysed: activation (red), desensitisation (orange), and deactivation (green).

tenuous (Colquhoun, 1998). In this chapter, GABA concentration response curves (CRC) are used, and fitted by the empirical Hill equation (Equation 2.1), to derive EC_{50} and Hill coefficient values to compare the functional properties between wild-type and mutated α_5-$GABA_A$Rs.

3.2 Results

3.2.1 Residues S^{374}, T^{379} and T^{380} in the gephyrin binding domain are predicted phosphorylation consensus sites for protein kinase C

I used the online prediction tool NetPhos 3.1 to identify novel phosphorylation consensus sites in the entire ICD of the mouse α_5 subunit (UniProt entry Q8BHJ7, residues 342-428 between transmembrane domains M3 and M4). Eleven residues in the mouse α_5 subunit were highlighted as potential sites for phosphorylation by either PKC or unspecified kinases (unsp.) (Table 3.1). Three of these residues (S^{374}, T^{379} and T^{380}) are in the GBD of the α_5 subunit (Brady and Jacob, 2015) and therefore, were targeted for this project. I hypothesized that the phosphorylation of GBD may negatively impact the interaction between the α_5 subunit and gephyrin and ultimately reduce the accumulation of α_5-$GABA_A$Rs at inhibitory synapses. The identification of PKC as a candidate for phosphorylating α_5 subunits was unsurprising because it is known to phosphorylate other $GABA_A$R subunits including α_4, $\beta_{1\text{-}3}$ and γ_2 (Moss and Smart 1996, Brandon et al 2000, Smart et al 2001, Abramian et al 2010, Bright and Smart 2013b, Nakamura et al 2015).

Table 3.1: Consensus phosphorylation sites in the large intracellular domain of the mouse α_5 subunit.
There are eleven residues in the ICD of the mouse α_5 subunit which are predicted to have a high likelihood of phosphorylation according to the prediction server NetPhos 3.1. These residues were predicted to be phosphorylation sites for unspecified kinases (unsp.) or by PKC. Each residue has a prediction score (range 0.000 (unlikely)-1.000 (very likely)) which shows how likely it is for this residue to be phosphorylated and by which kinase. Only residues with likelihood scores above 0.5 were considered as potential substrates.

Residue	Context	Kinase	Score
T^{345}	VNYF**T**KRGW	PKC	0.512
S^{374}	ILNK**S**TNAF	PKC	0.560
T^{379}	TNAF**T**TGKL	PKC	0.515
T^{380}	NAFT**T**GKLT	unsp.	0.958
S^{405}	APTV**S**IKAS	unsp.	0.891
S^{409}	SIKA**S**EEKT	unsp.	0.977
S^{416}	KTAE**S**KKTY	unsp.	0.894
T^{419}	ESKK**T**YNSI	PKC	0.668
Y^{420}	SKKT**Y**NSIS	unsp.	0.822
S^{422}	KTYN**S**ISKI	unsp.	0.939
S^{424}	YNSI**S**KIDK	unsp.	0.984

3.2.2 Mass spectrometry confirms phosphorylation of predicted residues in the gephyrin binding domain of recombinant and native α_5 subunits

I used mass spectrometry to experimentally confirm the predicted phosphorylation sites (Table 3.1). Two sets of samples were prepared: HEK293 cell lysates for recombinant receptors and adult rat hippocampal lysates for native receptors. HEK293 cells were transfected with cDNAs expressing myc-tagged α_5, flag-tagged β_3 and untagged γ_{2L} subunits 24 h before harvesting the cells. Recombinant receptor complexes were pulled down using immunoprecipitation directed against either the myc- or flag-epitope tags. To maximise phosphorylation by PKC, half of the cell samples were treated with the PKC activator phorbol 12-myristate 13-acetate (PMA – 200 nM for 15 min prior to cell lysis) whilst the other half were only exposed to the PMA vehicle, dimethyl sulfoxide (DMSO) as a control (Table 3.1). The second set of samples were taken from rat hippocampal lysates (for details see Section 2.1.1). The purpose of using rat brain to complement HEK293 cell samples was to assess phosphorylation of α_5 subunits assembled in native $GABA_AR$ complexes using immunoprecipitation targeted against the α_5 subunit.

Cell samples were analysed as described in Sections 2.1.2-2.1.5. Briefly, samples were run on 10% Bis-Tris gel and stained overnight using InstantBlue (Expedeon). The stained bands with molecular weights of approximately 50-70 kDa were excised and trypsin digested. Resulting peptides were separated by reverse phase nano-Ultra Performance Liquid Chromatography (nano-UPLC) and analysed using label-free liquid chromatography mass spectrometry in data-independent analysis mode (LC-MS^E). Data collected by LC-MS^E were processed using the Protein Lynx Global Server (PLGS) v3.0.2 (Waters Corporation) and queried against a Homo sapiens protein database (UniProt proteome: UP000005640) concatenated with a list of common contaminants obtained from the Global Proteome Machine (ftp://ftp.thegpm.org/fasta/cRAP) (Figure 3.2A). All peptides detected by mass spectrometry covered 27% of the entire α_5 subunit in HEK293 cell samples (for both PMA and DMSO treated cells) and 23% of native α_5 subunit in rat brain samples. Next, detected peptides were aligned against the ICD of either rat (UniProt

entry P19969 – native receptors) or human (UniProt entry P31644 – recombinant receptors) α_5 protein sequences (Figure 3.3) and only peptides carrying the phosphorylation motifs were included in further analysis.

Mass spectrometry analysis found one peptide from the rat hippocampal lysate and seven peptides from the HEK293 samples that were phosphorylated. The single phosphorylated α_5 peptide identified from rat hippocampal lysate contained two phosphorylated threonines, T^{379} and T^{380}. For the seven phosphorylated α_5 peptides detected in HEK293 cell lysates, in four peptides the residue that had undergone post-translational modification could be identified, whilst in three peptides the phosphorylated residue remained unidentified (Table 3.3).

There are several issues that complicate identification of the precise residue(s) of modification including low occupancy and two phosphorylation sites being too close together. In addition, same-sequence peptides, but phosphorylated on different residues, will have identical intact mass. To overcome this issue, phosphorylation-site localization relies on peptide fragmentation and when a peptide containing two sites is fragmented for MS, only those fragments resulting from breakage points located between the two sites can be used to distinguish them (Figure 3.2B). MS spectra rarely contain all possible fragment ions and therefore may not yield sufficient information to localize the site(s) within the peptide sequence (Dephoure et al 2013).

Often, there are multiple possible locations for a phosphate group on a peptide (Figure 3.2B). Because the intact masses would be the same for all of them, fragmentation is used to determine the exact location of the phosphate group. If multiple serines, threonines or tyrosines are close together, fragmentation must split the residues for successful identification. Unfortunately, not all fragments are produced and sometimes there is insufficient information to identify the phosphorylated residue in a particular peptide. In such cases the location of the phosphorylated residues is marked with an asterisk ($*$).

From the DMSO control samples, amino acids T^{393}, S^{402}, S^{408} and two more peptides (the location of the phosphorylation group was unidentified) were basally-

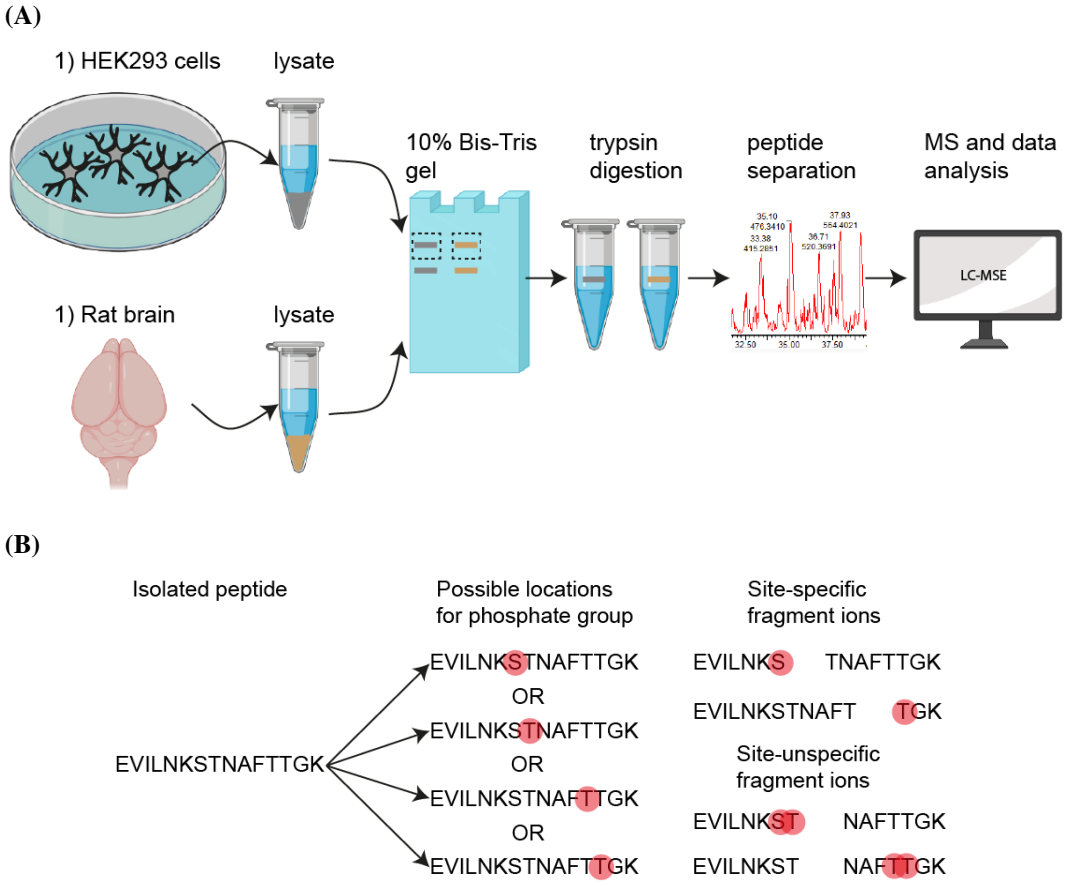

Figure 3.2: Schematic of sample preparation and mass spectrometry analysis. **(A)** Two sets of samples were used: transfected HEK293 cells and rat brains. Cells were lysed, α_5-GABA$_A$R complexes were separated using immunoprecipitation and run on 10% Bis-Tris gel. Protein bands with weight approximately 50-70 kDa were excised from the gel and then enzymatically digested by trypsin. Resultant peptides were separated, and mass spectrometry analysis was performed (see Section 2.1.2). **(B)** Example of phosphopeptide fragmentation to localize the exact residue carrying a phosphate group.

phosphorylated. In PMA treated cells, phosphorylation was detected on human residues S^{373}, T^{379}, S^{415} and T^{418} (Table 3.3). Therefore, six out of eleven predicted phosphorylation sites (mouse S^{374}, T^{379}, T^{380}, S^{409}, S^{416}, T^{419}) were confirmed to be phosphorylated in at least one of the samples, whilst the mass spectrometric analysis detected two phosphorylation sites, human T^{393} and S^{402} that are not conserved in the mouse sequence and therefore were not forecast by the NetPhos algorithm. Of the five predicted mouse sites that were not detected as phosphorylated by the MS analysis (mouse T^{345}, S^{405}, Y^{420}, S^{422}, S^{424}), T^{345} did not have any peptide coverage, whilst S^{405} is not conserved among all three species. Interestingly, some

residues were found in both forms: phosphorylated and not phosphorylated in the same sample, which may suggest low occupancy for these residues (Table 3.2).

To summarise, the three amino acids of interest located in the gephyrin binding domain of the α_5 subunit that were predicted to be sites of phosphorylation (mouse S^{374}, T^{379} and T^{380}) (Table 3.1) were all experimentally confirmed as phosphorylated by MS analysis (Tables 3.2 and 3.3, Figure 3.3). Complementary experiments performed in HEK293 cells by our collaborators (SJ Moss, Tufts University, Boston) confirmed only the phosphorylation of S^{374} (unpublished data), thus the role of the phosphorylation of residue S^{374} was selected for further investigation.

Table 3.2: Six predicted phosphorylation consensus sites were confirmed to be phosphorylated by mass spectrometry.
Six out of eleven predicted phosphorylation sites (mouse S^{374}, T^{379}, T^{380}, S^{409}, S^{416}, T^{419}) were confirmed to be phosphorylated in at least one of the lysate samples. Five predicted sites (mouse T^{345}, S^{405}, Y^{420}, S^{422}, S^{424}) were not detected as phosphorylated by the MS analysis.

Predicted phosphorylation sites in mouse	Corresponding residue in rat	Corresponding residue in HEK293
T^{345}	not covered	not covered
S^{374}	not phosphorylated	S^{373} phosphorylated
T^{379}	T^{379} phosphorylated	not confirmed
T^{380}	T^{380} phosphorylated	not confirmed
S^{405}	S^{406} not phosphorylated	not conserved
S^{409}	not covered	S^{408} phosphorylated
S^{416}	not covered	S^{415} phosphorylated
T^{419}	not covered	T^{418} phosphorylated
Y^{420}	not covered	Y^{419} not phosphorylated
S^{422}	not covered	S^{421} not phosphorylated
S^{424}	not covered	S^{423} not phosphorylated

Table 3.3: Mass-spectrometry analysis of phosphorylation of recombinant and native α_5 subunits.
Rat brain and HEK293 cell lysates were used to purify native and recombinant $GABA_ARs$ respectively. HEK293 cells were transfected with mouse cDNAs expressing myc-tagged α_5, flag-tagged β_3 and γ_{2L} subunits and incubated with PMA to activate PKC or DMSO solvent as a control. For immunoprecipitation (IP), myc and flag tags were used with HEK293 cell lysates and antibody directly against α_5 subunit was used for rat hippocampal lysates to pull down whole receptor complexes from the plasma membrane. Proteins were then separated, extracted, and digested with trypsin, and analysed by LC-MS^E (see Sections 2.1.1-2.1.5). From the ICD of the α_5 subunit mass spectrometry analysis identified one peptide in rat hippocampal lysates and seven in the HEK293 cell lysates that were phosphorylated. Where the exact location of the post-translational modification was known, it is highlighted in red in the second column and numerically marked in the peptide in the third column (counting from the left, first residue = 1). In other cases where the exact location was unknown (unsp.), an asterisk is shown. The location of the peptides and the phosphorylated residues are written in the fourth and fifth columns respectively.

Protein accession number	Peptide sequence	Modification	Peptide location on α_5	Phosph. residue on α_5	Sample	Transfected with	IP	Treatment
P19969	GWAWDGKK	none	348-355	N/A	Rat brain lysate	N/A	α_5	N/A
	ERELILNKSTNAFTTGK	Phosph.(14;15)	366-382	T^{379};T^{380}				
	STNAFTTGK	none	374-382	N/A				
	EQLPGGTGNAVGTASIR	none	392-408	N/A				
P31644	REVILNKSTNAFTTGK	Phosph.(*;*)	366-381	unsp.	HEK293 cell lysate	myc-α_5 + flag-β_3 + γ_{2L}	myc	DMSO
	STNAFTTGK	none	373-381	N/A			myc	DMSO
	EQTPAGTSNTTSVSVKPSEEK	Phosph.(12;18)	391-411	S^{402};S^{408}			myc	DMSO
	EQTPAGTSNTTSVSVKPSEEK	Phosph.(3;18)	391-411	T^{393};S^{408}			myc	DMSO
	GWAWDGKK	none	348-355	N/A			flag	DMSO
	EVILNKSTNAFTTGK	Phosph.(*;*)	367-381	unsp.			flag	DMSO
	STNAFTTGK	none	373-381	N/A			flag	DMSO
	MSHPPNIPK	none	382-390	N/A			flag	DMSO
	STNAFTTGK	none	373-381	N/A			myc	PMA
	STNAFTTGKMSHPPNIPK	Phosph.(1;7)	373-390	S^{373};T^{379}			myc	PMA
	EQTPAGTSNTTSVSVKPSEEK	Phosph.(*;*)	391-411	unsp.			myc	PMA
	TSESKKTYNSISK	Phosph.(4;7)	412-424	S^{415};T^{418}			myc	PMA
	TYNSISK	none	418-424	N/A			myc	PMA
	TYNSISKIDK	none	418-427	N/A			myc	PMA
	EVILNKSTNAFTTGK	none	367-381	N/A			flag	PMA
	KTYNSISK	none	417-424	N/A			flag	PMA

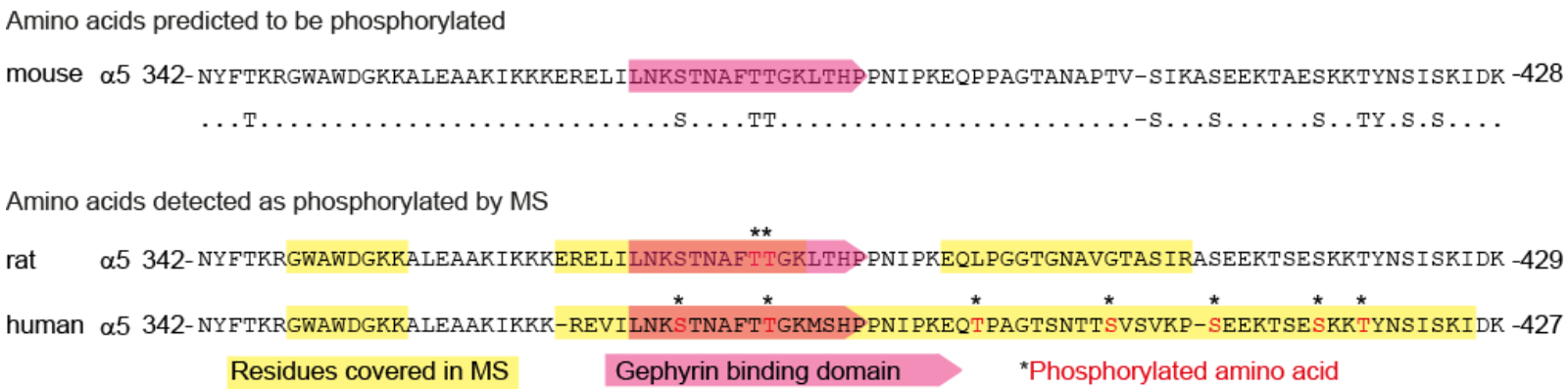

Figure 3.3: Phosphorylation in the gephyrin binding domain confirmed by mass spectrometry analysis.
Sequences of the intracellular domain of the α_5 subunit (large intracellular loop between TM3-TM4) from mouse, rat and human were aligned. The NetPhos 3.1 server was used to predict phosphorylated amino acids in mouse α_5 subunit and mass spectrometry was used to experimentally confirm predicted consensus sites in rat and human samples (see Sections 2.2 and 2.1). All residues covered in the mass spectrometry analysis were highlighted in yellow (exact sequences and conditions are shown in Table 3.3), gephyrin binding domain is in pink and overlapping residues shown in orange. Residues predicted to be phosphorylated are indicated on a separate line underneath the mouse sequence, phosphorylated residues confirmed experimentally are in red and marked with asterisks in the rat and human α_5 sequences. All three predicted phosphorylation sites in the gephyrin binding domain (Table 3.1) were detected as phosphorylated by mass spectrometry either in rat hippocampal lysate (mouse residues T^{379} and T^{380}) or in HEK293 cell lysates (mouse residues S^{374} and T^{380}) (Table 3.3).

3.2.3 Functional characterisation of wild-type and mutated α_5-GABA$_A$Rs expressed in HEK293 cells

To characterise the effects on receptor function of phosphorylating the intracellular domain of the α_5 subunit at residue S^{374} I generated a phospho-null mutant ($\alpha_5{}^{S374A}$) by replacing this serine with the neutral amino acid alanine (A) and a phospho-mimetic mutant ($\alpha_5{}^{S374D}$) by replacing S^{374} with the negatively-charged aspartic acid (D). These mutants and wild-type α_5 cDNAs were then transfected into HEK293 cells along with constructs encoding β_3 and γ_{2L} subunits to allow the expression of $\alpha_5\beta_3\gamma_{2L}$ receptors, an isoform that is thought to be widely expressed *in vivo* (Pirker et al 2000). Cells were also co-transfected with a plasmid expressing eGFP as a positive-transfection marker and studied using whole-cell patch clamp electrophysiology.

Whole-cell currents were recorded in response to brief (2-5 s) GABA applications via a U-tube and peak current responses were measured. Data for the GABA CRC were collected for each cell and fitted with the Hill equation (see Equation 2.1 in the Methods) to generate the mean CRC for wild-type and mutated receptors. Mutating serine to alanine ($\alpha_5{}^{S374A}$) shifted the CRC to the right (Figure 3.4A) and resulted in a significantly higher mean EC_{50} value compared to wild-type receptors (7.7 $\pm$ 1.0 μM and 4.3 $\pm$ 0.6 μM respectively; one-way ANOVA p=0.0235, Tukey's multiple comparisons test: $\alpha_5\beta_3\gamma_{2L}$ vs $\alpha_5{}^{S374A}\beta_3\gamma_{2L}$ adjusted p=0.0221; Figure 3.4B), which indicates that this mutation reduced GABA potency. Mutating serine to aspartate at position 374 ($\alpha_5{}^{S374D}$), to mimic phosphorylation, resulted in similar GABA curves (Figure 3.4A) and EC_{50} values compared to wild-type receptors (6.4 $\pm$ 1.3 μM and 4.3 $\pm$ 0.6 μM respectively; Figure 3.4B). The mean value of Hill coefficient was significantly lower for $\alpha_5{}^{S374A}\beta_3\gamma_{2L}$ compared to wild-type receptors (0.85 $\pm$ 0.07 and 1.08 $\pm$ 0.05 respectively; one-way ANOVA p=0.0182, Tukey multiple comparisons test: $\alpha_5\beta_3\gamma_{2L}$ vs $\alpha_5{}^{S374A}\beta_3\gamma_{2L}$ adjusted p=0.0179), which might suggest altered cooperativity of GABA binding to these receptors. In contrast, the mean Hill coefficient value for $\alpha_5{}^{S374D}\beta_3\gamma_{2L}$ receptors was very similar to wild-type receptors (1.06 $\pm$ 0.07 and 1.08$\pm$ 0.05 respectively; Figure 3.4C).

Taken together, these data indicate that S^{374} in α_5 subunit ($\alpha_5{}^{S374}$) is an important residue in terms of receptor function and mutating it to alanine causes a decrease in GABA potency (higher mean EC_{50}) and a less steep GABA CRC (lower mean Hill coefficient).

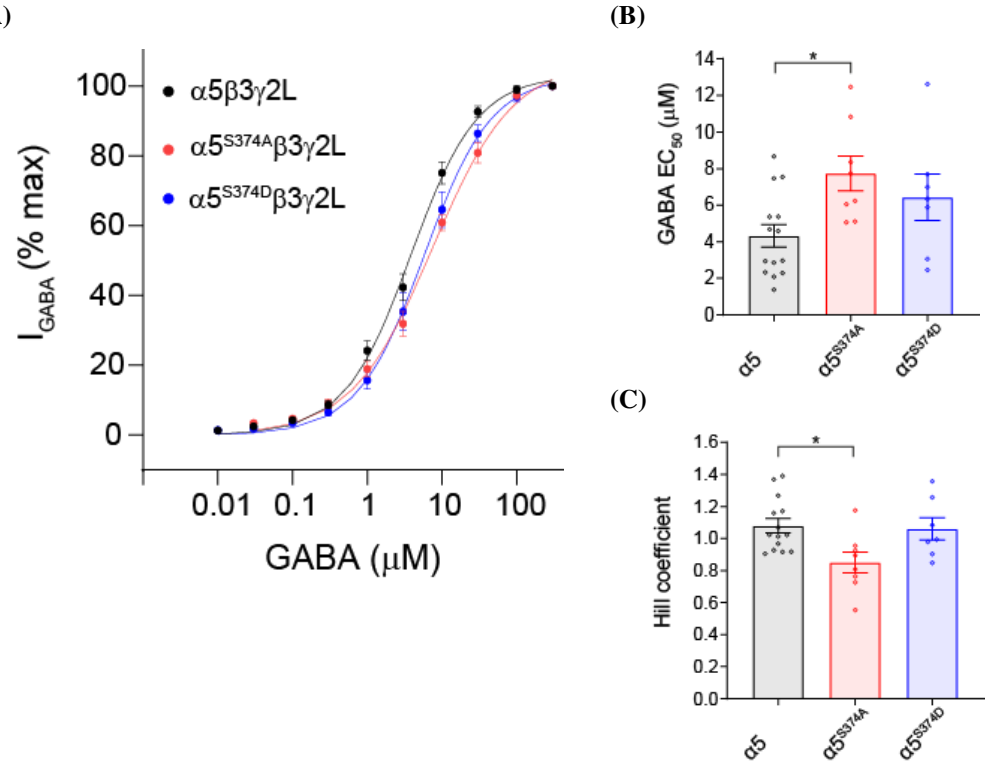

Figure 3.4: Effects of phospho-mutants of α_5 subunit on GABA activation of $\alpha_5\beta_3\gamma_{2L}$ receptors.
(A) GABA CRC for wild-type $\alpha_5\beta_3\gamma_{2L}$ (n=14, black), phospho-null $\alpha_5{}^{S374A}\beta_3\gamma_{2L}$ (n=8, red) or phospho-mimetic $\alpha_5{}^{S374D}\beta_3\gamma_{2L}$ (n=7, blue) receptors. Bars represent the mean values of **(B)** GABA EC_{50} (μM) and **(C)** Hill coefficient and are shown in black for wild-type $\alpha_5\beta_3\gamma_{2L}$ receptors and in red or blue for mutated $\alpha_5{}^{S374A}\beta_3\gamma_{2L}$ and $\alpha_5{}^{S374D}\beta_3\gamma_{2L}$ receptors respectively. Points represent values calculated for individual cells. Error bars represent SEM. $*$ $p< 0.05$, one-way ANOVA followed by Tukey's multiple comparisons test.

To explore the impact of mutating $\alpha_5{}^{S374}$ on receptor expression, I examined membrane currents elicited by a saturating concentration (300 μM) of GABA (Figure 3.5A). These maximum peak currents (pA) were normalized to whole cell capacitance (pF) to account for transfected cell-to-cell variability in size and are expressed as current density (pA/pF). The mean maximum peak current was significantly smaller for $\alpha_5{}^{S374A}\beta_3\gamma_{2L}$ compared to wild-type (-4960 $\pm$ 587.6 pA and

-7760 ± 634.7 pA respectively) or mutated $\alpha_5^{S374D}\beta_3\gamma_{2L}$ receptors (-7662 ± 671.4 pA; one-way ANOVA p=0.0128, Tukey multiple comparisons test: $\alpha_5\beta_3\gamma_{2L}$ vs $\alpha_5^{S374A}\beta_3\gamma_{2L}$ adjusted p=0.0140, $\alpha_5^{S374A}\beta_3\gamma_{2L}$ vs $\alpha_5^{S374D}\beta_3\gamma_{2L}$ adjusted p=0.0464; Figure 3.5B). As expected, there was no change in whole-cell capacitance ($\alpha_5\beta_3\gamma_{2L}$: 11.6 ± 1.07 pF, $\alpha_5^{S374A}\beta_3\gamma_{2L}$: 12.0 ± 1.69 pF, $\alpha_5^{S374D}\beta_3\gamma_{2L}$: 13.1 ± 1.95 pF; p=0.7676; Figure 3.5C). Therefore, the significant decrease seen in the mean maximum peak current for $\alpha_5^{S374A}\beta_3\gamma_{2L}$ compared to wild-type receptors was also reflected by reduced maximum GABA current densities (-455.5 ± 62.95 pA/pF and -712.0 ± 56.59 pA/pF respectively; one-way ANOVA p=0.0546, Tukey multiple comparisons test: $\alpha_5\beta_3\gamma_{2L}$ vs $\alpha_5^{S374A}\beta_3\gamma_{2L}$ adjusted p=0.0492), suggesting a reduction in cell surface expression levels for $\alpha_5^{S374A}\beta_3\gamma_{2L}$ receptors. Mean maximum GABA current density was similar comparing $\alpha_5\beta_3\gamma_{2L}$ and $\alpha_5^{S374D}\beta_3\gamma_{2L}$ receptors (-712.0 ± 56.59 pA/pF and -674.3 ± 119.3 pA/pF respectively; Figure 3.5D).

Next, I focused on whether mutating α_5^{S374} caused any effect on receptor kinetics by characterising the activation, desensitisation, and deactivation phases of maximal (300 μM) whole-cell GABA-activated currents (Figure 3.6) as described in Section 2.4.4. Mean activation time (ms) was measured as the interval between 20% and 80% of the peak current rise time (Figure 3.6A) and was significantly longer for $\alpha_5^{S374A}\beta_3\gamma_{2L}$ receptors by over 2-fold compared to wild-type (100.2 ± 9.5 ms and 44.9 ± 7.4 ms respectively) and $\alpha_5^{S374D}\beta_3\gamma_{2L}$ receptors (40.2 ± 4.4 ms; one way ANOVA p<0.0001, followed by Tukey multiple comparisons test: $\alpha_5\beta_3\gamma_{2L}$ vs $\alpha_5^{S374A}\beta_3\gamma_{2L}$ adjusted p=<0.0001, $\alpha_5^{S374A}\beta_3\gamma_{2L}$ vs $\alpha_5^{S374D}\beta_3\gamma_{2L}$ adjusted p=0.0002; Figure 3.6B). Although, the molecular mechanism of how altering residue α_5^{S374} affects the function of α_5-GABA$_A$Rs in HEK293 cells remains unknown, slower activation time may plausibly occur because of a slow rate of GABA binding, a slow exit from any preactivation states, or slowed channel gating (Sallard et al., 2021). These effects would also accord with the rightward shift of the GABA CRC for $\alpha_5^{S374A}\beta_3\gamma_{2L}$ receptors seemingly reducing the potency of GABA. The exponential time constants for desensitisation (mono-exponential) and deactivation (weighted tau, mono- or bi-exponential) were determined by fitting expo-

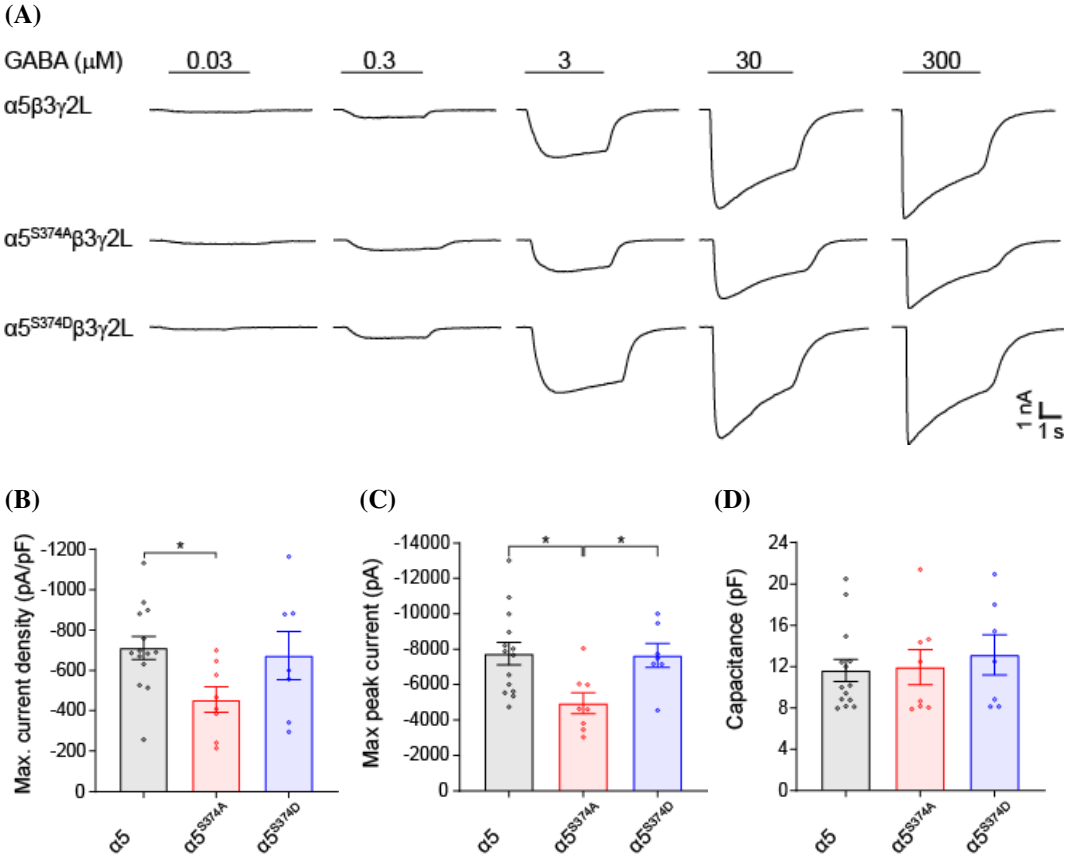

Figure 3.5: α_5^{S374A} reduces maximum GABA current of $\alpha_5\beta_3\gamma_{2L}$ receptors.
(A) Representative examples of membrane currents recorded from HEK293 cells expressing recombinant α_5-$GABA_A$Rs in response to increasing concentrations of GABA (0.03-300 μM). The black horizontal lines indicate the duration of GABA applications. Bars represent the mean values of **(B)** maximum current density (pA/pF), **(C)** maximum peak current (pA), and **(D)** capacitance (pF) and are shown in black for wild-type $\alpha_5\beta_3\gamma_{2L}$ receptors (n=14) and in red or blue for mutated $\alpha_5^{S374A}\beta_3\gamma_{2L}$ (n=8) and $\alpha_5^{S374D}\beta_3\gamma_{2L}$ (n=7) receptors respectively. Points represent values calculated for individual cells. Error bars represent SEM. $*$ $p<0.05$, one-way ANOVA with Tukey multiple comparisons test.

nential components to the current decay. More details about the analysis in Section 2.4.4. Desensitisation tau ($\alpha_5\beta_3\gamma_{2L}$: 2.95 ± 0.15 s, $\alpha_5^{S374A}\beta_3\gamma_{2L}$: 2.81 ± 0.17 s, $\alpha_5^{S374D}\beta_3\gamma_{2L}$: 2.86 ± 0.31 s; p=0.8533; Figures 3.6C) and deactivation weighted tau ($\alpha_5\beta_3\gamma_{2L}$: 0.76 ± 0.12 s, $\alpha_5^{S374A}\beta_3\gamma_{2L}$: 0.54 ± 0.11 s, $\alpha_5^{S374D}\beta_3\gamma_{2L}$: 0.63 ± 0.12 s; p=0.4706; Figure 3.6D) remained unchanged between the three receptors. Note that deactivation phase may be contaminated by some desensitisation.

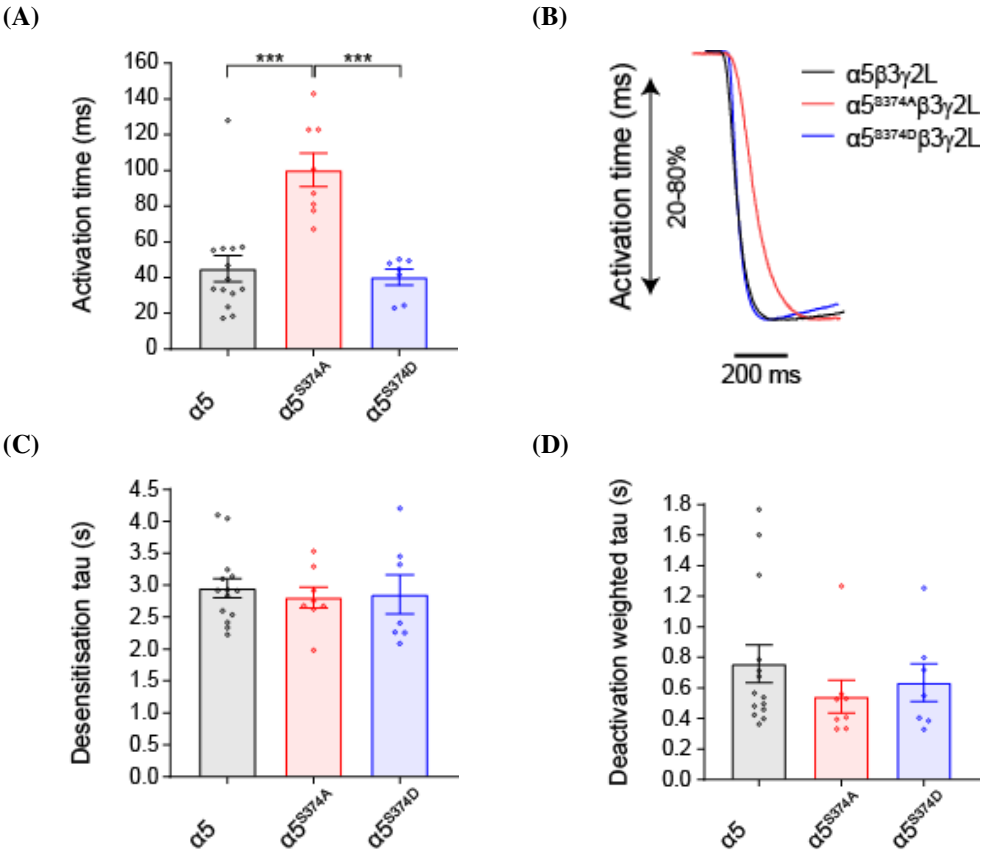

Figure 3.6: α_5^{S374A} slows the rate of GABA$_A$R activation.
Activation time was measured as the time taken to ascend from 20% to 80% of peak current following the application of 300 μM GABA. Bars represent the mean values of **(A)** activation time (ms), **(C)** desensitisation tau (s) and **(D)** deactivation weighted tau (s) and are shown in black for wild-type $\alpha_5\beta_3\gamma_{2L}$ receptors (n=14) and in red or blue for mutated $\alpha_5^{S374A}\beta_3\gamma_{2L}$ (n=8) and $\alpha_5^{S374D}\beta_3\gamma_{2L}$ receptors (n=7) respectively. **(B)** Example GABA currents for the activation of wild-type (black) and mutated $\alpha_5^{S374A}\beta_3\gamma_{2L}$ (red) and $\alpha_5^{S374D}\beta_3\gamma_{2L}$ (blue) receptors. More details about the analysis are in Section 2.4.4. Points represent values calculated for individual cells. Error bars represent SEM. $***$ $p < 0.001$, one-way ANOVA, Tukey multiple comparisons test.

3.2.4 Kinase(s) responsible for phosphorylating S^{374} in the α_5 subunit

The previous set of experiments using receptor expression in HEK293 cells demonstrated that mutating $\alpha_5{}^{S374}$ affects the function of α_5-$GABA_A$Rs. First, I showed that $\alpha_5{}^{S374A}\beta_3\gamma_{2L}$ receptors have significantly higher EC_{50} (Figure 3.4B) and a lower Hill coefficient (Figure 3.4C) compared to wild-type receptors, which indicates a reduced GABA potency for $\alpha_5{}^{S374A}\beta_3\gamma_{2L}$ receptors. Secondly, investigating the macroscopic kinetics of GABA-activated currents revealed more than a 2-fold increase in the activation time for $\alpha_5{}^{S374A}\beta_3\gamma_{2L}$ compared to wild-type receptors (Figure 3.6A). Since removal of this phosphorylation site by mutation to alanine leads to changes in receptor function, I speculated that this residue is likely to be phosphorylated in wild-type α_5 subunits under basal conditions in HEK293 cells.

Next, I wanted to know which kinase is responsible for phosphorylating S^{374} in wild-type α_5 subunits. Since PKC was predicted by the NetPhos 3.1 server to phosphorylate $\alpha_5{}^{S374}$ and mass spectrometry analyses confirmed that the same residue was indeed phosphorylated in PMA (PKC activator) treated HEK293 cells expressing $\alpha_5\beta_3\gamma_{2L}$ receptors (Table 3.3), I decided to test PKC first. Furthermore, PKC is known to phosphorylate other $GABA_A$R subunits including β_3 and γ_{2L} (Brandon et al., 2000, 2002b; Kittler et al., 2005; McDonald and Moss, 1994; Mcdonald and Moss, 1997; Moss et al., 1992). To specifically investigate the potential role of PKC in phosphorylating $\alpha_5{}^{S374}$, I used PMA to activate PKC and compared the effects on GABA CRC and EC_{50} values between wild-type $\alpha_5\beta_3\gamma_{2L}$ and mutated $\alpha_5{}^{S374A}\beta_3\gamma_{2L}$ receptors expressed in HEK293 cells. I excluded $\alpha_5{}^{S374D}\beta_3\gamma_{2L}$ receptors from this experiment, because this phospho-mimetic mutation appeared to have no significant impact upon receptor function from our previous set of experiments (Figures 3.4 and 3.6).

For $\alpha_5\beta_3\gamma_{2L}$ and $\alpha_5{}^{S374A}\beta_3\gamma_{2L}$ receptors, I first recorded the control GABA CRC, then applied 200 nM PMA for 3 min before re-evaluating the GABA CRC in the presence of the kinase activator. Adding PMA to wild-type receptors shifted the GABA CRC to the right (Figure 3.7A) and resulted in a significantly higher EC_{50} value, which indicates a decreased receptor sensitivity to GABA (2.7 ± 0.8 μM and

4.8 ± 1.0 μM respectively; two-way RM ANOVA: drug effect p=0.068, genotype effect p=0.578; followed by Sidak's multiple comparisons test: $\alpha_5\beta_3\gamma_{2L}$ no drug vs PMA, adjusted p=0.026; Figure 3.7C). Activating PKC in HEK293 cells expressing $\alpha_5^{S374A}\beta_3\gamma_{2L}$ receptors did not affect EC_{50} values (4.3 ± 0.60 μM and 4.3 ± 0.6 μM respectively; Figures 3.7B and 3.7C). Therefore, surprisingly, activation of PKC has a similar effect on wild-type receptors as introduction of the phospho-null α_5^{S374A} mutation, with both causing a decrease in GABA potency. However, given that there was no effect of PMA on $\alpha_5^{S374A}\beta_3\gamma_{2L}$ receptors, this suggests that α_5^{S374} is involved in mediating the PKC-evoked effect on wild-type receptors. Taken together, these results suggest that PKC does not directly phosphorylate α_5^{S374} to cause the decrease in GABA sensitivity but is probably involved in the signalling pathway.

Following our postulation that PKC may not act directly on α_5-$GABA_A$Rs, I returned to NetPhos 3.1 to expand the search criteria for identifying kinases that may phosphorylate residues in the mouse α_5 gephyrin binding domain. Instead of only allowing positive hits with scores higher than 0.5, I looked at the top three ranked kinases based on their scores. In addition to PKC, cyclin-dependent kinase 2 (cdc2) and GSK3 were predicted to phosphorylate α_5^{S374} (Table 3.4). Ca2+/calmodulin-dependent protein kinase II (CaMKII) was also highlighted as a potential kinase for phosphorylating another two residues, T^{379} and T^{380} in the gephyrin binding domain. All the aforementioned kinases are found at inhibitory synapses (Uezu et al., 2016).

To evaluate the probability of cdc2 and GSK3 phosphorylating residue S^{374} I searched for known short linear motifs in the intracellular domain of the α_5 subunit using the online prediction tool ELM. The prediction power was enhanced by applying additional filters such as the cell compartment (e.g, cytosol and plasma membrane) and species (e.g, *Mus musculus*). In addition to phosphorylation motifs, ELM found motifs for other classes of protein interaction across the intracellular domain of the α_5 subunit (see Table 3.4, column 3). All results are presented, but as the aim was to find kinase consensus motifs in the gephyrin binding domain of the

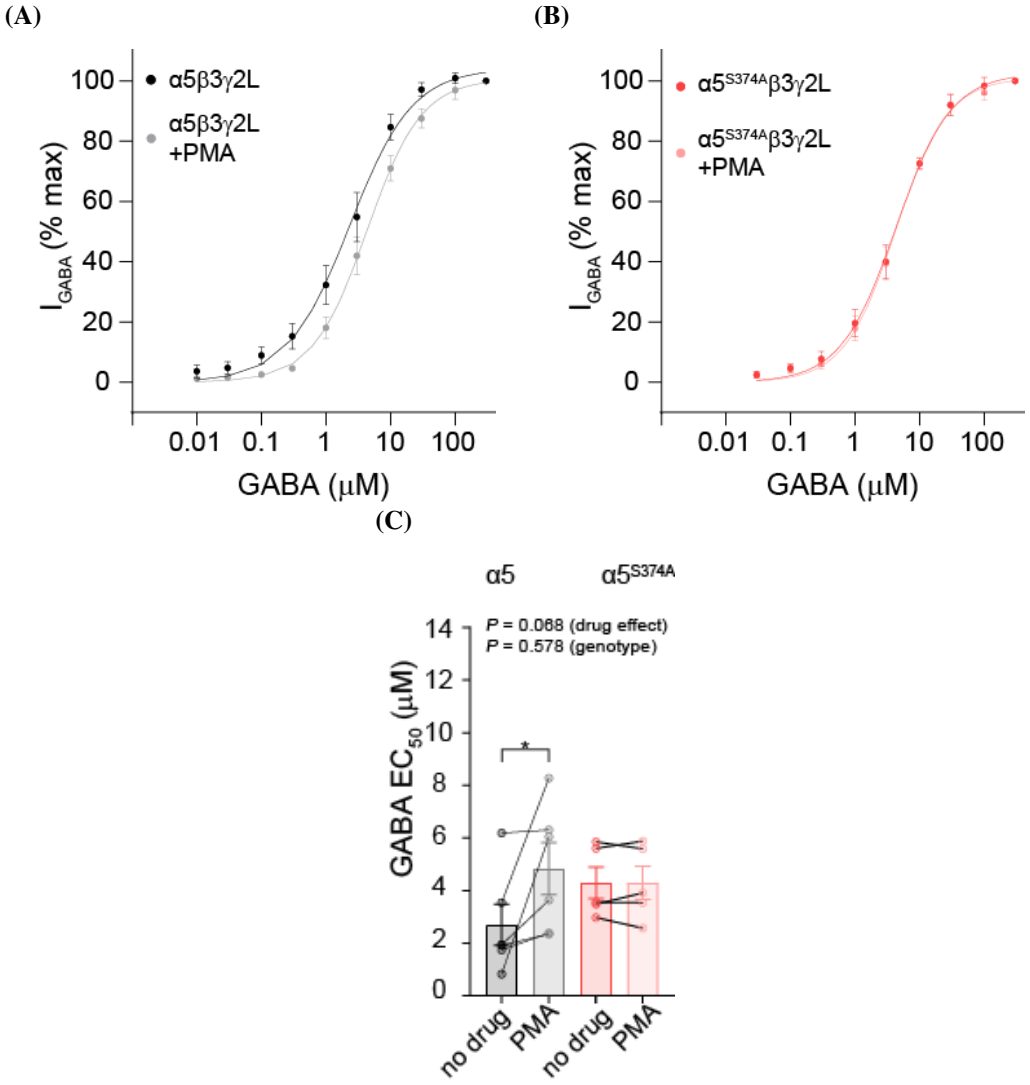

Figure 3.7: Activation of PKC decreases GABA sensitivity for wild-type $\alpha_5\beta_3\gamma_{2L}$ but not for $\alpha_5^{S374A}\beta_3\gamma_{2L}$ receptors.
GABA CRC for **(A)** wild-type $\alpha_5\beta_3\gamma_{2L}$ (n=6) and **(B)** mutated $\alpha_5{}^{S374A}\beta_3\gamma_{2L}$ (n=5) receptors recorded in the absence (black and red respectively) and presence (grey and pink respectively) of 200 nM PMA. **(C)** Bars represent mean GABA EC_{50} (μM) values and are shown in black or grey (before and after applying 200 nM PMA) for wild-type $\alpha_5\beta_3\gamma_{2L}$ receptors and in red or pink for mutated $\alpha_5{}^{S374A}\beta_3\gamma_{2L}$ receptors. Points represent EC_{50} values calculated for individual cells and are linked for no treatment and PMA data points as these were recorded from the same cell. Error bars represent SEM. $*$ $p < 0.05$, two-way RM ANOVA followed by Sidak's multiple comparisons test.

Table 3.4: Kinases predicted by NetPhos 3.1 server to phosphorylate α_5 subunit in the gephyrin binding domain.
There are three potential phosphorylation residues in the gephyrin binding domain of the α_5 subunit based on the prediction server NetPhos 3.1. Top ranked kinases for phosphorylating each of these residues based on kinase scores are PKC, GSK3, cdc2 and CaMKII.

Residue	Context	Kinase	Score
S^{374}	ILNK**S**TNAF	PKC	0.560
		cdc2	0.487
		GSK3	0.445
T^{379}	TNAF**T**TGKL	PKC	0.515
		GSK3	0.475
		CaMKII	0.439
T^{380}	NAFT**T**GKLT	unsp.	0.958
		PKC	0.792
		CaMKII	0.431

α_5 subunit, the other motifs were not investigated further. Serine 374 is part of the canonical consensus sequence for GSK3, which is composed of two key residues, either S or T, which are separated by 2-4 amino acids from a further S or T that acts as a priming phosphorylated residue (Sp/Tp). Both ${\alpha_5}^{S374}$ and T^{379} potentially fulfil the criterion of being a part of a GSK3 consensus motif of S/T-$X_{2\text{-}4}$-Sp/Tp, assuming that the residue T^{379} is previously phosphorylated by another unknown kinase to prime ${\alpha_5}^{S374}$ for phosphorylation by GSK3. The α_5 sequence is 374-STNAFT-379 (Figure 3.3).

Table 3.5: Classes of motif identified in the intracellular domain of the mouse α_5 subunit.
I used the ELM prediction tool to find different classes of motifs in the large intracellular domain of the α_5 subunit (UniProt entry Q8BHJ7, amino acids 342-428 between TM3-TM4). Only matches including the cell compartments cytosol and plasma membrane were included in the analysis. S^{374} is highlighted in red.

Matched sequence	Position	ELM description	Cell compartment
NY	342-343	N-terminal motif that initiates protein degradation	cytosol
YFTK	343-346	STAT5 Src homology 2 (SH2) domain binding motif	cytosol
KIKKKERELIL	361-371	MAPK interacting molecules carry docking motif that helps to regulate the specific interactions in the MAPK cascade	nucleus, cytosol
RELIL	367-371	Substrate recognition site that interacts with cyclin and thereby increases phosphorylation by cyclin/cdk complexes	cytosol, nucleous
LNKSTN	371-376	NEK2 phosphorylation motif	nucleus, cytosol
NKSTNAFT	372-379	GSK3 phosphorylation recognition site	cytosol, nucleus
AFTTGKLT	377-384		
PTVSIKAS	402-409		
IKASEEKT	406-413		

Matched sequence	Position	ELM description	Cell compartment
THPPNIP	384-390	Motif recognised by SH3 domains with a non-canonical class I recognition specificity	plasma membrane focal adhesion cytosol
PTVSIK	402-407	NEK2 phosphorylation motif	nucleus, cytosol
ASEE	408-411	Major TRAF2 binding consensus motif	cytosol
SKKTYNS	416-422	CK1 phosphorylation site	cytosol, nucleous
TYNSI	419-423	Canonical LIR motif that binds to Atg8 protein family members to mediate processes involved in autophagy	cytosol late endosome membrane
YNSI	420-423	Tyrosine-based sorting signal responsible for the interaction with the AP (adaptor protein) complex	plasma membrane endocytic vesicle cytosol

GSK3 is a multi-substrate, serine/threonine-protein kinase that is at the centre of numerous signalling pathways. Therefore, it is not surprising that GSK3 is involved in a range of biological processes. In addition, dysfunction of this kinase is associated with autism spectrum disorder, Alzheimer's disease, Parkinson's disease, Huntington's disease, stroke, Fragile X syndrome and several psychiatric diseases (Beurel et al., 2015; Pandey and DeGrado, 2016). The two isoforms of GSK3, GSK3α and GSK3β, are both expressed in the brain (Yao et al., 2002). At inhibitory synapses, GSK3β is best known for regulating postsynaptic plasticity via phosphorylating gephyrin, which reduces clustering (Tyagarajan et al., 2011, 2013). Given this link, I therefore chose this isoform for further investigation.

I took a similar approach to that previously adopted for PKC to investigate the potential role of GSK3β in phosphorylating $\alpha_5{}^{S374}$. Unfortunately, no direct activator of GSK3β has yet been developed, thus ruling out pharmacological activation of this kinase as an experimental approach. Therefore, I co-transfected HEK293 cells with a constitutively-active mutant form of GSK3β (GSK3β S9A) (Stambolic and Woodgett, 1994) and compared these cells in parallel to those transfected with just $\alpha_5\beta_3\gamma_{2L}$ alone. I hypothesized that expressing activated GSK3β should potentiate wild-type receptors by phosphorylating a higher percentage of receptors, unless all wild-type receptors are already fully phosphorylated, a scenario which seemed unlikely. Also, if S^{374} is the phosphorylation site for GSK3β, then in the absence of this target residue, in $\alpha_5{}^{S374A}\beta_3\gamma_{2L}$ receptors, adding GSK3β S9A should have no effect. Whilst I lack a specific activator of GSK3β, there is a specific inhibitor, CHIR99021 (CHIR). Using the inhibitor, I first recorded the control GABA CRC, before applying 1 μM CHIR (IC_{50} value is 6.7 nM for GSK3β (Kaku et al., 2008)) and then after a 5 min incubation period, I recorded GABA currents for compiling the CRC again.

As expected, co-expression of GSK3β S9A with wild-type receptors shifted the GABA CRC to the left (Figure 3.8A) and resulted in a significantly lower mean EC_{50} value (6.5 $\pm$ 1.4 μM and 3.3 $\pm$ 0.4 μM respectively; two-way ANOVA: GSK3β S9A effect p=0.114, genotype effect p=0.249; followed by Sidak's multi-

ple comparisons test: $\alpha_5\beta_3\gamma_{2L}$ receptors co-expressed with GSK3β S9A vs $\alpha_5\beta_3\gamma_{2L}$ receptors, adjusted p=0.023; Figure 3.8D), which suggests that GSK3β S9A potentiated the function of wild-type receptors. In contrast, co-expression of GSK3β S9A with mutated $\alpha_5{}^{S374A}\beta_3\gamma_{2L}$ receptors did not have any effect on the GABA CRC (Figure 3.8B) or EC_{50} values (5.8 ± 0.9 μM and 6.1 ± 1.1 μM respectively; Figure 3.8D). CHIR (1 μM) had no effect on the GABA EC_{50} values for wild-type receptors (6.5 ± 1.4 μM and 7.2 ± 1.4 μM, in the absence or presence of the inhibitor respectively; Figures 3.8A and 3.8C) or for mutated $\alpha_5{}^{S374A}\beta_3\gamma_{2L}$ receptors (5.8 ± 0.9 μM and 5.6 ± 1.1 μM, in the absence or presence of CHIR respectively; Figures 3.8B and 3.8C). It should also be noted that EC_{50} values were much higher in this experiment and the significant difference between wild-type and $\alpha_5{}^{S374A}\beta_3\gamma_{2L}$ receptors seen in previous experiments was not clear. It is likely that the phosphorylation status of residue $\alpha_5{}^{S374}$ in HEK293 cells has changed between experiments demonstrating the importance of controlling the extent of phosphorylation in such experiments. Nevertheless, the observation that co-expression of GSK3β S9A affects wild-type, but not mutated $\alpha_5{}^{S374A}\beta_3\gamma_{2L}$ receptors suggests that GSK3β could directly phosphorylate $\alpha_5{}^{S374}$ to increase receptor sensitivity to GABA activation.

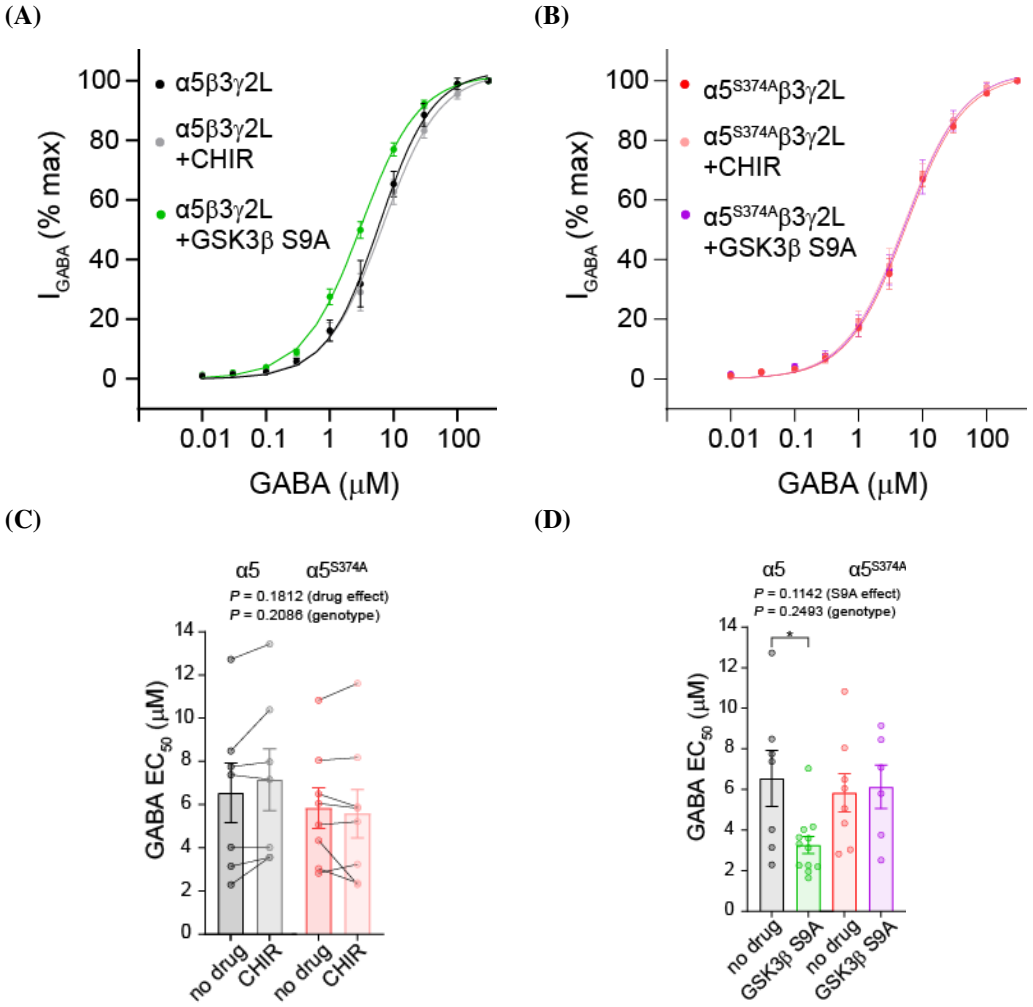

Figure 3.8: Constitutively-active GSK3β S9A increases GABA sensitivity for wild-type $\alpha_5\beta_3\gamma_{2L}$ but not for $\alpha_5^{S374A}\beta_3\gamma_{2L}$ receptors.
GABA CRC for **(A)** wild-type $\alpha_5\beta_3\gamma_{2L}$ or **(B)** mutated $\alpha_5^{S374A}\beta_3\gamma_{2L}$ receptors. Cells expressing wild-type or mutated receptors were untreated (n=7, black and n=8, red), exposed to 1 μM GSK3β inhibitor CHIR (grey or pink) or cells co-expressed a constitutively-active form of GSK3β S9A (n=12, green or n=6, purple respectively). **(C)** and **(D)** Bars represent mean GABA EC_{50} (μM) values and are shown in black, grey and green for wild-type $\alpha_5\beta_3\gamma_{2L}$ receptors and in red, pink and purple for mutated $\alpha_5^{S374A}\beta_3\gamma_{2L}$ receptors (no treatment, CHIR and +GSK3β S9A respectively). Points represent EC_{50} values calculated for individual cells and are linked for no treatment and CHIR data points as these were recorded from the same cells. Error bars represent SEM. $*$ $p< 0.05$, two-way ANOVA followed by Sidak's multiple comparisons test.

3.3 Discussion

Phosphorylation is one of the post-translational modifications that controls $GABA_AR$ function and subcellular location (see earlier sections). Many studies have addressed the location of phosphorylation sites in $GABA_ARs$, but so far, none have identified any such sites in the α_5 subunit until now (Nakamura et al., 2015). In this Chapter, I have identified three new phosphorylation sites in the gephyrin binding domain contained in the α_5 subunit ICD. I also investigated the effects of phosphorylating α_5^{S374} on α_5-$GABA_ARs$ function and surface expression in HEK293 cells. Finally, I demonstrated the involvement of both, PKC and GSK3β in phosphorylating residue α_5^{S374}.

I used mass-spectrometry and two online prediction tools, NetPhos 3.1 server and ELM, to identify novel phosphorylation sites in the α_5 subunit. I prepared two sets of biological samples, adult rat brain and transfected HEK293 cell lysates, to purify both native and recombinant α_5-$GABA_ARs$ respectively. Mass spectrometry analysis found one phosphopeptide from the rat hippocampal lysate and seven phosphopeptides from the HEK293 samples. In total, the online prediction tools forecasted eleven potential phosphorylated residues in the large intracellular domain of the α_5 subunit, of which six were confirmed by mass-spectrometry. Between the samples, residues S^{374}, T^{379} and T^{380}, located in the GBD of the α_5 subunit, were phosphorylated. Previously, it has been shown that the GBD of subunits α_1 and α_2 are also subject to phosphorylation (Mukherjee et al., 2011; Nakamura et al., 2020). I were not surprised to find multiple residues phosphorylated as there are also two phosphorylation sites described in the GBD for the α_2 subunit (Nakamura et al., 2020). Although the primary sequence of this domain varies significantly between different α subunits, I propose that phosphorylating GBD in a α subunit is a common mechanism to regulate the interaction between gephyrin and $GABA_ARs$. Here, I selected residue α_5^{S374} for further investigation. Future experiments will examine the importance and the interplay between all three identified phosphorylation sites.

The second set of experiments were designed to assess the importance of residue α_5^{S374} on receptor function using whole-cell patch-clamp electrophysiology

in HEK293 cells. Removing the phosphorylation site by mutating $\alpha_5{}^{S374A}$ increased EC_{50} values and reduced the Hill coefficient, indicating that this mutation reduced GABA sensitivity and potentially reduced the cooperativity of GABA binding for $\alpha_5{}^{S374A}\beta_3\gamma_{2L}$ receptors. Examination of the macroscopic parameters for GABA-evoked currents unveiled that mutating $\alpha_5{}^{S374A}$ increased the activation time by more than 2-fold, which supports the altered GABA binding hypothesis. Together, this data provides evidence that residue $\alpha_5{}^{S374}$ affects α_5-$GABA_A$Rs function.

Synaptic and extrasynaptic $GABA_A$Rs are composed of receptor subunits that convey electrophysiological properties ideally suited to generate transient phasic or persistent tonic inhibition in the brain (Banks and Pearce, 2000; Farrant and Nusser, 2005). Different $GABA_A$Rs subtypes exhibit a range of GABA potencies: extrasynaptic α_6 subunit-containing receptors have the highest potency for GABA, whereas synaptic $\alpha_2\beta_3\gamma_2$ and $\alpha_3\beta_3\gamma_2$ receptors exhibit the lowest potency (Mortensen et al., 2011). α_5-$GABA_A$Rs, found both at synaptic and extrasynaptic areas, have intermediate sensitivities to GABA. Based on our results, I assume that probably $\alpha_5{}^{S374}$ is phosphorylated under basal conditions in HEK293 cells and dephosphorylation makes α_5-$GABA_A$Rs less sensitive to GABA. I hypothesize that reduced GABA sensitivity could make unphosphorylated α_5-$GABA_A$Rs more suitable for synaptic localization compared to phosphorylated counterparts.

Next, I wanted to identify the kinase responsible for phosphorylating $\alpha_5{}^{S374}$ and based on the prediction server, PKC was the first kinase to be tested. Initially, I used PMA to activate PKC. If PKC is the kinase responsible for phosphorylating $\alpha_5{}^{S374}$, then I expected to see the opposite effects from mutating this serine to a phospho-null residue. Surprisingly, activating PKC had the same effect on GABA potency as mutating $\alpha_5{}^{S374}$ to alanine, which means it is unlikely to directly phosphorylate this residue, but instead perhaps engages with another kinase. PKC is known to phosphorylate other $GABA_A$R subunits (Nakamura et al., 2015), but these are probably not involved since comparing the effects of PMA between WT and mutated receptors clearly showed that the inhibitory effects of PMA on receptor function were mediated alone by $\alpha_5{}^{S374}$.

Although PKC did not directly phosphorylate $\alpha_5{}^{S374}$, it appeared to negatively affect the signalling pathway that does cause phosphorylation. GSK3β is one of the kinases that is negatively regulated by PKC (Moore et al., 2013). GSK3β is normally active in cells and is primarily regulated through inhibition of its activity (Doble and Woodgett, 2003). Interestingly, it is one of the kinases that requires prior phosphorylation of the target protein (called priming) by another kinase at a serine or threonine located 3-5 residues C-terminal to the GSK3β phosphorylation site (Hermida et al., 2017). The consensus sequence identified in the mouse α_5 subunit 374-STNAFT-379 shows that S^{374} together with T^{379} are ideally located for GSK3β phosphorylation of the α_5 subunit. Moreover, both residues were confirmed to be phosphorylated by mass-spectrometry analysis in the first set of experiments. This kinase has not been previously shown to directly phosphorylate any of the $GABA_A$Rs, but the scaffold protein gephyrin is a GSK3β substrate (Nakamura et al., 2015; Tyagarajan et al., 2011, 2013), thus making this kinase an ideal candidate for phosphorylating $\alpha_5{}^{S374}$, a residue located in the gephyrin binding domain (Brady and Jacob, 2015). As predicted, the constitutively active mutant GSK3β (GSK3β S9A) enhanced receptor sensitivity to GABA and the GSK3β inhibitor, CHIR, had a minor inhibitory effect in wt $\alpha_5\beta_3\gamma_{2L}$ but not with mutated $\alpha_5{}^{S374A}\beta_3\gamma_{2L}$ receptors.

Chapter 4

α_5^{S374} regulates phasic but not tonic inhibition mediated by α_5-GABA$_A$Rs

4.1 Introduction

The mechanisms underlying GABAergic plasticity can be categorised into presynaptic, postsynaptic, or mixed pre-and postsynaptic origins. In most cases, postsynaptic plasticity involves the modulation of GABA$_A$R number and/or their properties at the postsynaptic cell surface membrane (Barberis, 2020), whereas presynaptic plasticity involves a change in neurotransmitter release (Yang and Calakos, 2013). Traditionally, mean spontaneous GABA-mediated inhibitory postsynaptic current (sIPSC) frequency is used to monitor presynaptic effects (Choi and Lovinger, 1997) and mean sIPSC amplitude is used to provide insight into the dynamics of GABA$_A$R numbers at synapses (Nusser et al., 1998b). However, α_5-GABA$_A$Rs are also expressed at presynaptic terminals (Serwanski et al., 2006), but the functional consequences of presynaptic inhibition on neurotransmitter release varies across different synapses (Khatri et al., 2019). In this chapter, mean sIPSC frequency and amplitude are used to investigate the pre- and postsynaptic effects of mutating α_5^{S374}: a residue, that I propose impacts on the synaptic accumulation of α_5-GABA$_A$Rs.

The distinct response kinetics of GABA$_A$R subtypes are important for adapting the extent and duration of inhibition at inhibitory synaptic inputs (Banks and

Pearce, 2000; Farrant and Nusser, 2005). Thus, the specific requirements of individual synapses, at any particular moment, can be met by varying the expression levels of different $GABA_AR$ subtypes (Eyre et al., 2012; Picton and Fisher, 2007), each expressing distinctive kinetics (Bosman et al., 2002; Gingrich et al., 1995; Ortinski et al., 2004). Based on kinetic and amplitude profiles, sIPSCs can further be subdivided into $GABA_{A,fast}$ and $GABA_{A,slow}$ currents (Banks and Pearce, 2000; Banks et al., 2000). Slowly decaying sIPSCs are one of the key characteristic features generated by synaptic α_5-$GABA_ARs$ (Banks and Pearce, 2000; Cao et al., 2020; Capogna and Pearce, 2011; Magnin et al., 2019; Prenosil et al., 2006; Salesse et al., 2011; Schulz et al., 2018; Vargas-Caballero et al., 2010; Zarnowska et al., 2009). Using the benzodiazepine-insensitive, α_5^{H105R} mutant mice, Zarnowska and colleges demonstrated that multiple forms of $GABA_{A,slow}$ IPSCs exist, but α_5-$GABA_ARs$ are pre-eminent by contributing particularly to large-amplitude spontaneous and evoked responses in the hippocampus (Zarnowska et al., 2009). This unique kinetic profile of the α_5-$GABA_AR$ is therefore used to detect the presence of these receptors at inhibitory synapses. In addition, I classify sIPSCs into small and large amplitude groups to specifically determine the GABA synaptic currents most affected by mutating α_5^{S374}.

Using α_5 subtype-selective modulators is a useful technique to investigate the involvement of this particular $GABA_AR$ subtype in phasic and tonic inhibition (Maramai et al., 2020). As mentioned in Section 1.12, L-655,708 is a α_5 subunit-selective partial inverse agonist (or negative allosteric modulator, NAM) that specifically decreases GABAergic transmission via the α_5-$GABA_AR$ (Quirk et al., 1996). However, many modulators, including L-655,708, often exhibit only limited selectivity for $GABA_AR$ subtypes (Sieghart and Savić, 2018). L-655,708 binds to the benzodiazepine binding site, located at the interface between α_5 and γ_{2L} subunits and exhibits an 50-100-fold selectivity for α_5-$GABA_ARs$ compared to others containing α_1, α_2 or α_3 subunits. The inhibitory efficacy (35-50%) for L-655,708 is similar at all benzodiazepine-sensitive receptors, but the selectivity of L-655,708 for α_5-$GABA_ARs$ is determined by the higher binding affinity at this subunit (Ca-

sula et al., 2001; Quirk et al., 1996). Therefore, L-655,708 was used to investigate the synaptic contribution of α_5-GABA$_A$Rs by measuring the effect on sIPSCs and on the level of tonic inhibition by measuring a shift in the holding current after partially blocking α_5-GABA$_A$Rs with L-655,708 in neurons expressing wild-type or mutated α_5-GABA$_A$Rs.

To further explore the impact of the α_5-GABA$_A$Rs on inhibitory transmission, I target the α_5-GABA$_A$R-gephyrin protein complex (Khayenko and Maric, 2019; Schulte and Maric, 2021). This strategy relies upon the assumption that gephyrin is a key synaptic scaffold protein that regulates subcellular location and function of α_5-GABA$_A$Rs (Brady and Jacob, 2015; Tyagarajan and Fritschy, 2014). I investigate by blocking the interaction between α_5-GABA$_A$R and gephyrin using a competitive peptide that mimics the gephyrin binding domain (GBD) on the α_5 subunit (Brady and Jacob, 2015). Therefore, in these experiments, I expect to reduce the synaptic location of α_5-GABA$_A$Rs and hence their contribution to phasic inhibition.

4.2 Results

Experiments with recombinant $GABA_A$Rs in HEK293 cells demonstrated that mutating the putative phosphorylation site $\alpha_5{}^{S374}$ to alanine, to prevent phosphorylation by GSK3β, altered both α_5-receptor function and its cell surface expression. Whole-cell electrophysiological recordings from HEK cells expressing $\alpha_5{}^{S374A}\beta_3\gamma_{2L}$ receptors showed that this mutation resulted in receptors 2-fold less sensitive to GABA (Figure 3.4), with 2-fold slower macroscopic activation times (Figure 3.6), and reduced the number of receptors on the cell surface (Figure 3.5).

Whilst the HEK293 cell system provides an opportunity to investigate the functional properties of $GABA_A$Rs in relative isolation, it is also important to assess the impact of $\alpha_5{}^{S374}$ on receptors residing in their native environment with all other $GABA_A$R subtypes including the necessary regulatory proteins. Hence, I transfected cultured rat hippocampal neurons with wild-type α_5, phospho-null $\alpha_5{}^{S374A}$ or phospho-mimetic $\alpha_5{}^{S374D}$ constructs on the seventh day *in vitro* (7 DIV) and performed whole-cell recordings to examine sIPSCs and tonic currents on 12-16 DIV. Tonic currents were revealed by shifts in the holding current after applying 100 μM picrotoxin (PTX). As for HEK293 cell transfections, I also expressed eGFP to identify transfected neurons, and as a control treatment to confirm that the transfection process itself did not affect inhibitory transmission (for detailed description of methods see Section 2.5.1).

4.2.1 $\alpha_5{}^{S374A}$ prolongs the IPSC decay phase in hippocampal neurons

First, to investigate the impact of $\alpha_5{}^{S374A}$ on synaptic α_5-$GABA_A$Rs, I performed a detailed analysis of sIPSC properties and investigated how expressing wild-type or mutated forms of α_5 in cultured hippocampal neurons affected sIPSC mean frequency and amplitude. Neurons transfected with the phospho-null $\alpha_5{}^{S374A}$ construct showed a trend towards a reduced mean frequency of GABAergic events compared to eGFP transfected cells ($\alpha_5{}^{S374A}$: 0.96 $\pm$ 0.24 Hz and eGFP: 2.33 $\pm$ 0.52 Hz; one-way ANOVA, Tukey's multiple comparisons test adjusted p=0.0953). Neurons transfected with either the wild-type α_5 or phospho-mimetic $\alpha_5{}^{S374D}$ construct had similar sIPSC mean frequencies compared to eGFP transfected cells (α_5: 2.04

$\pm$ 0.74 Hz, α_5^{S374D}: 1.42 $\pm$ 0.37 Hz; Figures 4.1A and 4.1E, one-way ANOVA p=0.8768).

To examine how residue α_5^{S374} may influence the number of $GABA_A$Rs at inhibitory synapses, I compared sIPSC mean amplitudes between the four different transfected cell groups. sIPSC mean amplitudes were consistent across all transfected cell groups (eGFP: -77.40 $\pm$ 11.62 pA, α_5: -81.59 $\pm$ 17.79 pA, α_5^{S374A}: -106.3 $\pm$ 31.63 pA, α_5^{S374D}: -98.00 $\pm$ 37.46 pA; Figures 4.1B and 4.1E), therefore mutating α_5^{S374} does not appear to affect the mean number of $GABA_A$Rs at inhibitory synapses.

Secondly, for each transfected cell, a minimum of fifty GABAergic events were analysed for their kinetic profiles. sIPSCs were only selected for analysis if they presented 'clean' sIPSC profiles from which a mean IPSC was constructed (Figure 4.1F; for full details of analysis see Section 2.5.5). Neurons expressing α_5^{S374A} had significantly slower decaying sIPSCs compared to α_5 or eGFP transfected cells (eGFP: 41.1 $\pm$ 4.0 ms, α_5: 60.1 $\pm$ 4.9 ms, α_5^{S374A}: 88.0 $\pm$ 8.1 ms, α_5^{S374D}: 67.1 $\pm$ 8.3 ms; one-way ANOVA p=0.0002, Tukey's multiple comparisons tests, eGFP vs. α_5^{S374A} p<0.0001, α_5 vs. α_5^{S374A} p=0.0305, Figure 4.1C). Decay phase of α_5^{S374D} transfected neurons did not significantly differ from any other transfection groups. There were no changes to the mean IPSC 10 - 90% rise times (eGFP: 1.2 $\pm$ 0.2 ms, α_5: 1.0 $\pm$ 0.1 ms, α_5^{S374A}: 1.2 $\pm$ 0.1 ms, α_5^{S374D}: 1.2 $\pm$ 0.1 ms; one-way ANOVA p=0.5652; Figure 4.1D).

Together, these results indicate that the mean number of $GABA_A$Rs at individual synapses are likely to be similar between wild-type and α_5^{S374A} transfected cells (no change in sIPSC mean amplitudes). However, the increased decay time constant for α_5^{S374A} transfected cells suggest that the population of synaptic receptor subtypes was re-modelled in the neuronal environment, as experiments in HEK293 cells demonstrated that the α_5^{S374A} mutation does not appear to affect macroscopic receptor desensitisation or deactivation, the two receptor properties most likely to translate into altered IPSC decays.

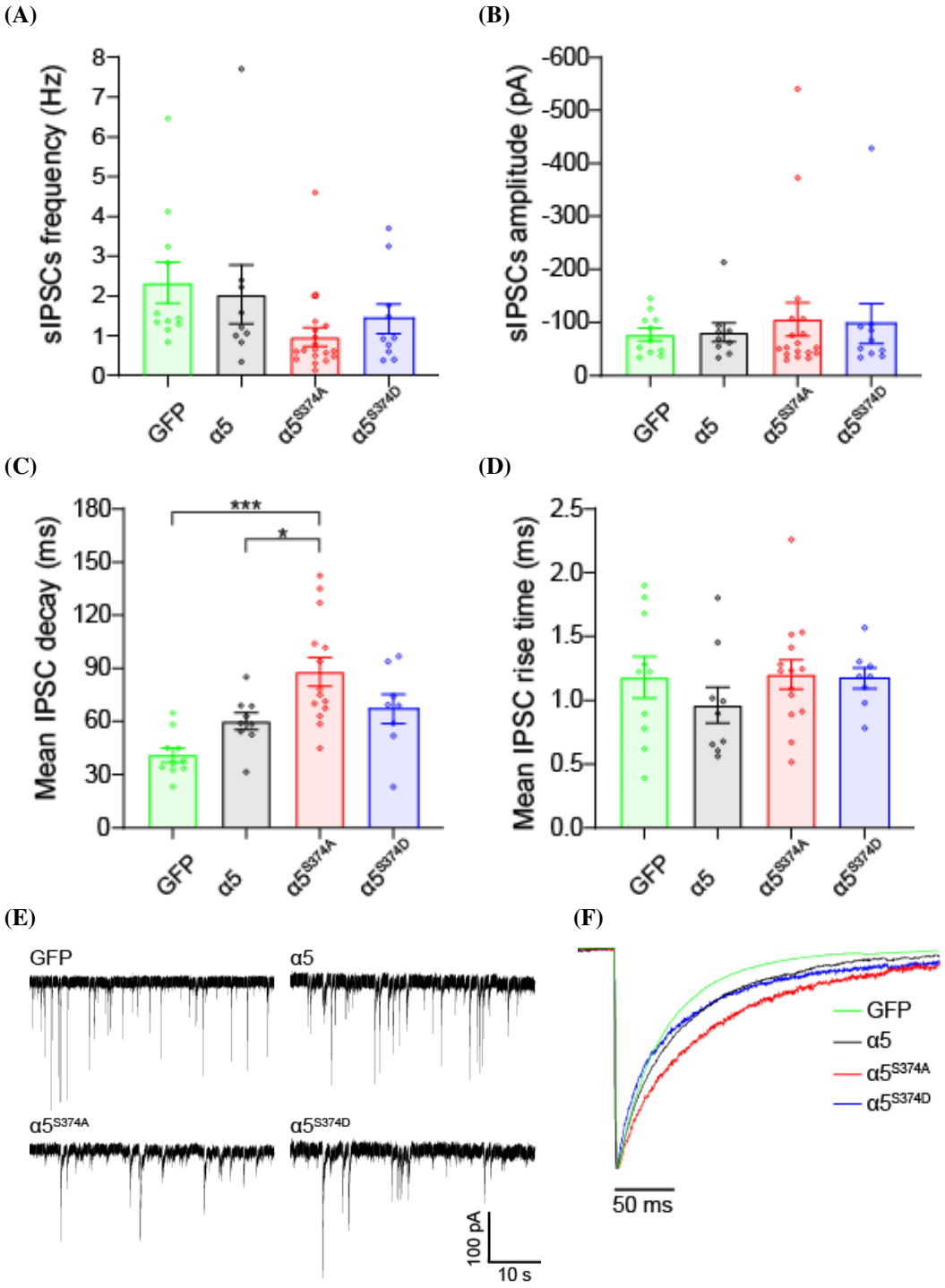
(A)
sIPSCs frequency (Hz)
0
1
2
3
4
5
6
7
8
GFP
α5
α5S374A
α5S374D
(B)
sIPSCs amplitude (pA)
-600
-500
-400
-300
-200
-100
0
GFP
α5
α5S374A
α5S374D
(C)
Mean IPSC decay (ms)
180
150
120
90
60
30
0
***
*
GFP
α5
α5S374A
α5S374D
(D)
Mean IPSC rise time (ms)
2.5
2.0
1.5
1.0
0.5
0.0
GFP
α5
α5S374A
α5S374D
(E)
GFP
α5
α5S374A
α5S374D
100 pA
10 s
(F)
GFP
α5
α5S374A
α5S374D
50 ms

Figure 4.1: Mutating α_5^{S374A} results in slower decaying sIPSCs in hippocampal neurons.
Bars represent the mean values of sIPSC **(A)** frequency (Hz), **(B)** amplitude (pA), **(C)** weighted tau decay time (ms) and **(D)** rise time (ms) and are shown in green for eGFP, black for wild-type α_5, red for the phospho-null α_5^{S374A} and blue for the phospho-mimetic α_5^{S374D} expressing neurons. Points represent mean values calculated for individual cells. sIPSC frequency and amplitude: eGFP n=11, α_5 n=9, α_5^{S374A} n=18, α_5^{S374D} n=10; sIPSC decay and rise time: eGFP n=10, α_5 n=9, α_5^{S374A} n=14, α_5^{S374D} n=8. Error bars represent SEM. $*\ p<0.05$, $***\ p<0.001$ one-way ANOVA followed by Tukey's multiple comparisons test. **(E)** Example sIPSC recordings and **(F)** mean peak-scaled IPSCs from representative GFP, α_5, α_5^{S374A} and α_5^{S374D} transfected cells.

4.2.2 L-655,708 blocks large-amplitude IPSCs in hippocampal neurons

To further investigate the synaptic effects seen with the α_5 subunit variants in the previous experiment, I used the α_5 subunit-selective partial inverse agonist L-655,708 (L655) to selectively inhibit these receptors. Recordings were made from cultured hippocampal neurons transfected with either eGFP, wild-type α_5, mutant α_5^{S374A} or α_5^{S374D} constructs as before. After a $\sim$15 min period of stable control recordings, L-655,708 (50 nM, IC_{50} 0.4 nM, Manzo et al 2021) was bath-applied and sIPSCs detected in the presence of L-655,708 were compared with control sIPSCs obtained before drug application in the same cell. I analysed sIPSC mean frequency and amplitude, as well as mean IPSC decay and rise times. Two-way repeated-measures (RM) ANOVA results indicate a significant overall effect of L-655,708 treatment (p=0.0170) but no overall effect of the transfected construct (p=0.4120) on the mean sIPSC frequency. A clear trend for a reduction of sIPSC frequency by L-655,708 was noted for all α_5 transfected neurons (wt, α_5^{S374A}, α_5^{S374D}), but not for eGFP (no drug vs. L-655,708; eGFP: 1.67 $\pm$ 0.42 vs. 1.83 $\pm$ 0.95 Hz, α_5: 1.58 $\pm$ 0.25 vs. 0.77 $\pm$ 0.17 Hz, α_5^{S374A}: 1.10 $\pm$ 0.38 vs. 0.68 $\pm$ 0.18 Hz, α_5^{S374D}: 1.97 $\pm$ 0.66 vs. 1.10 $\pm$ 0.57 Hz; Figure 4.2A). However, none of the individual pairwise comparisons were considered significant after correction for multiple comparisons. Interestingly, L-655,708 did not affect the mean sIPSC frequency in eGFP transfected control cells. Although, there were no significant effects of L-655,708 on mean sIPSC amplitudes, I noticed a trend for reduction of sIPSC amplitudes in neurons transfected with α_5^{S374A} and α_5^{S374D} (no drug vs.

L-655,708; α_5^{S374A}: -142.7 $\pm$ 49.27 vs. -74.16 $\pm$ 15.29 pA; α_5^{S374D}: -146.2 $\pm$ 71.15 vs. -73.97 $\pm$ 30.72 pA; two-way RM ANOVA, drug effect p=0.1440, transfected construct effect p=0.9899; Figure 4.2B). All results from this section are summarised in Table 4.1. Taken together, these data provide evidence that L-655,708 reduces sIPSC frequency and may also affect amplitude suggesting the involvement of synaptic α_5-GABA$_A$Rs.

The impact of L-655,708 on IPSC decay and rise times was assessed by examination of clean profile IPSC events as before. A two-way RM ANOVA analysis data revealed a significant overall effect of transfected construct on mean IPSC decay (p=0.0272); however, none of the individual pairwise comparisons reached significance after correction for multiple comparisons (Figure 4.2C). This result likely reflects the prolonged sIPSC decay time caused by transfection with α_5^{S374A} (Figure 4.1C). L-655,708 did not affect the mean IPSC decay time constants (overall drug effect p=0.6618) or rise times (overall drug effect p=0.8724, Figure 4.2D) in any of the transfected cell groups. All results from this section are summarised in Table 4.2.

Table 4.1: L-655,708 decreases mean sIPSC frequency in wild-type and mutated α_5 transfected neurons.
Summary of sIPSC frequency (Hz) and amplitude (pA) values (mean $\pm$ SEM) in control conditions and in the presence of 50 nM L-655,708. L-655,708 reduced the mean sIPSC frequency in wild-type and mutant α_5 but not in eGFP transfected neurons (two-way RM ANOVA: drug effect p=0.017, transfected construct effect alone p=0.412; followed by Sidak's multiple comparisons test). There were no significant changes in mean sIPSC amplitude in any transfection group (two-way RM ANOVA: drug effect p=0.1440, transfected construct effect p=0.9899).

Transfected with	Number of cells	Treatment	sIPSCs frequency (Hz)	sIPSCs amplitude (pA)
eGFP	4	N/A	1.67 $\pm$ 0.42	-110.5 $\pm$ 17.07
		L-655,708	1.83 $\pm$ 0.95	-128.4 $\pm$ 23.17
α_5	6	N/A	1.58 $\pm$ 0.25	-99.58 $\pm$ 23.49
		L-655,708	0.77 $\pm$ 0.17	-100.1 $\pm$ 30.37
α_5^{S374A}	11	N/A	1.10 $\pm$ 0.38	-142.7 $\pm$ 49.27
		L-655,708	0.68 $\pm$ 0.18	-74.16 $\pm$ 15.29
α_5^{S374D}	5	N/A	1.97 $\pm$ 0.66	-146.2 $\pm$ 71.15
		L-655,708	1.10 $\pm$ 0.57	-73.97 $\pm$ 30.72

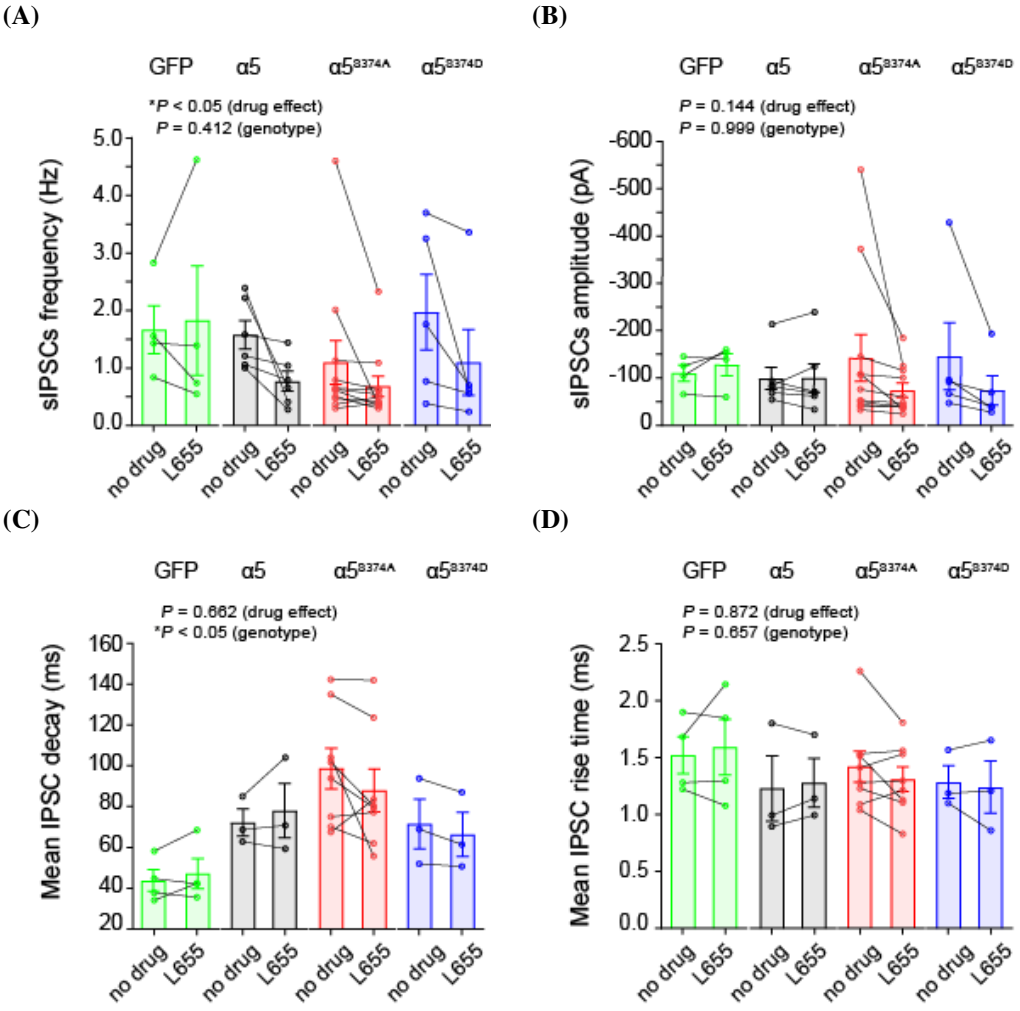

Figure 4.2: L-655,708 reduces the mean sIPSC frequency of wild-type and mutated α_5 transfected neurons.

Bars represent the mean values of sIPSC **(A)** frequency (Hz), **(B)** amplitude (pA), **(C)** decay time (ms) and **(D)** rise time (ms) and are shown in green for eGFP, black for wild-type α_5, red for the phospho-null α_5^{S374A} and blue for phospho-mimetic α_5^{S374D} expressing neurons. Points represent mean values calculated for individual cells and are linked for 'no drug' treatment and L-655,708 data points, recorded from the same cells. Mean sIPSC frequency and amplitude: eGFP n=4, α_5 n=6, α_5^{S374A} n=11, α_5^{S374D} n=5; mean IPSC decay and rise time: eGFP n=4, α_5 n=3, α_5^{S374A} n=8, α_5^{S374D} n=3. Error bars represent SEM. $*$ $p<0.05$, two-way RM ANOVA followed by Sidak's multiple comparisons test.

Table 4.2: L-655,708 does not affect mean sIPSC decay or rise times.
Summary of the mean IPSC decay (ms) and rise time (ms) values (mean ± SEM) in control conditions and in the presence of 50 nM L-655,708. L-655,708 did not affect mean IPSC decay or rise time values. Two-way RM ANOVA decay: drug effect p=0.662, transfected construct effect p=0.027; rise time: drug effect p=0.872, transfected construct effect p=0.657; followed by Sidak's multiple comparisons test.

Transfected with	Number of cells	Treatment	Mean IPSCs decay (ms)	Mean IPSCs rise time (ms)
eGFP	4	N/A	43.7 ± 5.3	1.5 ± 0.2
		L-655,708	47.1 ± 7.3	1.6 ± 0.3
α_5	3	N/A	72.2 ± 6.6	1.2 ± 0.3
		L-655,708	78.0 ± 13.4	1.3 ± 0.2
α_5^{S374A}	8	N/A	98.7 ± 10.0	1.4 ± 0.1
		L-655,708	88.0 ± 10.5	1.3 ± 0.1
α_5^{S374D}	3	N/A	71.6 ± 12.2	1.3 ± 0.1
		L-655,708	66.4 ± 10.8	1.2 ± 0.2

To further examine the reduction in mean sIPSC amplitudes, I combined all events from one transfection group before and after drug application and visualised the results using relative frequency plots (Figure 4.3). First, I noticed that both mutants, α_5^{S374A} (Figure 4.3C) and α_5^{S374D} (Figure 4.3D), had more large amplitude sIPSCs compared to wild-type (Figure 4.3B) and eGFP (Figure 4.3A) transfected neurons. Secondly, L-655,708 reduced the amplitude of the large-amplitude synaptic events in α_5^{S374A} and α_5^{S374D} and not in wild-type and eGFP transfected neurons. Finally, in each transfection group, sIPSCs with amplitudes 0 to -100 pA accounted for the majority (>70%) of all events (eGFP: 82.8%, α_5: 78.9%, α_5^{S374A}: 74.7%, α_5^{S374D}: 69.9%).

To quantify the observed differences in the effects of L-655,708 on different amplitude GABA synaptic currents, I subdivided the sIPSCs into small- and large-amplitude groups. First, I fitted amplitude distributions to the pooled sIPSCs in each transfection group under control conditions with the sum of three (eGFP, α_5^{S374A}, α_5^{S374D}) or four (α_5) Gaussian functions (Figure 4.4. Then, I evaluated the three parameters characterizing each individual component (A, amplitude; x, peak; c, peak centre; w, half-amplitude width). Our goal was to find one cut-off amplitude for all transfection groups that includes most of the data that had been fitted with the sum

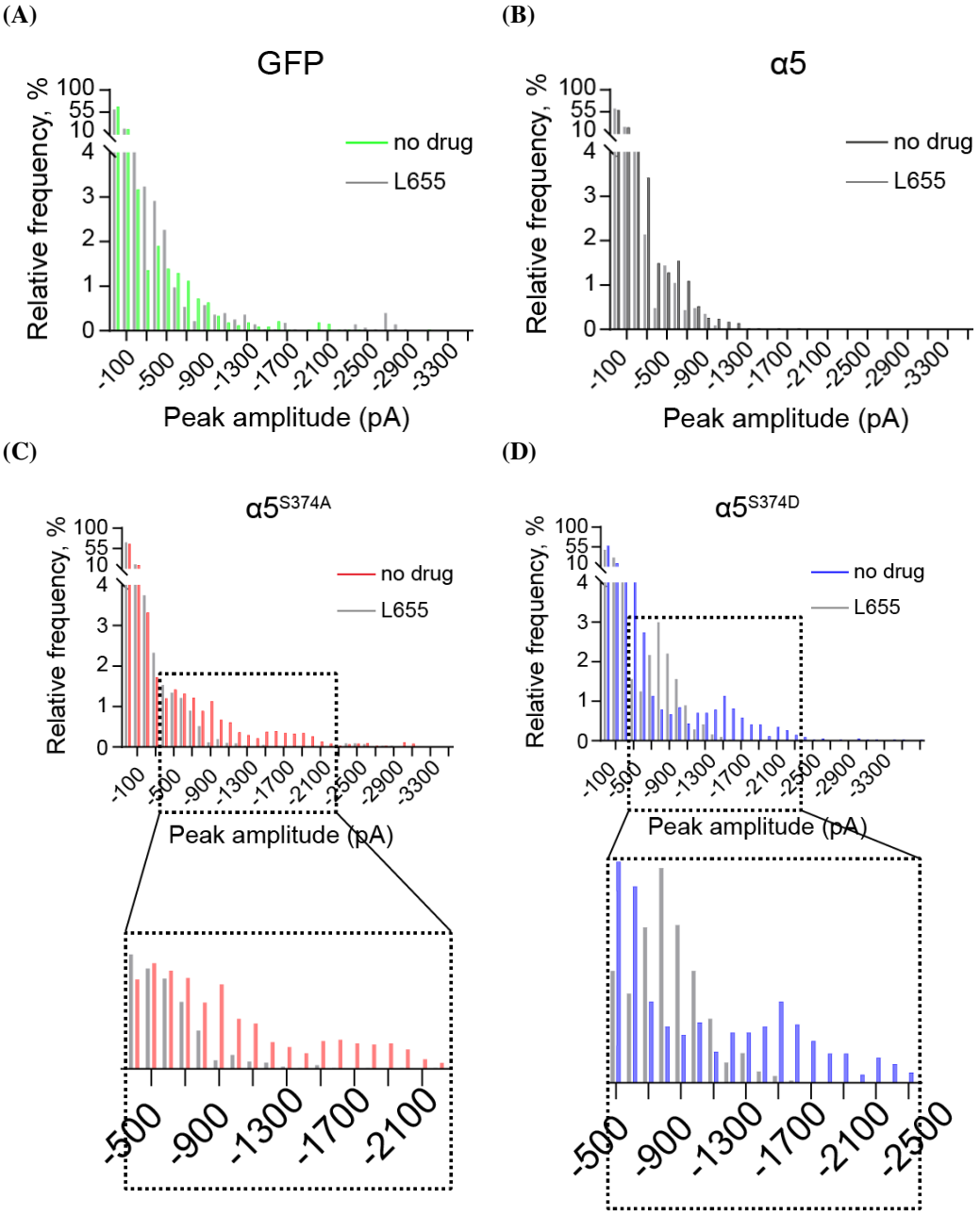

Figure 4.3: L-655,708 reduces the number of the largest amplitude sIPSCs in α_5^{S374A} and α_5^{S374D} transfected neurons.

Relative frequency plots for all sIPSC amplitudes recorded from **(A)** eGFP (n=4, green), **(B)** α_5 (n=6, black), **(C)** α_5^{S374A} (n=11, red) and **(D)** α_5^{S374D} (n=5, blue) transfected neurons. Coloured bars on the relative frequency plots represent the amplitude distributions under control conditions and grey bars reflect the presence of L-655,708. Selected areas on the α_5^{S374A} and α_5^{S374D} plots are shown zoomed in to emphasise the range of sIPSC amplitudes where L-655,708 seemed to have the largest effect.

of Gaussian functions. The relative frequency distributions of the largest amplitude sIPSCs were too low and spread to be adequately fit by a Gaussian function, thus I put these events into one group. Based on the peak centre and width of the third component (GFP peak c3=-51.57 $\pm$ 1.68 pA, w3=39.42 $\pm$ 1.76 pA, Figure 4.4A; α_5: peak c3=-42.51 $\pm$ 2.52 pA, w3=29.08 $\pm$ 3.01 pA, Figure 4.4B; α_5^{S374A}: peak c3=-78.89 $\pm$ 6.45 pA, w3=63.56 $\pm$ 7.97 pA, Figure 4.4C; α_5^{S374D}: peak c=-68.55 $\pm$ 3.58 pA, w3=65.26 $\pm$ 4.72 pA, Figure 4.4D), I defined small-amplitude sIPSCs with an absolute peak amplitude up to 100 pA and the remaining sIPSCs of $>$100pA as large-amplitude sIPSCs. Interestingly, I noticed that α_5 transfected neurons had a fourth group of sIPSCs: GABA currents with a larger amplitude (peak c4=-101.57 $\pm$ 8.26 pA, w4=157.37 $\pm$ 11.27 pA). However, as other transfection groups lacked the fourth component, I classified these events under the 'large-amplitude' category.

After sub-dividing the sIPSC-s, the data were re-analysed for control conditions and in the presence of L-655,708 to evaluate the drug effects on sIPSC frequency and amplitude in both (large and small) amplitude groups. L-655,708 affected the frequency of small- and large-amplitude sIPSCs similarly: eGFP transfected neurons were unaffected while the mean frequency of sIPSCs was reduced in wild-type and mutated α_5 transfected neurons (two-way RM ANOVA p=0.0224 drug effect for small-amplitude GABA currents, p=0.0589 drug effect for large-amplitude events; no statistically significant transfected construct effects; none of the individual pairwise comparisons reached significance after correction for multiple comparisons; Figures 4.5A and 4.5B).

Next, I reanalysed the sIPSC mean amplitudes to further investigate the trend in reduction caused by L-655,708 seen in α_5^{S374A} and α_5^{S374D} transfected neurons. First, I examined the small-amplitude events for each group by comparing the mean value of amplitudes (Figure 4.6A) and using cumulative probability plots obtained by pooling data from all cells in each group with or without L-655,708 treatment (Figure 4.6C). As expected, applying L-655,708 did not affect mean amplitudes for small IPSCs in any transfected cell group (Figures 4.6A-4.6C). By contrast, L-655,708 significantly reduced the mean amplitude of large-IPSCs in α_5^{S374A} and

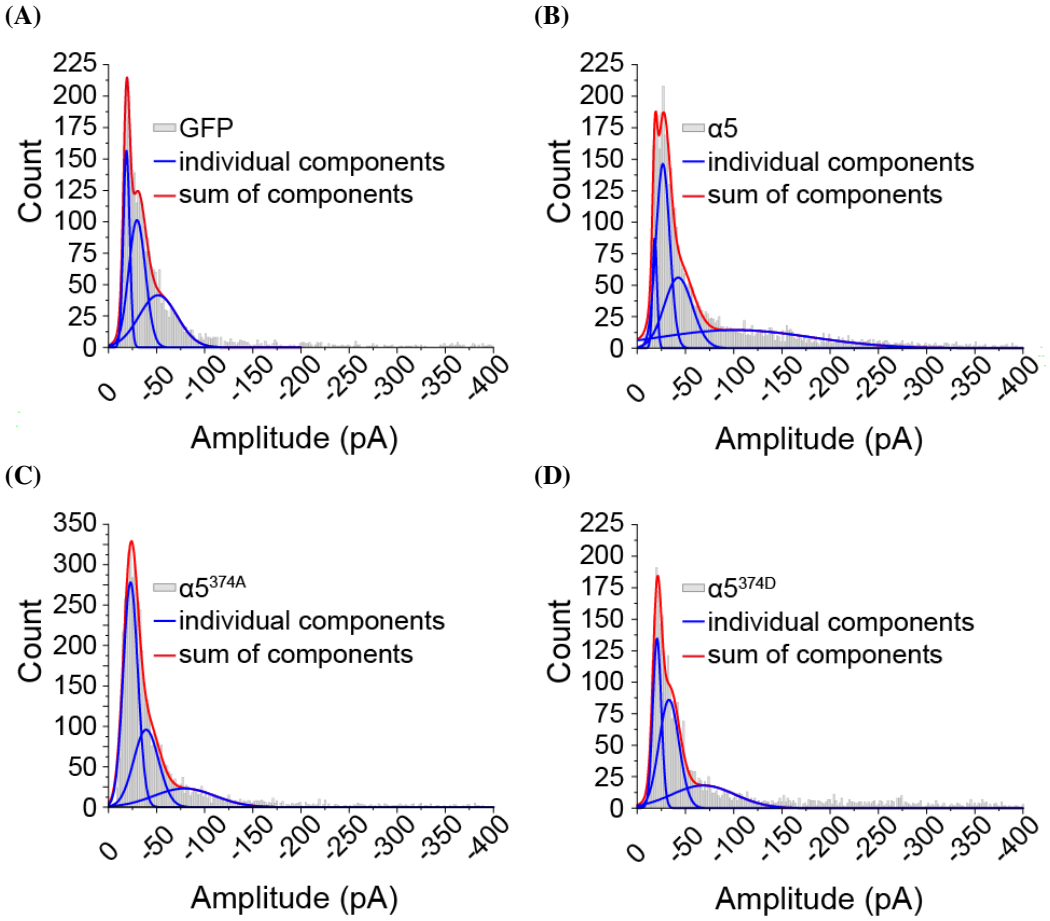

Figure 4.4: sIPSCs segregate into small- and large-amplitude groups.
The sIPSC amplitude distributions for pooled data from **(A)** eGFP (n=4), **(B)** α_5 (n=6), **(C)** α_5^{S374A} (n=11) and **(D)** α_5^{S374D} (n=5) transfected neurons are fitted with the sum of three or four Gaussian functions. Blue lines show individual component fits, red lines the sum of the three or four components. Grey bars represent the amplitude distributions.

α_5^{S374D} transfected neurons (no drug vs. L-655,708, α_5^{S374A}: -452.7 $\pm$ 117.6 pA vs. -284.4 $\pm$ 65.66 pA; α_5^{S374D}: -455.7 $\pm$ 79.86 pA vs. -235.4 $\pm$ 38.08 pA; two-way ANOVA: drug effect p=0.0025, transfected construct effect p=0.3860; followed by Sidak's multiple comparisons test: α_5^{S374A} adjusted p=0.0127, α_5^{S374D} adjusted p=0.0313; Figures 4.7A-4.7C). Based on this result I concluded that both mutants significantly contributed to large-amplitude synaptic currents. All the results from this section are shown together in Table 4.3.

To summarize, these results indicate that L-655,708 has pre- and postsynaptic effects by reducing the frequency and amplitude of sIPSCs. Interestingly, L-655,708 appears to cause a selective reduction in large amplitude sIPSCs and only

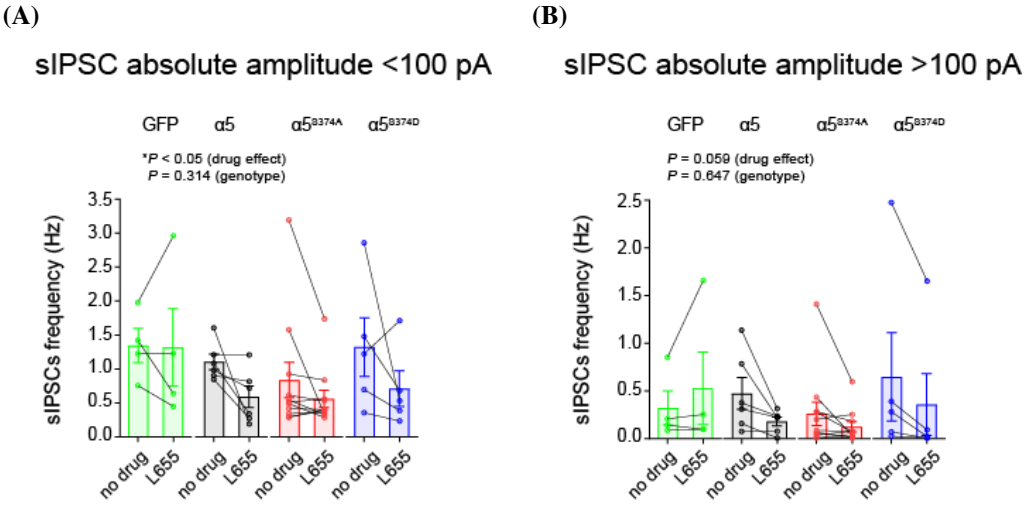

Figure 4.5: L-655,708 reduces the mean frequency of small- and large-amplitude IPSCs in wild-type and mutated α_5 transfected neurons similarly.
Bars represent the mean values for frequency (Hz) of **(A)** small amplitude and **(B)** large-amplitude sIPSCs and are shown in green for eGFP (n=4), black for wild-type α_5 (n=6), red for phospho-null α_5^{S374A} (n=11) and in blue for phospho-mimetic α_5^{S374D} (n=5) transfected neurons. Points represent mean values calculated for individual cells and are linked for no treatment and L-655,708 data points as these were recorded from the same cell. Error bars represent SEM. $*$ $p<0.05$, two-way RM ANOVA followed by Sidak's multiple comparisons test.

in cells transfected with α_5^{S374A} and α_5^{S374D}. Small amplitude sIPSCs were unaffected by L-655,708 in all transfected groups. These results further support the notion that α_5 receptors contribute to large-amplitude inhibitory synaptic currents.

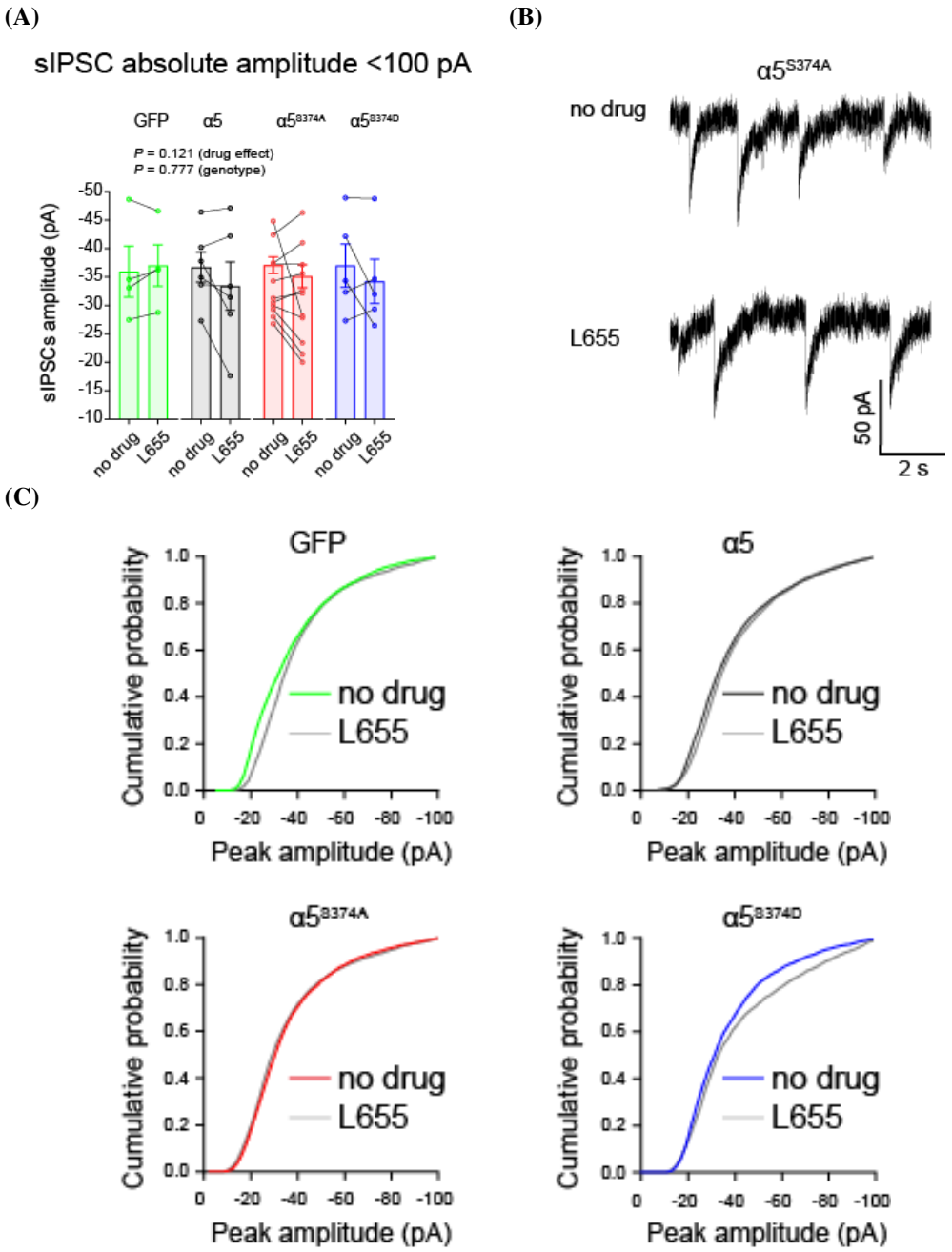

Figure 4.6: L-655,708 does not affect the mean amplitude of small sIPSCs.
(A) Bars represent the mean values of amplitude of small-amplitude sIPSCs and are shown in green for eGFP (n=4), black for wild-type α_5 (n=6), red for phospho-null α_5^{S374A} (n=11) and in blue for phospho-mimetic α_5^{S374D} (n=5) transfected neurons. Points represent mean values calculated for individual cells and are linked for no treatment and L-655,708 data points as these were recorded from the same cell. Error bars represent SEM. No statistically significant changes according to two-way RM ANOVA test. **(C)** All sIPSCs from all cells in one transfected group were pooled and analysed using cumulative probability plots. **(B)** Example recordings for small-amplitude sIPSCs.

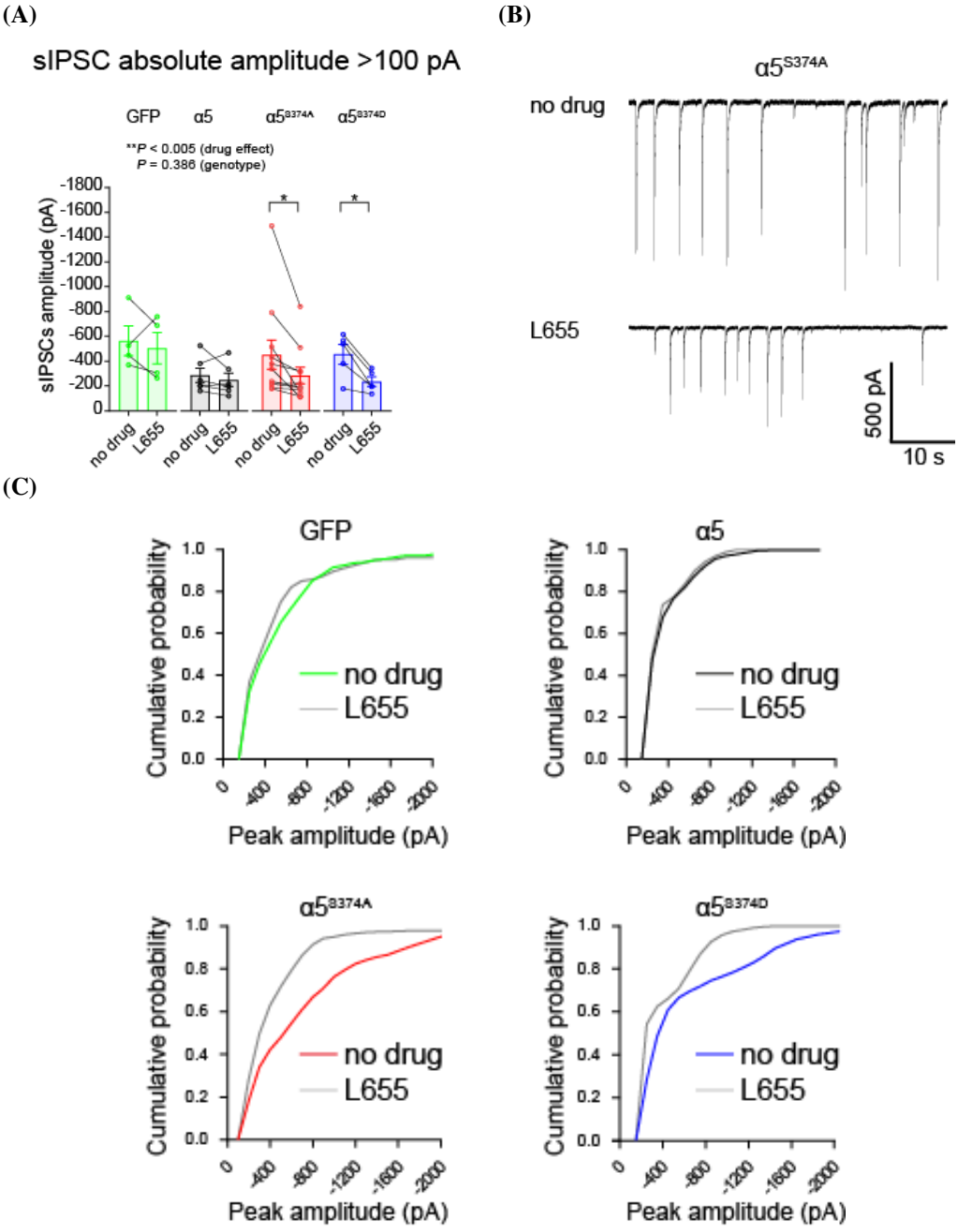

Figure 4.7: L-655,708 significantly reduces the mean amplitude of large sIPSCs in α_5^{S374A} and α_5^{S374D} transfected neurons.

(A) Bars represent the mean values of amplitude of large-amplitude sIPSCs and are shown in green for eGFP (n=4), black for wild-type α_5 (n=6), red for phospho-null α_5^{S374A} (n=11) and in blue for phospho-mimetic α_5^{S374D} (n=5) transfected neurons. Points represent mean values calculated for individual cells and are linked for no treatment and L-655,708 data points as these were recorded from the same cell. Error bars represent SEM. $*$ $p<0.05$, $**$ $p<0.005$ two-way RM ANOVA followed by Sidak's multiple comparisons test. **(C)** All sIPSCs from all cells in one transfected group were pooled and analysed using cumulative probability plots. **(B)** Example recordings for large-amplitude sIPSCs

Table 4.3: L-655,708 decreases mean amplitude of large-amplitude sIPSCs in α_5^{S374A} and α_5^{S374D} transfected neurons.
Summary of sIPSC frequency (Hz) and amplitude (pA) values (mean ± SEM) before and after applying L-655,708. Application of L-655,708 significantly reduced the sIPSC mean frequency in wild-type and mutant α_5 transfected neurons similarly. Two-way RM ANOVA: small-amplitude currents, drug effect p=0.022, transfected construct effect p=0.314; large-amplitude currents, drug effect p=0.059, transfected construct effect p=0.647; followed by Sidak's multiple comparisons test. L-655,708 significantly reduced the mean amplitude of large-amplitude sIPSCs in α_5^{S374A} and α_5^{S374D} transfected neurons. Two-way RM ANOVA: large-amplitude currents, drug effect p=0.003, transfected construct effect p=0.386; followed by Sidak's multiple comparisons test: α_5^{S374A} adjusted p=0.013, α_5^{S374D} adjusted p=0.031.

Transfected with	Number of cells	Treatment	Small-amplitude GABA currents		Large-amplitude GABA currents	
			sIPSCs frequency (Hz)	sIPSCs amplitude (pA)	sIPSCs frequency (Hz)	sIPSCs amplitude (pA)
eGFP	4	N/A	1.34 ± 0.25	-35.97 ± 4.50	0.32 ± 0.18	-564.1 ± 120.2
		L-655,708	1.32 ± 0.57	-37.03 ± 3.67	0.52 ± 0.38	-504.2 ± 127.7
α_5	6	N/A	1.10 ± 0.11	-36.73 ± 2.64	0.47 ± 0.17	-286.3 ± 57.03
		L-655,708	0.59 ± 0.16	-33.39 ± 4.23	0.18 ± 0.05	-250.1 ± 52.70
α_5^{S374A}	11	N/A	0.84 ± 0.26	-33.85 ± 1.80	0.26 ± 0.12	-452.7 ± 117.6
		L-655,708	0.56 ± 0.13	-31.45 ± 2.49	0.12 ± 0.05	-284.4 ± 65.66
α_5^{S374D}	5	N/A	1.32 ± 0.43	-37.02 ± 3.82	0.65 ± 0.46	-455.7 ± 79.86
		L-655,708	0.71 ± 0.26	-34.26 ± 3.88	0.36 ± 0.32	-235.4 ± 38.08

4.2.3 Competition for gephyrin binding leads to faster sIPSC decays in α_5^{S374A} transfected cells

Based on previous research that synaptic α_5-$GABA_A$Rs exhibit large-amplitude and slowly decaying synaptic GABA currents (Zarnowska et al., 2009), I hypothesized that an increased sIPSC decay time constant and more large-amplitude synaptic events for α_5^{S374A} transfected cells may represent an increased synaptic accumulation of α_5^{S374A}-$GABA_A$Rs (Figure 4.8B). To investigate this hypothesis, I designed a small blocking peptide that mimics the gephyrin binding domain sequence on the α_5 subunit to disrupt the interaction between α_5-$GABA_A$Rs and this important synaptic scaffold protein (sequences and modifications of peptides are described in Section 2.5.4) (Figure 4.8A). As a control, I also designed a scrambled version of the peptide. I postulated that the blocking peptide would prevent the localization of α_5^{S374A}-$GABA_A$Rs at inhibitory synapses by competing with the receptors' intracellular domain for the binding site on gephyrin (Figure 4.8C), whereas the scrambled peptide would not (Figure 4.8D). Using a competitive peptide to block the interaction between two proteins is a common technique used in $GABA_A$Rs research (Brandon et al., 2002b; Maric et al., 2017; Shen et al., 2019; Weltzien et al., 2012).

The peptides were dissolved in the patch pipette solution for intracellular delivery, and sIPSCs recorded over time. The presence of 30 μM blocking peptide, but not an equivalent concentration of the scrambled peptide, decreased sIPSC decay times in neurons expressing the α_5^{S374A} mutant (scrambled vs. blocking peptide: 76.33 ± 6.51 ms vs. 45.18 ± 4.90 ms; two-tailed unpaired t-test p=0.0034; Figure 4.9B). Mean sIPSC amplitude (scrambled vs. blocking peptide: -67.23 ± 17.94 pA vs. -92.02 ± 32.56 pA; two-tailed unpaired t-test p=0.5199; Figure 4.9A) and IPSC rise time (scrambled vs. blocking peptide: 1.75 ± 0.08 ms vs. 1.68 ± 0.17 ms; two-tailed unpaired t-test p=0.7288; Figure 4.9C) were unaffected by the blocking peptide.

By examining all synaptic GABA currents recorded from cells internally-perfused with either blocking or scrambled peptide, I noticed those with the block-

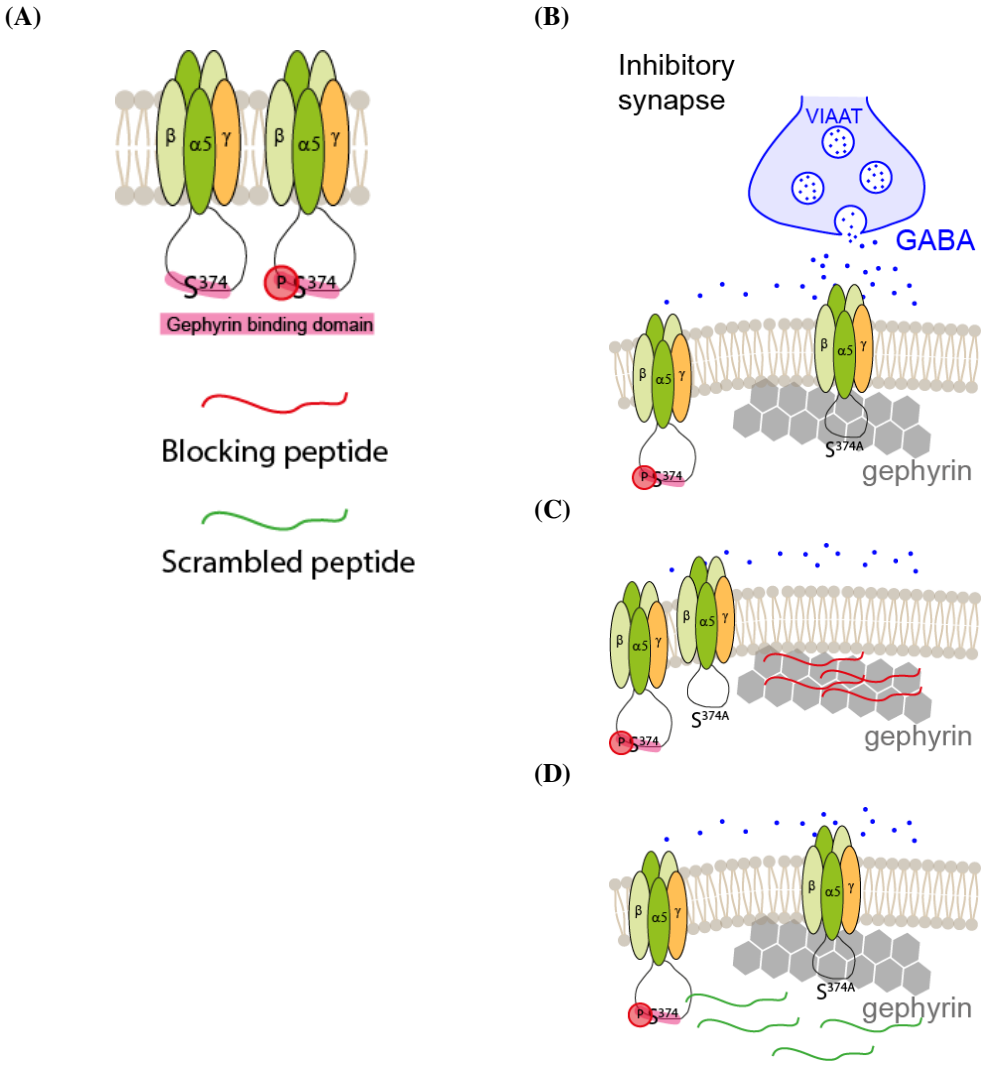

Figure 4.8: Schematic explaining the strategy with blocking peptide.
(A) Mass-spectrometry experiments showed that α_5^{S374}, a residue located in the gephyrin binding domain, exists in both phosphorylated and unphosphorylated forms. Based on the amino acid sequence of the gephyrin binding domain in the wild-type α_5 subunit, I designed a blocking peptide to act as a binding competitor, as well as a scrambled version of the same peptide. **(B)** I hypothesized that the increased decay time constant seen with sIPSCs recorded from α_5^{S374} transfected neurons may indicate increased synaptic accumulation of α_5^{S374A}-$GABA_A$Rs following interaction with gephyrin. **(C)** If this hypothesis is true, then I would expect this effect to be reversed by the blocking peptide, i.e., a faster decay rate. **(D)** In contrast, the scrambled peptide should not disturb the interaction between α_5^{S374A}-$GABA_A$Rs and gephyrin at inhibitory synapses.

ing peptide had less large-amplitude GABA currents (Figure 4.9E). However, subdividing the sIPSCs into small (< 100 pA, scrambled vs. blocking peptide: -26.15 ± 2.78 pA vs. -31.29 ± 2.34 pA; two-tailed unpaired t-test p=0.1874) and large (> 100 pA, scrambled vs. blocking peptide: -291.9 ± 72.15 pA vs. -232.2 ± 39.64 pA; two-tailed unpaired t-test p=0.4847) amplitude groups did not reveal any significant changes to mean sIPSCs amplitudes (Figure 4.9D and 4.9E). From these experiments, I concluded that the increased decay time constant of α_5^{S374A} transfected cells was most likely caused by increased synaptic accumulation of α_5-$GABA_A$Rs.

4.2.4 L-655,708 blocks tonic GABA current in neurons expressing all α_5 subunit variants

The preceding experiments with L-655,708 focused on synaptic $GABA_A$R, but it is also important to see if mutating α_5^{S374} affects tonic inhibition mediated by extrasynaptically located α_5-$GABA_A$Rs. To investigate GABA-mediated tonic currents, I first applied L-655,708 (50 nM) to measure the shift in the holding current revealing an estimate of the α_5-$GABA_A$R supported tonic current. Next, I applied a saturating concentration of the $GABA_A$R antagonist picrotoxin (100 μM, PTX) in the continued presence of L-655,708, to reveal any remaining tonic current mediated by unblocked α_5 and other $GABA_A$R subtypes, for example δ- subunit containing $GABA_A$Rs (Figures 4.10A to 4.10B).

Notably, for α_5 and α_5^{S374A} transfected neurons, significantly less total tonic current was evident when compared to eGFP expressing control cells (tonic blocked by L-655,708 + PTX, eGFP: 41 ± 8 pA, α_5: 19 ± 3 pA, α_5^{S374A}: 19 ± 3 pA, α_5^{S374D}: 32 ± 6 pA; one-way ANOVA p=0.0073; Tukey's multiple comparisons test, eGFP vs. α_5 adjusted p=0.0312, eGFP vs. α_5^{S374A} adjusted p=0.0196). A similar outcome was evident when applying just the α_5 selective inhibitor (tonic blocked by L-655,708 only, eGFP: 21.16 ± 7.70 pA, α_5: 5.73 ± 2.55 pA, α_5^{S374A}: 5.63 ± 1.59 pA, α_5^{S374D}: 8.20 ± 1.60 pA; one-way ANOVA p=0.0136; Tukey's multiple comparisons test, eGFP vs. α_5 adjusted p=0.0296, eGFP vs. α_5^{S374A} adjusted p=0.0114; Figure 4.10C). The proportion of the total tonic current that was sensitive to L-655,708 was very similar between transfections, indicating compara-

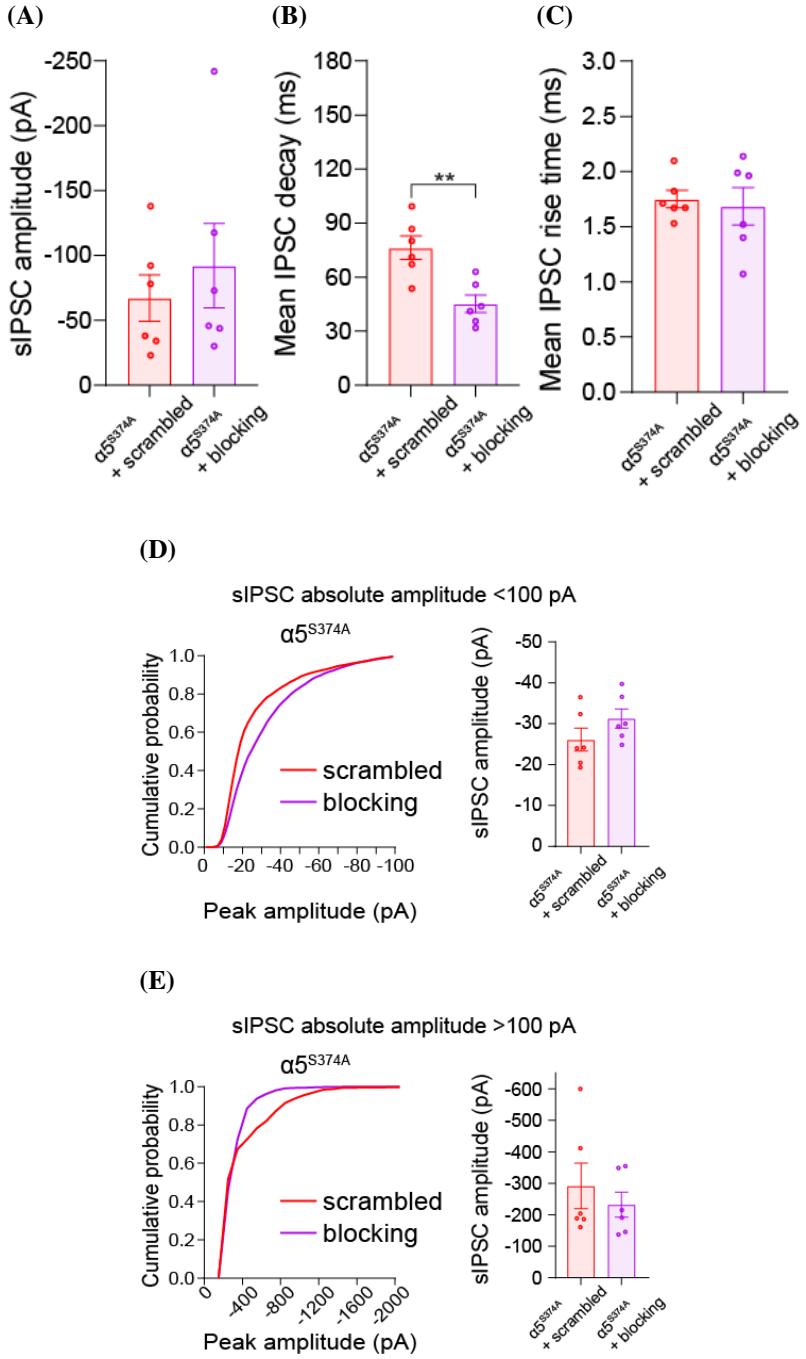

Figure 4.9: Blocking peptide reduces the decay time constant in α_5^{S374A} transfected neurons.

Bars represent the mean values of **(A)** sIPSC amplitude, **(B)** sIPSC decay and **(C)** rise times, **(D)** amplitude of small-amplitude and **(E)** large-amplitude IPSCs and are shown in red for α_5^{S374A} with the scrambled peptide (n=6) and purple for α_5^{S374A} with the blocking peptide (n=6) transfected neurons. Points represent mean values calculated for individual cells. Error bars represent SEM. $**$ $p<0.005$ two-tailed unpaired t-test. Cumulative probability plots for **(D)** small-amplitude and **(E)** large-amplitude sIPSCs.

ble contributions of extrasynaptic α_5-GABA$_A$Rs to tonic inhibition ($\sim$ 30%, Figure 4.10D). I concluded that mutating α_5^{S374} does not affect the tonic current mediated by α_5-GABA$_A$Rs.

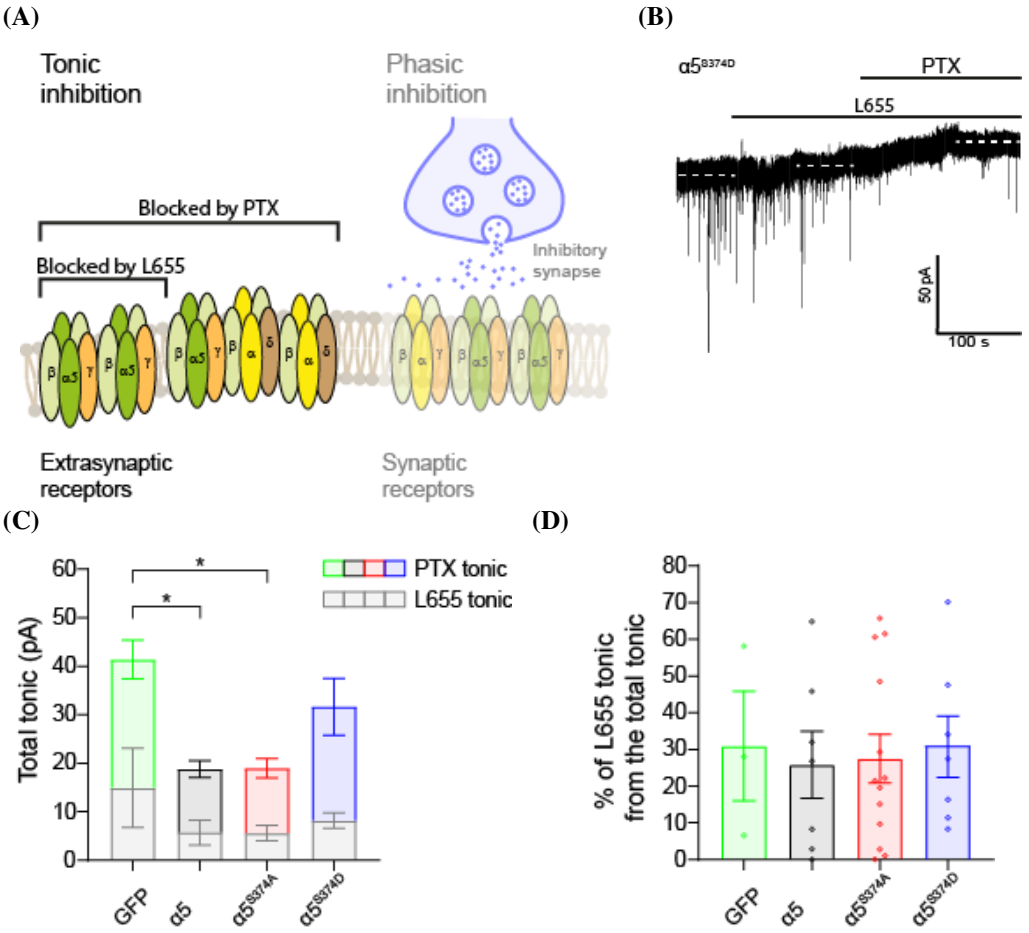

Figure 4.10: Expressing α_5 and α_5^{S374A} in neurons significantly reduces tonic current. **(A)** Schematic of GABA$_A$R isoforms blocked by 50 nM L-655,708 and 100 μM PTX. The selective partial inverse agonist L-655,708 only blocks a subset of α_5 containing GABA$_A$Rs, whilst PTX blocks tonic inhibition mediated by all GABA$_A$R subtypes. **(B)** Representative example membrane current recording for an α_5^{S374D} expressing cell showing a two-step block by first L-655,708 and then PTX. **(C)** Coloured bars represent total tonic (L-655,708+PTX) and grey bars represent tonic current blocked just by L-655,708. **(D)** Bars represent the percentage of the total tonic current sensitive to L-655,708. Bars are shown in green for eGFP (n=3), black for wild-type α_5 (n=7), red for phospho-null α_5^{S374A} (n=13) and in blue for phospho-mimetic α_5^{S374D} (n=7) transfected neurons. Points represent mean values calculated for individual cells. Error bars on both figures represent SEM. $*$ $p<0.05$ one-way ANOVA followed by Tukey's multiple comparisons test.

4.3 Discussion

Each $GABA_AR$ subtype, which corresponds to a specific subunit composition, differ in their electrophysiology and pharmacology (Mortensen et al., 2011). Although each GABAergic synapse likely comprises several different subtypes of $GABA_ARs$, collectively shaping sIPSCs (Kasugai et al., 2010), knowledge of receptor properties provides an opportunity to isolate and identify the components of GABAergic inhibition that originate from one particular subtype. In this chapter, I explored the functional effects of mutating $\alpha_5{}^{S374}$ on α_5-$GABA_AR$ mediated inhibitory transmission.

First, I examined the pre-and postsynaptic effects of S^{374} by comparing mean sIPSC frequency and amplitude respectively, for α_5 subunit expressing neurons. As there were no significant changes to either parameter, I concluded that mutation of residue $\alpha_5{}^{S374}$ does not regulate the neurotransmitter release or the mean number of $GABA_ARs$ at synapses. Instead, I demonstrated that the residue $\alpha_5{}^{S374}$ affects the combination of $GABA_ARs$ subtypes present at synapses as the mean IPSC decay time constant was significantly longer for $\alpha_5{}^{S374A}$ compared to wild-type α_5 transfected neurons. Previous research has shown a direct link between slower IPSC decay times and the increased presence of synaptic α_5-$GABA_ARs$ (Cao et al., 2020; Magnin et al., 2019; Salesse et al., 2011). Our previous experiments using heterologous expression of recombinant receptors in HEK cells demonstrated that mutating residue $\alpha_5{}^{S374}$ does not appear to affect macroscopic receptor desensitisation or deactivation. Therefore I speculate that the alteration in decay kinetics without changes to mean sIPSC amplitudes indicates a re-modelling of $GABA_ARs$ present at the synapse with an accumulation of α_5-$GABA_ARs$ replacing other α subunit-containing $GABA_ARs$ (van Rijnsoever et al., 2005). Thus, I propose that the residue $\alpha_5{}^{S374}$ may control the synaptic accumulation of α_5-$GABA_ARs$.

I used L-655,708 to block α_5-$GABA_ARs$ mediated inhibition to reveal the specific component of synaptic inhibition affected by $\alpha_5{}^{S374}$. Interestingly, L-655,708 caused a reduction in the sIPSC frequency for all α_5 transfected groups compared to eGFP transfected control cells. I speculate that L-655,708 acted via blocking

presynaptic α_5-GABA$_A$Rs (Serwanski et al., 2006) and reduced synaptic release of GABA. However, given our visual observations that transfection efficacy is smaller than 1% (data not shown), it is highly unlikely that presynaptic neurons were also substantially transfected. Thus L-655,708 could have acted via endogenous axonal α_5-GABA$_A$Rs. Recent studies have demonstrated that axonal GABA$_A$Rs, which can be activated by ambient GABA or by an autocrine GABA action, are often depolarising and exhibit excitatory action (Khatri et al., 2019; Kramer et al., 2020; Zorrilla de San Martin et al., 2017). Therefore, blocking presynaptic α_5-GABA$_A$Rs by L-655,708 would reduce the probability of GABA release. As the effect was not present in GFP transfected neurons, I hypothesize that over-expressing any of our α_5 constructs in postsynaptic pyramidal neurons induced some form of activity-dependent short-term inhibitory plasticity on presynaptic interneurons (Kawaguchi, 2019).

Next, I demonstrated that mutating S^{374} to either $\alpha_5{}^{S374A}$ or $\alpha_5{}^{S374D}$ increases the number of large-amplitude GABA currents that could be blocked by L-655,708, whereas small-amplitude events were unaffected by the α_5-NAM. This amplitude-dependent difference in L-655,708 modulation in transfected neurons agrees with previous work by Pearce and colleges where they showed that α_5-GABA$_A$Rs specifically contribute to large-amplitude GABA currents (Zarnowska et al., 2009). The origin of these large-amplitude currents is currently unknown, but I speculate that the largest sIPSCs may arise from spontaneous activity of multiple inhibitory synapses via synchronous possibly multi-vesicular release (Cohen et al., 2008; Ivenshitz and Segal, 2010).

Regarding the sIPSC decay rate, I speculated that sIPSCs would decay faster by blocking a proportion of synaptic α_5-GABA$_A$Rs. However, unexpectedly, application of L-655,708 did not decrease the prolonged IPSC decay phase in $\alpha_5{}^{S374A}$ transfected neurons. This result is in line with recent research showing that L-655,708 has no effect on mIPSCs (Manzo et al., 2021; Nuwer et al., 2021). The possible reason for this could be that insufficient numbers of receptors were blocked by the α_5-NAM due to its efficacy being only $\sim$35-50% in primary hippocampal neuron

cultures combined with the fact that most α_5-GABA$_A$Rs are extrasynaptic in hippocampal pyramidal neurons (Serwanski et al., 2006). Even using transfections, I would expect this scenario to be true due to the limited space at synaptic sites compared to the vast extrasynaptic area. Other NAMs could be explored to find one that is more efficacious and subunit-selective to block low numbers of synaptic α_5-GABA$_A$Rs (Hipp et al., 2021). Contrary to the experiments with L-655,708, an alternative strategy, using a blocking peptide to mimic the gephyrin binding domain on the α_5 subunit (Khayenko and Maric, 2019; Maric et al., 2017), successfully reversed the effects caused the α_5^{S374A} mutation on sIPSC decay times. This result supports the hypothesis, from the present study, that α_5^{S374} regulates the gephyrin-dependent synaptic accumulation of α_5-GABA$_A$Rs.

Finally, I investigated the effects of mutating residue α_5^{S374} on tonic inhibition. Interestingly, transfecting neurons with wild-type or α_5^{S374A} constructs significantly reduced the total tonic current compared to eGFP expressing neurons. Comparing the relative percentage of the tonic current sensitive to L-655,708, revealed no differences between the transfection groups. However, given the low efficacy of L-655,708, our results support the previous research which suggests that tonic current in hippocampal pyramidal cells is mediated predominantly by α_5-GABA$_A$Rs with a smaller contribution from other subtypes, for example δ subunit-containing GABA$_A$Rs (δ- GABA$_A$Rs). Moreover, for the *Gabra5 -/-* mouse model, the expression of the δ subunit is upregulated as a likely compensatory mechanism (Glykys and Mody, 2006; Glykys et al., 2008). Therefore, it is possible that the reduction of total tonic current is due to the overexpression of α_5 receptors, which may result in reduced expression of other GABA$_A$Rs subtypes mediating tonic inhibition in these cells.

In conclusion, in this chapter, I transfected cultured rat hippocampal neurons with wild-type α_5, phospho-null α_5^{S374A} or phospho-mimetic α_5^{S374D} constructs and explored the impact of α_5^{S374} on α_5-GABA$_A$R mediated inhibition. I measured sIPSC frequency and amplitude, characterized kinetics of sIPSCs and the level of tonic current in each transfection group. Then, I used the α_5 subtype spe-

cific inverse agonist L-655,708 to block synaptic and tonic currents mediated by α_5-GABA$_A$Rs, and a competitive peptide to block α_5-GABA$_A$R interactions with gephyrin. I showed that α_5^{S374A} prolongs the mean IPSC decay phase and neurons transfected with α_5^{S374A} had more large-amplitude GABA currents, which could be blocked by L-655,708. Furthermore, L-655,708 reduced the frequency of sIPSC in all α_5 transfection groups probably by blocking presynaptic axonal α_5-GABA$_A$R. By using a competitive blocking peptide to interrupt the association of α_5 subunits with gephyrin, I demonstrated that the effects of α_5^{S374A} on the sIPSC decay phase can be reversed by most likely preventing the accumulation of α_5-GABA$_A$Rs at the inhibitory postsynaptic density.

Chapter 5

Phosphorylation of α_5^{S374} regulates the synaptic accumulation of α_5-GABA$_A$Rs

5.1 Introduction

Recording from recombinant GABA$_A$Rs in HEK293 cells and transfected cultured hippocampal neurons strongly suggest that the function and subcellular location of α_5-GABA$_A$Rs are regulated by the residue α_5^{S374} in the large intracellular domain. To enable more accurate mapping of α_5-GABA$_A$R location, three-coloured, three-dimensional structured illumination microscopy (3D SIM) was used (Gustafsson, 2000). Super-resolution 3D-SIM microscopy was chosen over conventional confocal microscopy to characterize the nanoscale organization of the α_5 containing inhibitory synapse as it provides an enhanced resolution of $\sim$120 nm laterally and $\sim$300 nm axially (Crosby et al 2019).

3D SIM is a super-resolution microscopy technique that has been used to examine synapse structure and morphology (Crosby et al., 2019; Hong et al., 2017). This technique is easier to use in three-color and 3D mode compared to other super-resolution techniques previously used to investigate the nanoscale structure of inhibitory synapses such as stimulated emission depletion (STED) microscopy (Crosby et al., 2019; Dzyubenko et al., 2016), stochastic optical reconstruction mi-

croscopy (STORM) (Specht et al., 2013; Yang et al., 2021) or photoactivated localisation microscopy (PALM) (Battaglia et al., 2018; Pennacchietti et al., 2017; Specht et al., 2013). The level of resolution is more than sufficient to resolve individual synaptic compartments (Crosby et al., 2019; Hong et al., 2017). Furthermore, three-coloured SIM is preferred over a two-coloured approach as it permits both, pre-and postsynaptic markers to be used at the same time when imaging $GABA_ARs$.

Cultured hippocampal neurons were transfected at 7DIV with constructs expressing either wild-type α_5 or mutant α_5^{S374A} or α_5^{S374D} $GABA_A$ subunits. The N-terminus of each construct was myc-tagged to distinguish transfected from endogenously expressed α_5 subunits. Neurons were fixed and antibody labelled on day 14 (DIV) and imaged within a month using a Zeiss ELYRA PS.1 microscope at nanoscale resolution. I imaged cell surface α_5-$GABA_ARs$ and intracellular gephyrin clusters on hippocampal neuronal dendrites along with an inhibitory presynaptic marker, vesicular inhibitory amino acid transporter (VIAAT). To identify α_5 clusters colocalising with other synaptic compartments in an unbiased way, a semi-automated object-based 3D colocalization analysis tool, called DiAna, was used (Figure 5.1). DiAna is an ImageJ plugin that offers 3D segmentation for cluster extraction and determines the degree of colocalization and distance between clusters whilst providing quantitative measurements of cluster volume and mean grey value (Gilles et al 2017).

I defined α_5 clusters to be colocalised with another marker if both clusters overlapped. α_5 clusters were considered as synaptic when colocalised with both gephyrin (postsynaptic marker) and VIAAT (presynaptic marker) or with α_1 (postsynaptic marker) and VIAAT clusters (presynaptic marker) at the same time. In all images for the proceeding figures, myc-tagged α_5 clusters are shown in green colour, endogenous gephyrin or α_1-$GABA_ARs$ clusters are red, and VIAAT clusters are shown in blue.

Using a semi-automated analysis pipeline allowed the analysis of large numbers of immunostained clusters. For instance, for the α_5-gephyrin-VIAAT immunostaining, I analysed 1900 α_5, 2900 gephyrin and 1600 VIAAT clusters from

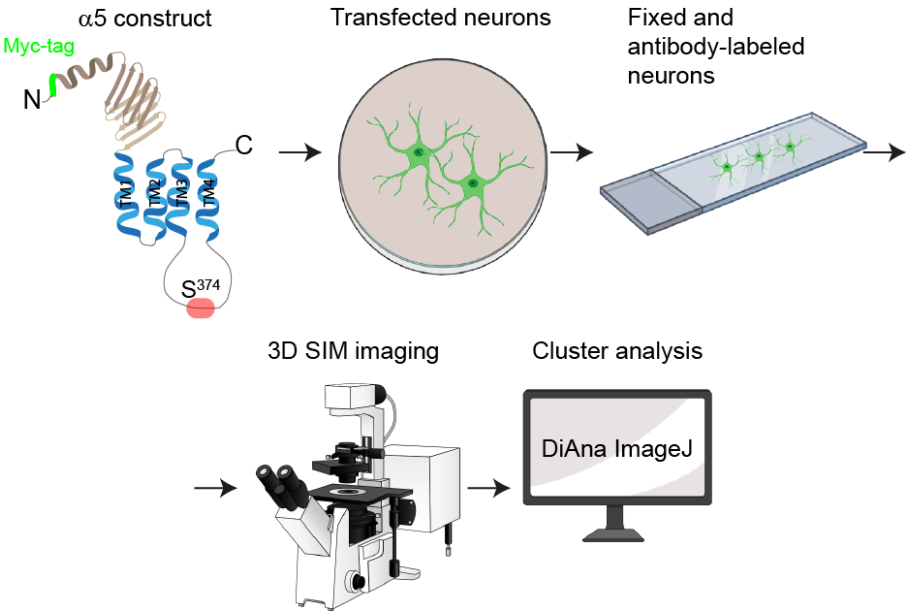

Figure 5.1: Schematic of the imaging workflow.
Constructs expressing myc-tagged wild-type or mutated α_5 subunits were transfected into cultured hippocampal neurons, which were fixed, antibody-labelled, imaged, and the data subsequently analysed. More details are included in Section 2.6

each neuron (18 cells for wild-type α_5, 17 cells for α_5^{S374A} and 18 cells for α_5^{S374D}). For the α_5-α_1-VIAAT imaging, I analysed 3500 α_5 and 2900 α_1 clusters from each untransfected neuron (16 cells), and 3400 α_5, 2500 α_1 and 2000 VIAAT clusters from each transfected neuron (21 cells for wild-type α_5, 19 cells for α_5^{S374A} and 19 cells for α_5^{S374D}). For each cell, mean cluster volumes and mean grey values were determined to characterise changes in the size and brightness of clusters. Both values were measured as previous research has shown that the density of gephyrin proteins can change independently from the cluster size during activity-dependent remodelling of inhibitory synapses (Battaglia et al., 2018; Pennacchietti et al., 2017). For measurements of the density of clusters along dendrites, I analysed dendritic areas of 100–300 μm^2 on each neuron. Previous research has shown that the surface area of a typical inhibitory postsynaptic density ranges between 0.04 and 0.15 μm^2 (Kasugai et al., 2010; Lushnikova et al., 2011; Nusser et al., 1997) and that $GABA_A$Rs and gephyrin clusters located opposite the release site are composed of a small number of receptors, ranging from tens to hundreds (Battaglia et al., 2018; Brickley et al., 1999; Nusser et al., 1997; Specht et al., 2013).

The correct internal organisation of inhibitory synapses is the foundation of efficient synaptic transmission (Yang and Specht, 2019). Recent advances in super-resolution microscopy techniques have demonstrated the higher nanoscale structure of inhibitory synaptic compartments. The large clusters of $GABA_ARs$, gephyrin and VIAAT previously seen by conventional microscopy, can now be resolved into smaller structural units called subsynaptic domains (SSD) (Crosby et al., 2019; Pennacchietti et al., 2017; Yang et al., 2021). One aim of this chapter is to also examine if the residue $\alpha_5{}^{S374}$ affects the number of SSDs. The exact role of a subsynaptic domain is yet to be described, but first insights suggest they may play a role in synaptic efficacy and GABAergic synaptic plasticity (Barberis, 2020; Crosby et al., 2019; Hruska et al., 2018; Pennacchietti et al., 2017). Interestingly, it should be noted that most inhibitory synapses contain only a single SSD with a smaller proportion containing up to 2-6 SSDs (Crosby et al., 2019; Pennacchietti et al., 2017). Thus, this paucity of SSDs suggests their function may be relevant only for the larger postsynaptic densities (Yang and Specht, 2019).

5.2 Results

5.2.1 Residue α_5^{S374} does not affect the mean density, volume, or the brightness of α_5-GABA$_A$ clusters

First, I assessed the effect of mutating residue α_5^{S374} on the surface expression of α_5-GABA$_A$Rs by examining the density (per 1 μm^2) of myc-tagged α_5 clusters along the dendrite as experiments with recombinant receptors in HEK293 cells suggested that there were less α_5^{S374A} receptors on the surface membrane compared to wild-type α_5 transfected cells (Figure 3.5). I also examined the cluster density of the pre- and postsynaptic markers, VIAAT and gephyrin respectively (Figure 5.2A), as I saw a reduction of sIPSC mean frequency in α_5^{S374A} transfected neurons in previous experiments (Figure 4.1A). No changes to the density of endogenous VIAAT clusters were noted in cells expressing α_5 (1.25 $\pm$ 0.19 clusters per 1 μm^2), α_5^{S374A} (1.46 $\pm$ 0.22 clusters per 1 μm^2), or α_5^{S374D} (1.28 $\pm$ 0.12 clusters per 1 μm^2; one-way ANOVA p=0.6838; Figure 5.2B). Gephyrin clusters were also unaffected in α_5 (2.65 $\pm$ 0.26 clusters per 1 μm^2), α_5^{S374A} (2.58 $\pm$ 0.29 clusters per 1 μm^2), or α_5^{S374D} expressing cells (2.43 $\pm$ 0.26 clusters per 1 μm^2; one-way ANOVA p=0.8338; Figure 5.2C). Moreover, the density of transfected myc-tagged α_5 clusters remained constant (α_5: 1.81 $\pm$ 0.14 clusters per 1 μm^2, α_5^{S374A}: 1.62 $\pm$ 0.15 clusters per 1 μm^2, α_5^{S374D}: 1.73 $\pm$ 0.13 clusters per 1 μm^2; one-way ANOVA p=0.6465; Figure 5.2D).

I then examined the impact of mutating α_5^{S374} on the size (mean volume) and brightness (mean grey value) of separate inhibitory synaptic components. I hypothesized that if the accumulation of α_5, gephyrin or VIAAT is affected by mutating residue α_5^{S374}, then I would see a reduction in either the mean volume or mean grey values. First, I noticed for transfected neurons that α_5 and gephyrin clusters were of a similar volume, whereas the presynaptic VIAAT clusters were approximately 2-fold larger in volume compared to α_5 and gephyrin clusters (Figures 5.3A to 5.3C). This indicates that α_5 clusters are of a suitable size to be clustered by gephyrin as the stoichiometry between gephyrin molecules and postsynaptic receptors is considered to be approximately 1:1 (Battaglia et al., 2018; Specht et al., 2013). Surprisingly, the mean grey value of VIAAT clusters was significantly smaller for α_5^{S374D} com-

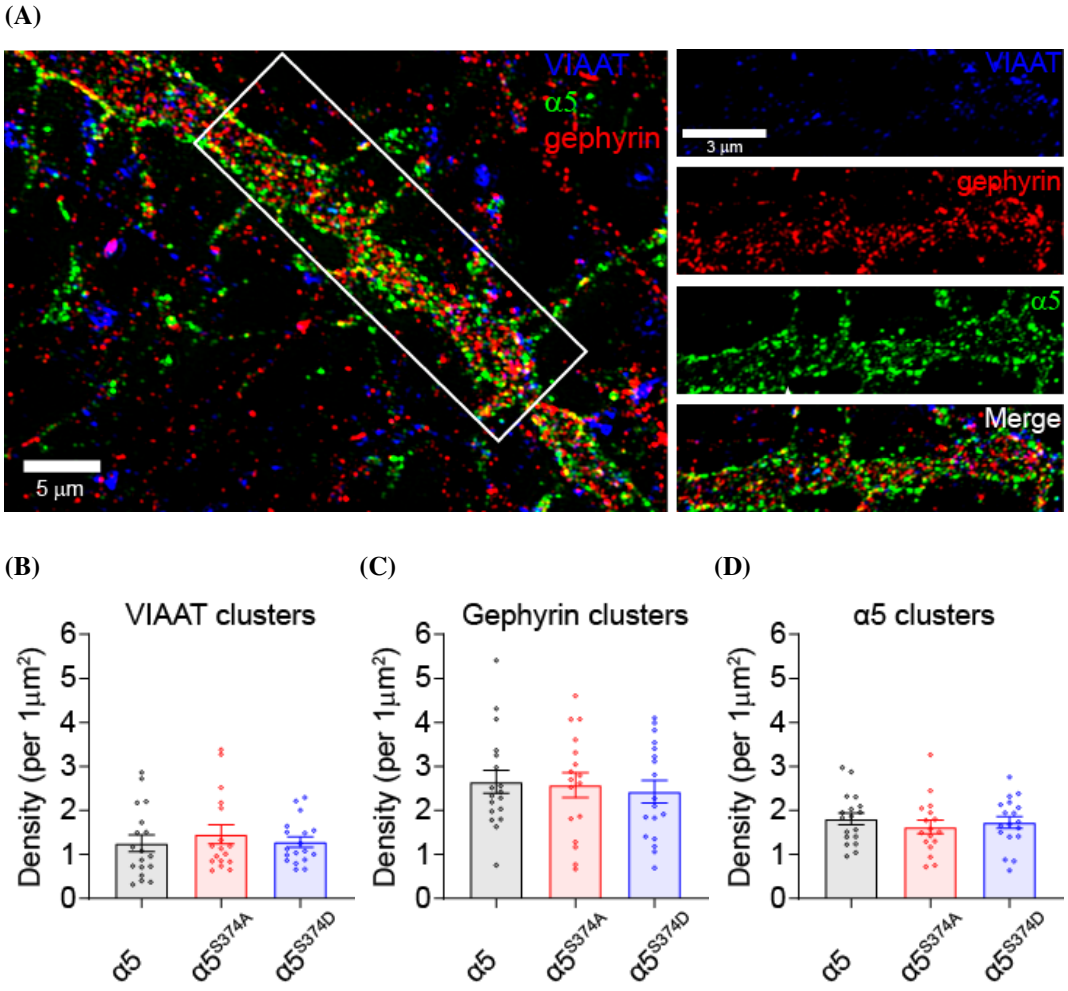

Figure 5.2: Residue α_5^{S374} does not affect the density of α_5, gephyrin or VIAAT clusters on hippocampal dendrites.
(A) Example SIM image of a hippocampal dendrite (left panel) illustrating three different markers: myc-tagged α_5 in green, the postsynaptic marker gephyrin in red, and the presynaptic marker VIAAT in blue. Right panels show separate staining patterns. Bar graphs representing the mean values for cluster density (clusters per 1 μm^2) of **(B)** VIAAT, **(C)** gephyrin and **(D)** α_5 clusters along the dendrites and are shown in black for wild-type α_5 (n=18), in red for phospho-null α_5^{S374A} (n=17) and in blue for phospho-mimetic α_5^{S374D} (n=18) transfected neurons. Points represent mean values calculated for individual cells. Error bars represent SEM. No significant effects according to one-way ANOVA.

pared to α_5^{S374A} transfected neurons, which may indicate a reduction of the number of VIAAT proteins per cluster (α_5: 1951 ± 32, α_5^{S374A}: 2030 ± 51, α_5^{S374D}: 1906 ± 21; one-way ANOVA p=0.0588; Tukey's multiple comparisons test, α_5^{S374A} vs. α_5^{S374D} adjusted p=0.0488; Figure 5.3E). By contrast, there were no changes in mean grey values for α_5 subunits (α_5: 5608 ± 87, α_5^{S374A}: 5688 ± 71, α_5^{S374D}: 5562 ± 80; one-way ANOVA p=0.5394; Figure 5.3D) and gephyrin clusters (α_5: 2854 ± 21, α_5^{S374A}: 2921 ± 25, α_5^{S374D}: 2875 ± 24; one-way ANOVA p=0.1299; Figure 5.3F). The mean volume of α_5 (α_5: 7.7 ± 0.4 x 10^{-3} μm^3, α_5^{S374A}: 7.8 ± 0.5 x 10^{-3} μm^3, α_5^{S374D}: 6.8 ± 0.5 x 10^{-3} μm^3; one-way ANOVA p=0.2386), gephyrin (α_5: 8.0 ± 0.5 x 10^{-3} μm^3, α_5^{S374A}: 8.3 ± 0.4 x 10^{-3} μm^3, α_5^{S374D}: 8.6 ± 0.5 x 10^{-3} μm^3; one-way ANOVA p=0.6349) and VIAAT clusters (α_5: 14.8 ± 0.7 x 10^{-3} μm^3, α_5^{S374A}: 14.0 ± 0.6 x 10^{-3} μm^3, α_5^{S374D}: 14.1 ± 0.5 x 10^{-3} μm^3; one-way ANOVA p=0.6191) were unaffected by the transfections. Note that here I measured all imaged clusters, regardless of whether they were colocalising or not.

5.2.2 Residue α_5^{S374} affects $GABA_AR$ interactions with gephyrin and VIAAT

To investigate the interaction between α_5 and gephyrin or VIAAT clusters separately, I first compared them pairwise. I calculated how many α_5 clusters were separately colocalising with VIAAT or gephyrin in each transfection group. Interestingly, the percentage of α_5 clusters colocalising with gephyrin clusters and not VIAAT clusters (most likely extrasynaptic α_5-gephyrin clusters) was unaltered by the α_5^{S374} mutations (α_5: 13.33 ± 1.33%, α_5^{S374A}: 13.82 ± 1.67%, α_5^{S374D}: 12.90 ± 1.44%; one-way ANOVA p=0.9096; Figure 5.4A). On the other hand, there were significantly more α_5^{S374A} clusters colocalising with VIAAT clusters only and not with the gephyrin clusters compared to wild-type α_5 or mutant α_5^{S374D} clusters (α_5: 6.87 ± 0.71%, α_5^{S374A}: 11.25 ± 1.94%, α_5^{S374D}: 7.03 ± 0.39%; one-way ANOVA p=0.0182; Tukey's multiple comparisons test, α_5 vs. α_5^{S374A} adjusted p=0.0314, α_5^{S374A} vs. α_5^{S374D} adjusted p=0.0393; Figure 5.4D). These data suggest that the clustering of α_5-$GABA_ARs$ at sites apposed to presynaptic terminals is not dependent solely on gephyrin. Although, colocalising with the presynaptic marker VIAAT alone without a postsynaptic marker is insufficient to categorically deter-

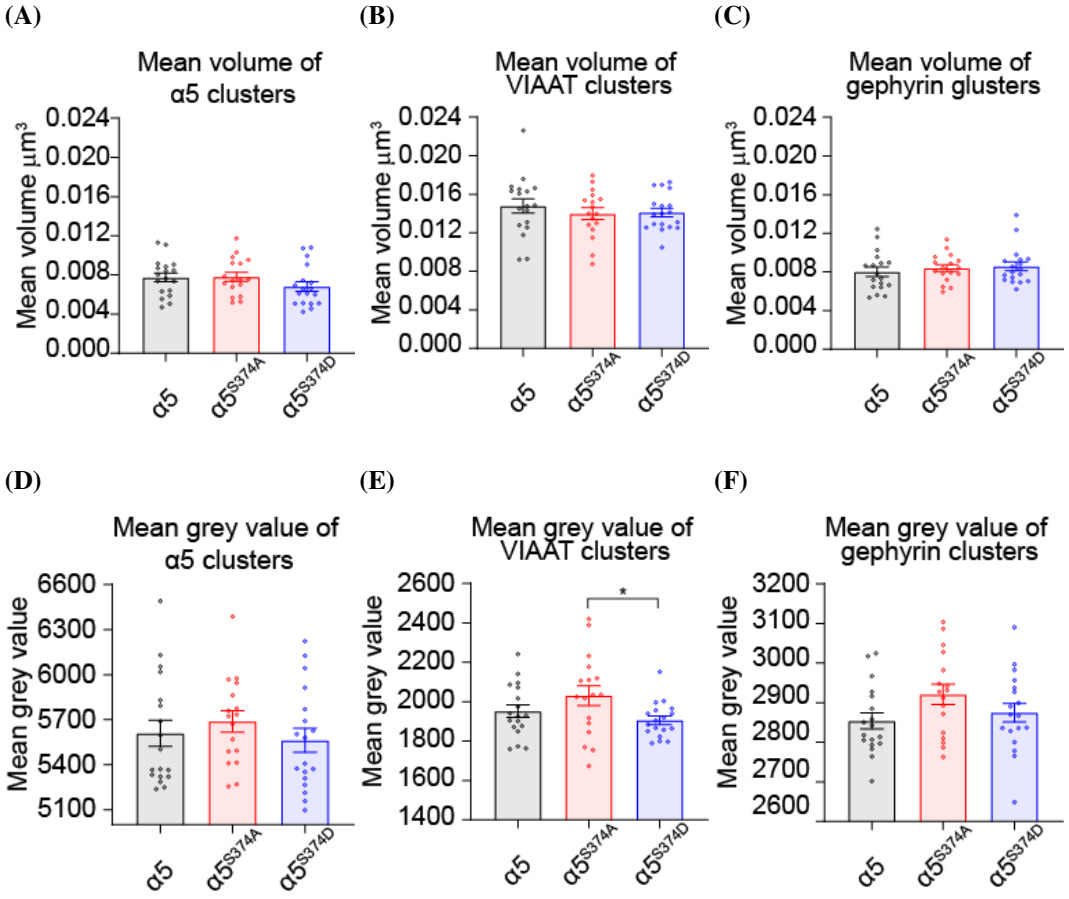

Figure 5.3: Residue α_5^{S374} does not affect the mean cluster size of α_5, gephyrin or VIAAT.
Bar graphs represent the mean volume (A-C) and mean grey values (D-F) of α_5, gephyrin and VIAAT clusters and are shown in black for wild-type α_5 (n=18), in red for phospho-null α_5^{S374A} (n=17) and in blue for phospho-mimetic α_5^{S374D} (n=18) transfected neurons. Points represent mean values calculated for individual cells. Error bars represent SEM. $*$ $p<0.05$, one-way ANOVA followed by Tukey's multiple comparisons test.

mine the location of inhibitory synapses, this result strongly supports our previous interpretation that there are more α_5^{S374A} receptors located at inhibitory synapses compared to transfected neurons expressing wild-type α_5 subunits.

An increase in number of clusters colocalising could potentially be due to an increase in cluster size as this might introduce overlap of adjacent clusters without an actual change in proximity. To examine this possibility, I compared the mean volumes of α_5 clusters colocalising with either VIAAT or gephyrin only. No changes in the mean volume of α_5 clusters colocalising with gephyrin and not with VIAAT

were observed (α_5: 12.48 $\pm$ 0.74 x 10^{-3} μm^3, α_5^{S374A}: 10.50 $\pm$ 0.75 x 10^{-3} μm^3, α_5^{S374D}: 9.82 $\pm$ 0.94 x 10^{-3} μm^3; one-way ANOVA p=0.0649; Figure 5.4B). Similarly, no changes were evident for α_5 clusters colocalising with VIAAT and not gephyrin (α_5: 12.43 $\pm$ 1.06 x 10^{-3} μm^3, α_5^{S374A}: 11.91 $\pm$ 0.93 x 10^{-3} μm^3, α_5^{S374D}: 11.64 $\pm$ 1.25 x 10^{-3} μm^3; one-way ANOVA p=0.8723; Figure 5.4E). Collectively, these data suggest that the increased number of α_5^{S374A} clusters colocalising with VIAAT clusters was not simply dependent on cluster size but by a genuine increase in cluster colocalization. Furthermore, there were no changes in mean grey values of α_5 clusters colocalising with gephyrin and not with VIAAT (α_5: 5897 $\pm$ 104, α_5^{S374A}: 5851 $\pm$ 90, α_5^{S374D}: 5764 $\pm$ 102; one-way ANOVA p=0.6269; Figure 5.4C) or colocalising with VIAAT and not with gephyrin (α_5: 6171 $\pm$ 167, α_5^{S374A}: 6350 $\pm$ 160, α_5^{S374D}: 6200 $\pm$ 152; one-way ANOVA p=0.7006; Figure 5.4F).

During the analysis, only a small number of α_5 clusters were noted to colocalise with either gephyrin (13%, Figure 5.4A) or VIAAT (7-11%, Figure 5.4D) only. Therefore, I decided to examine the percentage of α_5 clusters that did not colocalise with either of the two markers (designated as extrasynaptic α_5 clusters) and α_5 clusters that colocalised with both markers (defined as synaptic α_5 clusters). The majority of α_5 clusters (69-77%) were classed as extrasynaptic and did not colocalise with either pre- or postsynaptic marker. Interestingly, there were significantly less extrasynaptic α_5 clusters in α_5^{S374A} compared to wild-type α_5 or mutated α_5^{S374D} transfected cells (α_5: 76.78 $\pm$ 1.42%, α_5^{S374A}: 68.96 $\pm$ 2.45%, α_5^{S374D}: 76.91 $\pm$ 1.71%; one-way ANOVA p=0.0059; Tukey's multiple comparisons test, α_5 vs. α_5^{S374A} p=0.0147, α_5^{S374A} vs. α_5^{S374D} p=0.0128, Figure 5.5A). In comparison, there were significantly more synaptic α_5 clusters in α_5^{S374A} compared to wild-type α_5 or mutant α_5^{S374D} transfected cells (α_5: 2.30 $\pm$ 0.26%, α_5^{S374A}: 4.67 $\pm$ 0.84%, α_5^{S374D}: 2.4 $\pm$ 0.31%; one-way ANOVA p=0.0036; Tukey's multiple comparisons test, α_5 vs. α_5^{S374A} p=0.0072, α_5^{S374A} vs. α_5^{S374D} p=0.0113, Figure 5.5D). In addition, I observed that extrasynaptic α_5 clusters were small volume (α_5: 5.72 $\pm$ 0.32 x 10^{-3} μm^3, α_5^{S374A}: 5.39 $\pm$ 0.26 x 10^{-3} μm^3, α_5^{S374D}: 5.33 $\pm$ 0.33 x 10^{-3} μm^3; one-way ANOVA p=0.3222; Figure 5.5B) compared to the increased

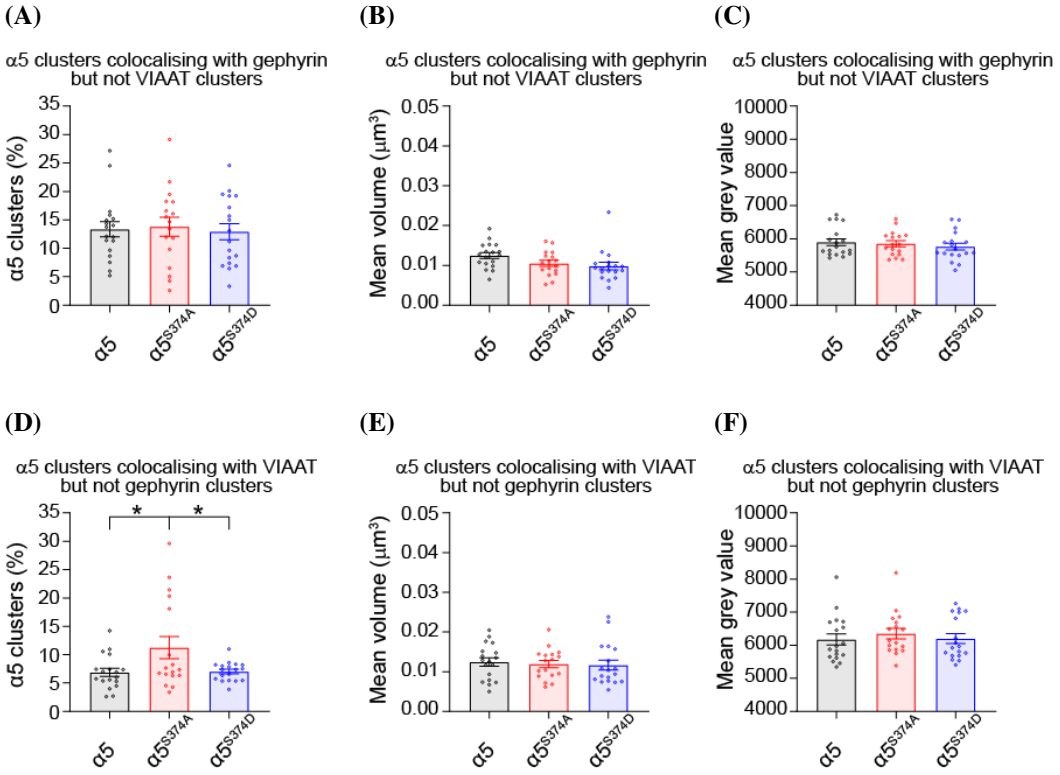

Figure 5.4: α_5^{S374A} increases the number of α_5 clusters colocalising with VIAAT clusters independent of gephyrin.
Bar graphs representing the mean number of clusters (%; A, D), mean volume (μm^3, B, E) and mean grey values (C, F) of α_5 clusters colocalising with gephyrin or VIAAT clusters only. These are shown in black for wild-type α_5 (n=18), in red for phospho-null α_5^{S374A} (n=17) and in blue for phospho-mimetic α_5^{S374D} (n=18) transfected neurons. Points represent mean values calculated for individual cells. Error bars represent SEM. $*$ $p<0.05$, one-way ANOVA followed by Tukey's multiple comparisons test.

size of synaptic α_5 clusters (α_5: 19.82 $\pm$ 1.53 x 10^{-3} μm^3, α_5^{S374A}: 22.27 $\pm$ 2.54 x 10^{-3} μm^3, α_5^{S374D}: 18.93 $\pm$ 1.76 x 10^{-3} μm^3; one-way ANOVA p=0.4744; Figure 5.5E). This profile was repeated for the mean grey value with extrasynaptic α_5 clusters the dimmest (α_5: 5463 $\pm$ 74, α_5^{S374A}: 5475 $\pm$ 55, α_5^{S374D}: 5418 $\pm$ 62; one-way ANOVA p=0.8044; Figure 5.5C) and synaptic α_5 clusters clearly the brightest (α_5: 6574 $\pm$ 197, α_5^{S374A}: 6774 $\pm$ 294, α_5^{S374D}: 6619 $\pm$ 205; one-way ANOVA p=0.8211; Figure 5.5F). There were no transfection group specific changes in mean cluster volume or in mean grey values.

Together, these results suggest that gephyrin and VIAAT can produce larger and brighter clusters of α_5-$GABA_AR$, but the largest and brightest clusters need the presence of both, pre-and postsynaptic markers. Increased cluster size and bright-

ness occurs also for synaptic α_5-GABA$_A$R clusters in the absence of gephyrin at VIAAT positive synapses, presumably due to other postsynaptic scaffolding proteins.

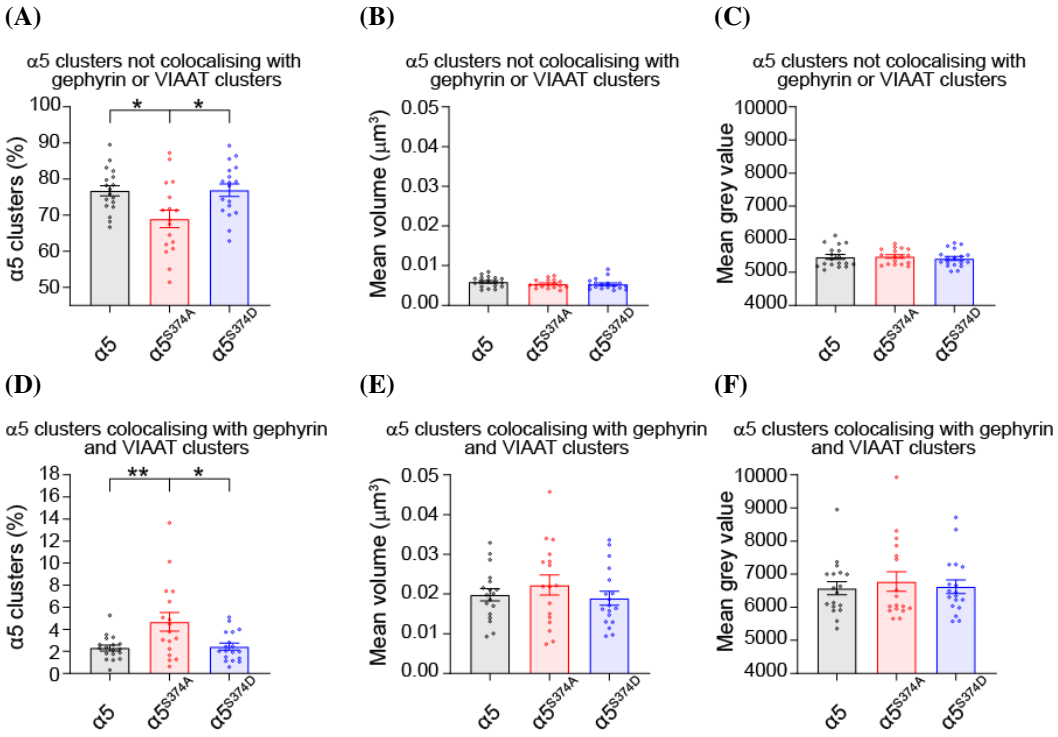

Figure 5.5: Synaptic α_5 clusters have the largest volume.
Bar graphs represent the mean cluster (%, A, C), mean volume (μm^3,B, E) and mean grey value (C, F) of extrasynaptic α_5 clusters not colocalising with gephyrin or VIAAT, and synaptic α_5 clusters colocalising with both markers. These are shown in black for wild-type α_5 (n=18), in red for phospho-null α_5^{S374A} (n=17) and in blue for phospho-mimetic α_5^{S374D} (n=18) transfected neurons. Points represent mean values calculated for individual cells. Error bars represent SEM. $*$ $p<0.05$, $**$ $p<0.01$, one-way ANOVA followed by Tukey's multiple comparisons test.

5.2.3 α_5^{S374A} increases the number of synaptic α_5-gephyrin clusters

After investigating the α_5-GABA$_A$Rs interaction with gephyrin and VIAAT individually, I focused our attention onto synaptic α_5-gephyrin clusters. The α_5-gephyrin cluster was defined as being synaptically-located if all three markers (α_5, gephyrin, VIAAT) were colocalised (Figure 5.6A). The α_5-gephyrin clusters were designated as extrasynaptic when these cluster combinations did not colocalise with VIAAT (Figures 5.4A-5.4C). Then, I compared the percentage of synaptic α_5-gephyrin clus-

ters in all three transfection groups (α_5, α_5^{S374A} and α_5^{S374D}). There were significantly more synaptic α_5^{S374A}-gephyrin clusters compared to wild-type α_5 or mutated α_5^{S374D} clusters which strongly supports the hypothesis that residue α_5^{S374} regulates the subcellular location of α_5-$GABA_A$Rs (α_5: 14.50 $\pm$ 1.29%, α_5^{S374A}: 23.74 $\pm$ 3.33%, α_5^{S374D}: 15.09 $\pm$ 0.91%; one-way ANOVA p=0.0041; Tukey's multiple comparisons test, α_5 vs. α_5^{S374A} adjusted p=0.0077, α_5^{S374A} vs. α_5^{S374D} adjusted p=0.0134; Figure 5.6B). The mean volume (Figure 5.4E) and mean grey value (Figure 5.4F) of synaptic α_5 clusters were the same for all three transfection groups, thus the increased percentage of synaptic α_5 was cluster size independent. Furthermore, line scans through a typical synaptic 3D-image illustrates the expected structural arrangement of presynaptic and postsynaptic markers where α_5 and gephyrin clusters colocalise closely with each other with a VIAAT cluster located further away (Figure 5.6C).

5.2.4 α_5^{S374A} increases the number and proximity of α_5 and neighbouring gephyrin or VIAAT SSDs

Several studies have investigated the nanoscale structure of inhibitory synapses and it has been established that a synapse can be composed of multiple nanoscale subsynaptic domains (SSDs) (Crosby et al., 2019; Pennacchietti et al., 2017; Yang and Specht, 2019; Yang et al., 2021). The mean volume of α_5, gephyrin and VIAAT clusters in this project appear to correspond to individual SSD volumes rather than to whole pre- and postsynaptic compartments (mean individual $GABA_A$Rs SSD volume 0.02 μm^3, mean postsynaptic compartment volume 0.05 μm^3) (Crosby et al., 2019). Thus, I decided to quantify the number of α_5 SSDs per VIAAT (presynaptic marker) or gephyrin cluster (postsynaptic marker) and vice versa. This was achieved by counting the number of α_5 clusters that colocalise with the same VIAAT or gephyrin cluster.

I pooled the number of SSDs in each cell within one transfection group and investigated the relative frequency of the number of α_5, gephyrin and VIAAT SSDs. Analysis revealed that the majority (89.3% to 97.1%) of α_5-gephyrin and α_5-VIAAT pairwise clusters comparisons had a 1:1 ratio, with a mean number of SSDs of

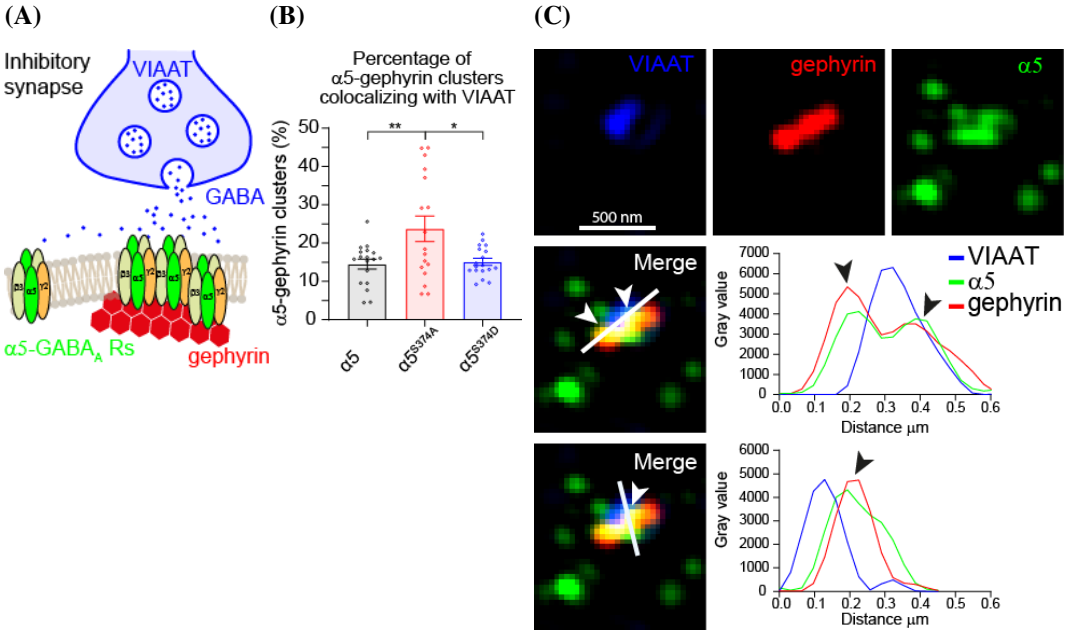

Figure 5.6: α_5^{S374A} increases the number of synaptic α_5-gephyrin clusters.
(A) Schematic of synaptic and extrasynaptic α_5-GABA$_A$R clusters. **(B)** Bar graph representing mean percentage of α_5-gephyrin clusters that colocalise with VIAAT, shown in black for wild-type α_5 (n=18), in red for phospho-null α_5^{S374A} (n=17) and in blue for phospho-mimetic α_5^{S374D} (n=18) transfected neurons. Points represent mean values calculated for individual cells. Error bars represent SEM. **(C)** Example cell showing synaptic α_5-gephyrin clusters with line scans parallel to and across the synaptic axis from α_5^{S374A} transfected cells. $*$ $p<0.05$, $**$ $p<0.01$, one-way ANOVA followed by Tukey's multiple comparisons test.

1.03–1.13 and a range of 1–7 SSDs (Figure 5.7). α_5^{S374A} transfected neurons had more often 2:1 ratio for gephyrin-α_5 clusters and 2:1 or 3:1 ratio for VIAAT-α_5 clusters compared to α_5 and α_5^{S374D} transfected cells (Figures 5.7A and 5.7B). The ratio between α_5-gephyrin clusters did not change across transfection groups (Figure 5.7C) and the ratio for α_5-VIAAT was more often 2:1 in α_5 compared to α_5^{S374A} or α_5^{S374D} transfected cells (Figure 5.7D).

There were significantly more gephyrin and VIAAT SSDs per α_5 cluster for α_5^{S374A} compared to α_5 or α_5^{S374D} transfected cells (gephyrin SSDs: α_5: 1.076 $\pm$ 0.004, α_5^{S374A}: 1.091 $\pm$ 0.004, α_5^{S374D}: 1.064 $\pm$ 0.004; Kruskal-Wallis test $p<0.0001$; Dunn's multiple comparisons test, α_5 vs. α_5^{S374A} adjusted $p=0.0032$, α_5^{S374A} vs. α_5^{S374D} adjusted $p<0.001$; VIAAT SSDs: α_5: 1.035 $\pm$ 0.003, α_5^{S374A}: 1.067 $\pm$ 0.005, α_5^{S374D}: 1.030 $\pm$ 0.003; Kruskal-Wallis test $p<0.0001$; Dunn's

multiple comparisons test, α_5 vs. α_5^{S374A} adjusted $p<0.0001$, α_5^{S374A} vs. α_5^{S374D} adjusted $p<0.0001$; Figures 5.7E and 5.7F). The mean number of α_5 SSDs per gephyrin cluster did not change between transfection groups (α_5: 1.109 $\pm$ 0.005, α_5^{S374A}: 1.110 $\pm$ 0.005, α_5^{S374D}: 1.118 $\pm$ 0.006; Kruskal-Wallis test p=0.3582; Figure 5.7G). By contrast, the mean number of α_5 SSDs per VIAAT cluster was significantly higher for α_5 compared to α_5^{S374A} or α_5^{S374D} transfected cells (α_5: 1.135 $\pm$ 0.007, α_5^{S374A}: 1.105 $\pm$ 0.006, α_5^{S374D}: 1.097 $\pm$ 0.006; Kruskal-Wallis test $p<0.0001$; Dunn's multiple comparisons test, α_5 vs. α_5^{S374A} adjusted p=0.0006, α_5 vs. α_5^{S374D} adjusted p=0.0003; Figure 5.7H).

Together, these data indicate that residue α_5^{S374} affects the number of gephyrin and VIAAT SSDs. The molecular mechanism is currently unknown, but I speculate that an increased number of gephyrin and VIAAT SSDs in α_5^{S374A} transfected neurons could potentially be due to the increased presence of α_5-$GABA_A$Rs at synaptic sites (see discussion for more details) and that α_5 subunits play a key role in regulating the number of gephyrin and VIAAT SSD at these synapses.

To further investigate the effect of residue α_5^{S374} on the apposition of α_5 clusters with gephyrin or VIAAT clusters, I determined the distance between the centre of each α_5 cluster and its nearest neighbouring gephyrin or VIAAT cluster and compared these distances in all three α_5 transfection groups. The centre of the cluster of interest was automatically determined by using thresholding and segmentation masks (see Methods for more details, Section 2.6.3). As expected, the mean distance between centres of colocalised α_5 and VIAAT clusters is greater than mean distance between centres of colocalised α_5 and gephyrin clusters as both α_5 and gephyrin are localised on the postsynaptic membrane, whereas VIAAT is presynaptic (Figures 5.8C and 5.8D). The mean distance between the centres of α_5^{S374A} clusters and colocalised gephyrin clusters was significantly shorter compared to wild-type α_5 or α_5^{S374D} transfected cells (α_5: 0.1801 $\pm$ 0.0012 µm, α_5^{S374A}: 0.1678 $\pm$ 0.0012 µm, α_5^{S374D}: 0.1803 $\pm$ 0.0014 µm; Kruskal-Wallis test $p<0.0001$; Dunn's multiple comparisons test, α_5 vs. α_5^{S374A} adjusted $p<0.0001$, α_5^{S374A} vs. α_5^{S374D} adjusted $p<0.0001$; Figure 5.8A and 5.8C). The mean distance between α_5 clus-

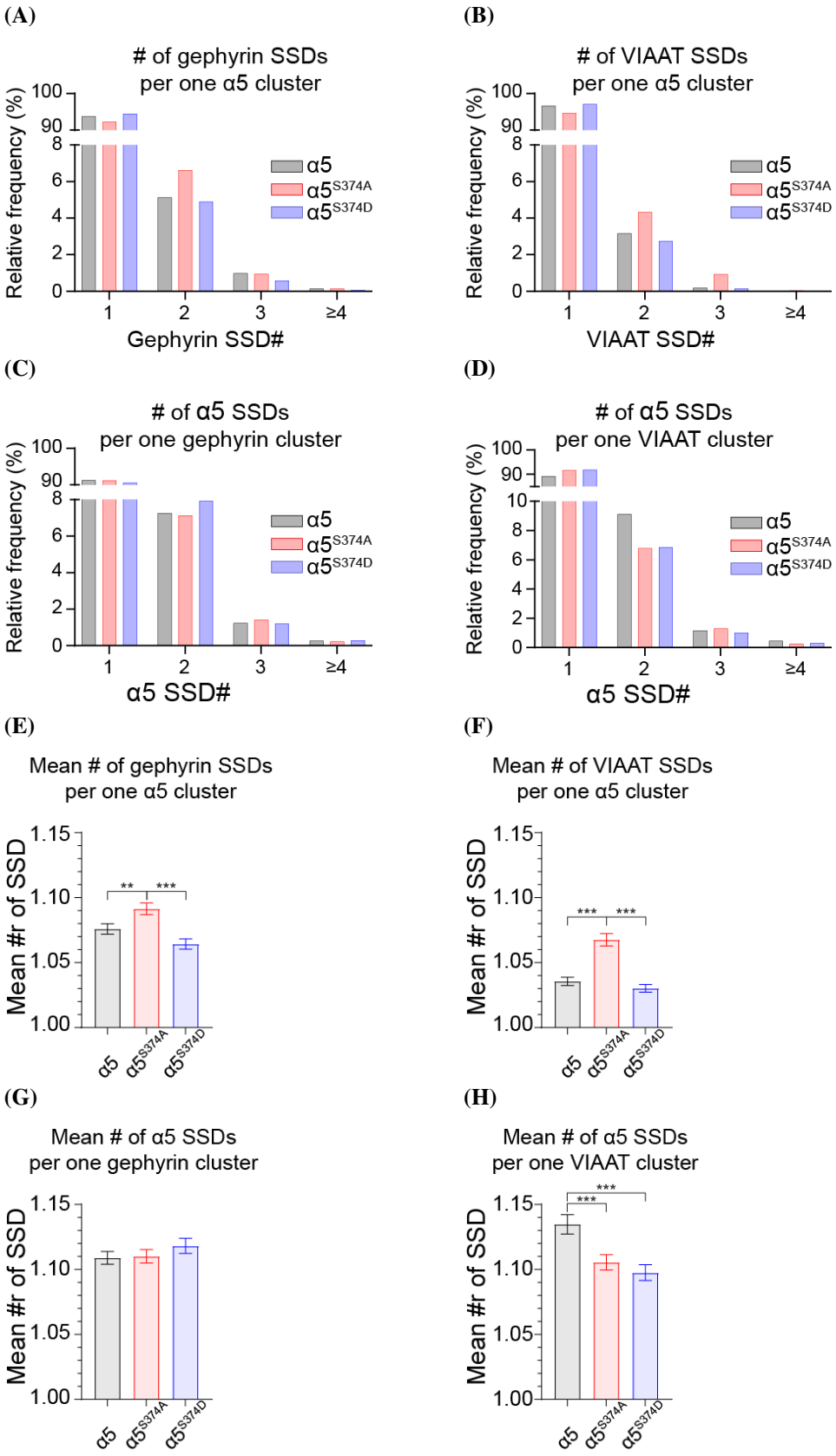
(A)
# of gephyrin SSDs
per one α5 cluster
Relative frequency (%)
Gephyrin SSD#
α5
α5S374A
α5S374D
(B)
# of VIAAT SSDs
per one α5 cluster
VIAAT SSD#
(C)
# of α5 SSDs
per one gephyrin cluster
α5 SSD#
(D)
# of α5 SSDs
per one VIAAT cluster
(E)
Mean # of gephyrin SSDs
per one α5 cluster
Mean #r of SSD
(F)
Mean # of VIAAT SSDs
per one α5 cluster
(G)
Mean # of α5 SSDs
per one gephyrin cluster
(H)
Mean # of α5 SSDs
per one VIAAT cluster

Figure 5.7: α_5^{S374A} increases the number of gephyrin and VIAAT SSDs per α_5 cluster. **(A-D)** Frequency distribution plots of the number (#) of α_5 SSDs per VIAAT or per gephyrin cluster and vice versa. **(E-H)** Bar graphs representing the mean numbers of SSDs. **(A,E)** Mean number of gephyrin SSDs per α_5 cluster, **(B,F)** mean number of VIAAT SSDs per α_5 cluster, **(C,G)** mean number of α_5 SSDs per gephyrin cluster, **(D,H)** mean number of α_5 SSDs per VIAAT cluster. Data shown in black are for wild-type α_5 (n=18), in red for phospho-null α_5^{S374A} (n=17) and in blue for phospho-mimetic α_5^{S374D} (n=18) transfected neurons. Error bars represent SEM. $**$ $p<0.01$, $***$ $p<0.001$ Kruskal-Wallis test followed by Dunn's multiple comparisons test.

ters and colocalised VIAAT clusters varied significantly between all three transfection groups and was longest in α_5 and shortest in α_5^{S374A} transfected neurons (α_5: 0.2160 ± 0.0020 µm, α_5^{S374A}: 0.1886 ± 0.0015 µm, α_5^{S374D}: 0.2003 ± 0.0019 µm; Kruskal-Wallis test $p<0.0001$; Dunn's multiple comparisons test, α_5 vs. α_5^{S374A} adjusted $p<0.0001$, α_5^{S374A} vs. α_5^{S374D} adjusted $p=0.0018$, α_5 vs. α_5^{S374D} adjusted $p<0.0001$; Figure 5.8B and 5.8D). I speculate that the change in distance between neighbouring α_5-gephyrin and α_5-VIAAT clusters could represent the conformational changes of receptor and/or gephyrin.

5.2.5 α_5^{S374} affects the clustering of other synaptic $GABA_ARs$

Given the increased number of synaptic α_5-gephyrin clusters, it was of interest to examine if expressing more α_5 receptors in neurons affected the clustering of other synaptic $GABA_AR$ α subunits. The $GABA_AR$ is a pentamer and composed of two α, two β and either a γor δ subunit. I hypothesized that the clustering of $GABA_ARs$ composed of other α subunits could be compromised in α_5 transfected neurons as a result of competition for available β and γsubunits. I examined this hypothesis using α_1 subunits as this is most widely expressed α subunit in the brain (Heldt and Ressler, 2007; Hörtnagl et al., 2013; Müller Herde et al., 2017; Pirker et al., 2000; Sun et al., 2004) and is an important contributor to synaptic $GABA_AR$ inhibition (Fujiyama et al., 2000; Nusser et al., 1996; Sassoè-Pognetto et al., 2000). I used an antibody directed against the α_5 subunit to detect native α_5 clusters in neurons and an antibody against the myc-tag to identify transfected α_5 clusters (Figure 5.9E). The mean volume of α_5 clusters in α_5-transfected neurons (detected by myc-tag only) was significantly higher compared to α_5 clusters in untransfected neurons (detected

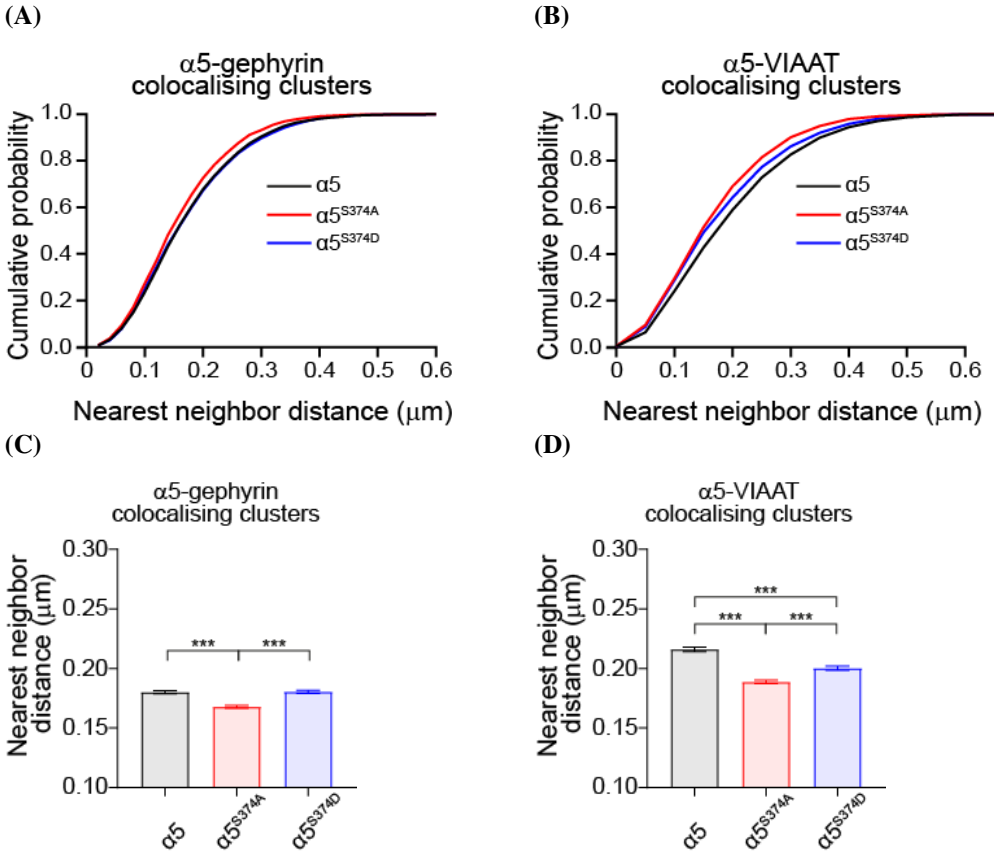

Figure 5.8: α_5^{S374A} decreases the distance between α_5 and neighbouring gephyrin or VIAAT clusters.
The mean distance between nearest neighbouring α_5-gephyrin and α_5-VIAAT clusters measuring from centre to centre of the clusters. Cumulative probability plots (A-B) and bar graphs (C-D) for the distance between α_5 and its nearest colocalised neighbouring (A,C) gephyrin, or (B,D) VIAAT cluster. Black indicates wild-type α_5 (n=18), red is for phospho-null α_5^{S374A} (n=17) and blue is phospho-mimetic α_5^{S374D} (n=18) transfected neurons. Error bars represent SEM. $***$ $p<0.001$ Kruskal-Wallis test followed by Dunn's multiple comparisons test.

by antibody directly against α_5 subunit) (untransfected: $5.26 \pm 0.40 \times 10^{-3}$ μm^3, α_5: $11.07 \pm 0.76 \times 10^{-3}$ μm^3, α_5^{S374A}: $10.20 \pm 0.67 \times 10^{-3}$ μm^3, α_5^{S374D}: $10.99 \pm 0.97 \times 10^{-3}$ μm^3; one-way ANOVA $p<0.001$; Tukey's multiple comparisons test, untransfected vs. α_5, α_5^{S374A}, α_5^{S374D} all pairwise adjusted $p=<0.001$; Figure 5.9A). To detect endogenous α_1 subunits, I used an antibody directed against the α_1 subunit. The mean volume of α_1 clusters in α_5 transfected neurons was significantly lower compared to the mean volume of α_1 clusters in untransfected cells (untransfected: $12.39 \pm 0.83 \times 10^{-3}$ μm^3, α_5: $8.93 \pm 0.59 \times 10^{-3}$ μm^3, α_5^{S374A}: $8.50 \pm 0.52 \times 10^{-3}$ μm^3, α_5^{S374D}: $8.23 \pm 0.50 \times 10^{-3}$ μm^3; one-way ANOVA $p<0.001$; Tukey's mul-

tiple comparisons test, untransfected vs. α_5, α_5^{S374A}, α_5^{S374D} all pairwise adjusted p=<0.001; Figure 5.9A). Interestingly, I noticed that the mean volume of endogenous α_5 clusters in untransfected cells (Figure 5.9A) was 2-fold smaller compared to endogenous α_1 clusters in untransfected cells (Figure 5.9C). The mean grey value of α_5 (untransfected: 5715 $\pm$ 90, α_5: 5924 $\pm$ 50, α_5^{S374A}: 5837 $\pm$ 56, α_5^{S374D}: 5831 $\pm$67; one-way ANOVA p=0.1776; Figure 5.9B) and α_1 receptors (untransfected: 3203 $\pm$ 56, α_5: 3183 $\pm$ 54, α_5^{S374A}: 3187 $\pm$ 48, α_5^{S374D}: 3133 $\pm$ 43; one-way ANOVA p=0.7894, Figure 5.9D) were similar compared to untransfected and transfected cells. From these results I concluded that expressing extra α_5 subunits in neurons reduces the clustering of cell surface α_1 subunits. There were no changes within different α_5 transfection groups, which suggests that residue α_5^{S374} does not affect the clustering of α_1 subunits specifically.

Previous imaging results showed that generally, synaptic (colocalised with both gephyrin and VIAAT) $GABA_AR$ clusters have the largest volume and $GABA_AR$ clusters that do not colocalise with VIAAT or gephyrin are the smallest in volume. Thus, changes in receptor cluster volumes may reflect their interaction with other components of the postsynaptic density that is the inhibitory synapse. As the α_1 mean cluster volume was reduced in all α_5 transfection groups compared to untransfected neurons (Figure 5.9C), I decided to examine, by imaging, if residue α_5^{S374} affects the subcellular location of α_1 subunits. First, I quantified the number of endogenous α_1 clusters that did not colocalise with either, α_5 or VIAAT clusters. Most likely these represented extrasynaptic α_1 clusters. There were significantly less extrasynaptic α_1 clusters in α_5^{S374A} and α_5^{S374D} compared to wild-type α_5 transfected neurons (α_5: 76.70 $\pm$ 1.83%, α_5^{S374A}: 61.69 $\pm$ 3.57%, α_5^{S374D}: 65.20 $\pm$ 3.00%; one-way ANOVA p=0.0011; Tukey's multiple comparisons test, α_5 vs. α_5^{S374A} adjusted p=0.0013, α_5 vs. α_5^{S374D} adjusted p=0.0148; Figure 5.10A).

Next, I quantified the number of extrasynaptic α_1 clusters that colocalised with α_5 but not with VIAAT clusters. There were significantly more extrasynaptic α_1-α_5 clusters in α_5^{S374A} and α_5^{S374D} compared to wild-type α_5 transfected neurons (α_5: 11.41 $\pm$ 1.24%, α_5^{S374A}: 24.25 $\pm$ 3.38%, α_5^{S374D}: 24.45 $\pm$ 3.22%; one-

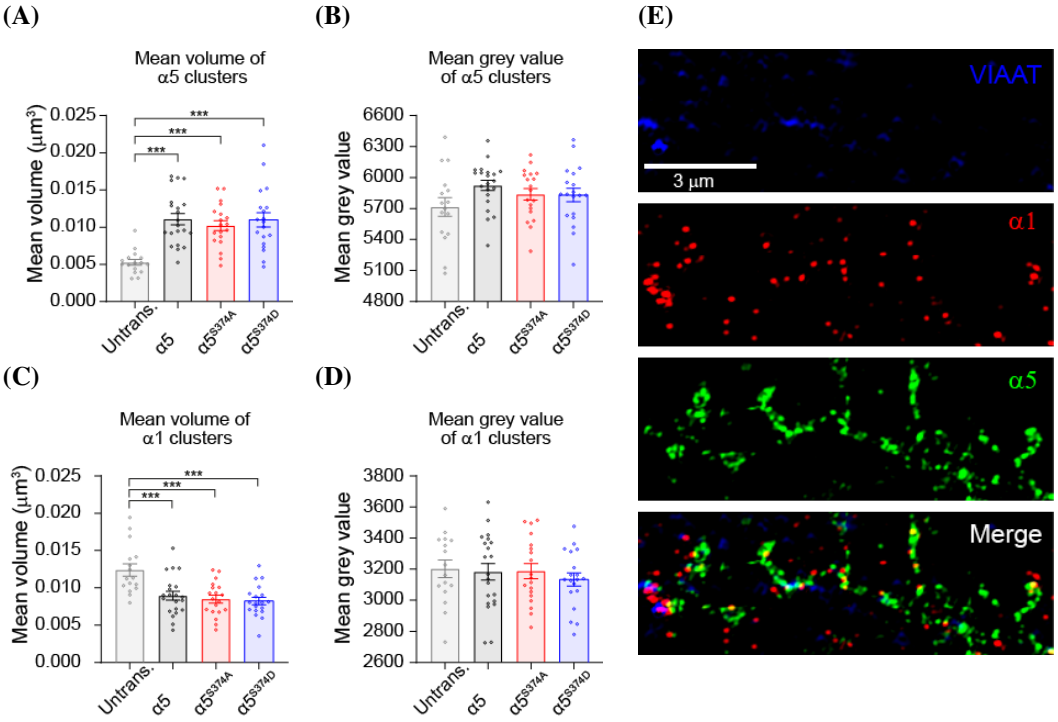

Figure 5.9: Transfecting α_5 constructs increased α_5 and decreased α_1 cluster volumes compared to untransfected cells.
Bar graphs representing **(A)** mean volume of α_5 clusters, **(B)** mean grey value of α_5 clusters, **(C)** mean volume of α_1 clusters, **(D)** mean grey value of α_1 clusters. Grey represents untransfected cells (n=16), black is wild-type α_5 (n=21), red is phospho-null α_5^{S374A} (n=19) and blue is phospho-mimetic α_5^{S374D} (n=19) transfected neurons. Points represent mean values calculated for individual cells. $***p<0.001$, one-way ANOVA followed by Tukey's multiple comparisons test. **(E)** Example image showing α_5 clusters in green, α_1 clusters in red and VIAAT clusters in blue along the hippocampal dendrite.

way ANOVA p=0.0010; Tukey's multiple comparisons test, α_5 vs. α_5^{S374A} adjusted p=0.0038, α_5 vs. α_5^{S374D} adjusted p=0.0033; Figure 5.10B). The number of synaptic α_1 clusters (α_1 colocalising with VIAAT) that did not contain α_5-GABA$_A$Rs remained constant across all the transfection groups (α_5: 9.34 $\pm$ 0.81%, α_5^{S374A}: 8.74 $\pm$ 1.16%, α_5^{S374D}: 6.84 $\pm$ 0.89%; one-way ANOVA p=0.1552; Figure 5.10C). By contrast, there were significantly more synaptic α_1 clusters that contained α_5-GABA$_A$Rs (α_1 colocalising with VIAAT and α_5) in α_5^{S374A} compared to wild-type α_5 transfected neurons (α_5: 2.07 $\pm$ 0.33%, α_5^{S374A}: 4.24 $\pm$ 0.68%, α_5^{S374D}: 2.90 $\pm$ 0.36%; one-way ANOVA p=0.0076; Tukey's multiple comparisons test, α_5 vs. α_5^{S374A} adjusted p=0.0055; Figure 5.10D). These results suggest that residue

α_5^{S374} regulates the colocalization of α_5 with α_1 subunits either in separate, or the same, receptor complex.

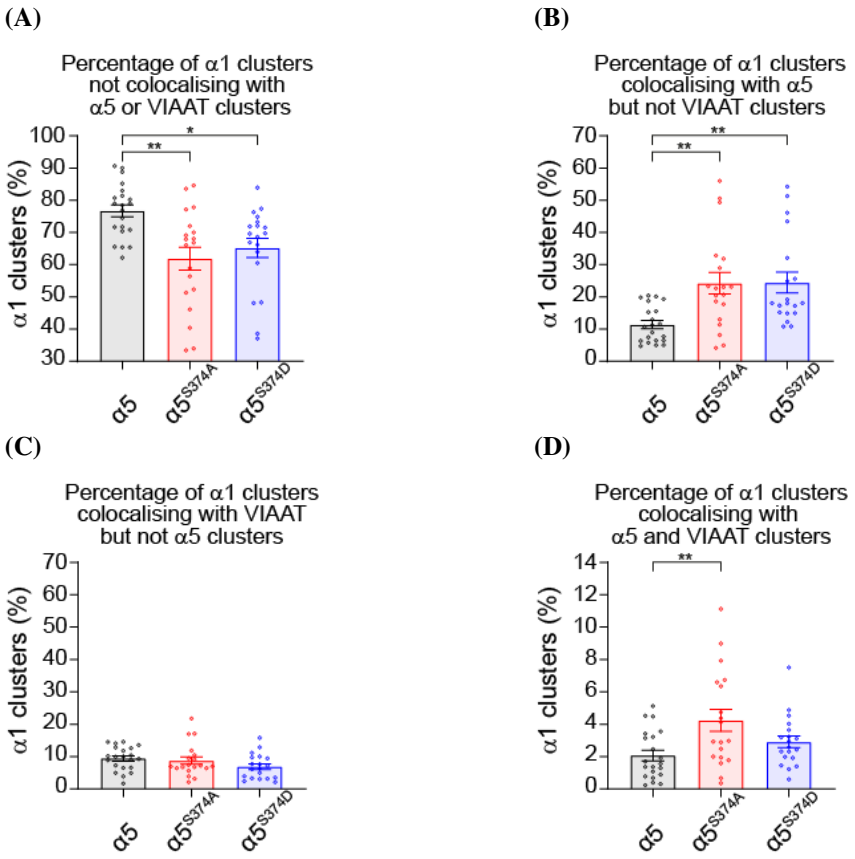

Figure 5.10: α_5^{S374} affects the colocalization of α_5 with α_1 subunits.
Bar graphs representing the percentage of α_1 clusters that **(A)** did not colocalise with α_5 or VIAAT clusters, **(B)** colocalised with α_5 but not with VIAAT clusters, **(C)** colocalised with VIAAT but not with α_5 clusters and **(D)** colocalised with both α_5 and VIAAT clusters. These are shown in black for wild-type α_5 (n=21), in red for phospho-null α_5^{S374A} (n=19) and in blue for phospho-mimetic α_5^{S374D} (n=19) transfected neurons. Points represent mean values calculated for individual cells. $*$ $p<0.05$, $**$ $p<0.01$ one-way ANOVA followed by Tukey's multiple comparisons test.

As the number of α_1 clusters colocalising with α_5 and VIAAT clusters was the highest in α_5^{S374} transfected cells, I examined synapses containing both α_1 and α_5 subunits to investigate the effects of α_5^{S374} on synaptic α_1-GABA$_A$Rs (Figures 5.11A and 5.11G). The number of fluorophore channels imaged at one time was limited to three, therefore I could not use another postsynaptic marker. Thus, I treated α_1 as a postsynaptic marker in these images if it colocalised with the presynaptic marker VIAAT. I calculated the percentage of synapses (α_1 colocalising with

VIAAT) that contained α_5 clusters. There were significantly more α_1-VIAAT clusters that colocalised with α_5 clusters in α_5^{S374A} and α_5^{S374D} transfected neurons compared to wild-type α_5 transfected neurons (α_5: 16.43 $\pm$ 1.91%, α_5^{S374A}: 30.30 $\pm$ 4.19%, α_5^{S374D}: 29.81 $\pm$ 3.75%; one-way ANOVA p=0.0056; Tukey's multiple comparisons test, α_5 vs. α_5^{S374A} adjusted p=0.0127, α_5 vs. α_5^{S374D} adjusted p=0.0168; Figure 5.11B). I concluded that in both mutated α_5^{S374A} and α_5^{S374D} transfected cells, there were significantly more α_1 positive synapses that include α_5 receptors compared to wild-type transfected cells. I noticed that the synaptic α_5 clusters were more than 2-fold larger and brighter than synaptic α_1 clusters. The mean volume of synaptic α_5 clusters (α_5: 41.03 $\pm$ 3.76 x 10^{-3} μm^3, α_5^{S374A}: 34.31 $\pm$ 3.59 x 10^{-3} μm^3, α_5^{S374D}: 37.63 $\pm$ 3.19 x 10^{-3} μm^3; one-way ANOVA p=0.4071; Figure 5.11C) or synaptic α_1 clusters (α_5: 18.47 $\pm$ 2.39 x 10^{-3} μm^3, α_5^{S374A}: 15.11 $\pm$ 1.02 x 10^{-3} μm^3, α_5^{S374D}: 16.83 $\pm$ 1.69 x 10^{-3} μm^3; one-way ANOVA p=0.4349; Figure 5.11D) did not change between transfected groups. Also, there were no changes in mean grey values of synaptic α_5 (α_5: 7706 $\pm$ 163, α_5^{S374A}: 7237 $\pm$ 133, α_5^{S374D}: 7351 $\pm$ 134; one-way ANOVA p=0.0633; Figure 5.11E) or synaptic α_1 clusters (α_5: 3672 $\pm$ 93, α_5^{S374A}: 3638 $\pm$ 71, α_5^{S374D}: 3679 $\pm$ 101; one-way ANOVA p=0.9445; Figure 5.11F) between transfection groups. Taken together, I concluded that residue α_5^{S374} alters the colocalization between α_5-$GABA_A$Rs and α_1-$GABA_A$Rs at both, synaptic and extrasynaptic areas which is probably due to the redistribution of α_5-$GABA_A$Rs at both sites.

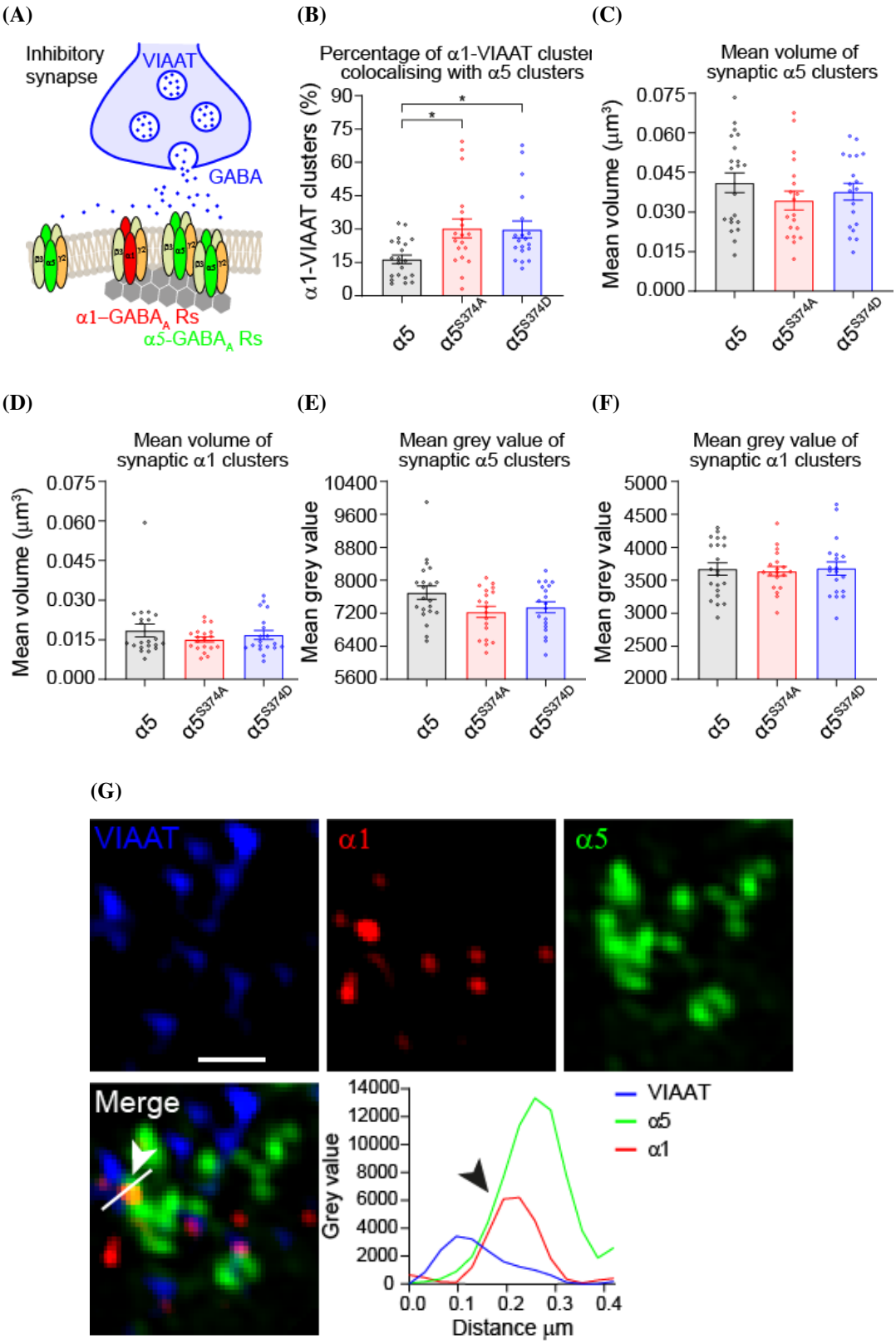
(A)
Inhibitory synapse
VIAAT
GABA
α1–GABA$_A$ Rs
α5-GABA$_A$ Rs
(B)
Percentage of α1-VIAAT cluster colocalising with α5 clusters
α1-VIAAT clusters (%)
90
75
60
45
30
15
0
*
*
α5
α5^{S374A}
α5^{S374D}
(C)
Mean volume of synaptic α5 clusters
Mean volume (µm^3)
0.075
0.060
0.045
0.030
0.015
0.000
α5
α5^{S374A}
α5^{S374D}
(D)
Mean volume of synaptic α1 clusters
Mean volume (µm^3)
0.075
0.060
0.045
0.030
0.015
0.000
α5
α5^{S374A}
α5^{S374D}
(E)
Mean grey value of synaptic α5 clusters
Mean grey value
10400
9600
8800
8000
7200
6400
5600
α5
α5^{S374A}
α5^{S374D}
(F)
Mean grey value of synaptic α1 clusters
Mean grey value
5000
4500
4000
3500
3000
2500
2000
α5
α5^{S374A}
α5^{S374D}
(G)
VIAAT
α1
α5
Merge
Grey value
14000
12000
10000
8000
6000
4000
2000
0
0.0
0.1
0.2
0.3
0.4
Distance µm
VIAAT
α5
α1

Figure 5.11: α_5^{S374} affects the colocalization of α_5 with α_1 subunits at synapses. **(A)** Schematic of inhibitory synapse composed of VIAAT as a presynaptic marker, α_1-$GABA_A$ as a postsynaptic marker and α_5-$GABA_A$Rs. Bar graphs represent **(B)** percentage of α_1-VIAAT clusters that colocalised with α_5 clusters, **(C)** mean volume of synaptic α_5 clusters, **(D)** mean volume of synaptic α_1 clusters, **(E)** mean grey value of synaptic α_5 clusters, **(F)** mean grey value of synaptic α_1 clusters. These are shown in black for wild-type α_5 (n=21), in red for phospho-null α_5^{S374A} (n=19) and in blue for phospho-mimetic α_5^{S374D} (n=19) transfected neurons. Points represent mean values calculated for individual cells. $*$ $p<0.05$, one-way ANOVA followed by Tukey's multiple comparisons test. **(G)** Example cell showing synaptic α_1-α_5 clusters with line scan across the synaptic axis.

5.3 Discussion

Super-resolution imaging is an effective way to visualise the nanoscale organization of inhibitory synapses. 3D SIM provides sufficient resolution to separate pre-and postsynaptic compartments and measure their physical properties such as the volume and mean grey value of clustered proteins. Using a semi-automated, unbiased, and high-throughput analysis workflow, I were able to analyse tens of thousands α_5-GABA$_A$Rs, gephyrin and VIAAT clusters.

Experiments on recombinant GABA$_A$Rs in HEK293 cells showed a reduction in cell surface expression levels for $\alpha_5{}^{S374A}\beta_3\gamma_{2L}$ receptors compared to $\alpha_5\beta_3\gamma_{2L}$ and $\alpha_5{}^{S374D}\beta_3\gamma_{2L}$ receptors. Therefore, I first analysed the cluster density of three markers – myc-tagged α_5 subunits, native gephyrin and VIAAT, along the dendrites together with the mean cluster volume and mean grey value in transfected hippocampal neurons expressing wild-type α_5 or mutant $\alpha_5{}^{S374A}$ or $\alpha_5{}^{S374D}$ GABA$_A$ subunits. No changes were observed in the density, mean volume or mean grey values of α_5-GABA$_A$Rs in the different transfection groups. Interestingly, these results were different from previous experiments modifying the gephyrin binding domain in GABA$_A$Rs containing the α_1 or α_2 subunits (Hines et al., 2018; Mukherjee et al., 2011; Nakamura et al., 2020). Phosphorylation of residue S^{359} in the gephyrin/collybistin binding domain of the α_2 subunit negatively impacted on the binding of α_2-GABA$_A$Rs to gephyrin/collybistin. Hippocampal neurons expressing phospho-mimetic S^{359D} construct had a reduced cluster density on the dendrites and a reduced enrichment of α_2-GABA$_A$Rs at the axon initial segment (Nakamura et al., 2020). Phosphorylation of residue T^{375} in gephyrin binding domain of the α_1 subunit also negatively regulated the affinity of the α_1 subunit for gephyrin. The density of α_1-GABA$_A$Rs clusters was also significantly reduced in hippocampal neurons transfected with a construct expressing phospho-mimetic $\alpha_1{}^{T375D}$ subunits (Mukherjee et al., 2011). Thus, phosphorylation of residues within the gephyrin binding domain of α_1 and α_2 subunits seems to affect the cluster density of GABA$_A$Rs containing these subunits. However, in our experiments, mimicking

the phosphorylation on S^{374} in the gephyrin binding domain of α_5 subunits did not affect the clustering or the surface expression levels of α_5-$GABA_A$Rs.

I quantified the number of α_5-$GABA_A$Rs clusters colocalizing with the pre- and postsynaptic markers, VIAAT and gephyrin respectively, and measured mean cluster size and brightness in neurons expressing wild-type or S^{374} mutant α_5 subunits. In all transfection groups, I routinely observed three classes of α_5-$GABA_A$Rs clusters in our imaging study: (1) the smallest and dimmest α_5-$GABA_A$Rs clusters which did not colocalise with either of the synaptic markers gephyrin and VIAAT (presumably extrasynaptic α_5-$GABA_A$Rs), (2) α_5-$GABA_A$Rs clusters colocalised with either gephyrin or VIAAT exhibit mid-range volume and brightness, and (3) α_5-$GABA_A$Rs colocalised with both markers (presumably synaptic α_5-$GABA_A$Rs) were the largest in volume and the brightest. These three classes of α_5-$GABA_A$Rs have been previously described in rat hippocampal cultures using immunofluorescence (Serwanski et al., 2006). Extrasynaptic α_5-$GABA_A$Rs were most likely clustered by radixin (Hausrat et al., 2015; Loebrich et al., 2006), while synaptic α_5-$GABA_A$Rs were presumably clustered by gephyrin (Brady and Jacob, 2015). In addition to its role at synaptic sites, gephyrin also reduces the lateral diffusion, and confines $GABA_A$Rs, at extrasynaptic locations (Battaglia et al., 2018). Thus, the extrasynaptic α_5-$GABA_A$Rs-gephyrin clusters could serve as a reserve pool for synaptic α_5-$GABA_A$Rs, diffusing to synaptic sites as pre-formed receptor-scaffold complexes, similar to extrasynaptic complexes formed between glycine receptors and gephyrin (Chapdelaine et al., 2021; Ehrensperger et al., 2007; Hakim and Ranft, 2020).

However, it should be emphasised that the majority of transfected α_5-$GABA_A$Rs did not colocalise with either marker, therefore most of the α_5-$GABA_A$Rs clusters appear to be extrasynaptic. Although I observed considerable heterogeneity in cluster colocalization, comparing different transfection groups revealed that there were significantly more α_5^{S374A} clusters colocalising with VIAAT clusters without gephyrin compared to wild-type or α_5^{S374D} transfected cells. By contrast, there were no transfection group specific changes in α_5 clusters colocalising with

gephyrin clusters without VIAAT (representing extrasynaptic α_5-gephyrin clusters). By quantifying the percentage of synaptic and extrasynaptic α_5-gephyrin clusters, there were significantly more synaptic α_5-gephyrin clusters in α_5^{S374A} compared to wild-type or α_5^{S374D} transfected cells. These results showing increased colocalization of α_5 clusters with key inhibitory synaptic markers suggest an increased accumulation of α_5-$GABA_A$Rs at postsynaptic sites in α_5^{S374A} transfected cells. However, there is evidence to suggest that the mechanism(s) for these changes could be, at least in part, gephyrin-independent.

Previous studies have shown that the α_5-$GABA_A$R interaction with radixin is necessary for the formation of extrasynaptic α_5-$GABA_A$Rs clusters (Loebrich et al., 2006) and dispersal of α_5-$GABA_A$Rs-radixin complexes increase their accumulation at synapses (Hausrat et al., 2015). An interaction with gephyrin is also important for the synaptic localisation of α_5-$GABA_A$Rs (Brady and Jacob, 2015), but gephyrin *per se* is not crucial for the synaptic clustering of α_5-$GABA_A$Rs as it was unaltered in spinal cord sections derived from gephyrin knock-out mice ((geph-/-)) (Kneussel et al., 2001). This suggests that although gephyrin and radixin both play a dynamic role in regulating the subcellular localisation of α_5-$GABA_A$Rs, other, unidentified proteins could be involved as well. The list of proteins involved in $GABA_A$Rs clustering at synapses is continuously expanding (Ko et al., 2015), but none of these proteins seem to have strong links to α_5-$GABA_A$Rs. Thus, more work is needed to identify proteins directly interacting with α_5-$GABA_A$Rs at synaptic and extrasynaptic sites.

It is important to consider the possibility that other subunits in the receptor pentamer may play a supportive role for a gephyrin/radixin independent clustering of α_5-$GABA_A$Rs at synaptic or extrasynaptic sites. Interestingly, the fourth transmembrane domain of the γ_2 subunit is reported to be sufficient for $GABA_A$R clustering *per se*, also, notably, both the cytoplasmic domain and the fourth transmembrane domain of the γ_2 subunit are required for the recruitment of gephyrin at synaptic sites (Alldred et al., 2005; Essrich et al., 1998). In the absence of the γ_2 subunit, the γ_3 subunit can also initiate clustering of $GABA_A$Rs at synaptic sites

(Kerti-Szigeti et al., 2014). In addition, post-translational modifications such as the phosphorylation of $\gamma_{2L}{}^{S327}$ have been shown to play a central role in gephyrin-independent $GABA_A$Rs clustering (Bannai et al., 2009; Muir et al., 2010; Niwa et al., 2012). For example, increased acute excitatory synaptic activity caused the dephosphorylation of residue $\gamma_{2L}{}^{S327}$, which in turn increased the lateral mobility of $GABA_A$Rs on the cell surface and led to reduced postsynaptic clustering and dispersal of $GABA_A$Rs and gephyrin from inhibitory synapses (Bannai et al., 2009; Muir et al., 2010). In this case, the de-clustering of synaptic $GABA_A$Rs was independent of gephyrin and gephyrin loss was a consequence only of receptor dispersal (Niwa et al., 2012). Therefore, increased synaptic accumulation of α_5-$GABA_A$Rs with or without gephyrin in $\alpha_5{}^{S374A}$ transfected cells seen in this study could be a combination of enhanced interaction with gephyrin, interaction with novel synaptic protein(s) and/or altered phosphorylation of other subunits in the pentamer.

The organisation of inhibitory synaptic compartments into discrete SSDs has been described, but the exact function or the regulation of the number of SSDs per synapse remains elusive (Crosby et al., 2019; Lushnikova et al., 2011; Pennacchietti et al., 2017; Yang et al., 2021). I demonstrated that the $\alpha_5{}^{S374A}$ transfected cells had significantly more gephyrin and VIAAT SSDs per α_5 cluster and the mean distance between α_5 and colocalising gephyrin or VIAAT clusters was the shortest compared to other transfection groups. There were no changes in SSD volumes between transfection groups, thus changes in the number of and proximities between SSDs could not be due to the cluster size. Instead, I speculate that it may represent an altered conformation of gephyrin and/or α_5-$GABA_A$Rs. Based on the existence of 'open' and 'closed' structural conformations for gephyrin (Sander et al., 2013), Battaglia and colleagues hypothesized that the distance between and/or the total number of gephyrin nanodomains, may depend on the conformational changes caused by the phosphorylation of gephyrin (Battaglia et al., 2018). The two different functional conformations for gephyrin depend on the folding of the linker domain (C-domain) and as gephyrin phosphorylation sites have been mapped in this domain (Pizzarelli et al., 2020; Zacchi et al., 2014), they suggested that phosphorylation could be a

switch between open and closed states within gephyrin nanodomains (Battaglia et al., 2018). Indeed, Yang and colleagues recently demonstrated that gephyrin SSDs contain high levels of phosphorylated gephyrin molecules at residue pS270 (Yang et al., 2021). The phosphorylation of residue S270 in gephyrin is primed by cyclin-dependent kinase 5 (CDK5) (Kalbouneh et al., 2014) and phosphorylated by GSK3β (Tyagarajan et al., 2011). GSK3β is also a kinase that I propose to directly phosphorylate α_5^{S374}. Therefore, it is plausible that GSK3β could be a central kinase in inhibitory transmission by phosphorylating several proteins such α_5-$GABA_A$Rs and gephyrin at inhibitory synapses to affect their structure and receptor accumulation.

An increased number of gephyrin nanodomains have been observed in hippocampal pyramidal cells during inhibitory long-term potentiation (Lushnikova et al., 2011; Pennacchietti et al., 2017) and in response to elevated neural activity by incubating neurons for 24h with bicuculline to block $GABA_A$R mediated inhibition (Crosby et al., 2019). Decreased numbers of gephyrin nanodomains have been seen after acute increased neural activity by 4-aminopyridine treatment in spinal cord neurons (Yang et al., 2021). Hence, I propose that the increased number of gephyrin and perhaps also VIAAT SSDs in α_5^{S374A} transfected cells could be caused by increased inhibitory transmission due to the increased synaptic accumulation of α_5-$GABA_A$Rs at these synapses.

In final part of this chapter, I asked whether the increased synaptic accumulation of α_5-$GABA_A$Rs in α_5^{S374A} transfected cells affects the colocalization of α_5-$GABA_A$Rs with other $GABA_A$Rs. I chose to investigate the colocalization between α_5-$GABA_A$Rs and α_1-$GABA_A$Rs clusters as the latter are 'classically' synaptic receptors and the most widely expressed in the brain (Pirker et al., 2000). Interestingly, the colocalization between α_5-$GABA_A$Rs and α_1-$GABA_A$Rs clusters was increased at both synaptic and extrasynaptic sites in neurons expressing either phospho-mimetic or phospho-dead, α_5^{S374A} and α_5^{S374D} respectively, constructs compared to neurons expressing wild-type α_5 subunits. Thus, this effect seemed to be dependent on residue α_5^{S374} but independent from phosphorylation.

In regard to synaptic inhibition mediated by α_5-GABA$_A$Rs, Zarnowska and colleges discussed that the larger amplitude subpopulation of GABA$_{A,slow}$ IPSCs, generated by synaptic/perisynaptic α_5-GABA$_A$Rs, may also have contained α_1-GABA$_A$Rs. Their experiments with diazepam and α_5^{H105R} mice support the idea that various receptor types could be present at the same synapses, either with synaptic α_1-GABA$_A$Rs and perisynaptic α_5-GABA$_A$Rs or possibly with α_1-α_5 present in the same hetero-alpha subunit receptor complex (Zarnowska et al., 2009). The GABA$_A$R pentamer has two non-equivalent positions for α subunits at β-α-β and β-α-γlocations. The existence of α_5-GABA$_A$Rs containing an α_1 subunit in a single receptor complex, where α_5 is positioned next to the γ_2 subunit, has been well documented, based largely on imaging and immunoprecipitation studies (Araujo et al., 1999; Balic et al., 2009; Benke et al., 2004; Christie and de Blas, 2002b; Ghafari et al., 2017; Ju et al., 2009; Müller Herde et al., 2017; del Río et al., 2001). In Chapter 4 I demonstrated that both mutants, α_5^{S374A} and α_5^{S374D}, had more large amplitude sIPSCs which could be blocked by the α_5-NAM, L-655,708. In this chapter, I showed increased colocalization for α_1 and α_5 subunits at extrasynaptic and synaptic areas for both α_5^{S374A} and α_5^{S374D} expressing cells. Therefore, based on previous findings and our results, I propose that the larger amplitude subpopulation of GABA$_{A,slow}$ IPSCs is potentially generated by GABA$_A$Rs containing both α_1 and α_5 subunits. I hypothesize that the phosphorylation of residue α_5^{S374} controls the subsynaptic location of α_5-GABA$_A$Rs, and that this residue, independently from phosphorylation, is important for α_5 to interact with α_1 subunits.

Chapter 6

General Discussion

6.1 Overall rationale for this project

The α_5-GABA$_A$R isoform has received a lot of interest in recent years due to their unique distribution in the brain accompanied by their dual, synaptic and extrasynaptic, subcellular location. Moreover, this receptor subtype has an important role in inhibitory postsynaptic plasticity (Davenport et al., 2021; Martin et al., 2010; Schulz et al., 2019; Wyroślak et al., 2021), cognition (Atack et al., 2006; Ballard et al., 2009; Chambers et al., 2003; Dawson et al., 2006; Gacsályi et al., 2017; Knust et al., 2009; Martínez-Cué et al., 2013) and memory (Collinson et al., 2002, 2006; Crestani et al., 2002; Davenport et al., 2021; Engin et al., 2015, 2020; Ghafari et al., 2017; Martin et al., 2009, 2010; Möhler and Rudolph, 2017; Prut et al., 2010; Zurek et al., 2012). Thus, promoting α_5-GABA$_A$Rs as an ideal target for the treatment of pathological conditions particularly involving cognitive dysfunction (Jacob, 2019; Mohamad and Has, 2019). Despite their considerable therapeutic potential, no study to date has examined the effects of phosphorylation on synaptic targeting of α_5-GABA$_A$Rs to identify molecular mechanisms of action that could be significant in these physiological processes.

6.2 Summary of key findings

In this project I identified several phosphorylation sites within the large intracellular domain of the α_5 subunit including three that are located in the gephyrin binding domain and of these, residue S^{374} was selected for further investigation. Using

phospho-mimetic and phospho-null mutations of this S^{374} site, I provided evidence that phosphorylation of $\alpha_5{}^{S374}$, possibly by kinase GSK3β, affects receptor function and favours extrasynaptic location whereas dephosphorylation of S^{374} increases the synaptic accumulation of α_5-$GABA_A$Rs. This type of phosphoregulation relies on the dynamic and transient interactions between the receptor and the postsynaptic scaffold protein gephyrin (Brady and Jacob, 2015; Tretter et al., 2012). Moreover, previous research has shown that the phosphorylation of other $GABA_A$Rs subunits (e.g. $\alpha_{1\text{-}2}$) (Kowalczyk et al., 2013; Nakamura et al., 2020; Petrini et al., 2014; Tretter et al., 2008) as well as gephyrin (Battaglia et al., 2018; Flores et al., 2015; Tyagarajan et al., 2011) is a key step in regulating the number of $GABA_A$Rs at postsynaptic sites during GABAergic postsynaptic plasticity (Barberis, 2020; Tyagarajan and Fritschy, 2010). Similarly, the main conclusion derived from this study is that the role of phosphorylating $\alpha_5{}^{S374}$ is most likely to modulate α_5-GABAergic postsynaptic plasticity via receptor interaction with gephyrin.

6.3 Relocation of extrasynaptic α_5-$GABA_A$Rs to synaptic areas

Although the source of the increased number of synapses containing α_5-$GABA_A$Rs in $\alpha_5{}^{S374A}$ transfected cells was not addressed in this study, I presumed, from prior work on other $GABA_A$Rs by others, that these receptors laterally diffuse into synapses from extrasynaptic areas either as receptors alone or receptor-gephyrin complexes (Davenport et al., 2021; Hakim and Ranft, 2020; Hausrat et al., 2015). I demonstrated that increased synaptic accumulation of α_5-$GABA_A$Rs resulted from replacing a phosphorylation consensus residue with alanine ($\alpha_5{}^{S374A}$) in the gephyrin binding domain of the α_5 subunit. Under physiological conditions, the targeted relocation of extrasynaptic α_5-$GABA_A$Rs to synaptic sites can be trigged by enhanced neuronal activity which increases the number of synaptic α_5-$GABA_A$Rs and strengthens phasic inhibitory transmission mediated by these receptors (Davenport et al., 2021; Hausrat et al., 2015).

In the hippocampus, activity-dependent plasticity of synaptic transmission, classically represented by excitatory as well as inhibitory long-term potentiation and depression (LTP and iLTP, LTD and iLTD respectively), is a neural correlate of learning and memory (Gaiarsa et al., 2002). As α_5-GABA$_A$Rs have a direct role in these physiological processes, LTP and iLTP have been used to examine the molecular changes that occur during a variety of cognitive tasks. Recent studies have focused on how synaptic transmission is affected by the induction of both LTP and iLTP within the hippocampus. For example, induction of iLTP enhanced tonic current in hippocampal CA1 pyramidal neurons by increasing the pool of extrasynaptic α_5-GABA$_A$Rs (Wyroślak et al., 2021). By contrast, induction of LTP in CA1 pyramidal neurons was shown to drive initially extrasynaptic α_5-GABA$_A$Rs into synapses which in turn strengthened synaptic inhibition and supressed the LTP (Davenport et al., 2021). This dynamic relocation of α_5-GABA$_A$Rs required the dissociation of the α_5-GABA$_A$Rs-radixin complex and the presence of gephyrin at inhibitory synapses. Increased accumulation of synaptic α_5-GABA$_A$Rs was associated with impaired short-termed memory and reversal learning which was rescued by photo-blocking α_5-GABA$_A$Rs (Davenport et al., 2021; Hausrat et al., 2015). Hence, I hypothesize that dephosphorylation of α_5^{S374} is part of the molecular mechanism involved in activity-dependent relocation of extrasynaptic α_5-GABA$_A$Rs into synapses in conjunction with dephosphorylation of radixin residue T564 (Davenport et al., 2021; Hausrat et al., 2015). Although the exact role in cognitive function of these changes in postsynaptic α_5-GABA$_A$R localisation remains elusive, the emerging evidence emphasises its critical importance for stabilizing learned associations (Davenport et al., 2021). A delicate balance in synaptic receptor recruitment has to be achieved, since abnormal increased relocation of extrasynaptic α_5-GABA$_A$Rs to synapses may lead to pathological conditions, such as Huntington's disease (Rosas-Arellano et al., 2017).

6.4 Therapeutic potential of α_5-GABA$_A$Rs

The α_5-GABA$_A$R isoform can also directly affect the generation of LTP. For example, genetic deletion (*Gabra5 -/-* mouse model) or pharmacological inhibition of α_5-GABA$_A$Rs (via L-655,708) reduced the threshold for LTP induction in CA1 stratum radiatum neurons (Martin et al., 2010). Previous studies have shown that Ts65Dn mice, a mouse model for Down Syndrome (DS,) exhibits excessive α_5-GABAergic inhibition which contributes to cognitive dysfunction in these mice (Block et al., 2017; Braudeau et al., 2011; Duchon et al., 2019; Kleschevnikov et al., 2004; Martínez-Cué et al., 2013, 2014; Möhler, 2012; Schulz et al., 2019; Vidal et al., 2017). In Ts65Dn mice, *in vivo* LTP at hippocampal CA3-CA1 synapses could not be evoked by a high-frequency stimulation (HFS) protocol. However, LTP was sustainably restored in these mice by blocking α_5-GABA$_A$Rs with an α_5-selective inverse agonist (α5IA) (Duchon et al., 2019). In the same mouse model, another α_5-GABA$_A$R-selective inverse agonist, RO4938581, also completely restored LTP induced by theta burst stimulation in CA1 stratum radiatum neurons (Martínez-Cué et al., 2013). Importantly, all mentioned NAMs of α_5-GABA$_A$Rs enhance cognition in both, wild-type and Down syndrome mouse model (Jacob, 2019; Möhler, 2012). As there are no gross changes in the distribution or expression levels of α_5-GABA$_A$Rs in the hippocampus of Ts65Dn mice, over-inhibition is likely caused by the changes in the properties of individual GABAergic synapses (Kleschevnikov et al., 2012; Zorrilla de San Martin et al., 2018). This could involve both pre- and postsynaptic mechanisms. I propose that the dysregulation to the phosphorylation/dephosphorylation balance of α_5^{S374} results in increased extrasynaptic/synaptic accumulation of α_5-GABA$_A$Rs that could play a significant role in the excessive inhibition observed in Ts65Dn mice (Schulz et al., 2018, 2019). Therefore, the molecular mechanisms revealed in this study could significantly contribute to further research about the treatment of cognitive disability in Down syndrome as well as cognitive deficits in other neuropathological diseases.

Interestingly, the ability of α_5-GABA$_A$Rs to regulate the threshold for induction of LTP depends on the brain region and is the highest at ventral hippocampal

CA1 synapses (Pofantis and Papatheodoropoulos, 2014) which is in agreement with the higher expression levels of these receptors in the CA1 region of ventral compared to dorsal hippocampus (Sotiriou et al., 2005). The dominant view is that the cognitive functions such as spatial memory and navigation, assessed with the water maze and radial maze for example, are thought to involve the dorsal hippocampus, whereas the ventral segment of the hippocampus mediates anxiety-related behaviours and is involved in unconditioned fear responses often studied by the elevated plus maze (EPM) (Strange et al., 2014).

α_5-GABA$_A$Rs in the ventral hippocampus may play an important role in schizophrenia as patients have increased hippocampal activity at rest (Medoff et al., 2001) which is the result of reduced GABAergic inhibition (Heckers and Konradi, 2015) most likely caused by the reduction in the number of SST INs (Konradi et al., 2011). Given that α_5-GABA$_A$Rs are more highly expressed at synapses onto SST INs (Magnin et al., 2019; Salesse et al., 2011), this may imply that a specific deficit in α_5-GABA$_A$Rs inhibition is important. Indeed, overexpression of α_5-GABA$_A$Rs in ventral hippocampus of the methylazoxymethanol (MAM) model of schizophrenia, by viral-mediated gene transfer, rescued inhibitory signalling, normalized pyramidal cell activity and rescued impaired cognitive functions (Donegan et al., 2019). The deficits in α_5-GABA$_A$Rs mediated inhibition in the MAM model were also reversed by the α_5 selective positive allosteric modulator, SH-053-2'F-R-CH3 (Gill et al., 2011).

6.5 α_5-GABA$_A$Rs control dendritic outgrowth and spine morphology

Most GABAergic contacts are formed onto dendritic shafts and small protrusions known as dendritic spines. Dendritic spines are postsynaptic compartments consisting of postsynaptic density (PSD) and receive the majority of excitatory input in the brain (Higley, 2014). Following synaptic plasticity, including LTP and LTD, spines can undergo morphological plasticity (Matsuzaki et al., 2004; Nishiyama, 2019; Oh et al., 2013; Zhou et al., 2004). Spine morphology studies in cultured hippocampal

neurons have shown that the shift in extrasynaptic/synaptic membrane localisation of α_5-GABA$_A$Rs significantly disrupts dendritic outgrowth and spine morphology. A relocation of synaptic α_5-GABA$_A$Rs to extrasynaptic areas resulted in enhanced dendritic outgrowth and a less mature dendritic spine phenotype (Brady and Jacob, 2015). Treatment with the α_5 NAM L-655,708 (50 nM for 48 h) also reduced dendritic spine maturation but without affecting dendritic branch complexity (Nuwer et al., 2021). By contrast, treatment of cultured cortical neurons with the α_5 PAM, GL-II-73 (1 μM for 24h), increased dendritic branch complexity and the number of spines (Prevot et al., 2021). Although dendritic spine morphology and complexity of dendritic branching were not assessed in this study, future work should explore these aspects of neuronal structure in α_5^{S374A} and α_5^{S374D} transfected neurons.

6.6 α_5-GABA$_A$Rs in other brain regions

In contrast to high expression levels of α_5-GABA$_A$Rs in the hippocampus, these receptors are expressed at low-to-moderate levels in the amygdala (Heldt and Ressler, 2007; Müller Herde et al., 2017). As *Gabra5 -/-* mice exhibit deficits in learning and memory, but normal anxiety levels (Collinson et al., 2002; Martin et al., 2009), there have not been many papers investigating the role of extrasynaptic and synaptic α_5-GABA$_A$Rs in the amygdala until recently. The amygdala is a brain region known for processing emotion and is broadly divided into the basolateral complex (BLA) and the central nucleus of the amygdala (CeA). The CeA is made up of a lateral (CeL) and a medial (CeM) subdivision with the CeL projecting to the CeM. Neurons in both subdivisions are primarily GABAergic (Janak and Tye, 2015). There are different types of neurons, but the best characterised are those expressing the protein kinase C-delta isoform (PKCδ+), and those expressing SST but negative for PKCδ (PKCδ-). Approximately 50% of CeL GABAergic neurons are expressing PKCδ+ (Haubensak et al., 2010) and, in turn, about 70% of PKCδ+ neurons in CeA are also expressing the α_5 subunit (Botta et al., 2015). It was recently demonstrated that extrasynaptic α_5-GABA$_A$Rs, mediating tonic inhibition in PKCδ+ neurons, contribute to the regulation of anxiety. After auditory fear

conditioning, PKCδ+ neurons exhibited a reduced tonic conductance, mediated by α_5-containing receptors. The authors suggested that the reduced extrasynaptic inhibition in these cells is most likely caused by alternations in the numbers and/or properties of α_5-$GABA_A$Rs expressed by CeA PKCδ+ neurons (Botta et al., 2015). Therefore, it is plausible that regulation of extrasynaptic or synaptic accumulation of α_5-$GABA_A$Rs by phosphorylation studied in cultured hippocampal neurons in this project, is also relevant for other brain areas, including the amygdala.

6.7 Similar slow kinetic profiles for α_5-$GABA_A$Rs and NMDARs

As described in Section 1.9, α_5-$GABA_A$R-mediated currents have slow decay kinetics, a feature that makes this isoform unique for $GABA_A$Rs (Cao et al., 2020; Capogna and Pearce, 2011; Magnin et al., 2019; Prenosil et al., 2006; Salesse et al., 2011; Schulz et al., 2018; Vargas-Caballero et al., 2010; Zarnowska et al., 2009). Schulz and colleagues found that the decay time and voltage-dependent activation threshold of α_5-$GABA_A$R-mediated currents closely match with the time profile for currents mediated by excitatory N-methyl-D-aspartate (NMDA) receptors (NMDARs) (Schulz et al., 2019). Indeed, there appears to be a complex interplay between α_5-$GABA_A$Rs and NMDARs, both participate in the bidirectional control of excitatory and inhibitory synaptic transmission. Inhibitory LTP, induced by the pharmacological activation of NMDARs, increased the proportion of extrasynaptic α_5-GABARs (Wyroślak et al., 2021), recruited extrasynaptic gephyrin to synaptic compartments (Pennacchietti et al., 2017; Petrini et al., 2014) and increased the complexity of inhibitory postsynaptic densities (PSD) (Pennacchietti et al., 2017). Activation of NMDARs by theta burst stimulation (TBS) and corresponding Ca^{2+} influx during excitatory LTP, caused the relocation of extrasynaptic α_5-GABARs to synapses. This accumulation of synaptically-clustered α_5-GABARs prevented not only NMDAR activation but also the following excitatory LTP (Davenport et al., 2021). Furthermore, the previously described Down syndrome mouse model, Ts65Dn, have impaired NMDAR activation, which could be rescued by

blocking approximately 50% of the α_5-GABARs in dendritic synapses by acute application of α_5-NAM RO4938581 (1 μM) (Martínez-Cué et al., 2013, Schulz et al., 2018). Thus, noting the functional synchrony and physical proximity of these α_5- and NMDA-receptors in CA1 pyramidal cells, I propose that dephosphorylation of α_5^{S374} followed by relocation of α_5-$GABA_A$Rs to synaptic sites in hippocampal neurons likely requires nearby NMDAR-mediated signalling and a concurrent increase in cytoplasmic Ca^{2+}. Conversely, phosphorylation of α_5^{S374} by GSK3β at synaptic sites promotes the transfer of α_5-GABARs to extrasynaptic areas, thus allowing more activation of synaptic NMDARs.

The direct interplay between GSK3β and NMDA receptors has been described in many studies. For example, Ppp1r2cre/Grin1 knockout (KO) mice, a model of NMDAR hypofunction relevant to schizophrenia, exhibit reduced function of NMDARs due to the lack of the essential NMDAR subunit Grin1 in 50% of cortical and hippocampal GABAergic neurons and over-activation of GSK3β. The genetic deletion of GSK3β in GABAergic neurons reversed the synaptic and cognitive deficits described in this mouse model (Nakao et al., 2020). Similarly, conditional cell-type–specific deletion of GSK3β in neurons expressing dopamine D2 receptors, resulted in increased NMDA function in the medial prefrontal cortex (Li et al., 2020). In another study, NMDA receptor expression in prefrontal cortical neurons was increased by lithium treatment, a common drug that blocks GSK3β activity by increasing phosphorylation on S9 in GSK3β (Monaco et al., 2018). Moreover, NMDAR subunit expression and synaptic content is directly affected by the activity of α_5-GABARs (Nuwer et al., 2021).

6.8 Remaining questions and future work

Although the present study sheds light on molecular mechanisms of inhibitory postsynaptic plasticity mediated by α_5-$GABA_A$Rs, and lays a strong foundation for further studies, several questions remain unanswered.

6.8.1 Experiments for elaborating the current findings

First, multiple phosphorylation sites were detected in the large intracellular domain of the α_5 subunit. Although this study focused on the role of $\alpha_5{}^{S374}$, it would be interesting to further investigate the role(s) of the other phosphorylation consensus sites identified by mass-spectrometry. Residues $\alpha_5{}^{T379}$ and/or $\alpha_5{}^{T380}$ most likely serve as a priming residue for phosphorylation of $\alpha_5{}^{S374}$ by GSK3β. Further along the intracellular loop more potential phosphorylation consensus residues (Q8BHJ7, amino acids 400-428) could regulate the binding of other unidentified proteins. Thus, a new mass-spectrometry analysis to identify novel binding partners should be performed. Secondly, the binding affinities of wild-type and mutated α_5-GABA$_A$Rs to gephyrin were not assessed in this study. This could be addressed in future experiments using a binding affinity assay. A biochemical assay to show direct phosphorylation of $\alpha_5{}^{S374}$ by GSK3β and dephosphorylation by phosphatases *in vitro* is also needed. To quantify the amount of phosphorylated $\alpha_5{}^{S374}$ *in vivo*, a phospho-antibody directed against phosphorylated $\alpha_5{}^{S374}$ should be generated. This could be used in biochemical (e.g., Western blot) and imaging studies.

The α_5 NAM, L-655,708, was chosen as it is the most widely used drug in α_5-GABA$_A$Rs research (Quirk et al., 1996). Yet, there are several other α_5-NAMs available (Maramai et al., 2020). Recent studies have shown that L-655,708 has little effect on synaptic α_5-GABA$_A$Rs acting more so via extrasynaptic α_5-GABA$_A$Rs instead (Manzo et al., 2021; Nuwer et al., 2021). Thus, other α_5-NAMs and α_5-PAMs should be tested to refine the functional signature of synaptic α_5-GABA$_A$Rs.

The peptide approach used in electrophysiology studies could also be used in 3D SIM imaging. Blocking the binding between α_5-GABA$_A$Rs and gephyrin by using a competitive peptide was successful as demonstrated by electrophysiology. Hence, it is likely that 3D SIM imaging could detect a reduced synaptic location for α_5-GABA$_A$Rs after incubating cells with a cell-permeable version of the blocking peptide.

6.8.2 Future directions

As discussed previously, the synaptic accumulation of α_5-GABA$_A$Rs is highly cell-type and brain region-specific. Thus, future studies should specifically target the distinct subcellular populations, extrasynaptic or synaptic, α_5-GABA$_A$Rs in defined cell types. To investigate the role of α_5-GABA$_A$Rs in the control of anxiety, phospho-regulation of α_5-GABA$_A$Rs should be addressed within specific neuronal circuits responsible for that behaviour as demonstrated by the virus-based approach adopted by Botta and colleges (Botta et al., 2015). Most work to date has centred on the hippocampus, but other brain regions where α_5-GABA$_A$Rs are expressed such as amygdala and olfactory bulb would expand our understanding of the physiological role of α_5-GABA$_A$Rs in other behavioural processes.

The role of α_5-GABA$_A$Rs in pathological conditions has been well documented and ongoing efforts are being made to specifically target α_5-GABA$_A$Rs using NAMs and PAMs. The studies described in this thesis offer new understanding about the control of synaptic and extrasynaptic accumulation of the α_5-GABA$_A$R at a molecular level, orchestrated by α_5 subunit phosphorylation. Thus, future studies in terms of pathological conditions should focus on one subsynaptic population at time, for example, by targeting phosphorylated α_5-GABA$_A$R.

Appendix A

Details of primers, constructs, drugs, antibodies and software used in experiments.

Table A.1: Details of primers used for mutagenesis.

Primer	Sequence 5'-3'	Template
Forward	CTTTTACAACTGGAAAGCTGACC	α_5-GABA$_A$R
374A-Reverse	CATTTGTTGcCTTATTTAGTATGAG	or
S^{374D}-Reverse	CATTTGTgtcCTTATTTAGTATGAG	myc-α_5-GABA$_A$R

Table A.2: Details of constructs used in experiments.

Construct	Vector	Insert	Tag
pRK5-eGFP	pRK5	eGFP	-
α_5		α_5	-
α_5^{S374A}		α_5^{S374A}	-
α_5^{S374D}		α_5^{S374D}	-
Myc-α_5		Myc-α_5	Myc-tag (replacing amino acids 28 and 29 in mouse α_5 subunit)
Myc-α_5^{S374A}		Myc-α_5^{S374A}	
Myc-α_5^{S374D}		Myc-α_5^{S374D}	
β_3		β_3	-
Flag-β_3		Flag-β_3	Flag-tag (inserted between amino-acids 23 and 24 in mouse β_3 subunit)
γ_{2L}		γ_{2L}	-
pcDNA3-HA-GSK3β S9A	pcDNA3	HA-GSK3β S9A	HA-tag (C terminal on insert)

Table A.3: Details of drugs and peptides used in experiments.

Compound	Abbrev.	Source	Stock	Solvent	Working concentration
Dimethyl sulfoxide	DMSO	Sigma-Aldrich	-	-	0.0001% v/v
Phorbol 12-myristate 13-acetate	PMA	Calbiochem	2 mM	DMSO	200 nM
CHIR99021	CHIR	Calbiochem	10 mM	DMSO	1 μM
Gamma-aminobutyric acid	GABA	Sigma-Aldrich	1 M	water	0.01-300 μM
L-655,708	L655	Santa Cruz Biochemicals	5 mM	DMSO	50 nM
Picrotoxin	PTX	Sigma-Aldrich	100 mM	DMSO	100 μM
CH_3CO-KSNAFTTGKLTHPPN-NH_2CO	Blocking peptide	Biomatik	3 mM	water	30 μM
CH_3CO-TSTLFPTHKKPNNAG-NH_2CO	Scrambled peptide	Biomatik	3 mM	water	30 μM

Table A.4: Details of antibodies used in experiments.

Antibody	IP dilution	Immunostaining	Epitope details	Source
Primary antibodies				
Guinea pig anti-α_5 subunit	2.5 µl per 500 µl	1:2000	Amino acids 32 –41 (QMPTSSVQDE) of rat α_5 subunit	gift from Dr Jean-Marc Fritschy
Mouse anti-myc	15 µl per 500 µl	1:500	Myc-tag at the start of the mature protein	Abcam, ab32
Rabbit anti-myc	-	1:500		Abcam, ab9106
Mouse anti-flag tag	15 µl per 500 µl	-	Flag-tag at the start of the mature protein	Sigma, M2
Rabbit anti-α_1 subunit	-	1:200	Amino acids 28-42 (QPSQDELKDNTTVFT) of rat α_1 subunit	Abcam, ab33299
Guinea pig anti-VIAAT	-	1:500	Amino acids 106-120 (GEFGGHDKPKITAWE) of rat VIAAT protein	Alomone labs, AGP-129
Mouse anti-gephyrin	-	1:200	Amino acids 326-550 (SSKENILRASHSAVDITKVARRHRMSPFPL) from rat gephyrin protein	Synaptic Systems, SYSY3B11

Antibody	IP dilution	Immunostaining	Epitope details	Source
Secundary antibodies				
Anti-rabbit Alexa Flour 488	-	1:500	IgG	Invitrogen, A-11034
Anti-mouse Alexa Flour 555	-	1:500	IgG (H+L)	Invitrogen, A-21424
Anti-guinea pig Alexa Flour 647	-	1:500	IgG (H+L)	Invitrogen, A-21450

Table A.5: Details of software used in experiments and analysis.

Software	Reference/source	Website
NetPhos 3.1 server	(Blom et al., 2004)	https://www.cbs.dtu.dk/services/NetPhos/
ELM	(Kumar et al., 2020)	https://elm.eu.org
ImageJ	National Institutes of Health	https://imagej.nih.gov/ij/
Prism	GraphPad	https://www.graphpad.com/scientific-software/prism/
MATLAB	Mathworks	https://www.mathworks.com
Adobe Illustrator CS6	Adobe	https://www.adobe.com/
WinEDR	Strathclyde Electrophysiology Software	https://spider.science.strath.ac.uk/sipbs/software_ses.htm
WinWCP	Origin OriginLab	https://www.originlab.com/

Bibliography

Abramian, A. M., Comenencia-Ortiz, E., Vithlani, M., Tretter, E. V., Sieghart, W., Davies, P. A., & Moss, S. J. (2010). Protein kinase C phosphorylation regulates membrane insertion of $GABA_A$ receptor subtypes that mediate tonic inhibition. *Journal of Biological Chemistry*, *285*(53), 41795–41805.

Ali, A. B., & Thomson, A. M. (2008). Synaptic α_5 subunit–containing $GABA_A$ receptors mediate IPSPs elicited by dendrite-preferring cells in rat neocortex. *Cerebral cortex*, *18*(6), 1260–1271.

Alldred, M. J., Mulder-Rosi, J., Lingenfelter, S. E., Chen, G., & Lüscher, B. (2005). Distinct γ_2 subunit domains mediate clustering and synaptic function of postsynaptic $GABA_A$ receptors and gephyrin. *Journal of Neuroscience*, *25*(3), 594–603.

Araujo, F., Ruano, D., & Vitorica, J. (1998). Absence of association between δ and γ_2 subunits in native $GABA_A$ receptors from rat brain. *European journal of pharmacology*, *347*(2-3), 347–353.

Araujo, F., Ruano, D., & Vitorica, J. (1999). Native $GABA_A$ receptors from rat hippocampus, containing both α_1 and α_5 subunits, exhibit a single benzodiazepine binding site with α_5 pharmacological properties. *Journal of Pharmacology and Experimental Therapeutics*, *290*(3), 989–997.

Atack, J. R. (2011). $GABA_A$ receptor subtype-selective modulators. II. α_5-selective inverse agonists for cognition enhancement. *Current topics in medicinal chemistry*, *11*(9), 1203–1214.

Atack, J. R., Bayley, P. J., Seabrook, G. R., Wafford, K. A., McKernan, R. M., & Dawson, G. R. (2006). L-655,708 enhances cognition in rats but is not

proconvulsant at a dose selective for α_5-containing $GABA_A$ receptors. *Neuropharmacology*, *51*(6), 1023–1029.

Baker, P. M., Pennefather, P. S., Orser, B. A., & Skinner, F. K. (2002). Disruption of coherent oscillations in inhibitory networks with anesthetics: role of $GABA_A$ receptor desensitization. *Journal of neurophysiology*, *88*(5), 2821–2833.

Balic, E., Rudolph, U., Fritschy, J.-M., Mohler, H., & Benke, D. (2009). The α_5 (H105R) mutation impairs α_5 selective binding properties by altered positioning of the α_5 subunit in $GABA_A$ receptors containing two distinct types of α subunits. *Journal of neurochemistry*, *110*(1), 244–254.

Ballard, T. M., Knoflach, F., Prinssen, E., Borroni, E., Vivian, J. A., Basile, J., Gasser, R., Moreau, J.-L., Wettstein, J. G., Buettelmann, B., et al. (2009). RO4938581, a novel cognitive enhancer acting at α_5 subunit-containing $GABA_A$ receptors. *Psychopharmacology*, *202*(1-3), 207–223.

Banks, M. I., & Pearce, R. A. (2000). Kinetic differences between synaptic and extrasynaptic $GABA_A$ receptors in CA1 pyramidal cells. *Journal of Neuroscience*, *20*(3), 937–948.

Banks, M. I., White, J. A., & Pearce, R. A. (2000). Interactions between distinct $GABA_A$ circuits in hippocampus. *Neuron*, *25*(2), 449–457.

Bannai, H., Lévi, S., Schweizer, C., Inoue, T., Launey, T., Racine, V., Sibarita, J.-B., Mikoshiba, K., & Triller, A. (2009). Activity-dependent tuning of inhibitory neurotransmission based on $GABA_A$ receptor diffusion dynamics. *Neuron*, *62*(5), 670–682.

Barberis, A. (2020). Postsynaptic plasticity of GABAergic synapses. *Neuropharmacology*, *169*, 107643.

Battaglia, S., Renner, M., Russeau, M., Côme, E., Tyagarajan, S. K., & Lévi, S. (2018). Activity-dependent inhibitory synapse scaling is determined by gephyrin phosphorylation and subsequent regulation of $GABA_A$ receptor diffusion. *Eneuro*, *5*(1).

Baumann, S. W., Baur, R., & Sigel, E. (2001). Subunit arrangement of $GABA_A$ receptors. *Journal of Biological Chemistry*, *276*(39), 36275–36280.

Baumann, S. W., Baur, R., & Sigel, E. (2002). Forced subunit assembly in $\alpha_1\beta_2\gamma_2$ $GABA_A$ receptors: insight into the absolute arrangement. *Journal of Biological Chemistry*, *277*(48), 46020–46025.

Baumann, S. W., Baur, R., & Sigel, E. (2003). Individual properties of the two functional agonist sites in $GABA_A$ receptors. *Journal of Neuroscience*, *23*(35), 11158–11166.

Benke, D., Fakitsas, P., Roggenmoser, C., Michel, C., Rudolph, U., & Mohler, H. (2004). Analysis of the presence and abundance of $GABA_A$ receptors containing two different types of α subunits in murine brain using point-mutated α subunits. *Journal of Biological Chemistry*, *279*(42), 43654–43660.

Beurel, E., Grieco, S. F., & Jope, R. S. (2015). Glycogen synthase kinase-3 (GSK3): regulation, actions, and diseases. *Pharmacology & therapeutics*, *148*, 114–131.

Bianchi, M. T., & Macdonald, R. L. (2002). Slow phases of $GABA_A$ receptor desensitization: structural determinants and possible relevance for synaptic function. *The Journal of physiology*, *544*(1), 3–18.

Bianchi, M., Haas, K., & Macdonald, R. (2002). A_1 and α_6 subunits specify distinct desensitization, deactivation and neurosteroid modulation of $GABA_A$ receptors containing the δ subunit. *Neuropharmacology*, *43*(4), 492–502.

Block, A., Ahmed, M. M., Rueda, N., Hernandez, M.-C., Martinez-Cué, C., & Gardiner, K. (2018). The α_5-$GABA_A$ -selective modulator, RO4938581, rescues protein anomalies in the Ts65Dn mouse model of Down syndrome. *Neuroscience*, *372*, 192–212.

Blom, N., Sicheritz-Pontén, T., Gupta, R., Gammeltoft, S., & Brunak, S. (2004). Prediction of post-translational glycosylation and phosphorylation of proteins from the amino acid sequence. *Proteomics*, *4*(6), 1633–1649.

Bogdanov, Y., Michels, G., Armstrong-Gold, C., Haydon, P. G., Lindstrom, J., Pangalos, M., & Moss, S. J. (2006). Synaptic $GABA_A$ receptors are directly

recruited from their extrasynaptic counterparts. *The EMBO journal*, *25*(18), 4381–4389.

Bonin, R. P., Martin, L. J., MacDonald, J. F., & Orser, B. A. (2007). α_5-$GABA_A$ receptors regulate the intrinsic excitability of mouse hippocampal pyramidal neurons. *Journal of neurophysiology*, *98*(4), 2244–2254.

Bonnert, T. P., McKernan, R. M., Farrar, S., le Bourdellès, B., Heavens, R. P., Smith, D. W., Hewson, L., Rigby, M. R., Sirinathsinghji, D. J., Brown, N., et al. (1999). Θ, a novel $GABA_A$ receptor subunit. *Proceedings of the National Academy of Sciences*, *96*(17), 9891–9896.

Bosman, L. W., Rosahl, T. W., & Brussaard, A. B. (2002). Neonatal development of the rat visual cortex: synaptic function of $GABA_A$ receptor α subunits. *The Journal of physiology*, *545*(1), 169–181.

Botta, P., Demmou, L., Kasugai, Y., Markovic, M., Xu, C., Fadok, J. P., Lu, T., Poe, M. M., Xu, L., Cook, J. M., et al. (2015). Regulating anxiety with extrasynaptic inhibition. *Nature neuroscience*, *18*(10), 1493–1500.

Brady, M. L., & Jacob, T. C. (2015). Synaptic localization of α_5-$GABA_A$ receptors via gephyrin interaction regulates dendritic outgrowth and spine maturation. *Developmental neurobiology*, *75*(11), 1241–1251.

Brandon, N. J., Delmas, P., Kittler, J. T., McDonald, B. J., Sieghart, W., Brown, D. A., Smart, T. G., & Moss, S. J. (2000). $GABA_A$ receptor phosphorylation and functional modulation in cortical neurons by a protein kinase C-dependent pathway. *Journal of Biological Chemistry*, *275*(49), 38856–38862.

Brandon, N. J., Jovanovic, J. N., & Moss, S. J. (2002). Multiple roles of protein kinases in the modulation of $GABA_A$ receptor function and cell surface expression. *Pharmacology & therapeutics*, *94*(1-2), 113–122.

Brandon, N. J., Jovanovic, J. N., Smart, T. G., & Moss, S. J. (2002). Receptor for activated C kinase-1 facilitates protein kinase C-dependent phosphorylation and functional modulation of $GABA_A$ receptors with the activation of G-protein-coupled receptors. *Journal of Neuroscience*, *22*(15), 6353–6361.

Brandon, N., Delmas, P., Hill, J., Smart, T., & Moss, S. (2001). Constitutive tyrosine phosphorylation of the $GABA_A$ receptor γ_2 subunit in rat brain. *Neuropharmacology*, *41*(6), 745–752.

Braudeau, J., Delatour, B., Duchon, A., Pereira, P. L., Dauphinot, L., de Chaumont, F., Olivo-Marin, J.-C., Dodd, R. H., Hérault, Y., & Potier, M.-C. (2011). Specific targeting of the $GABA_A$ receptor α_5 subtype by a selective inverse agonist restores cognitive deficits in Down syndrome mice. *Journal of psychopharmacology*, *25*(8), 1030–1042.

Brickley, S. G., Cull-Candy, S. G., & Farrant, M. (1999). Single-channel properties of synaptic and extrasynaptic $GABA_A$ receptors suggest differential targeting of receptor subtypes. *Journal of Neuroscience*, *19*(8), 2960–2973.

Brickley, S. G., & Mody, I. (2012). Extrasynaptic $GABA_A$ receptors: their function in the CNS and implications for disease. *Neuron*, *73*(1), 23–34.

Bright, D., & Smart, T. G. (2013). Methods for recording and measuring tonic $GABA_A$ receptor-mediated inhibition. *Frontiers in neural circuits*, *7*, 193.

Bright, D. P., & Smart, T. G. (2013). Protein kinase C regulates tonic $GABA_A$ receptor-mediated inhibition in the hippocampus and thalamus. *European Journal of Neuroscience*, *38*(10), 3408–3423.

Brünig, I., Scotti, E., Sidler, C., & Fritschy, J.-M. (2002). Intact sorting, targeting, and clustering of $GABA_A$ receptor subtypes in hippocampal neurons *in vitro*. *Journal of Comparative Neurology*, *443*(1), 43–55.

Cao, J.-W., Guan, W., Yu, Y.-C., & Fu, Y. (2020). Synaptic transmission from somatostatin-expressing interneurons to excitatory neurons mediated by α_5 subunit-containing $GABA_A$ receptors in the developing visual cortex. *Neuroscience*, *449*, 147–156.

Capogna, M., & Pearce, R. A. (2011). $GABA_{A,slow}$: causes and consequences. *Trends in neurosciences*, *34*(2), 101–112.

Caraiscos, V. B., Elliott, E. M., You-Ten, K. E., Cheng, V. Y., Belelli, D., Newell, J. G., Jackson, M. F., Lambert, J. J., Rosahl, T. W., Wafford, K. A., et al. (2004). Tonic inhibition in mouse hippocampal CA1 pyramidal neurons is

mediated by α_5 subunit-containing $GABA_A$ receptors. *Proceedings of the National Academy of Sciences*, *101*(10), 3662–3667.

Casula, M. A., Bromidge, F. A., Pillai, G. V., Wingrove, P. B., Martin, K., Maubach, K., Seabrook, G. R., Whiting, P. J., & Hadingham, K. L. (2001). Identification of amino acid residues responsible for the α_5-subunit binding selectivity of L-655,708, a benzodiazepine binding site ligand at the $GABA_A$ receptor. *Journal of neurochemistry*, *77*(2), 445–451.

Chambers, M. S., Atack, J. R., Broughton, H. B., Collinson, N., Cook, S., Dawson, G. R., Hobbs, S. C., Marshall, G., Maubach, K. A., Pillai, G. V., et al. (2003). Identification of a novel, selective α_5-$GABA_A$ receptor inverse agonist which enhances cognition. *Journal of medicinal chemistry*, *46*(11), 2227–2240.

Chapdelaine, T., Hakim, V., Triller, A., Ranft, J., & Specht, C. G. (2021). Reciprocal stabilization of glycine receptors and gephyrin scaffold proteins at inhibitory synapses. *Biophysical Journal*, *120*(5), 805–817.

Charych, E. I., Yu, W., Miralles, C. P., Serwanski, D. R., Li, X., Rubio, M., & De Blas, A. L. (2004). The brefeldin a-inhibited GDP/GTP exchange factor 2, a protein involved in vesicular trafficking, interacts with the β subunits of the $GABA_A$ receptors. *Journal of neurochemistry*, *90*(1), 173–189.

Chen, X., Keramidas, A., & Lynch, J. W. (2017). Physiological and pharmacological properties of inhibitory postsynaptic currents mediated by $\alpha_5\beta_1\gamma_2$, $\alpha_5\beta_2\gamma_2$ and $\alpha_5\beta_3\gamma_2$ $GABA_A$ receptors. *Neuropharmacology*, *125*, 243–253.

Chen, Z.-W., Fuchs, K., Sieghart, W., Townsend, R. R., & Evers, A. S. (2012). Deep amino acid sequencing of native brain $GABA_A$ receptors using high-resolution mass spectrometry. *Molecular & Cellular Proteomics*, *11*(1).

Cheng, A. T.-A., Loh, E.-W., Cheng, C.-Y., Wang, Y.-C., & Hsu, Y.-P. P. (1997). Polymorphisms and intron sequences flanking the alternatively spliced 8-amino-acid exon of γ_2 subunit gene for $GABA_A$ receptors. *Biochemical and biophysical research communications*, *238*(2), 683–685.

Chiu, C. Q., Barberis, A., & Higley, M. J. (2019). Preserving the balance: diverse forms of long-term GABAergic synaptic plasticity. *Nature Reviews Neuroscience*, *20*(5), 272–281.

Choi, S., & Lovinger, D. M. (1997). Decreased frequency but not amplitude of quantal synaptic responses associated with expression of corticostriatal long-term depression. *Journal of Neuroscience*, *17*(21), 8613–8620.

Christensen, R. K., Petersen, A. V., Schmitt, N., & Perrier, J.-F. (2014). Fast detection of extrasynaptic GABA with a whole-cell sniffer. *Frontiers in cellular neuroscience*, *8*, 133.

Christie, S. B., & de Blas, A. L. (2002). A_5 subunit-containing $GABA_A$ receptors form clusters at GABAergic synapses in hippocampal cultures. *Neuroreport*, *13*(17), 2355–2358.

Clarkson, A. N., Huang, B. S., MacIsaac, S. E., Mody, I., & Carmichael, S. T. (2010). Reducing excessive GABA-mediated tonic inhibition promotes functional recovery after stroke. *Nature*, *468*(7321), 305–309.

Cohen, E., Ivenshitz, M., Amor-Baroukh, V., Greenberger, V., & Segal, M. (2008). Determinants of spontaneous activity in networks of cultured hippocampus. *Brain research*, *1235*, 21–30.

Collinson, N., Atack, J., Laughton, P., Dawson, G., & Stephens, D. (2006). An inverse agonist selective for α_5 subunit-containing $GABA_A$ receptors improves encoding and recall but not consolidation in the morris water maze. *Psychopharmacology*, *188*(4), 619–628.

Collinson, N., Kuenzi, F. M., Jarolimek, W., Maubach, K. A., Cothliff, R., Sur, C., Smith, A., Otu, F. M., Howell, O., Atack, J. R., et al. (2002). Enhanced learning and memory and altered GABAergic synaptic transmission in mice lacking the α_5 subunit of the $GABA_A$ receptor. *Journal of Neuroscience*, *22*(13), 5572–5580.

Colquhoun, D. (1998). Binding, gating, affinity and efficacy: the interpretation of structure-activity relationships for agonists and of the effects of mutating receptors. *British journal of pharmacology*, *125*(5), 923–947.

Connolly, C. N., Krishek, B. J., McDonald, B. J., Smart, T. G., & Moss, S. J. (1996). Assembly and cell surface expression of heteromeric and homomeric $GABA_A$ receptors. *Journal of Biological Chemistry*, *271*(1), 89–96.

Corringer, P.-J., Poitevin, F., Prevost, M. S., Sauguet, L., Delarue, M., & Changeux, J.-P. (2012). Structure and pharmacology of pentameric receptor channels: from bacteria to brain. *Structure*, *20*(6), 941–956.

Crestani, F., Keist, R., Fritschy, J.-M., Benke, D., Vogt, K., Prut, L., Blüthmann, H., Möhler, H., & Rudolph, U. (2002). Trace fear conditioning involves hippocampal α_5-$GABA_A$ receptors. *Proceedings of the National Academy of Sciences*, *99*(13), 8980–8985.

Crosby, K. C., Gookin, S. E., Garcia, J. D., Hahm, K. M., Dell'Acqua, M. L., & Smith, K. R. (2019). Nanoscale subsynaptic domains underlie the organization of the inhibitory synapse. *Cell reports*, *26*(12), 3284–3297.

Danglot, L., Triller, A., & Bessis, A. (2003). Association of gephyrin with synaptic and extrasynaptic $GABA_A$ receptors varies during development in cultured hippocampal neurons. *Molecular and Cellular Neuroscience*, *23*(2), 264–278.

Davenport, C. M., Rajappa, R., Katchan, L., Taylor, C. R., Tsai, M.-C., Smith, C. M., de Jong, J. W., Arnold, D. B., Lammel, S., & Kramer, R. H. (2021). Relocation of an extrasynaptic $GABA_A$ receptor to inhibitory synapses freezes excitatory synaptic strength and preserves memory. *Neuron*, *109*(1), 123–134.

Davenport, E. C., Pendolino, V., Kontou, G., McGee, T. P., Sheehan, D. F., López-Doménech, G., Farrant, M., & Kittler, J. T. (2017). An essential role for the tetraspanin LHFPL4 in the cell-type-specific targeting and clustering of synaptic $GABA_A$ receptors. *Cell reports*, *21*(1), 70–83.

Dawson, G. R., Maubach, K. A., Collinson, N., Cobain, M., Everitt, B., MacLeod, A., Choudhury, H., McDonald, L., Pillai, G., Rycroft, W., et al. (2006). An inverse agonist selective for α_5 subunit-containing $GABA_A$ receptors en-

hances cognition. *Journal of Pharmacology and Experimental Therapeutics*, *316*(3), 1335–1345.

del Rıo, J. C., Araujo, F., Ramos, B., Ruano, D., & Vitorica, J. (2001). Prevalence between different αsubunits performing the benzodiazepine binding sites in native heterologous $GABA_A$ receptors containing the alpha2 subunit. *Journal of neurochemistry*, *79*(1), 183–191.

Dephoure, N., Gould, K. L., Gygi, S. P., & Kellogg, D. R. (2013). Mapping and analysis of phosphorylation sites: a quick guide for cell biologists. *Molecular biology of the cell*, *24*(5), 535–542.

Doble, B. W., & Woodgett, J. R. (2003). GSK3: tricks of the trade for a multi-tasking kinase. *Journal of cell science*, *116*(7), 1175–1186.

Donegan, J., Boley, A., Yamaguchi, J., Toney, G., & Lodge, D. (2019). Modulation of extrasynaptic α_5-$GABA_A$ receptors in the ventral hippocampus normalizes physiological and behavioral deficits in a circuit specific manner. *Nature communications*, *10*(1), 1–12.

Duchon, A., Gruart, A., Albac, C., Delatour, B., Zorrilla de San Martin, J., Delgado-Garcıa, J. M., Hérault, Y., & Potier, M.-c. (2020). Long-lasting correction of *in vivo* LTP and cognitive deficits of mice modelling Down syndrome with an α_5-selective $GABA_A$ inverse agonist. *British journal of pharmacology*, *177*(5), 1106–1118.

Duncalfe, L. L., Carpenter, M. R., Smillie, L. B., Martin, I. L., & Dunn, S. M. (1996). The major site of photoaffinity labeling of the $GABA_A$ receptor by [3H] flunitrazepam is histidine 102 of the α subunit. *Journal of Biological Chemistry*, *271*(16), 9209–9214.

Dzyubenko, E., Rozenberg, A., Hermann, D. M., & Faissner, A. (2016). Colocalization of synapse marker proteins evaluated by STED-microscopy reveals patterns of neuronal synapse distribution *in vitro*. *Journal of neuroscience methods*, *273*, 149–159.

Ehrensperger, M.-V., Hanus, C., Vannier, C., Triller, A., & Dahan, M. (2007). Multiple association states between glycine receptors and gephyrin identified by SPT analysis. *Biophysical journal*, *92*(10), 3706–3718.

Engin, E., Sigal, M., Benke, D., Zeller, A., & Rudolph, U. (2020). Bidirectional regulation of distinct memory domains by α_5 subunit-containing $GABA_A$ receptors in CA1 pyramidal neurons. *Learning & Memory*, *27*(10), 423–428.

Engin, E., Zarnowska, E. D., Benke, D., Tsvetkov, E., Sigal, M., Keist, R., Bolshakov, V. Y., Pearce, R. A., & Rudolph, U. (2015). Tonic inhibitory control of dentate gyrus granule cells by α_5-containing $GABA_A$ receptors reduces memory interference. *Journal of Neuroscience*, *35*(40), 13698–13712.

Essrich, C., Lorez, M., Benson, J. A., Fritschy, J.-M., & Lüscher, B. (1998). Postsynaptic clustering of major $GABA_A$ receptor subtypes requires the γ_2 subunit and gephyrin. *Nature neuroscience*, *1*(7), 563–571.

Eyre, M. D., Renzi, M., Farrant, M., & Nusser, Z. (2012). Setting the time course of inhibitory synaptic currents by mixing multiple $GABA_A$ receptor α subunit isoforms. *Journal of Neuroscience*, *32*(17), 5853–5867.

Farrant, M., & Nusser, Z. (2005). Variations on an inhibitory theme: phasic and tonic activation of $GABA_A$ receptors. *Nature Reviews Neuroscience*, *6*(3), 215–229.

Fatima-Shad, K., & Barry, P. H. (1993). Anion permeation in GABA and glycine-gated channels of mammalian cultured hippocampal neurons. *Proceedings of the Royal Society of London. Series B: Biological Sciences*, *253*(1336), 69–75.

Fee, C., Prevot, T. D., Misquitta, K., Knutson, D. E., Li, G., Mondal, P., Cook, J. M., Banasr, M., & Sibille, E. (2021). Behavioral deficits induced by somatostatin-positive GABA neuron silencing are rescued by α_5 $GABA_A$ receptor potentiation. *International Journal of Neuropsychopharmacology*.

Field, M., Dorovykh, V., Thomas, P., & Smart, T. G. (2021). Physiological role for $GABA_A$ receptor desensitization in the induction of long-term potentiation at inhibitory synapses. *Nature communications*, *12*(1), 1–16.

Flores, C. E., Nikonenko, I., Mendez, P., Fritschy, J.-M., Tyagarajan, S. K., & Muller, D. (2015). Activity-dependent inhibitory synapse remodeling through gephyrin phosphorylation. *Proceedings of the National Academy of Sciences*, *112*(1), E65–E72.

Fritschy, J.-M., Johnson, D. K., Mohler, H., & Rudolph, U. (1998). Independent assembly and subcellular targeting of $GABA_A$-receptor subtypes demonstrated in mouse hippocampal and olfactory neurons *in vivo*. *Neuroscience letters*, *249*(2-3), 99–102.

Fritschy, J.-M., Benke, D., Johnson, D., Mohler, H., & Rudolph, U. (1997). $GABA_A$-receptor α-subunit is an essential prerequisite for receptor formation *in vivo*. *Neuroscience*, *81*(4), 1043–1053.

Fujiyama, F., Fritschy, J.-M., Stephenson, F. A., & Bolam, J. P. (2000). Synaptic localization of $GABA_A$ receptor subunits in the striatum of the rat. *Journal of Comparative Neurology*, *416*(2), 158–172.

Gacsályi, I., Móricz, K., Gigler, G., Wellmann, J., Nagy, K., Ling, I., Barkóczy, J., Haller, J., Lambert, J. J., Szénási, G., et al. (2017). Behavioural pharmacology of the α_5-$GABA_A$ receptor antagonist S44819: enhancement and remediation of cognitive performance in preclinical models. *Neuropharmacology*, *125*, 30–38.

Gaiarsa, J.-L., Caillard, O., & Ben-Ari, Y. (2002). Long-term plasticity at GABAergic and glycinergic synapses: mechanisms and functional significance. *Trends in neurosciences*, *25*(11), 564–570.

Gallagher, M. J., Ding, L., Maheshwari, A., & Macdonald, R. L. (2007). The $GABA_A$ receptor α_1 subunit epilepsy mutation A322D inhibits transmembrane helix formation and causes proteasomal degradation. *Proceedings of the National Academy of Sciences*, *104*(32), 12999–13004.

George, S., Chiou, T.-T., Kanamalla, K., & De Blas, A. L. (2021). Recruitment of plasma membrane $GABA_A$ receptors by submembranous gephyrin/collybistin clusters. *Cellular and molecular neurobiology*, 1–20.

Ghafari, M., Falsafi, S. K., Szodorai, E., Kim, E.-J., Li, L., Höger, H., Berger, J., Fuchs, K., Sieghart, W., & Lubec, G. (2017). Formation of $GABA_A$ receptor complexes containing α_1 and α_5 subunits is paralleling a multiple t-maze learning task in mice. *Brain Structure and Function*, *222*(1), 549–561.

Gielen, M., Thomas, P., & Smart, T. G. (2015). The desensitization gate of inhibitory cys-loop receptors. *Nature communications*, *6*(1), 1–10.

Gill, K. M., Lodge, D. J., Cook, J. M., Aras, S., & Grace, A. A. (2011). A novel α_5-$GABA_A$ receptor allosteric modulator reverses hyperactivation of the dopamine system in the MAM model of schizophrenia. *Neuropsychopharmacology*, *36*(9), 1903–1911.

Gilles, J.-F., Dos Santos, M., Boudier, T., Bolte, S., & Heck, N. (2017). DiAna, an ImageJ tool for object-based 3D co-localization and distance analysis. *Methods*, *115*, 55–64.

Gingrich, K., Roberts, W., & Kass, R. (1995). Dependence of the $GABA_A$ receptor gating kinetics on the α-subunit isoform: implications for structure-function relations and synaptic transmission. *The Journal of physiology*, *489*(2), 529–543.

Glykys, J., Mann, E. O., & Mody, I. (2008). Which $GABA_A$ receptor subunits are necessary for tonic inhibition in the hippocampus? *Journal of Neuroscience*, *28*(6), 1421–1426.

Glykys, J., & Mody, I. (2006). Hippocampal network hyperactivity after selective reduction of tonic inhibition in $GABA_A$ receptor α_5 subunit–deficient mice. *Journal of neurophysiology*, *95*(5), 2796–2807.

Gross, A., Sims, R., Swinny, J., Sieghart, W., Bolam, J., & Stanford, I. (2011). Differential localization of $GABA_A$ receptor subunits in relation to rat striatopallidal and pallidopallidal synapses. *European Journal of Neuroscience*, *33*(5), 868–878.

Grosskreutz, Y., Hermann, A., Kins, S., Fuhrmann, J. C., Betz, H., & Kneussel, M. (2001). Identification of a gephyrin-binding motif in the GDP/GTP exchange factor collybistin.

Gustafsson, M. G. (2000). Surpassing the lateral resolution limit by a factor of two using structured illumination microscopy. *Journal of microscopy*, *198*(2), 82–87.

Hakim, V., & Ranft, J. (2020). Lifetime of a structure evolving by cluster aggregation and particle loss, and application to postsynaptic scaffold domains. *Physical Review E*, *101*(1), 012411.

Hannan, S., Minere, M., Harris, J., Izquierdo, P., Thomas, P., Tench, B., & Smart, T. G. (2020). $GABA_A$ receptor isoform and subunit structural motifs determine synaptic and extrasynaptic receptor localisation. *Neuropharmacology*, *169*, 107540.

Hannan, S., Wilkins, M. E., Thomas, P., & Smart, T. G. (2013). Tracking cell surface mobility of GPCRs using α-bungarotoxin-linked fluorophores. *Methods in enzymology*, *521*, 109–129.

Harris, K. D., Hochgerner, H., Skene, N. G., Magno, L., Katona, L., Bengtsson Gonzales, C., Somogyi, P., Kessaris, N., Linnarsson, S., & Hjerling-Leffler, J. (2018). Classes and continua of hippocampal CA1 inhibitory neurons revealed by single-cell transcriptomics. *PLoS biology*, *16*(6), e2006387.

Haubensak, W., Kunwar, P. S., Cai, H., Ciocchi, S., Wall, N. R., Ponnusamy, R., Biag, J., Dong, H.-W., Deisseroth, K., Callaway, E. M., et al. (2010). Genetic dissection of an amygdala microcircuit that gates conditioned fear. *Nature*, *468*(7321), 270–276.

Hauser, J., Rudolph, U., Keist, R., Möhler, H., Feldon, J., & Yee, B. (2005). Hippocampal α_5 subunit-containing $GABA_A$ receptors modulate the expression of prepulse inhibition. *Molecular psychiatry*, *10*(2), 201–207.

Hausrat, T. J., Muhia, M., Gerrow, K., Thomas, P., Hirdes, W., Tsukita, S., Heisler, F. F., Herich, L., Dubroqua, S., Breiden, P., et al. (2015). Radixin regulates

synaptic $GABA_A$ receptor density and is essential for reversal learning and short-term memory. *Nature communications*, *6*(1), 1–17.

He, Q., Duguid, I., Clark, B., Panzanelli, P., Patel, B., Thomas, P., Fritschy, J.-M., & Smart, T. G. (2015). Interneuron-and $GABA_A$ receptor-specific inhibitory synaptic plasticity in cerebellar purkinje cells. *Nature communications*, *6*(1), 1–13.

Heckers, S., & Konradi, C. (2015). GABAergic mechanisms of hippocampal hyperactivity in schizophrenia. *Schizophrenia research*, *167*(1-3), 4–11.

Hedblom, E., & Kirkness, E. F. (1997). A novel class of $GABA_A$ receptor subunit in tissues of the reproductive system. *Journal of Biological Chemistry*, *272*(24), 15346–15350.

Heldt, S. A., & Ressler, K. J. (2007). Forebrain and midbrain distribution of major benzodiazepine-sensitive $GABA_A$ receptor subunits in the adult C57 mouse as assessed with in situ hybridization. *Neuroscience*, *150*(2), 370–385.

Herd, M. B., Brown, A. R., Lambert, J. J., & Belelli, D. (2013). Extrasynaptic $GABA_A$ receptors couple presynaptic activity to postsynaptic inhibition in the somatosensory thalamus. *Journal of Neuroscience*, *33*(37), 14850–14868.

Herde, A. M., Benke, D., Ralvenius, W. T., Mu, L., Schibli, R., Zeilhofer, H. U., & Krämer, S. D. (2017). $GABA_A$ receptor subtypes in the mouse brain: regional mapping and diazepam receptor occupancy by *in vivo* [18F] flumazenil PET. *Neuroimage*, *150*, 279–291.

Hermida, M. A., Kumar, J. D., & Leslie, N. R. (2017). GSK3 and its interactions with the PI3K/AKT/mTOR signalling network. *Advances in biological regulation*, *65*, 5–15.

Higley, M. J. (2014). Localized GABAergic inhibition of dendritic Ca^{2+} signalling. *Nature Reviews Neuroscience*, *15*(9), 567–572.

Hines, R. M., Maric, H. M., Hines, D. J., Modgil, A., Panzanelli, P., Nakamura, Y., Nathanson, A. J., Cross, A., Deeb, T., Brandon, N. J., et al. (2018). Devel-

opmental seizures and mortality result from reducing $GABA_A$ receptor α_2 -subunit interaction with collybistin. *Nature communications*, *9*(1), 1–15.

Hipp, J. F., Knoflach, F., Comley, R., Ballard, T. M., Honer, M., Trube, G., Gasser, R., Prinssen, E., Wallace, T. L., Rothfuss, A., et al. (2021). Basmisanil, a highly selective α_5-$GABA_A$ negative allosteric modulator: preclinical pharmacology and demonstration of functional target engagement in man. *Scientific reports*, *11*(1), 1–20.

Hong, S., Wilton, D. K., Stevens, B., & Richardson, D. S. (2017). Structured illumination microscopy for the investigation of synaptic structure and function. *Synapse development* (pp. 155–167). Springer.

Hörtnagl, H., Tasan, R., Wieselthaler, A., Kirchmair, E., Sieghart, W., & Sperk, G. (2013). Patterns of mRNA and protein expression for 12 $GABA_A$ receptor subunits in the mouse brain. *Neuroscience*, *236*, 345–372.

Houston, C. M., He, Q., & Smart, T. G. (2009). CaMKII phosphorylation of the $GABA_A$ receptor: receptor subtype-and synapse-specific modulation. *The Journal of physiology*, *587*(10), 2115–2125.

Houston, C. M., Hosie, A. M., & Smart, T. G. (2008). Distinct regulation of β_2 and β_3 subunit-containing cerebellar synaptic $GABA_A$ receptors by calcium/calmodulin-dependent protein kinase II. *Journal of Neuroscience*, *28*(30), 7574–7584.

Hruska, M., Henderson, N., Le Marchand, S. J., Jafri, H., & Dalva, M. B. (2018). Synaptic nanomodules underlie the organization and plasticity of spine synapses. *Nature neuroscience*, *21*(5), 671–682.

Inoue, T., Takamatsu, Y., Okamura, M., Mani, H., Hasegawa, N., & Maejima, H. (2021). Specific inhibition of α_5 subunit-containing $GABA_A$ receptors enhances locomotor activity and neuronal activity in the motor cortex. *Biomedical Research*, *42*(3), 103–108.

Ivenshitz, M., & Segal, M. (2010). Neuronal density determines network connectivity and spontaneous activity in cultured hippocampus. *Journal of neurophysiology*, *104*(2), 1052–1060.

Jacob, T. C. (2019). Neurobiology and therapeutic potential of α_5-$GABA_A$ receptors. *Frontiers in molecular neuroscience*, *12*, 179.

Jacob, T. C., Moss, S. J., & Jurd, R. (2008). $GABA_A$ receptor trafficking and its role in the dynamic modulation of neuronal inhibition. *Nature Reviews Neuroscience*, *9*(5), 331–343.

Janak, P. H., & Tye, K. M. (2015). From circuits to behaviour in the amygdala. *Nature*, *517*(7534), 284–292.

Jones, B. L., & Henderson, L. P. (2007). Trafficking and potential assembly patterns of ε-containing $GABA_A$ receptors. *Journal of neurochemistry*, *103*(3), 1258–1271.

Ju, Y. H., Guzzo, A., Chiu, M. W., Taylor, P., Moran, M. F., Gurd, J. W., MacDonald, J. F., & Orser, B. A. (2009). Distinct properties of murine α_5-$GABA_A$ receptors revealed by biochemical fractionation and mass spectroscopy. *Journal of neuroscience research*, *87*(8), 1737–1747.

Jurd, R., Tretter, V., Walker, J., Brandon, N. J., & Moss, S. J. (2010). Fyn kinase contributes to tyrosine phosphorylation of the $GABA_A$ receptor γ_2 subunit. *Molecular and Cellular Neuroscience*, *44*(2), 129–134.

Kaku, S., Chaki, S., & Muramatsu, M. (2008). GSK3 inhibitors: recent developments and therapeutic potential. *Current Signal Transduction Therapy*, *3*(3), 195–205.

Kalbouneh, H., Schlicksupp, A., Kirsch, J., & Kuhse, J. (2014). Cyclin-dependent kinase 5 is involved in the phosphorylation of gephyrin and clustering of $GABA_A$ receptors at inhibitory synapses of hippocampal neurons. *PloS one*, *9*(8), e104256.

Kang, S. U., Fuchs, K., Sieghart, W., & Lubec, G. (2008). Gel-based mass spectrometric analysis of recombinant $GABA_A$ receptor subunits representing strongly hydrophobic transmembrane proteins. *Journal of proteome research*, *7*(8), 3498–3506.

Kang, S. U., Heo, S., & Lubec, G. (2011). Mass spectrometric analysis of $GABA_A$ receptor subtypes and phosphorylations from mouse hippocampus. *Proteomics*, *11*(11), 2171–2181.

Kang, S. U., & Lubec, G. (2009). Complete sequencing of $GABA_A$ receptor subunit β_3 by a rapid technique following in-gel digestion of the protein. *Electrophoresis*, *30*(12), 2159–2167.

Kang, S.-U., Fuchs, K., Sieghart, W., Pollak, A., Csaszar, E., & Lubec, G. (2009). Gel-based mass spectrometric analysis of a strongly hydrophobic $GABA_A$-receptor subunit containing four transmembrane domains. *Nature protocols*, *4*(7), 1093–1102.

Kasugai, Y., Swinny, J. D., Roberts, J. D. B., Dalezios, Y., Fukazawa, Y., Sieghart, W., Shigemoto, R., & Somogyi, P. (2010). Quantitative localisation of synaptic and extrasynaptic $GABA_A$ receptor subunits on hippocampal pyramidal cells by freeze-fracture replica immunolabelling. *European Journal of Neuroscience*, *32*(11), 1868–1888.

Kawaguchi, S.-y. (2019). Dynamic factors for transmitter release at small presynaptic boutons revealed by direct patch-clamp recordings. *Frontiers in cellular neuroscience*, *13*, 269.

Kerti-Szigeti, K., Nusser, Z., & Eyre, M. D. (2014). Synaptic $GABA_A$ receptor clustering without the γ_2 subunit. *Journal of Neuroscience*, *34*(31), 10219–10233.

Khatri, S. N., Wu, W.-C., Yang, Y., & Pugh, J. R. (2019). Direction of action of presynaptic $GABA_A$ receptors is highly dependent on the level of receptor activation. *Journal of neurophysiology*, *121*(5), 1896–1905.

Khayenko, V., & Maric, H. M. (2019). Targeting $GABA_A$ receptor-associated proteins: new modulators, labels and concepts. *Frontiers in molecular neuroscience*, *12*, 162.

Khodaei, S., Avramescu, S., Wang, D.-S., Sheng, H., Chan, N. K., Lecker, I., Fernandez-Escobar, A., Lei, G., Dewar, M. B., Whissell, P. D., et al. (2020). Inhibiting α_5 subunit-containing $GABA_A$ receptors attenuates cogni-

tive deficits after traumatic brain injury. *Critical care medicine*, *48*(4), 533–544.

Kim, J. J., Gharpure, A., Teng, J., Zhuang, Y., Howard, R. J., Zhu, S., Noviello, C. M., Walsh, R. M., Lindahl, E., & Hibbs, R. E. (2020). Shared structural mechanisms of general anaesthetics and benzodiazepines. *Nature*, *585*(7824), 303–308.

Kim, J. J., & Hibbs, R. E. (2021). Direct structural insights into $GABA_A$ receptor pharmacology. *Trends in Biochemical Sciences*.

Kins, S., Betz, H., & Kirsch, J. (2000). Collybistin, a newly identified brain-specific GEF, induces submembrane clustering of gephyrin. *Nature neuroscience*, *3*(1), 22–29.

Kittler, J. T., Chen, G., Honing, S., Bogdanov, Y., McAinsh, K., Arancibia-Carcamo, I. L., Jovanovic, J. N., Pangalos, M. N., Haucke, V., Yan, Z., et al. (2005). Phospho-dependent binding of the clathrin AP2 adaptor complex to $GABA_A$ receptors regulates the efficacy of inhibitory synaptic transmission. *Proceedings of the National Academy of Sciences*, *102*(41), 14871–14876.

Kittler, J. T., Chen, G., Kukhtina, V., Vahedi-Faridi, A., Gu, Z., Tretter, V., Smith, K. R., McAinsh, K., Arancibia-Carcamo, I. L., Saenger, W., et al. (2008). Regulation of synaptic inhibition by phospho-dependent binding of the AP2 complex to a YECL motif in the $GABA_A$ receptor γ_2 subunit. *Proceedings of the National Academy of Sciences*, *105*(9), 3616–3621.

Kittler, J. T., Delmas, P., Jovanovic, J. N., Brown, D. A., Smart, T. G., & Moss, S. J. (2000). Constitutive endocytosis of $GABA_A$ receptors by an association with the adaptin AP2 complex modulates inhibitory synaptic currents in hippocampal neurons. *Journal of Neuroscience*, *20*(21), 7972–7977.

Kittler, J. T., Thomas, P., Tretter, V., Bogdanov, Y. D., Haucke, V., Smart, T. G., & Moss, S. J. (2004). Huntingtin-associated protein 1 regulates inhibitory synaptic transmission by modulating $GABA_A$ receptor membrane trafficking. *Proceedings of the National Academy of Sciences*, *101*(34), 12736–12741.

Kleschevnikov, A. M., Belichenko, P. V., Gall, J., George, L., Nosheny, R., Maloney, M. T., Salehi, A., & Mobley, W. C. (2012). Increased efficiency of the $GABA_A$ and $gaba_B$ receptor-mediated neurotransmission in the Ts65Dn mouse model of Down syndrome. *Neurobiology of disease*, *45*(2), 683–691.

Kleschevnikov, A. M., Belichenko, P. V., Villar, A. J., Epstein, C. J., Malenka, R. C., & Mobley, W. C. (2004). Hippocampal long-term potentiation suppressed by increased inhibition in the Ts65Dn mouse, a genetic model of Down syndrome. *Journal of Neuroscience*, *24*(37), 8153–8160.

Kneussel, M., Brandstätter, J. H., Gasnier, B., Feng, G., Sanes, J. R., & Betz, H. (2001). Gephyrin-independent clustering of postsynaptic $GABA_A$ receptor subtypes. *Molecular and Cellular Neuroscience*, *17*(6), 973–982.

Kneussel, M., Brandstätter, J. H., Laube, B., Stahl, S., Müller, U., & Betz, H. (1999). Loss of postsynaptic $GABA_A$ receptor clustering in gephyrin-deficient mice. *Journal of Neuroscience*, *19*(21), 9289–9297.

Knust, H., Achermann, G., Ballard, T., Buettelmann, B., Gasser, R., Fischer, H., Hernandez, M.-C., Knoflach, F., Koblet, A., Stadler, H., et al. (2009). The discovery and unique pharmacological profile of RO4938581 and RO4882224 as potent and selective α_5-$GABA_A$ inverse agonists for the treatment of cognitive dysfunction. *Bioorganic & medicinal chemistry letters*, *19*(20), 5940–5944.

Ko, J., Choii, G., & Um, J. W. (2015). The balancing act of GABAergic synapse organizers. *Trends in molecular medicine*, *21*(4), 256–268.

Kofuji, P., Wang, J. B., Moss, S. J., Huganir, R. L., & Burt, D. R. (1991). Generation of two forms of the $GABA_A$ receptor γ_2 -subunit in mice by alternative splicing. *Journal of neurochemistry*, *56*(2), 713–715.

Koh, M. T., Rosenzweig-Lipson, S., & Gallagher, M. (2013). Selective α_5-$GABA_A$ positive allosteric modulators improve cognitive function in aged rats with memory impairment. *Neuropharmacology*, *64*, 145–152.

Konradi, C., Yang, C. K., Zimmerman, E. I., Lohmann, K. M., Gresch, P., Pantazopoulos, H., Berretta, S., & Heckers, S. (2011). Hippocampal interneurons are abnormal in schizophrenia. *Schizophrenia research*, *131*(1-3), 165–173.

Kowalczyk, S., Winkelmann, A., Smolinsky, B., Förstera, B., Neundorf, I., Schwarz, G., & Meier, J. C. (2013). Direct binding of $GABA_A$ receptor β_2 and β_3 subunits to gephyrin. *European Journal of Neuroscience*, *37*(4), 544–554.

Kramer, P. F., Twedell, E. L., Shin, J. H., Zhang, R., & Khaliq, Z. M. (2020). Axonal mechanisms mediating $GABA_A$ inhibition of striatal dopamine release. *Elife*, *9*, e55729.

Krishek, B. J., Xie, X., Blackstone, C., Huganir, R. L., Moss, S. J., & Smart, T. G. (1994). Regulation of $GABA_A$ receptor function by protein kinase C phosphorylation. *Neuron*, *12*(5), 1081–1095.

Kumar, M., Gouw, M., Michael, S., Sámano-Sánchez, H., Pancsa, R., Glavina, J., Diakogianni, A., Valverde, J. A., Bukirova, D., Čalyševa, J., et al. (2020). ELM—the eukaryotic linear motif resource in 2020. *Nucleic acids research*, *48*(D1), D296–D306.

Laha, K. T., & Tran, P. N. (2013). Multiple tyrosine residues at the GABA binding pocket influence surface expression and mediate kinetics of the $GABA_A$ receptor. *Journal of neurochemistry*, *124*(2), 200–209.

Lake, E. M., Chaudhuri, J., Thomason, L., Janik, R., Ganguly, M., Brown, M., McLaurin, J., Corbett, D., Stanisz, G. J., & Stefanovic, B. (2015). The effects of delayed reduction of tonic inhibition on ischemic lesion and sensorimotor function. *Journal of Cerebral Blood Flow & Metabolism*, *35*(10), 1601–1609.

Laverty, D., Desai, R., Uchański, T., Masiulis, S., Stec, W. J., Malinauskas, T., Zivanov, J., Pardon, E., Steyaert, J., Miller, K. W., et al. (2019). Cryo-EM structure of the human $\alpha_1\beta_3$ $GABA_A$ receptor in a lipid bilayer. *Nature*, *565*(7740), 516–520.

Lee, V., & Maguire, J. (2014). The impact of tonic $GABA_A$ receptor-mediated inhibition on neuronal excitability varies across brain region and cell type. *Frontiers in neural circuits*, *8*, 3.

Lévi, S., Logan, S. M., Tovar, K. R., & Craig, A. M. (2004). Gephyrin is critical for glycine receptor clustering but not for the formation of functional GABAergic synapses in hippocampal neurons. *Journal of Neuroscience*, *24*(1), 207–217.

Li, Y.-C., Panikker, P., Xing, B., Yang, S.-S., Alexandropoulos, C., McEachern, E. P., Akumuo, R., Zhao, E., Gulchina, Y., Pletnikov, M. V., et al. (2020). Deletion of glycogen synthase kinase-3β in D2 receptor–positive neurons ameliorates cognitive impairment via NMDA receptor–dependent synaptic plasticity. *Biological psychiatry*, *87*(8), 745–755.

Lisman, J., & Buzsáki, G. (2008). A neural coding scheme formed by the combined function of gamma and theta oscillations. *Schizophrenia bulletin*, *34*(5), 974–980.

Loebrich, S., Bähring, R., Katsuno, T., Tsukita, S., & Kneussel, M. (2006). Activated radixin is essential for $GABA_A$ receptor α_5 subunit anchoring at the actin cytoskeleton. *The EMBO journal*, *25*(5), 987–999.

Lorenz-Guertin, J. M., & Jacob, T. C. (2018). $GABA_A$ trafficking and the architecture of synaptic inhibition. *Developmental neurobiology*, *78*(3), 238–270.

Luscher, B., Fuchs, T., & Kilpatrick, C. L. (2011). $GABA_A$ receptor trafficking-mediated plasticity of inhibitory synapses. *Neuron*, *70*(3), 385–409.

Lushnikova, I., Skibo, G., Muller, D., & Nikonenko, I. (2011). Excitatory synaptic activity is associated with a rapid structural plasticity of inhibitory synapses on hippocampal CA1 pyramidal cells. *Neuropharmacology*, *60*(5), 757–764.

M Gill, K., & A Grace, A. (2014). The role of α_5-$GABA_A$ receptor agonists in the treatment of cognitive deficits in schizophrenia. *Current pharmaceutical design*, *20*(31), 5069–5076.

Magnin, E., Francavilla, R., Amalyan, S., Gervais, E., David, L. S., Luo, X., & Topolnik, L. (2019). Input-specific synaptic location and function of the α_5-

$GABA_A$ receptor subunit in the mouse CA1 hippocampal neurons. *Journal of Neuroscience*, *39*(5), 788–801.

Manzo, M. A., Wang, D.-S., Li, W. W., Pinguelo, A., Popa, M. O., Khodaei, S., Atack, J. R., Ross, R. A., & Orser, B. A. (2021). Inhibition of a tonic inhibitory conductance in mouse hippocampal neurones by negative allosteric modulators of α_5 subunit-containing $GABA_A$ receptors: implications for treating cognitive deficits. *British Journal of Anaesthesia*, *126*(3), 674–683.

Maramai, S., Benchekroun, M., Ward, S. E., & Atack, J. R. (2019). Subtype selective γ-aminobutyric acid type A receptor ($GABA_A$) modulators acting at the benzodiazepine binding site: an update. *Journal of medicinal chemistry*, *63*(7), 3425–3446.

Marchionni, I., Kasap, Z., Mozrzymas, J., Sieghart, W., Cherubini, E., & Zacchi, P. (2009). New insights on the role of gephyrin in regulating both phasic and tonic GABAergic inhibition in rat hippocampal neurons in culture. *Neuroscience*, *164*(2), 552–562.

Maric, H. M., Hausrat, T. J., Neubert, F., Dalby, N. O., Doose, S., Sauer, M., Kneussel, M., & Strømgaard, K. (2017). Gephyrin-binding peptides visualize postsynaptic sites and modulate neurotransmission. *Nature chemical biology*, *13*(2), 153–160.

Martin, L. J., Oh, G. H., & Orser, B. A. (2009). Etomidate targets α_5-$GABA_A$ receptors to regulate synaptic plasticity and memory blockade. *The Journal of the American Society of Anesthesiologists*, *111*(5), 1025–1035.

Martin, L. J., Zurek, A. A., MacDonald, J. F., Roder, J. C., Jackson, M. F., & Orser, B. A. (2010). α_5-$GABA_A$ receptor activity sets the threshold for long-term potentiation and constrains hippocampus-dependent memory. *Journal of Neuroscience*, *30*(15), 5269–5282.

Martinez-Cué, C., Delatour, B., & Potier, M.-C. (2014). Treating enhanced GABAergic inhibition in Down syndrome: use of GABA α_5-selective inverse agonists. *Neuroscience & Biobehavioral Reviews*, *46*, 218–227.

Martınez-Cué, C., Martınez, P., Rueda, N., Vidal, R., Garcıa, S., Vidal, V., Corrales, A., Montero, J. A., Pazos, Á., Flórez, J., et al. (2013). Reducing α_5-$GABA_A$ receptor-mediated inhibition rescues functional and neuromorphological deficits in a mouse model of Down syndrome. *Journal of Neuroscience*, *33*(9), 3953–3966.

Masiulis, S., Desai, R., Uchański, T., Martin, I. S., Laverty, D., Karia, D., Malinauskas, T., Zivanov, J., Pardon, E., Kotecha, A., et al. (2019). $GABA_A$ receptor signalling mechanisms revealed by structural pharmacology. *Nature*, *565*(7740), 454–459.

Matsuzaki, M., Honkura, N., Ellis-Davies, G. C., & Kasai, H. (2004). Structural basis of long-term potentiation in single dendritic spines. *Nature*, *429*(6993), 761–766.

McDonald, B. J., Amato, A., Connolly, C. N., Benke, D., Moss, S. J., & Smart, T. G. (1998). Adjacent phosphorylation sites on $GABA_A$ receptor β subunits determine regulation by cAMP-dependent protein kinase. *Nature neuroscience*, *1*(1), 23–28.

McDonald, B. J., & Moss, S. J. (1994). Differential phosphorylation of intracellular domains of $GABA_A$ receptor subunits by Ca^{2+}/calmodulin type II-dependent protein kinase. *Journal of Biological Chemistry*, *269*(27), 18111–18117.

Mcdonald, B. J., & Moss, S. J. (1997). Conserved phosphorylation of the intracellular domains of $GABA_A$ receptor β_2 and β_3 subunits by cAMP-dependent protein kinase, cGMP-dependent protein kinase, protein kinase C and Ca^{2+}/calmodulin type II-dependent protein kinase. *Neuropharmacology*, *36*(10), 1377–1385.

Medoff, D. R., Holcomb, H. H., Lahti, A. C., & Tamminga, C. A. (2001). Probing the human hippocampus using rCBF: contrasts in schizophrenia. *Hippocampus*, *11*(5), 543–550.

Mesbah-Oskui, L., Penna, A., Orser, B. A., & Horner, R. L. (2017). Reduced expression of α_5-$GABA_A$ receptors elicits autism-like alterations in eeg pat-

terns and sleep-wake behavior. *Neurotoxicology and teratology*, *61*, 115–122.

Milić, M., Timić, T., Joksimović, S., Biawat, P., Rallapalli, S., Divljaković, J., Radulović, T., Cook, J. M., & Savić, M. M. (2013). PWZ-029, an inverse agonist selective for α_5-$GABA_A$ receptors, improves object recognition, but not water-maze memory in normal and scopolamine-treated rats. *Behavioural brain research*, *241*, 206–213.

Miller, P. S., & Aricescu, A. R. (2014). Crystal structure of a human $GABA_A$ receptor. *Nature*, *512*(7514), 270–275.

Miller, P. S., Masiulis, S., Malinauskas, T., Kotecha, A., Rao, S., Chavali, S., De Colibus, L., Pardon, E., Hannan, S., Scott, S., et al. (2018). Heteromeric $GABA_A$ receptor structures in positively-modulated active states. *BioRxiv*, 338343.

Miller, P. S., Scott, S., Masiulis, S., De Colibus, L., Pardon, E., Steyaert, J., & Aricescu, A. R. (2017). Structural basis for $GABA_A$ receptor potentiation by neurosteroids. *Nature structural & molecular biology*, *24*(11), 986–992.

Mody, I., & Pearce, R. A. (2004). Diversity of inhibitory neurotransmission through $GABA_A$ receptors. *Trends in neurosciences*, *27*(9), 569–575.

Mohamad, F. H., & Has, A. T. C. (2019). The α_5-containing $GABA_A$ receptors—a brief summary. *Journal of Molecular Neuroscience*, *67*(2), 343–351.

Möhler, H., Fritschy, J., & Rudolph, U. (2002). A new benzodiazepine pharmacology. *Journal of Pharmacology and Experimental Therapeutics*, *300*(1), 2–8.

Möhler, H. (2012). Cognitive enhancement by pharmacological and behavioral interventions: the murine Down syndrome model. *Biochemical pharmacology*, *84*(8), 994–999.

Möhler, H., & Rudolph, U. (2017). Disinhibition, an emerging pharmacology of learning and memory. *F1000Research*, *6*.

Monaco, S. A., Ferguson, B. R., & Gao, W.-J. (2018). Lithium inhibits GSK3β and augments GluN2A receptor expression in the prefrontal cortex. *Frontiers in cellular neuroscience*, *12*, 16.

Moore, S. F., van den Bosch, M. T., Hunter, R. W., Sakamoto, K., Poole, A. W., & Hers, I. (2013). Dual regulation of glycogen synthase kinase 3 (GSK3)α/β by protein kinase C (PKC)α and akt promotes thrombin-mediated integrin $\alpha_{IIb}\beta_3$ activation and granule secretion in platelets. *Journal of Biological Chemistry*, *288*(6), 3918–3928.

Mortensen, M., Patel, B., & Smart, T. G. (2012). Gaba potency at $GABA_A$ receptors found in synaptic and extrasynaptic zones. *Frontiers in cellular neuroscience*, *6*, 1.

Mortensen, M., & Smart, T. G. (2006). Extrasynaptic αβ subunit $GABA_A$ receptors on rat hippocampal pyramidal neurons. *The Journal of physiology*, *577*(3), 841–856.

Mortensen, M., & Smart, T. G. (2007). Single-channel recording of ligand-gated ion channels. *Nature protocols*, *2*(11), 2826–2841.

Moss, S. J., Doherty, C., & Huganir, R. (1992). Identification of the cAMP-dependent protein kinase and protein kinase C phosphorylation sites within the major intracellular domains of the β_1, γ_{2S} and γ_{2L} subunits of the $GABA_A$ receptor. *Journal of Biological Chemistry*, *267*(20), 14470–14476.

Mozrzymas, J. W. (2004). Dynamism of $GABA_A$ receptor activation shapes the "personality" of inhibitory synapses. *Neuropharmacology*, *47*(7), 945–960.

Mozrzymas, J. W., Żarmowska, E. D., Pytel, M., & Mercik, K. (2003). Modulation of $GABA_A$ receptors by hydrogen ions reveals synaptic GABA transient and a crucial role of the desensitization process. *Journal of Neuroscience*, *23*(22), 7981–7992.

Muir, J., Arancibia-Carcamo, I. L., MacAskill, A. F., Smith, K. R., Griffin, L. D., & Kittler, J. T. (2010). NMDA receptors regulate $GABA_A$ receptor lateral mobility and clustering at inhibitory synapses through serine 327 on the γ_2

subunit. *Proceedings of the National Academy of Sciences*, *107*(38), 16679–16684.

Mukherjee, J., Kretschmannova, K., Gouzer, G., Maric, H.-M., Ramsden, S., Tretter, V., Harvey, K., Davies, P. A., Triller, A., Schindelin, H., et al. (2011). The residence time of $GABA_A$ receptors at inhibitory synapses is determined by direct binding of the receptor α_1 subunit to gephyrin. *Journal of Neuroscience*, *31*(41), 14677–14687.

Nakamura, Y., Darnieder, L. M., Deeb, T. Z., & Moss, S. J. (2015). Regulation of $GABA_A$ receptors by phosphorylation. *Advances in pharmacology*, *72*, 97–146.

Nakamura, Y., Morrow, D. H., Modgil, A., Huyghe, D., Deeb, T. Z., Lumb, M. J., Davies, P. A., & Moss, S. J. (2016). Proteomic characterization of inhibitory synapses using a novel pHluorin-tagged γ-aminobutyric acid receptor, type A $GABA_A$, α_2 subunit knock-in mouse. *Journal of Biological Chemistry*, *291*(23), 12394–12407.

Nakamura, Y., Morrow, D. H., Nathanson, A. J., Henley, J. M., Wilkinson, K. A., & Moss, S. J. (2020). Phosphorylation on Ser-359 of the α_2 subunit in GABA type A receptors down-regulates their density at inhibitory synapses. *Journal of Biological Chemistry*, *295*(35), 12330–12342.

Nakao, K., Singh, M., Sapkota, K., Hagler, B. C., Hunter, R. N., Raman, C., Hablitz, J. J., & Nakazawa, K. (2020). GSK3β inhibition restores cortical gamma oscillation and cognitive behavior in a mouse model of NMDA receptor hypofunction relevant to schizophrenia. *Neuropsychopharmacology*, *45*(13), 2207–2218.

Nathanson, A. J., Davies, P. A., & Moss, S. J. (2019). Inhibitory synapse formation at the axon initial segment. *Frontiers in molecular neuroscience*, *12*, 266.

Navarro, J. F., Burón, E., & Martın-López, M. (2002). Anxiogenic-like activity of L-655,708, a selective ligand for the benzodiazepine site of $GABA_A$ receptors which contain the α_5 subunit, in the elevated plus-maze test. *Progress*

in Neuro-Psychopharmacology and Biological Psychiatry, *26*(7-8), 1389–1392.

Neelands, T. R., Fisher, J. L., Bianchi, M., & Macdonald, R. L. (1999). Spontaneous and γ-aminobutyric acid (GABA)-activated $GABA_A$ receptor channels formed by ε subunit-containing isoforms. *Molecular pharmacology*, *55*(1), 168–178.

Nishiyama, J. (2019). Plasticity of dendritic spines: molecular function and dysfunction in neurodevelopmental disorders. *Psychiatry and clinical neurosciences*, *73*(9), 541–550.

Niwa, F., Bannai, H., Arizono, M., Fukatsu, K., Triller, A., & Mikoshiba, K. (2012). Gephyrin-independent $GABA_A$ receptor mobility and clustering during plasticity. *PloS one*, *7*(4), e36148.

Nusser, Z., Cull-Candy, S., & Farrant, M. (1997). Differences in synaptic $GABA_A$ receptor number underlie variation in GABA mini amplitude. *Neuron*, *19*(3), 697–709.

Nusser, Z., Hajos, N., Somogyi, P., & Mody, I. (1998). Increased number of synaptic $GABA_A$ receptors underlies potentiation at hippocampal inhibitory synapses. *Nature*, *395*(6698), 172–177.

Nusser, Z., Sieghart, W., Benke, D., Fritschy, J.-M., & Somogyi, P. (1996). Differential synaptic localization of two major $GABA_A$ receptor α subunits on hippocampal pyramidal cells. *Proceedings of the National Academy of Sciences*, *93*(21), 11939–11944.

Nusser, Z., Sieghart, W., & Somogyi, P. (1998). Segregation of different $GABA_A$ receptors to synaptic and extrasynaptic membranes of cerebellar granule cells. *Journal of Neuroscience*, *18*(5), 1693–1703.

Nuwer, J. L., Brady, M. L., Povysheva, N. V., Coyne, A., & Jacob, T. C. (2021). Sustained treatment with an α_5-$GABA_A$ receptor negative allosteric modulator delays excitatory circuit development while maintaining GABAergic neurotransmission. *Neuropharmacology*, *197*, 108724.

Nyitrai, G., Kékesi, K. A., & Juhász, G. (2006). Extracellular level of GABA and glu: *in vivo* microdialysis-HPLC measurements. *Current topics in medicinal chemistry*, *6*(10), 935–940.

Oh, W. C., Hill, T. C., & Zito, K. (2013). Synapse-specific and size-dependent mechanisms of spine structural plasticity accompanying synaptic weakening. *Proceedings of the National Academy of Sciences*, *110*(4), E305–E312.

Olsen, R. W. (2018). $GABA_A$ receptor: positive and negative allosteric modulators. *Neuropharmacology*, *136*, 10–22.

Olsen, R. W., & Sieghart, W. (2008). International union of pharmacology. LXX. subtypes of $GABA_A$ receptors: classification on the basis of subunit composition, pharmacology, and function. Update. *Pharmacological reviews*, *60*(3), 243–260.

Olsen, R. W., & Sieghart, W. (2009). $GABA_A$ receptors: subtypes provide diversity of function and pharmacology. *Neuropharmacology*, *56*(1), 141–148.

Olsen, R. W., & Tobin, A. J. (1990). Molecular biology of $GABA_A$ receptors. *The FASEB journal*, *4*(5), 1469–1480.

Ortinski, P. I., Lu, C., Takagaki, K., Fu, Z., & Vicini, S. (2004). Expression of distinct α subunits of $GABA_A$ receptor regulates inhibitory synaptic strength. *Journal of neurophysiology*, *92*(3), 1718–1727.

Pandey, M. K., & DeGrado, T. R. (2016). Glycogen synthase kinase-3 (GSK3)-targeted therapy and imaging. *Theranostics*, *6*(4), 571.

Papadopoulos, T., Korte, M., Eulenburg, V., Kubota, H., Retiounskaia, M., Harvey, R. J., Harvey, K., O'Sullivan, G. A., Laube, B., Hülsmann, S., et al. (2007). Impaired GABAergic transmission and altered hippocampal synaptic plasticity in collybistin-deficient mice. *The EMBO journal*, *26*(17), 3888–3899.

Patrizi, A., Viltono, L., Frola, E., Harvey, K., Harvey, R. J., & Sassoè-Pognetto, M. (2012). Selective localization of collybistin at a subset of inhibitory synapses in brain circuits. *Journal of Comparative Neurology*, *520*(1), 130–141.

Pennacchietti, F., Vascon, S., Nieus, T., Rosillo, C., Das, S., Tyagarajan, S. K., Diaspro, A., Del Bue, A., Petrini, E. M., Barberis, A., et al. (2017). Nanoscale

molecular reorganization of the inhibitory postsynaptic density is a determinant of GABAergic synaptic potentiation. *Journal of Neuroscience*, *37*(7), 1747–1756.

Petrache, A. L., Khan, A. A., Nicholson, M. W., Monaco, A., Kuta-Siejkowska, M., Haider, S., Hilton, S., Jovanovic, J. N., & Ali, A. B. (2020). Selective modulation of α_5-$GABA_A$ receptors exacerbates aberrant inhibition at key hippocampal neuronal circuits in APP mouse model of alzheimer's disease. *Frontiers in cellular neuroscience*, *14*.

Petrini, E. M., Ravasenga, T., Hausrat, T. J., Iurilli, G., Olcese, U., Racine, V., Sibarita, J.-B., Jacob, T. C., Moss, S. J., Benfenati, F., et al. (2014). Synaptic recruitment of gephyrin regulates surface $GABA_A$ receptor dynamics for the expression of inhibitory LTP. *Nature communications*, *5*(1), 1–19.

Phulera, S., Zhu, H., Yu, J., Claxton, D. P., Yoder, N., Yoshioka, C., & Gouaux, E. (2018). Cryo-EM structure of the benzodiazepine-sensitive $\alpha_1\beta_1\gamma_{2S}$ tri-heteromeric $GABA_A$ receptor in complex with GABA. *Elife*, *7*, e39383.

Picton, A. J., & Fisher, J. L. (2007). Effect of the α subunit subtype on the macroscopic kinetic properties of recombinant $GABA_A$ receptors. *Brain research*, *1165*, 40–49.

Pirker, S., Schwarzer, C., Wieselthaler, A., Sieghart, W., & Sperk, G. (2000). $GABA_A$ receptors: immunocytochemical distribution of 13 subunits in the adult rat brain. *Neuroscience*, *101*(4), 815–850.

Pizzarelli, R., Griguoli, M., Zacchi, P., Petrini, E. M., Barberis, A., Cattaneo, A., & Cherubini, E. (2020). Tuning GABAergic inhibition: gephyrin molecular organization and functions. *Neuroscience*, *439*, 125–136.

Pofantis, H., & Papatheodoropoulos, C. (2014). The α_5-$GABA_A$ receptor modulates the induction of long-term potentiation at ventral but not dorsal CA1 hippocampal synapses. *Synapse*, *68*(9), 394–401.

Poulopoulos, A., Aramuni, G., Meyer, G., Soykan, T., Hoon, M., Papadopoulos, T., Zhang, M., Paarmann, I., Fuchs, C., Harvey, K., et al. (2009). Neuroligin

2 drives postsynaptic assembly at perisomatic inhibitory synapses through gephyrin and collybistin. *Neuron*, *63*(5), 628–642.

Prenosil, G. A., Schneider Gasser, E. M., Rudolph, U., Keist, R., Fritschy, J.-M., & Vogt, K. E. (2006). Specific subtypes of $GABA_A$ receptors mediate phasic and tonic forms of inhibition in hippocampal pyramidal neurons. *Journal of neurophysiology*, *96*(2), 846–857.

Prevot, T. D., Sumitomo, A., Tomoda, T., Knutson, D. E., Li, G., Mondal, P., Banasr, M., Cook, J. M., & Sibille, E. (2021). Reversal of age-related neuronal atrophy by α_5-$GABA_A$ receptor positive allosteric modulation. *Cerebral Cortex*, *31*(2), 1395–1408.

Prut, L., Prenosil, G., Willadt, S., Vogt, K., Fritschy, J.-M., & Crestani, F. (2010). A reduction in hippocampal $GABA_A$ receptor α_5 subunits disrupts the memory for location of objects in mice. *Genes, brain and behavior*, *9*(5), 478–488.

Quirk, K., Blurton, P., Fletcher, S., Leeson, P., Tang, F., Mellilo, D., Ragan, C., & McKernan, R. (1996). [3H] L-655,708, a novel ligand selective for the benzodiazepine site of $GABA_A$ receptors which contain the α_5 subunit. *Neuropharmacology*, *35*(9-10), 1331–1335.

Rappsilber, J., Mann, M., & Ishihama, Y. (2007). Protocol for micro-purification, enrichment, pre-fractionation and storage of peptides for proteomics using StageTips. *Nature protocols*, *2*(8), 1896–1906.

Rosas-Arellano, A., Tejeda-Guzmán, C., Lorca-Ponce, E., Palma-Tirado, L., Mantellero, C. A., Rojas, P., Missirlis, F., & Castro, M. A. (2018). Huntington's disease leads to decrease of $GABA_A$ tonic subunits in the D2 neostriatal pathway and their relocalization into the synaptic cleft. *Neurobiology of disease*, *110*, 142–153.

Rudolph, U., & Knoflach, F. (2011). Beyond classical benzodiazepines: novel therapeutic potential of $GABA_A$ receptor subtypes. *Nature reviews Drug discovery*, *10*(9), 685–697.

Rudolph, U., & Möhler, H. (2014). $GABA_A$ receptor subtypes: therapeutic potential in Down syndrome, affective disorders, schizophrenia, and autism. *Annual review of pharmacology and toxicology*, *54*, 483–507.

Saiepour, L., Fuchs, C., Patrizi, A., Sassoè-Pognetto, M., Harvey, R. J., & Harvey, K. (2010). Complex role of collybistin and gephyrin in $GABA_A$ receptor clustering. *Journal of Biological Chemistry*, *285*(38), 29623–29631.

Salesse, C., Mueller, C. L., Chamberland, S., & Topolnik, L. (2011). Age-dependent remodelling of inhibitory synapses onto hippocampal CA1 oriens-lacunosum moleculare interneurons. *The Journal of physiology*, *589*(20), 4885–4901.

Saliba, R. S., Kretschmannova, K., & Moss, S. J. (2012). Activity-dependent phosphorylation of $GABA_A$ receptors regulates receptor insertion and tonic current. *The EMBO journal*, *31*(13), 2937–2951.

Sallard, E., Letourneur, D., & Legendre, P. (2021). Electrophysiology of ionotropic GABA receptors. *Cellular and Molecular Life Sciences*, 1–30.

Sarto-Jackson, I., & Sieghart, W. (2008). Assembly of $GABA_A$ receptors. *Molecular membrane biology*, *25*(4), 302–310.

Sassoè-Pognetto, M., Panzanelli, P., Sieghart, W., & Fritschy, J.-M. (2000). Colocalization of multiple $GABA_A$ receptor subtypes with gephyrin at postsynaptic sites. *Journal of Comparative Neurology*, *420*(4), 481–498.

Savić, M. M., Huang, S., Furtmüller, R., Clayton, T., Huck, S., Obradović, D. I., Ugrešić, N. D., Sieghart, W., Bokonjić, D. R., & Cook, J. M. (2008). Are $GABA_A$ receptors containing α_5 subunits contributing to the sedative properties of benzodiazepine site agonists? *Neuropsychopharmacology*, *33*(2), 332–339.

Schulte, C., & Maric, H. M. (2021). Expanding $GABA_A$ receptor pharmacology via receptor-associated proteins. *Current Opinion in Pharmacology*, *57*, 98–106.

Schulz, J. M., Knoflach, F., Hernandez, M.-C., & Bischofberger, J. (2018). Dendrite-targeting interneurons control synaptic NMDA-receptor activa-

tion via nonlinear α_5-GABA$_A$ receptors. *Nature communications*, *9*(1), 1–16.

Schulz, J. M., Knoflach, F., Hernandez, M.-C., & Bischofberger, J. (2019). Enhanced dendritic inhibition and impaired NMDAR activation in a mouse model of Down syndrome. *Journal of Neuroscience*, *39*(26), 5210–5221.

Schweizer, C., Balsiger, S., Bluethmann, H., Mansuy, I. M., Fritschy, J.-M., Mohler, H., & Lüscher, B. (2003). The γ_2 subunit of GABA$_A$ receptors is required for maintenance of receptors at mature synapses. *Molecular and Cellular Neuroscience*, *24*(2), 442–450.

Scimemi, A., & Beato, M. (2009). Determining the neurotransmitter concentration profile at active synapses. *Molecular neurobiology*, *40*(3), 289–306.

Serwanski, D. R., Miralles, C. P., Christie, S. B., Mehta, A. K., Li, X., & De Blas, A. L. (2006). Synaptic and nonsynaptic localization of GABA$_A$ receptors containing the α_5 subunit in the rat brain. *Journal of Comparative Neurology*, *499*(3), 458–470.

Shen, Z.-C., Wu, P.-F., Wang, F., Xia, Z.-X., Deng, Q., Nie, T.-L., Zhang, S.-Q., Zheng, H.-L., Liu, W.-H., Lu, J.-J., et al. (2019). Gephyrin palmitoylation in basolateral amygdala mediates the anxiolytic action of benzodiazepine. *Biological psychiatry*, *85*(3), 202–213.

Sieghart, W. (2006). Structure, pharmacology, and function of GABA$_A$ receptor subtypes. *Advances in pharmacology*, *54*, 231–263.

Sieghart, W., & Savić, M. M. (2018). International union of basic and clinical pharmacology. CVI: GABA$_A$ receptor subtype-and function-selective ligands: key issues in translation to humans. *Pharmacological reviews*, *70*(4), 836–878.

Sigel, E. (2002). Mapping of the benzodiazepine recognition site on GABA$_A$ receptors. *Current topics in medicinal chemistry*, *2*(8), 833–839.

Simon, J., Wakimoto, H., Fujita, N., Lalande, M., & Barnard, E. A. (2004). Analysis of the set of GABA$_A$ receptor genes in the human genome. *Journal of Biological Chemistry*, *279*(40), 41422–41435.

Solomon, V. R., Tallapragada, V. J., Chebib, M., Johnston, G., & Hanrahan, J. R. (2019). GABA allosteric modulators: an overview of recent developments in non-benzodiazepine modulators. *European journal of medicinal chemistry*, *171*, 434–461.

Sotiriou, E., Papatheodoropoulos, C., & Angelatou, F. (2005). Differential expression of $GABA_A$ receptor subunits in rat dorsal and ventral hippocampus. *Journal of neuroscience research*, *82*(5), 690–700.

Specht, C. G., Izeddin, I., Rodriguez, P. C., El Beheiry, M., Rostaing, P., Darzacq, X., Dahan, M., & Triller, A. (2013). Quantitative nanoscopy of inhibitory synapses: counting gephyrin molecules and receptor binding sites. *Neuron*, *79*(2), 308–321.

Sperk, G., Schwarzer, C., Tsunashima, K., Fuchs, K., & Sieghart, W. (1997). $GABA_A$ receptor subunits in the rat hippocampus I: immunocytochemical distribution of 13 subunits. *Neuroscience*, *80*(4), 987–1000.

Sperk, G., Kirchmair, E., Bakker, J., Sieghart, W., Drexel, M., & Kondova, I. (2020). Immunohistochemical distribution of 10 $GABA_A$ receptor subunits in the forebrain of the rhesus monkey macaca mulatta. *Journal of Comparative Neurology*, *528*(15), 2551–2568.

Stambolic, V., & Woodgett, J. R. (1994). Mitogen inactivation of glycogen synthase kinase-3 β in intact cells via serine 9 phosphorylation. *Biochemical Journal*, *303*(3), 701–704.

Stamenić, T. T., Poe, M. M., Rehman, S., Santrač, A., Divović, B., Scholze, P., Ernst, M., Cook, J. M., & Savić, M. M. (2016). Ester to amide substitution improves selectivity, efficacy and kinetic behavior of a benzodiazepine positive modulator of $GABA_A$ receptors containing the α_5 subunit. *European journal of pharmacology*, *791*, 433–443.

Strange, B. A., Witter, M. P., Lein, E. S., & Moser, E. I. (2014). Functional organization of the hippocampal longitudinal axis. *Nature Reviews Neuroscience*, *15*(10), 655–669.

Sun, C., Sieghart, W., & Kapur, J. (2004). Distribution of α_1, α_4, γ_2 and δ subunits of $GABA_A$ receptors in hippocampal granule cells. *Brain research*, *1029*(2), 207–216.

Sun, M.-Y., Shu, H.-J., Benz, A., Bracamontes, J., Akk, G., Zorumski, C. F., Steinbach, J. H., & Mennerick, S. J. (2018). Chemogenetic isolation reveals synaptic contribution of δ-$GABA_A$ receptors in mouse dentate granule neurons. *Journal of Neuroscience*, *38*(38), 8128–8145.

Sur, C., Fresu, L., Howell, O., McKernan, R. M., & Atack, J. R. (1999). Autoradiographic localization of α_5 subunit-containing $GABA_A$ receptors in rat brain. *Brain research*, *822*(1-2), 265–270.

Sur, C., Quirk, K., Dewar, D., Atack, J., & McKernan, R. (1998). Rat and human hippocampal α_5 subunit-containing $GABA_A$ receptors have $\alpha_5\beta_3\gamma_2$ pharmacological characteristics. *Molecular pharmacology*, *54*(5), 928–933.

Terejko, K., Kaczor, P. T., Michałowski, M. A., Dąbrowska, A., & Mozrzymas, J. W. (2020). The C loop at the orthosteric binding site is critically involved in $GABA_A$ receptor gating. *Neuropharmacology*, *166*, 107903.

Terejko, K., Michałowski, M. A., Iżykowska, I., Dominik, A., Brzóstowicz, A., & Mozrzymas, J. W. (2021). Mutations at the m2 and m3 transmembrane helices of the $GABA_A$ receptors α_1 and β_2 subunits affect primarily late gating transitions including opening/closing and desensitization. *ACS Chemical Neuroscience*.

Thomas, P., Mortensen, M., Hosie, A. M., & Smart, T. G. (2005). Dynamic mobility of functional $GABA_A$ receptors at inhibitory synapses. *Nature neuroscience*, *8*(7), 889–897.

Thomas, P., & Smart, T. G. (2005). HEK293 cell line: a vehicle for the expression of recombinant proteins. *Journal of pharmacological and toxicological methods*, *51*(3), 187–200.

Towers, S., Gloveli, T., Traub, R., Driver, J., Engel, D., Fradley, R., Rosahl, T., Maubach, K., Buhl, E., & Whittington, M. (2004). A_5 subunit-containing $GABA_A$ receptors affect the dynamic range of mouse hippocampal kainate-

induced gamma frequency oscillations *in vitro*. *The Journal of physiology*, *559*(3), 721–728.

Tretter, V., Jacob, T. C., Mukherjee, J., Fritschy, J.-M., Pangalos, M. N., & Moss, S. J. (2008). The clustering of $GABA_A$ receptor subtypes at inhibitory synapses is facilitated via the direct binding of receptor α_2 subunits to gephyrin. *Journal of Neuroscience*, *28*(6), 1356–1365.

Tretter, V., Kerschner, B., Milenkovic, I., Ramsden, S. L., Ramerstorfer, J., Saiepour, L., Maric, H.-M., Moss, S. J., Schindelin, H., Harvey, R. J., et al. (2011). Molecular basis of the $GABA_A$ receptor α_3 subunit interaction with the clustering protein gephyrin. *Journal of Biological Chemistry*, *286*(43), 37702–37711.

Tretter, V. E., Mukherjee, J., Maric, H. M., Schindelin, H., Sieghart, W., & Moss, S. J. (2012). Gephyrin, the enigmatic organizer at GABAergic synapses. *Frontiers in cellular neuroscience*, *6*, 23.

Triller, A., & Choquet, D. (2005). Surface trafficking of receptors between synaptic and extrasynaptic membranes: and yet they do move! *Trends in neurosciences*, *28*(3), 133–139.

Tyagarajan, S. K., & Fritschy, J.-M. (2010). $GABA_A$ receptors, gephyrin and homeostatic synaptic plasticity. *The Journal of physiology*, *588*(1), 101–106.

Tyagarajan, S. K., & Fritschy, J.-M. (2014). Gephyrin: a master regulator of neuronal function? *Nature Reviews Neuroscience*, *15*(3), 141–156.

Tyagarajan, S. K., Ghosh, H., Yévenes, G. E., Imanishi, S. Y., Zeilhofer, H. U., Gerrits, B., & Fritschy, J.-M. (2013). Extracellular signal-regulated kinase and glycogen synthase kinase 3β regulate gephyrin postsynaptic aggregation and GABAergic synaptic function in a calpain-dependent mechanism. *Journal of Biological Chemistry*, *288*(14), 9634–9647.

Tyagarajan, S. K., Ghosh, H., Yévenes, G. E., Nikonenko, I., Ebeling, C., Schwerdel, C., Sidler, C., Zeilhofer, H. U., Gerrits, B., Muller, D., & Fritschy, J.-M. (2011). Regulation of GABAergic synapse formation and plasticity

by GSK3β-dependent phosphorylation of gephyrin. *Proceedings of the National Academy of Sciences*, *108*(1), 379–384.

Uezu, A., Kanak, D. J., Bradshaw, T. W., Soderblom, E. J., Catavero, C. M., Burette, A. C., Weinberg, R. J., & Soderling, S. H. (2016). Identification of an elaborate complex mediating postsynaptic inhibition. *Science*, *353*(6304), 1123–1129.

Van Rijnsoever, C., Sidler, C., & Fritschy, J.-M. (2005). Internalized $GABA_A$-receptor subunits are transferred to an intracellular pool associated with the postsynaptic density. *European Journal of Neuroscience*, *21*(2), 327–338.

van Niel, M. B., Wilson, K., Adkins, C. H., Atack, J. R., Castro, J. L., Clarke, D. E., Fletcher, S., Gerhard, U., Mackey, M. M., Malpas, S., Maubach, K., Newman, R., O'Connor, D., Pillai, G. V., Simpson, P. B., Thomas, S. R., & MacLeod, A. M. (2005). A new pyridazine series of α_5-$GABA_A$ ligands. *Journal of medicinal chemistry*, *48*(19), 6004–6011.

Vargas-Caballero, M., Martin, L. J., Salter, M. W., Orser, B. A., & Paulsen, O. (2010). A_5 subunit-containing $GABA_A$ receptors mediate a slowly decaying inhibitory synaptic current in CA1 pyramidal neurons following schaffer collateral activation. *Neuropharmacology*, *58*(3), 668–675.

Varoqueaux, F., Jamain, S., & Brose, N. (2004). Neuroligin 2 is exclusively localized to inhibitory synapses. *European journal of cell biology*, *83*(9), 449–456.

Vidal, V., Garcıa-Cerro, S., Martınez, P., Corrales, A., Lantigua, S., Vidal, R., Rueda, N., Ozmen, L., Hernández, M.-C., & Martınez-Cué, C. (2018). Decreasing the expression of α_5 subunit-containing $GABA_A$ receptors partially improves cognitive, electrophysiological, and morphological hippocampal defects in the Ts65Dn model of Down syndrome. *Molecular neurobiology*, *55*(6), 4745–4762.

Vinnakota, C., Govindpani, K., Tate, W. P., Peppercorn, K., Anekal, P. V., Waldvogel, H. J., Faull, R. L. M., & Kwakowsky, A. (2020). An α_5-$GABA_A$ receptor inverse agonist, $\alpha_5$ia, attenuates amyloid beta-induced neuronal death in

mouse hippocampal cultures. *International journal of molecular sciences*, *21*(9), 3284.

Wagner, S., Lee, C., Rojas, L., Specht, C. G., Rhee, J., Brose, N., & Papadopoulos, T. (2021). The α_3 subunit of $GABA_A$ receptors promotes formation of inhibitory synapses in the absence of collybistin. *Journal of Biological Chemistry*, *296*.

Wei, W., Zhang, N., Peng, Z., Houser, C. R., & Mody, I. (2003). Perisynaptic localization of δ subunit-containing $GABA_A$ receptors and their activation by GABA spillover in the mouse dentate gyrus. *Journal of Neuroscience*, *23*(33), 10650–10661.

Weltzien, F., Puller, C., O'Sullivan, G. A., Paarmann, I., & Betz, H. (2012). Distribution of the glycine receptor β-subunit in the mouse CNS as revealed by a novel monoclonal antibody. *Journal of Comparative Neurology*, *520*(17), 3962–3981.

Whiting, P., McKernan, R. M., & Iversen, L. L. (1990). Another mechanism for creating diversity in $GABA_A$ receptors: RNA splicing directs expression of two forms of γ_2 phosphorylation site. *Proceedings of the National Academy of Sciences*, *87*(24), 9966–9970.

Whiting, P. J., McKernan, R. M., & Wafford, K. A. (1995). Structure and pharmacology of vertebrate $GABA_A$ receptor subtypes. *International review of neurobiology*, *38*, 95–138.

Wieland, H. A., Lüddens, H., & Seeburg, P. H. (1992). A single histidine in $GABA_A$ receptors is essential for benzodiazepine agonist binding. *Journal of Biological Chemistry*, *267*(3), 1426–1429.

Wu, M., Tian, H.-L., Liu, X., Lai, J. H. C., Du, S., & Xia, J. (2018). Impairment of inhibitory synapse formation and motor behavior in mice lacking the NL2 binding partner LHFPL4/GARLH4. *Cell reports*, *23*(6), 1691–1705.

Wyroślak, M., Lebida, K., & Mozrzymas, J. W. (2021). Induction of inhibitory synaptic plasticity enhances tonic current by increasing the content of α_5

subunit-containing $GABA_A$ receptors in hippocampal pyramidal neurons. *Neuroscience*.

Xu, N. Z., Ernst, M., Treven, M., Wakulchik, M., Li, X., Jones, T. M., Gleason, S. D., Morrow, D., Schkeryantz, J. M., Rahman, M. T., et al. (2018). Negative allosteric modulation of α_5-containing $GABA_A$ receptors engenders antidepressant-like effects and selectively prevents age-associated hyperactivity in tau-depositing mice. *Psychopharmacology*, *235*(4), 1151–1161.

Yamasaki, T., Hoyos-Ramirez, E., Martenson, J. S., Morimoto-Tomita, M., & Tomita, S. (2017). GARLH family proteins stabilize $GABA_A$ receptors at synapses. *Neuron*, *93*(5), 1138–1152.

Yang, X., Le Corronc, H., Legendre, P., Triller, A., & Specht, C. G. (2021). Differential regulation of glycinergic and GABAergic nanocolumns at mixed inhibitory synapses. *EMBO reports*, e52154.

Yang, X., & Specht, C. G. (2019). Subsynaptic domains in super-resolution microscopy: the treachery of images. *Frontiers in molecular neuroscience*, *12*, 161.

Yang, Y., & Calakos, N. (2013). Presynaptic long-term plasticity. *Frontiers in synaptic neuroscience*, *5*, 8.

Yao, H.-B., Shaw, P.-C., Wong, C.-C., & Wan, D. C.-C. (2002). Expression of glycogen synthase kinase-3 isoforms in mouse tissues and their transcription in the brain. *Journal of chemical neuroanatomy*, *23*(4), 291–297.

Ye, J., Zou, G., Zhu, R., Kong, C., Miao, C., Zhang, M., Li, J., Xiong, W., & Wang, C. (2021). Structural basis of GABARAP-mediated $GABA_A$ receptor trafficking and functions on GABAergic synaptic transmission. *Nature communications*, *12*(1), 1–12.

Yee, B. K., Hauser, J., Dolgov, V. V., Keist, R., Möhler, H., Rudolph, U., & Feldon, J. (2004). $GABA_A$ receptors containing the α_5 subunit mediate the trace effect in aversive and appetitive conditioning and extinction of conditioned fear. *European Journal of Neuroscience*, *20*(7), 1928–1936.

Zacchi, P., Antonelli, R., & Cherubini, E. (2014). Gephyrin phosphorylation in the functional organization and plasticity of GABAergic synapses. *Frontiers in cellular neuroscience*, *8*, 103.

Zarnowska, E. D., Keist, R., Rudolph, U., & Pearce, R. A. (2009). $GABA_A$ receptor α_5 subunits contribute to $GABA_{A,slow}$ synaptic inhibition in mouse hippocampus. *Journal of neurophysiology*, *101*(3), 1179–1191.

Zhou, Q., Homma, K. J., & Poo, M.-m. (2004). Shrinkage of dendritic spines associated with long-term depression of hippocampal synapses. *Neuron*, *44*(5), 749–757.

Zhu, S., Noviello, C. M., Teng, J., Walsh, R. M., Kim, J. J., & Hibbs, R. E. (2018). Structure of a human synaptic $GABA_A$ receptor. *Nature*, *559*(7712), 67–72.

Zorrilla de San Martin, J., Delabar, J.-M., Bacci, A., & Potier, M.-C. (2018). GABAergic over-inhibition, a promising hypothesis for cognitive deficits in Down syndrome. *Free Radical Biology and Medicine*, *114*, 33–39.

Zorrilla de San Martin, J., Trigo, F. F., & Kawaguchi, S.-y. (2017). Axonal $GABA_A$ receptors depolarize presynaptic terminals and facilitate transmitter release in cerebellar purkinje cells. *The Journal of physiology*, *595*(24), 7477–7493.

Zurek, A. A., Bridgwater, E. M., & Orser, B. A. (2012). Inhibition of α_5-$GABA_A$ receptors restores recognition memory after general anesthesia. *Anesthesia & Analgesia*, *114*(4), 845–855.

Zurek, A. A., Kemp, S. W., Aga, Z., Walker, S., Milenkovic, M., Ramsey, A. J., Sibille, E., Scherer, S. W., & Orser, B. A. (2016). α_5-$GABA_A$ receptor deficiency causes autism-like behaviors. *Annals of clinical and translational neurology*, *3*(5), 392–398.

Zurek, A. A., Yu, J., Wang, D.-S., Haffey, S. C., Bridgwater, E. M., Penna, A., Lecker, I., Lei, G., Chang, T., Salter, E. W., et al. (2014). Sustained increase in α_5-$GABA_A$ receptor function impairs memory after anesthesia. *The Journal of clinical investigation*, *124*(12), 5437–5441.